

Covalent Adaptable Networks to Create Dynamic, Tunable, and Actuatable Materials from Molecular Self Assembly

by
Alina Marissa Martinez

B.S. University of New Mexico – 2016
M.S. University of Colorado Boulder – 2018

A thesis submitted to the
Faculty of the Graduate School of the
University of Colorado in partial fulfillment
of the requirement for the degree of
Doctor of Philosophy
Department of Materials Science & Engineering
2022

Committee:

Christopher N. Bowman
Jeffrey W. Stansbury
Ryan C. Hayward
Timothy J. White
Yifu Ding

Martinez, Alina Marissa (PhD, Materials Science and Engineering)

Covalent Adaptable Networks to Create Dynamic, Tunable, and Actuable Materials from Molecular Self Assembly

Thesis directed by Professor Christopher N. Bowman at the University of Colorado Boulder

The work in this thesis focuses on molecular-level self-assembly to achieve autonomous shape change in polymer materials. The breadth of this work ranges from macroscopic to microscopic shape programming of polymers. These autonomous, shape switching materials rely on post-polymerization modifications to the polymer network facilitated by dynamic covalent chemistry (DCC) incorporated into crosslinked polymers to form covalent adaptable networks (CANs). The DCC significantly utilized in this work is light activated addition-fragmentation chain-transfer (AFT), which provides spatial and temporal control of bond rearrangement. Furthermore, the self-assembly capabilities afforded by liquid crystals (LCs) tethered to a polymer network create the structure through which these micro and macroscopic shape changes are made possible, enabling molecular assembly to generate 3D structures. By disrupting LC alignment tethered to the polymer network in a liquid crystal elastomer (LCE), reversible shape switching is achieved by heating past the LC phase transition temperature. These shape switching structures were programmed by simple mechanical deformations under illumination and deployed via a thermal stimulus to reversibly actuate the material. Investigating the complex LC alignment also allows for the achievement of visible color changes linked to structure, that are reversibly modified.

AFT-LCEs on the order of millimeters in length, were designed and programmed into a variety of complex shapes post polymerization. These programmed shapes were also erased by

irradiating the materials above their phase transition temperature to erase any alignment that existed prior. Furthermore, incorporation of a chiral LC monomer induced a handedness of alignment throughout the thickness of the film, which resulted in a Bragg reflection on visible wavelengths of light. The cholesteric LCE (CLCE) exhibited a red reflective character and upon uniaxial deformation to modify the underlying structure, resulted in a blue shift of the material. Light exposures performed programmed the strain and color change in the material. Color was erased by irradiating the CLCE above the phase transition temperature, resulting in a transparent, clear film.

CANs were then translated to micro-networks. AFT-LCEMPs were generated via a thiol-Michael dispersion polymerization, yielding particles with a diameter of $7 \pm 2 \mu\text{m}$. These particles doped with photoinitiator were compressed and irradiated with light to program them into a variety of geometries including prolate and oblate, by tuning the temperature with which programming was done. Switchable shapes were investigated, and these programmed shapes were also erased by exposure of the particles to light above their phase transition temperature, which erased any programming or alignment that existed prior.

Amorphous CAN microparticles with a diameter of $4.0 \pm 0.4 \mu\text{m}$ were generated by a thiol-Michael dispersion polymerization. These particles were designed with DCC to enable interparticle bond exchange to generate new permanent structures. The DCC utilized here was the thiol-thioester exchange, which is base catalyzed. The ultra-violet visible spectroscopy (UV-vis) of the particle coalescence process indicated that change to the transmission cease to occur at 3 days. The integrity of the films generated from microparticle coalescence was evaluated by performing tensile tests, finding that films made directly from monomer and films made from

particles had similar mechanical properties after 7 days. The modulus values were measured to be 5 ± 1 MPa and 6 ± 1 MPa for the monomer-films and particle-films respectively.

Ultimately in this work, investigation of the stress relaxation mechanism for network reorganization enables the programming of new, permanent, and temporarily reversible structures post-polymerization, while simultaneously utilizing molecular self-assembly to generate 3D structures. Demonstrations of programming and re-programming were reported, showcasing the adaptability achieved by polymer networks designed as CANs.

Dedication

This work is dedicated to those like myself. To the underdogs and minorities, who defy standards even when you are doubted, overlooked, and underestimated. To the women and men who came before me, who have made this journey possible. We must remember not to take our freedom to practice science for granted. And to those after me, who continue to push the limits.

Querer es Poder.

Acknowledgements

To Carmen, mi hermana, the strongest and most determined person I know. A doctor in engineering. My best friend and teacher, who always has time for me, and who always believes in me. I cherish our discussions and I don't know what I would do without you. Having a sibling is the greatest gift I could've been given. To my parents for their countless sacrifices and unconditional love and support throughout life, I wouldn't be here without them. My mom, the kindest and hardest working person I know. A very rare person, she has taught me to have empathy and compassion, which I cherish greatly. And for always taking care of me, no matter how old I am. My dad, my hero, the best engineer I know, who raised me to defy standards and to have high standards for myself and others. To have mental strength, which has helped me succeed again and again. He taught me that "rocket science is for real". I cannot put into words the appreciation I have for the lessons they have taught me. To my brother-in-law, Nick, for always believing in me, even when I didn't. Thank you and Carmen for my perfect sobrina Rosario Maria Villalobos. I can't wait to be best friends. To Toki, my rabbit sized roommate and my soul companion. Who has lived with me these past 5.5 years without complaint.

Jill, Emma, and Jordan, my lifelong and best friends, who have carried me through my worst times, and laughed with me at my best times.

To my New Mexico friends, the ones who are no longer with us, who would be proud of me, and the ones who have continued to support me. To my Angry Dragons soccer team and lifelong friends. We have come a long way since high school. To Tracy Davis, a badass engineer, my peer but someone I look up to. Who also always believed in me and had my back through anything. And of course, to your family, Kalvin and Blair, our number one fans. To my New Mexico culture and pride. It shaped me to be the person I am.

To having the opportunity to live in paradise, and to my Colorado friends who I consider family, who have made this experience extraordinary. The biking and skiing have been world class.

To Dr. Repine, for putting my legs back together so I could continue to pursue my academics and passions.

To my first mentor, Dr. Brad Jones, who showed me what a PhD should look like and who I look up to as a scientist and thrill seeker. I highly valued my time at Sandia National Labs. To my mentors Dr. Lewis Cox and Dr. Matt McBride, for the intellectual conversations, for always making time for me to think through problems or ideas, and more importantly, shredding the mountain, or grabbing a beer, and always being in my corner.

To my past and future boss Dr. Rafael Zaldivar, at The Aerospace Corporation, a Latino like myself, for inspiring me to continue to strive for greatness but to also have fun doing the work. To the GEM foundation and fellowship I received, for letting me spend an unforgettable summer in Los Angeles, CA. I guess I am heading back there!

To my lab mate and great friend Nick Bongiardina, for experiencing this journey with me and always being there to talk about science or life, the hardships, and successes in both, and being a

genuinely kind person. For being a wealth of knowledge. The late nights, the long weekends. 5.5 years flies by. And to my lab mates, who have been there every step of the way on this journey.

To my committee, Dr. Jeff Stansbury, Dr. Yifu Ding, Dr. Tim White, and Dr. Ryan Hayward. For having genuine interest in my work, asking thoughtful and probing questions, making me a better scientist, and for letting me use their equipment. To the Materials Science and Engineering program at CU Boulder, for this unforgettable journey, education, and opportunities.

Finally, and very importantly, to my advisor, Dr. Chris Bowman, for the overwhelming support and belief in me and my work. For pushing me to be a better scientist. For giving me the opportunities to travel and go to Japan, one of the greatest experiences in my life. For the opportunities this lab has given me. I have had so much fun and freedom with my work and research. None of this would have been possible without his help.

Two quotes I've carried with me over the years...

“Fortune Favors the Bold”

-Vergil-

“Happiness, only real when shared”

-Chris McCandless-

Table of Contents

Chapter 1: Introduction	1
1.1 – Overview.....	1
1.2 – Polymer Structure and Polymerizations.....	2
1.2.1 – Polymer Structure.....	2
1.2.2 – Chain-Growth Polymerization.....	4
1.2.3 – Step-Growth Polymerization.....	5
1.2.4 – Polymer Characterization.....	6
1.3 – Covalent Adaptable Networks.....	7
1.3.1 – Mechanisms of CANs.....	7
1.3.2 – Addition Fragmentation Chain Transfer.....	9
1.3.3 – Thiol-Thioester Exchange.....	10
1.4 – Shape Switching Materials.....	10
1.4.1 – Shape Switching Polymers.....	11
1.4.2 – Liquid Crystal Elastomers.....	11
1.4.3 – Color Switching.....	13
1.5 – Microparticles.....	15
1.5.1 – Shape Switching Microparticles.....	15
1.5.2 – Microparticles to Generate Tunable Surfaces and Films.....	17
1.6 – Summary.....	17
1.7 – References.....	18
Chapter 2: Objectives	25
Chapter 3: Investigating Molecular Level Self-Assembly to Program and Re-write Tunable Materials	30
3.1 – Introduction.....	30
3.2 – Results and Discussion.....	32
3.3 – Conclusions.....	42
3.4 – Experimental.....	42
3.5 – Acknowledgements.....	47
3.6 – Supporting Information.....	48
3.7 – References.....	50
Chapter 4: Reconfigurable and Spatially Programmable Chameleon-Skin Like Material Utilizing Light Responsive Covalent Adaptable Cholesteric Liquid Crystal Elastomers	52
4.1 – Introduction.....	52
4.2 – Results and Discussion.....	56
4.3 – Conclusions.....	67
4.4 – Experimental.....	68
4.5 – Acknowledgements.....	74
4.6 – Supporting Information.....	75
4.7 – References.....	79
Chapter 5: One- and Two-way Shape Switching Liquid Crystal Elastomer Microparticles	81
5.1 – Introduction.....	81
5.2 – Results and Discussion.....	83
5.3 – Conclusions.....	90
5.4 – Experimental.....	90

5.5 – Acknowledgements.....	92
5.6 – Supporting Information.....	93
5.7 – References.....	94
Chapter 6: Permanent and Reversibly Programmable Shapes in Liquid Crystal Elastomer Microparticles Capable of Shape Switching.....	96
6.1 – Introduction.....	96
6.2 – Results and Discussion.....	98
6.3 – Conclusions.....	110
6.4 – Experimental.....	111
6.5 – Acknowledgements.....	116
6.6 – Supporting Information.....	117
6.7 – References.....	123
Chapter 7: Tunable Surfaces and Films from Thioester Containing Microparticles.....	127
7.1 – Introduction.....	127
7.2 – Results and Discussion.....	129
7.3 – Conclusions.....	142
7.4 – Experimental.....	143
7.5 – Acknowledgements.....	147
7.6 – Supporting Information.....	148
7.7 – References.....	153
7.A – Appendix.....	156
Chapter 8: Conclusions and Future Recommendations.....	160
8.1 – Shape and Color Changing Structures.....	160
8.2 – Shape Changing Microstructures.....	164
8.3 – Processable Polymer Microparticles with Potential in 3D Printing.....	166
8.4 – Summary.....	167
Bibliography.....	169

List of Tables

Table 5.1: For System A, B and C; monomer stoichiometry and polymer properties of particles. Where r is the ratio of thiol to acrylate, P_{gel} is the probability of gelation, Alignment is LC alignment determined by WAXS, D_n is average particle diameter, CV is coefficient of variance = $(StDev/D_n * 100)$, and T_{NI} is the temperature for the LC phase transition from nematic to isotropic.....85

Table 7.1: Mechanical properties for films made from monomer, and particles (P) after 3 and 7 days. Modulus (M) = Stress/Strain, toughness (T) found by area under the tensile curve, and strain to break (S to B).....139

List of Figures

Figure 1.1: Examples of structurally colored materials. Image used from references (61,62)....14

Figure 3.1: a.) Programming the LCE occurs by straining the material and irradiating with light. Heating the film returns it to its temporary starting shape. b.) AFT exchange mechanism c.) POM of LCE A – Before programming, B – After programming, 45 degrees to the polarizer, C – Aligned with the polarizer. d.) AFT-LCE reprogrammed by irradiating the film above the T_{NI} in its temporary recovered shape.....34

Figure 3.2: Strain measurements of the AFT-LCE programmed at varying light exposure durations measured in a.) the LC Phase at room temperature. b.) the isotropic phase at 120°C. c.) Erasing programming. Samples were initially programmed with 100 s, 365 nm, 30 mW/cm². They were then erased by heating to 100°C and irradiated with 320-500 nm 30 mW/cm². The LC (grey) and isotropic (blue) phase shape was then measured.....36

Figure 3.3: a.) Box shape programming at 25°C, 365 nm, 50mW/cm², 120 s. b.) Flower shape programming at 40°C, 365 nm, 50mW/cm², 200 s.....38

Figure 3.4: a.) LCE starting at 25°C (top) and heated above T_{NI} (bottom) b.) LCE viewed at 25°C, cooled after programming c.) LCE heated above the T_{NI} displaying a bent shape d.) LCE after irradiating at step c. e.) LCE cooled to 25°C displaying the new permanent starting shape.....39

Figure 3.5: a.) Scheme for utilizing light attenuation to program LC alignment. b.) Bending LCE programmed by light attenuation. By increasing exposure time, network reorganization and alignment stabilization is increased resulting in enhanced 3D deformations. c.) Twisting LCE programmed in a similar manner.....40

Figure 3.6: Programming the AFT-LCE in a variety of complex geometries using T-328 a.) Saddle. Using a photomask, programming a b.) Box and c.) Pyramid is achieved.....41

Figure S3.1: DMA for three LCE stoichiometries being RM82:NPGDA:ADT, displaying the modulation of NPGDA content, denoted diacrylate (DA), (full stoichiometry RM82:NPGDA:ADT at 0.9 x Acrylate EQ). Data displaying a change in the LC phase transitions as the concentration of LC monomer is changed a.) Tan Delta b.) Storage modulus.....48

Figure S3.2: Stress relaxation behavior of LCE at 120°C (gray), 67°C (blue), and 25°C (red). Conditions: 10% strain, light on at 100 s (30 mW/cm², 320-500 nm).....48

Figure S3.3: Strain measurements of the AFT-LCE programmed at varying strains in the LC Phase (green) and isotropic phase (grey).....49

Figure S3.4: Strain to break experiments for 1:0.5:1.35 RM82/NPGDA/allyl dithiol. Conditions: 3.14×0.25×6 mm was stretched at 0.1 mm/s until slip or break on a TA RSA-G2. Experiment was run in triplicate.....49

Figure S3.5: UV-vis for LCE doped with 0.5 wt% T328. Light attenuation is confirmed at the programming wavelength of 365 nm.....49

Figure 4.1: a.) Monomers used to prepare the CLCE: (1) RM82, (2) NPGDA, and (3) allyl dithiol were oligomerized as diacrylate functionalized oligomers and acrylate homopolymerized with chiral LC monomer (4) LC756. b.) Schematic of chiral nematic alignment in the film as the material is strained. Overall alignment improves along with a decrease and some deformation of the pitch. c.) Schematic of the polymerization and programming process. LC resin was repeatedly cooled and heated just below the T_{NI} while manual shearing between glass to align the monomers into the chiral nematic phase, polymerized with visible light and later programmed via straining and irradiating with UV light. Alignment follows Figure 1b depiction.....57

Figure 4.2: a.) Camera images of the CLCE being mechanically strained and corresponding b.) UV-Vis spectroscopy upon straining. c.) Wavelength of the film taken at the center minimum of the reflection notch at corresponding strain values. d.) Optical microscopy of the CLCE unstrained and strained. e.) WAXS on an unstrained film and then strained to 60% displaying chiral nematic alignment initially, then localization of intensity indicating a deformed chiral nematic.....59

Figure 4.3: Values for CLCEs of the wavelength measured at the center minimum of the reflection notch and % strain from the initial length after programming, measured in the a.) LC phase and b.) Isotropic phase: programming done at 25°C, strained to 100%, exposed with light at 320-390 nm and 70 mW/cm² intensity for varying amounts of time (20 s, 60 s, 120 s, 600 s) and corresponding images. c.) Schematic of chiral nematic alignment before and after programming in the LC and isotropic phase with improvement to overall alignment but some deformation to the pitch.....62

Figure 4.4: a.) UV-vis on erasing reflection band for samples fixed between glass, exposed with light at 320-390 nm and 70 mW/cm² intensity, at 120°C for varying amounts of time (10 s, 60 s) b.) Same experimental conditions done on free standing films (10 s, 60 s, 600 s).....64

Figure 4.5: Demonstration of cycling back and forth between red and blue shifts. a.) Wavelength of the sample measured at the center minimum reflection notch of the curve done at each step and b.) the representative UV-vis curves for those values at each step.....65

Figure 4.6: a.) Photo patterned lines of varying distances indicated in the bottom left corner of each photo, shown at room temperature in the LC phase and at 120°C in the isotropic phase. Cross-Polarized POM images are inset in the corners. b.) Photo patterned chameleon skin, (top) shown in the LC phase (25°C) and (bottom) shown in the isotropic phase (120°C). Chameleon background image used from Teyssier *et al.* [5] c.) The CLCE is wrapped around plastic tubing to demonstrate strain mapping when the tube is pulled with the top region of the film appearing blue under strain while the sides undergo little to no strain and remain red.....66

Figure S4.1: DSC on the cholesteric doped resin. Working temperature to shear resin between glass is done at 60°C, between the two-phase transitions, chiral nematic phase at 40°C and T_{NI} at 70°C.....75

Figure S4.2: Analysis of CLCE mechanical properties a.) DMA T_g and storage modulus for the CLCE with a T_g around 6.5°C. b.) DMA Stress vs. Strain to break, showing how the CLCE has an altered strain profile due to the deformation of the chiral nematic phase.....75

Figure S4.3: Control UV-Vis as the material is strained to 100%. Transmission improves as the material is strained.....76

Figure S4.4: SEM on a cryo-microtomed unstrained and unprogrammed sample with imperfect lamellar orientation indicative of random alignment.....76

Figure S4.5: Control WAX for a.) unstrained material and b.) material strained to 60%. Weak localization of intensity at the top and bottom of the unstrained WAX diffraction pattern confirming some alignment induced by slightly shearing the sample before polymerization. Straining the sample reorients mesogens to display a nematic with a biased ordering pattern....76

Figure S4.6: AFT exchange mechanism. A radical from the photoinitiator or a thiyl radical can induce bond exchange.....77

Figure S4.7: Polarized optical microscopy of the CLCE initially unprogrammed and unstrained, and programmed samples in the LC phase and Isotropic phase as indicated for varying exposure times (20 s, 60 s, 120 s, 600 s).....77

Figure S4.8: Image analysis done on photopatterned films measured in the (left-blue) LC phase, and (right-red) isotropic phase a.) 3 mm line spacing b.) 1.5 mm line spacing c.) 1 mm line spacing. Measurements in ImageJ were taken across the profile of each film from left to right recording the change of intensity vs. distance measured. Blue shifted regions were recoded to have a lower intensity value and the unexposed red regions recorded a higher intensity value, graphically displayed.....78

Figure S4.9: Image analysis done using ImageJ on the CLCE wrapped around a plastic tube and strained. Yellow arrows portray direction of measurement for three measurements done. The three measurements were taken down the center of the film, recording the intensity values across the measured region. Normalized intensity increases as strain on the material decreases and the color of the material shifts from blue, highly strained region, to red, unstrained region.....79

Figure 5.1: a.) Monomers and surfactant for dispersion polymerization (1) PETMP, (2) PDT, (3) RM82, (4) PVP surfactant, and TEA catalyst b.) OM of System A particles c.) POM of System A particles at room temperature d.) POM of System A particles at 120°C showing change in birefringence.....84

Figure 5.2: For all particle Systems A, B, and C a.) OM (left) and POM (right) with all scale bars representing 100 nm b.) WAXS c.) DSC traces.....86

Figure 5.3: a.) Particle deformation and shape switching scheme. System A: One-way shape switching demonstration of LCEMPs top row OM and bottom row POM b.) Particles as polymerized initially at room temperature c.) Particles after manual compression at room

temperature displaying prolate deformation d.) Particles after being thermally cycled from room temperature past their T_{NI} to 120°C and back to room temperature, displaying recovery of shape.....88

Figure 5.4: a.) Particle programming and shape switching scheme. System C: Two-way shape switching demonstration of LCCEMPs top row OM and bottom row POM b.) Particle after being compressed and irradiated at room temperature c.) Particle in a temporary recovered shape above the T_{NI} at 120°C d.) Particle returned to room temperature demonstrating recovery to programmed shape.....89

Figure S5.1: Particle size distribution for system A, B, and C.....93

Figure 6.1: a.) Monomers and surfactant for the thiol-Michael dispersion polymerization (1) PETMP, (2) ADT the AFT moiety, (3) RM82, (4) PVP surfactant b.) AFT exchange mechanism. Crosslink density is maintained due to the exchange type mechanism where a radical adds into the exchangeable moiety before a sulfide bond is broken. c.) Thiol-Michael dispersion polymerization scheme with catalyst TEA added to start the reaction. AFT-LCCEMPs as polymerized d.) Optical microscopy e.) Polarized optical microscopy f.) g.) SEM.....100

Figure 6.2: a.) Schematic of programming particles and shape switching behavior of particles after programming. b.) Particles after programming displaying a prolate shape at room temperature (top) OM (bottom) POM c.) Particles at 120 °C recovering their temporary spherical shape and appearing almost fully isotropic in POM with birefringence almost completely gone. d.) Aspect ratio plot for particles undergoing temperature cycles and switching shape from prolate to spherical. Dashed line for ease of viewing. e.) Aspect ratio plot of particles undergoing three programming steps: **1st Stage** - Particles pictured after compression and irradiated with light, programmed to the prolate shape at Temp. Step 1. Particles cycle shape between Temp. Step 2 and 3. **2nd Stage** - Particles undergo a re-programming step, light exposure at high temperature, back to the spherical shape at Temp. Step 4. **3rd Stage** - Particles undergo a final programming step, particles pictured after compression and irradiated with light, programmed back to the prolate shape at Temp. Step 9. Particles cycle shape between Temp. Step 10 and 11. Dashed line for ease of viewing.....103

Figure 6.3: a.) SEM of particles after undergoing NIL, run with a flat superstrate under compression at 140 °C to program a permanent oblate shape b.) AFM of an oblate programmed particle displaying the flat particle aspect ratio of 15:3 length to height ratio.....110

Figure 6.4: a.) AFM of multiple particles imaged at 125 °C displaying the patterned surface topography incurred by NIL programming, compressed at 140 °C using a diffraction grating mold as the superstrate. b.) AFM of a particle surface imaged at 35 °C displaying pattern disruption c.) AFM of the same particle surface imaged at 125 °C displaying pattern recovery. Axes for b.) and c.) are in nm as indicated by b.).....128

Figure S6.1: Bar graph detailing particle size dispersity for the reported system.....117

Figure S6.2: Differential scanning calorimetry for the AFT-LCCEMPs.....117

Figure S6.3: Scanning electron microscopy (SEM) of particles after programming displaying a prolate shape.....118

Figure S6.4: Compressed AFT-LCEMPs under POM. Inset represents a microparticle and the LC alignment director within. a.) Particles aligned with polarizers displaying a skewed alignment along the particle long axis b.) Particles 45 degrees to polarizers displaying a disappearance of birefringence.....118

Figure S6.5: Stress-Strain profile for bulk LCE analog of the LCEMPs. Data taken until sample slipped or broke.....118

Figure S6.6: Particles after programming. a.) Programmed particles display a permanent prolate shape. b.) Particles recover temporarily to their initial shape when heated above their T_{NI}119

Figure S6.7: Control 1: light exposed - Particles were pre-irradiated with UV light for 30 s to ensure any excess acrylates and thiols were reacted. AFT-LCEMPs without photoinitiator (no pi) a.) Particles were compressed and exposed to light for 30 s. b.) Particles were heated past the T_{NI} and returned to room temperature displaying the recovered original spherical shape. Non-AFT capable LCEMPs swollen with photoinitiator (pi) c.) Particles were compressed and exposed to light for 30 s. b.) Particles were heated past the T_{NI} and returned to room temperature displaying the recovered original spherical shape.....119

Figure S6.8: Control 2: no photoinitiator, no light exposure - Particles were pre-irradiated with UV light for 30 s to ensure any excess acrylates and thiols were reacted. AFT-LCEMPs without photoinitiator a.) Particles were compressed at room temperature. b.) Particles were heated past the T_{NI} and returned to room temperature displaying the recovered original spherical shape. Non-AFT capable LCEMPs without photoinitiator c.) Particles were compressed at room temperature. d.) Particles were heated past the T_{NI} and returned to room temperature displaying the recovered original spherical shape.....120

Figure S6.9: Fourier Transform Infrared Spectroscopy for a.) Dried AFT-LCEMPs not containing photoinitiator b.) Zoomed in on the faint acrylate region at 800 to 830 cm^{-1}121

Figure S6.10: Particles undergoing reverse programming. a.) Programmed particles display a permanent prolate shape. b.) Particles recover temporarily to their initial shape when heated above their T_{NI} and are exposed to light again c.) Particles are cooled back to room temperature displaying their re-programmed permanent spherical shape. d.) Aspect ratio for particles during temperature steps demonstrating the initial prolate shape is re-programmed to a permanent sphere. Dotted line for ease of viewing.....121

Figure S6.11: Particles undergoing 1st through 3rd Stage programming. Particles were initially swollen with Irg-819 and DMPA a.) Programmed particles display a permanent prolate shape. b.) Particles recover temporarily to their initial spherical shape when heated above their T_{NI} and are exposed to light again at high temperature, followed by cooling to room temperature, maintaining a spherical shape c.) Particles are compressed and exposed to light again to re-program the prolate

shape. d.) Particles are heated above the T_{NI} and are cooled back to room temperature to recover the prolate shape and demonstrate shape switching. The shape can be toggled between prolate and spherical by thermally cycling past the T_{NI}122

Figure S6.12: Zoomed in AFM cross-section of a single particle surface after undergoing NIL programming with a diffraction grating mold utilizing spacers, imaged at 125 °C displaying pattern profile. Axes in microns.....122

Figure S6.13: SEM of particles after NIL programming at high temperature with a diffraction grating mold, without the use of spacers, yielding a complex surface topography.....123

Figure 7.1: a.) Monomers and reaction constituents for the thiol-Michael dispersion polymerization b.) Optical microscopy of thioester containing microparticles.....130

Figure 7.2: a.) Schematic of the particle deposition and coalescence process b.) Images from the actual particle casting and coalescence process over time. c.) Mechanism for the thiol-thioester exchange.....131

Figure 7.3: Optical microscopy of the particle coalescence process over time at varying concentrations of base, 5, 10, and 20 wt% loadings. Imaged immediately after swelling, 1 hour, 6 hours, and 24 hours after swelling displaying particle coalescence through the bulk of the film over time. A red arrow has been placed in the same position for each catalyst loading as a reference to monitor particle coalescence.....132

Figure 7.4: a.) Images of films undergoing particle coalescence over time b.) UV-vis for particle coalescence over time at 5, 10, and 20 wt% catalyst loadings reported at 600 nm. c.) Profilometry for the 20 wt% catalyst loading at time increments of 10, 20, 30 min, and 1 hour.....134

Figure 7.5: AFM modulus map for an interface between two particles (P1 and P2) at a.) 1 hour and b.) 3 days of compression. The modulus continues to evolve over time, with information still needed at later timepoints.....138

Figure 7.6: a.) Tensile tests for films prepared from monomer (blue + repeats), particles after 3 days (red, dashed + repeats), particles after 7 days (black, long dash + repeats).....139

Figure 7.7: SEM for particles welding to the secondary network. at a.) 1 hour showing a visible interface between the films, and b.) 2 week time points, with a nearly indiscernible interface between films. The film made from the secondary network is positioned in the top of each photo and the film made from particles is on the bottom. To the right is an image of the joined materials at the corresponding weld times.....140

Figure 7.8: Images of particles being welded to the secondary network in a complex geometry. The particles are initially cast, compressed with base added, and allowed to coalesce and weld over time, resulting in a free-standing polymer film.....141

Figure S7.1: Particle size distribution for the thioester containing microparticles.....148

Figure S7.2: DSC traces for microparticles and bulk film made from monomer.....	148
Figure S7.3: FTIR for thioester containing particles with 40% excess thiol.....	149
Figure S7.4: Images of particles coalescing into films for the designated catalyst loadings (5, 10, and 20 wt% PMDETA).....	149
Figure S7.5: Optical microscopy paired with camera images of control experiment, particles not swollen with base a.) Initial time point b.) After 24 hours. Camera images show particles clamped between glass (top) and open and un-clamped (bottom).....	150
Figure S7.6: Camera images (top) of particle coalescence over time at the designated catalyst loadings (5, 10, and 20 wt% PMDETA) and corresponding UV-vis spectra (bottom).....	150
Figure S7.7: UV-vis spectra for control experiment of thioester particles not swollen with base.....	151
Figure S7.8: Stress strain profiles for bulk films made from monomer at different PMDETA catalyst loadings, demonstrating control of stress relaxation rate. The control contains no base..	151
Figure S7.9: UV-vis for samples after thermal treatments. Thermal treatment after a.) 30 min. of coalescence treated at 70°C for 6 min. b.) 1 hour of coalescence treated at 100°C for 10 min. Image to the right displaying evaporation of base from the polymer film at the elevated processing conditions. Black curves are representative data for 1 hr. and 3 hr. spectra to demonstrate insignificant shift in UV-vis after heating.....	151
Figure S7.10: AFM topography scans at varying time points showing the evolution of the nm length scale features on the surface, evolving until 3 days.....	152
Figure S7.11: Images of particle coalescence over time and evolution of the “stained glass” appearance seen through the bulk of the film upon angling the film to light.....	152
Figure S7.12: UV-vis of films made from particles after 3 and 7 days of compression in comparison to a bulk film made from monomer.....	152
Figure S7.13: DSC trace for the secondary network.....	153
Figure A7.1: Table for particle stoichiometry and summary of properties. Stoichiometry read as PETMP to TEDA.....	156
Figure A7.2: Optical microscopy for particle formulations.....	158
Figure A7.3: a.) Example of dry thioester particles. b.) Thioester particles with a 1:1 stoichiometry after allowing to dry over two days resulting in coalescence of particles. c.) A piece of the coalesced polymer mass from b.) under the microscope.....	158

Figure A7.4: FTIR for particle formulations.....159
Figure A7.5: DSC for particle formulations.....159

List of Schemes

Scheme 1.1: Network formation of a (Left) of a chain-growth polymerization, where homopolymerization occurs and functional groups can react twice to form a network. (Right) step-growth polymerization, where A functional group can only react with B functional group.....	4
Scheme 1.2: Chain-growth acrylate homopolymerization.....	4
Scheme 1.3: Step-growth reaction pathways.....	5
Scheme 1.4: a.) Upon input of a stimulus, bonds can be broken and reformed, in a CAN, which can follow one of two pathways i.) Addition type (Dissociative), or ii.) Exchange type (Associative).....	8
Scheme 1.5: Illustration for liquid crystalline elastomer thermotropic phase transitions. LC mesogens (dark blue) are tethered to a polymer network (light blue).....	12
Scheme 1.6: Microparticle programming and shape switching.....	15
Scheme 1.7: Depiction of a dispersion polymerization to generate microparticles.....	16
Scheme 3.1: AFT-LCE Design Scheme. Monomers for the AFT-LCE (1) Liquid Crystal, RM82, (2) NPGDA (3) CANs moiety, ADT. Thiol-Michael oligomerization done in DCM followed by a light facilitated acrylate homopolymerization. Light facilitated AFT programming done to result in a thermoreversible shape switching material.....	33

Chapter 1: Introduction

1.1 – Overview

Autonomously shape changing materials are unceasingly captivating to not only the scientific community, but to non-scientists as well. The ability for a material to behave or react to a stimulus on its own has always been of great interest for a variety of applications, from soft robots,¹ optics,² and drug delivery.³ Designing a material that reversibly changes shape without requiring repeated programming steps reduces the work input done by the user. The ideal approach is to design a material that is reconfigurable and adaptable, allowing for the recycling and reusability of materials and thus a potential device or application.

For polymeric shape changing materials, it is important to understand the underlying structure of the polymer network when designing a material with shape changing capabilities. A variety of stimuli exist to actuate these materials which will be discussed in depth later. Also, there are different methods used to program these shape changing materials which include programming done before polymerization, during polymerization, or post-polymerization. Often, polymer materials are designed with one functionality in mind and are not necessarily recoverable or adaptable. This work aims to utilize dynamic covalent chemistry (DCC) to enable reconfigurations to the polymer network post-polymerization enabling re-processability.

Overall, the work reported here will focus on the polymerization and network reconfigurations undergone utilizing DCC. The scope of the work includes macroscopic networks to microscopic networks and reconfigurations. Discussed in chapter one, will be chemistries used to generate and manipulate the network for shape changing structures, followed by examples of shape switching materials utilizing a variety of these methods. A study of the underlying self-assembled structure will also be important to controlling shape programming and actuation.

Finally, microparticles and their applications will be discussed. The sections in this chapter will continue as such: 1.2 Polymer Structure and Polymerizations, 1.3 Covalent Adaptable Networks, 1.4 Shape Switching Materials, and 1.5 Microparticles. This chapter will create an understanding of the background for the work discussed throughout this thesis.

1.2 – Polymer Structure and Polymerizations

1.2.1 – Polymer Structure

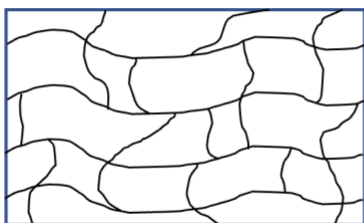
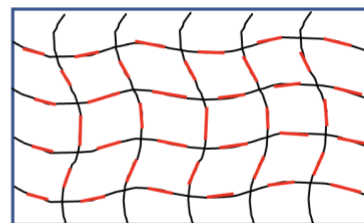
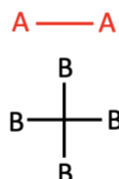
The underlying network structure of polymer materials is important for translating materials to appropriate applications. These structures fall under two main classifications, linear polymers commonly referred to as thermoplastics, or crosslinked polymers referred to as thermosets.⁴ Each of these polymer categories yield materials with varying mechanical properties for specific applications. Thermoplastics can be heated or solvated and be made to flow like a liquid. This makes them desirable for reprocessing, but they cannot be used for high temperature applications. In contrast, thermosets are durable and maintain network structure at high temperatures and are insoluble, but with that, they lack reprocess-ability. The glass transition temperature or T_g of polymer materials is an important characteristic, which determines the temperature with which the material is glassy and stiff or rubbery and pliable. Below the T_g , segmental motion of polymer chains is severely limited or prohibited and as the material is heated, these chains have the ability to move. The modulus will significantly change from the glassy to rubbery regime, from a few GPa's to MPa's. Thermoplastics will eventually degrade and behave as a liquid at high enough temperatures, with a drop in the storage modulus, but thermosets will maintain their network fidelity and the storage modulus will eventually plateau. The functionality and characteristics of monomers determines the T_g of these materials and if they are to be a

thermoplastic or thermoset. Highly functional monomers lead to highly crosslinked thermosets, whereas lower functionality monomers lead to more loosely crosslinked thermosets or even thermoplastics. Monomers with stiff cores can lead to higher T_g 's. For monomers with long aliphatic chains, depending on the combinations, this can lead to more rubbery materials or in contrast enable chain packing and crystallize. Controlling the crystallinity of a material can be achieved by modulating the monomers and network structure including crosslink density, along with polymerization rates and heating and cooling rates of the material. The work discussed here will focus on covalently crosslinked polymer networks, or thermosets.

To generate crosslinked thermosets, a variety of polymerization techniques are employed. Traditionally, chain-growth polymerizations generate high molecular weight polymers rapidly and often result in heterogeneous networks. Due to the ability for functional groups to react unregulated, molecular weight between crosslinks can vary greatly. In contrast, the step-growth polymerization results in a slower increase of the polymers overall molecular weight and more homogenous network formation.⁴ **Scheme 1.1** depicts simplified network formation for chain and step-growth polymerizations. The polymerizations utilized in this work include the the chain-growth radical initiated acrylate homopolymerization, and the thiol-Michael step-growth polymerization.

Chain-growth

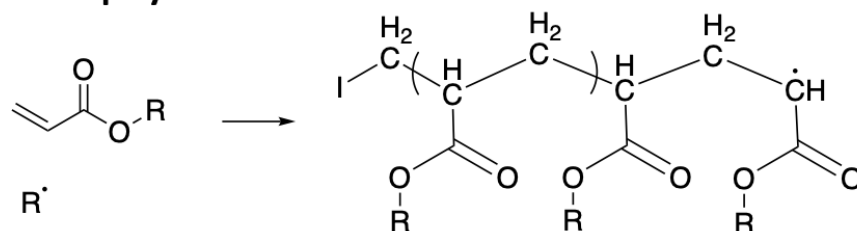
A — A
Ex: Functional groups can react twice

**Step-growth**

Scheme 1.1: Network formation of a (Left) of a chain-growth polymerization, where homopolymerization occurs and functional groups can react twice to form a network. (Right) step-growth polymerization, where A functional groups can only react with B functional groups.

1.2.2 – Chain-Growth Polymerization

A variety of chain-growth polymerizations exist, which include the acrylate and methacrylate homopolymerization. Radical based polymerizations are sensitive to oxygen inhibition due to radical scavenging.⁵ These can often yield highly crosslinked in contrast to their step growth counterparts, where polymerization is more readily controlled by functionality of monomers.⁶ **Scheme 1.2** depicts the mechanism for a chain-growth acrylate homopolymerization.

Acrylate Homopolymerization

Scheme 1.2: Chain-growth acrylate homopolymerization

Often, the crosslink density of chain-growth polymerizations is much greater than that of a step-growth mechanism. This is important to keep in mind when designing CANs to achieve optimal stress relaxation. The more dense the network, the less stress relaxation occurs. Rearrangement of crosslinks in a densely crosslinked network yields little change in the overall network structure in

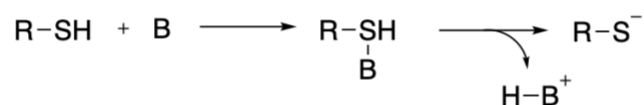
contrast to a relatively loosely crosslinked system, where the available free volume more significantly affects rearrangement of crosslinks and network relaxation.

1.2.3 – Step-Growth Polymerization

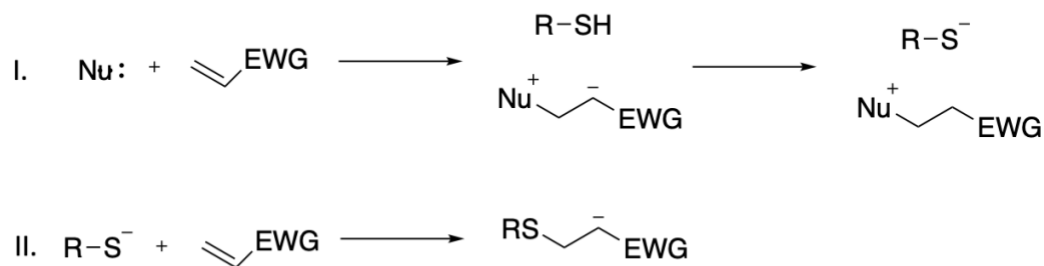
Some step-growth polymerizations include thiol-Michael, and thiol-ene click chemistry. There is also the radical-mediated thiol-acrylate polymerization where there is a competition between the chain-growth acrylate homopolymerization and the step-growth thiol-acrylate polymerization.^{7,8} The thiol-Michael polymerization proceeds by catalysis via a nucleophile or base, whereas thiol-ene proceeds radically, depicted in **Scheme 1.3**.^{9,10}

Thiol-Michael Reaction Pathways

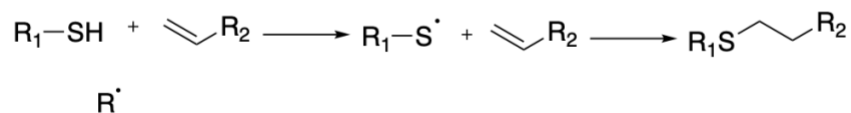
a.) Base Catalyzed



b.) Nucleophile Catalyzed



Thiol-ene Reaction Pathway



Scheme 1.3: Step-growth reaction pathways.

The radical initiated thiol-ene or thiol-acrylate polymerization is less sensitive to oxygen inhibition than the (meth)acrylate homopolymerization and the reaction proceeds more efficiently, with

insignificant change to the polymerization rate, due to the chain transfer step provided by the thiols present.⁷ The -ene functional monomers in the ideal thiol-ene do not readily homopolymerize making for a more homogenous polymerization overall. Also, oxygen sensitivity can become an issue for dilute thiol-ene reaction. The thiol-Michael polymerization becomes attractive, due to its lack of sensitivity to ambient environments.

1.2.4 – Polymer Characterization

To characterize these networks a variety of analyses are routinely done. Dynamic mechanical analysis or DMA, subjects rectangular shaped polymer samples to stress or strain controlled mechanical tests, often in tension. The force applied can be an oscillating or static mode. This determines the materials T_g , loss (E''), and storage (E') moduli, young's modulus, or strain to break. The T_g of a material is measured via an oscillatory loading of the sample at a chosen frequency along with a ramp in temperature. The T_g is measured as the tan delta or the tangent to the phase angle between the loss and the storage modulus seen in **equation 1.1**.

$$\tan \delta = \frac{E''}{E'} \quad (1.1)$$

This represents the ratio of a materials viscous to elastic response.⁴ The T_g is a measure in the change of the molecular mobility of polymer chains. A variety of attachments can enable measurement of viscosity or samples in compression. There are also a variety of attachments that can be used in the DMA such as compression to measure low viscosity materials including thermoplastics at higher temperature or materials that flow.

Differential scanning calorimetry (DSC) is another method of polymer characterization which subjects a sample to a controlled temperature ramp. This is used to determine the materials T_g , which is a first order process. DSC can also determine second order processes such as

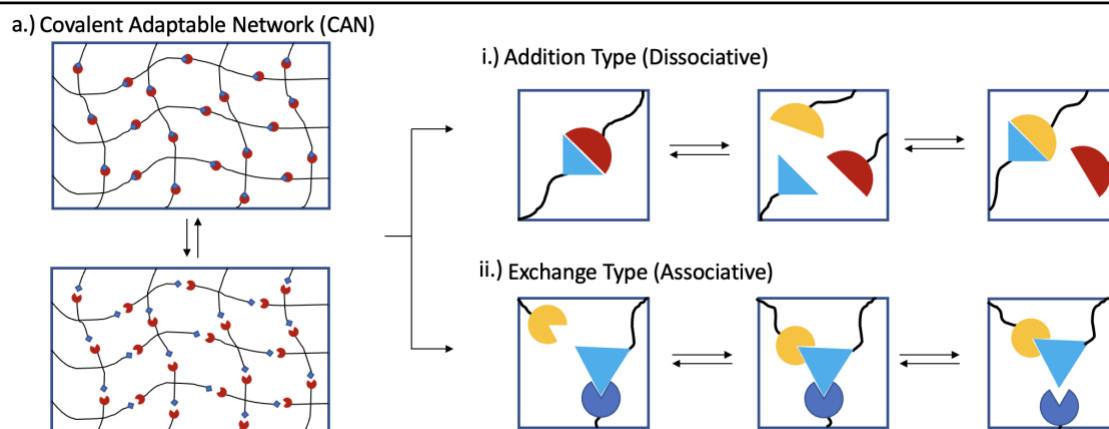
crystalline melting transitions or T_m and crystal formation or T_c . Heterogenous networks will have broader T_g 's while homogenous networks will have sharper T_g 's.⁴

It is important to measure these material properties when designing polymers to determine if they are appropriate for the desired application. Glass transition and crystallinity are a basis for understanding the behavior and capabilities of the polymer network.

1.3 – Covalent Adaptable Networks (CANs)

1.3.1 – Mechanisms of CANs

Covalent adaptable networks or CANs, transiently modify a crosslinked thermoset network to behave like a fluid thermoplastic, upon application of a stimulus, depicted in **Scheme 1.4a**.^{11,12,13} The stimulus effectively allows for the breaking and reforming of the networks covalent bonds, or total degradation of a network if desired. Often, CANs are used to modify the shape of materials or recycle starting materials. These mechanisms have been utilized in polymerizations as well, but this work will focus on networks and post-polymerization modifications of those networks.¹⁴ CAN mechanisms fall into two overarching categories, addition type mechanisms (dissociative) and, exchange type mechanisms (associative) (**Scheme 1.4, i, ii**). A variety of stimuli include thermal,^{15,16} light,¹⁷ or chemoresponsive.¹⁸ These dynamic covalent chemistries (DCC) enable post polymerization processing of polymer materials. Ultimately, these bond exchange mechanisms work to relieve stress in a polymer network. A stress is input to the network and upon activation of the bond exchange, the network will move towards a thermodynamic equilibrium to relieve that stress to a relatively stress-free state, depending on the time scale of the reaction and longevity of the applied stimulus.



Scheme 1.4: a.) Upon input of a stimulus, bonds can be broken and reformed, in a CAN, which can follow one of two pathways i.) Addition type (Dissociative), or ii.) Exchange type (Associative).

We will proceed with using the terminology as the addition type mechanism. In the addition mechanism, a covalent bond is broken before it can be reformed, resulting in a change to the crosslinking density and results in temporary depolymerization of the polymer network (**Figure 1.4,i**). Some addition type CANs include urethane dissociation¹⁹ and the Diels-Alder reaction.²⁰ Both reactions require elevated temperatures to facilitate bond rearrangement. Another important type of bond exchange reaction includes vitrimers, where upon elevation to a certain temperature, bond exchange can occur, but below the activation temperature, or upon vitrification, there is no longer mobility for the exchange to occur.²¹

For the exchange type mechanism, a species must add into the covalent bond before the bond is broken, maintaining the fidelity of the crosslinked network (**Figure 1.4,ii**). Some examples of the Exchange Type include transesterification,¹⁶ boronic ester exchange,²² addition-fragmentation chain-transfer (AFT)²³ and thiol-thioester exchange.²⁴ AFT and thiol-thioester exchange are the two mechanisms that will be utilized as DCC in the work reported here.

1.3.2 – Addition-Fragmentation Chain-Transfer

As mentioned above, a variety of stimuli exist to activate bond exchange in CANs. There is much interest in light facilitated bond exchange reactions for the spatial and temporal control it affords. Bond exchange can occur in a network through a photothermal or photochemical stimulus. It is more desirable to eliminate heating as a stimulus because it can often confound crystal phase behavior or network characteristics that need to be controlled. Radical mediated reactions follow thermal, or light activated pathways. A few examples of materials that are triggered via radical activation include trithiocarbonates,¹⁷ disulfides,²⁵ and allyl sulfides.²³ Utilizing allyl sulfide functionality in polymer networks allows for a variety of enhanced applications including stress relaxation to minimize shrinkage stress,²⁶ shape programming,^{23,27,28} mechanopatterning,²⁹ and self-healing materials.³⁰ For the AFT reaction, radical initiation is required for a radical to add into the double bond of the allyl sulfide functionality embedded in the network backbone. This then generates a cascading bond exchange reaction where sulfide bonds are broken to form thiyl radicals, which then reform as covalent bonds. This mechanism is shut off once radicals have been terminated upon depletion of initiator or removal of the stimulus. As mentioned above, this process can be light activated, allowing for spatiotemporal control. These radical mediated processes don't necessarily require the presence of a photoinitiator, but bond exchange is significantly slower and less efficient without it.

Although photo activation has advantages, some disadvantages can include light attenuation, or some added heating effects depending on light intensities used. These materials can be limited in thickness due to light attenuation. The radical mediated reaction is also reliant on the availability of initiator, which can potentially be reswollen into the network.

1.3.3 – Thiol-Thioester Exchange

The thiol-thioester exchange was initially studied in peptide ligation³¹ or prebiotic chemistries.²⁴ Some newer applications include their implementation into polymer networks as CANs with rapid relaxation time constants dependent on environmental conditions and network stoichiometry.^{32,33,34} Fluid-like flow was achieved upon activation of the bond exchange in a study performed by Worrell et al.³² Hydrogels are another example of networks the thiol-thioester mechanism has been incorporated into to create tunable viscoelastic properties for cell differentiation.³⁵

For the thiol-thioester exchange, the presence of thiolate anions is necessary, which is induced upon addition of a base as a catalyst. Formation of thiolate anions occur, which then add into the carbonyl before breaking a sulfur bond.²⁴ The bond exchange propagates until removal of the stimulus and there is no longer formation of thiolate anions. Elevated temperature will also enhance this exchange mechanism. Worrell et al. did a comprehensive investigation of the thiol-thioester exchange to be used in linear or crosslinked polymer networks.³⁶

CANs have enabled reprocessing and recyclability of polymer materials that has not been achieved before.

1.4 – Shape Switching Materials

Shape switching materials come in a variety of network structures and actuation modes. In many cases, materials switch shape once, but require subsequent deformation events to return them to their starting deformed shape. With more complex chemistry and design, autonomous and reversibly shape switching materials can be achieved, which are known as two-way shape switching.

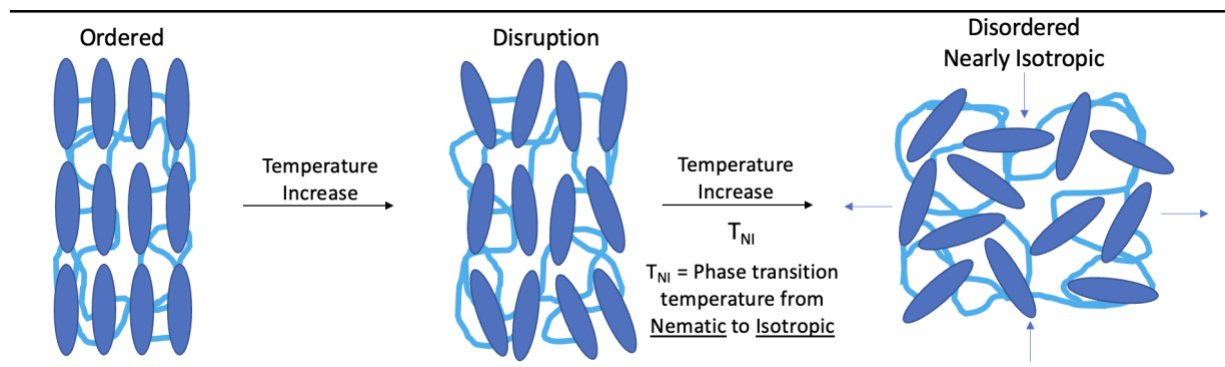
1.4.1 – Shape Switching Polymers

Thermoplastics are often used as one-way shape switching materials.³⁷ Temporary shapes can be fixed when the material is heated above the T_g to a state where chains can be made extensible without degradation, and then fixed by cooling in that temporary position. Upon heating above the glass transition the material shape can be actuated if it is heated below the degradation or melting temperature of the polymer.^{38,39} Thermosets can also act as shape switching materials, although without complex chemistries, both these systems are limited to single modes of actuation and cannot recover their initial deformed shape without subsequent deformation events.⁴⁰ Semicrystalline polymers are another class of shape switching materials. The mechanism with which this works is a material's shape is fixed above crystalline melting transitions and cooled in place, allowing re-crystallization to maintain the shape. Upon heating the material through these melting transitions, the shape can be actuated, which allows for actuation of multiple modes if there are multiple T_m 's.^{25,41,42,43,44} Some demonstrations of swelling and deswelling to actuate have been reported for hydrogels.⁴⁵ Alternately, employing DCC allows for programmable and autonomously shape switching materials, which was discussed at length in the previous section.⁴⁶ These materials can be programmed to a new permanent shape that demonstrate two or more way shape switching.

1.4.2 – Liquid Crystal Elastomers

Another means to achieve stimuli responsive materials is by coupling liquid crystals (LCs) with a crosslinked polymer network, which can enable autonomous and reversible shape switching without subsequent deformation events. This enables two-way or multiple shape switching capabilities. The anisotropy afforded by LC mesogens tethered to a polymer network results in macroscopic actuation when this anisotropic order is disrupted by a stimulus to transition from an

ordered nematic state to a disrupted isotropic state, depicted in **Scheme 1.5**.⁴⁷ A variety of stimuli exist to disrupt the LC phase including thermal,⁴⁷ light,⁴⁸ and electrical.⁴⁹



Scheme 1.5: Illustration for liquid crystalline elastomer thermotropic phase transitions. LC mesogens (dark blue) are tethered to a polymer network (light blue).

For thermotropic LCs, the temperature at which the material goes from the ordered nematic phase to the disordered isotropic phase is known as the T_{NI} . Liquid crystal elastomers (LCEs), amongst other shape memory materials are often limited by the programming technique to set a new geometry. LC alignment is necessary for reversible shape switching. Typically, a two-stage polymerization method permanently sets the alignment and geometry, where an initial loose crosslinking is done, the material is strained to align the LCs, and a secondary polymerization preserves the alignment.^{50,51} Another means of generating shape switching structures is to pre-align the LCs and polymerize the network around them.⁵² DCC has more recently been utilized to program alignment by altering the polymer structure post-polymerization around the LCs. Static covalent bonds are made dynamic and rearrange the network upon application of a stimulus, afforded by a CAN.^{11,53} After the network undergoes a straining event and activation of the DCC, the network will relax the stress imparted on the network towards a thermodynamic equilibrium. A variety of DCCs have been coupled with LCE materials to program switchable shapes, including transesterification,⁵⁴ transcarbamylation,⁵⁵ and disulfide exchange.⁵⁶ Many of these DCCs require

a thermal stimulus to activate bond exchange, but the work in this thesis relies on light mediated bond exchange of the AFT reaction mechanism to decouple the thermal LC phase transitions from the network programming. Furthermore, the AFT reaction maintains network crosslink density and material fidelity during radical mediated bond rearrangement due to its exchange type nature.⁵³

These shape switching LCEs are attractive for their autonomous behavior, but it has been a challenge to translate these behaviors to meaningful work outputs. In glassy LC networks (LCNs), a work output of 3.6 kJ/m³ has been reported.⁵² Another LCE was capable of lifting a 10 g weight upon heating through its phase transition.⁴⁹ A summary of LCE work outputs can be found in Liu et al.'s review on the subject.⁵⁷ The underlying network architecture is important for achieving a variety of strain changes in LCEs. The LC content relative to the polymer network is also important to achieve these strain changes. A variety of configurations exist to attach the LC mesogen to the network including a side-on, end-on, and main-chain coupling. Main-chain configurations have been shown to demonstrate the most dramatic shape changes. These actuation modes are also dependent on the efficiency of the stimuli.

1.4.2 – Color Switching

An important aspect of structural change is the capacity to modulate color. The color of a material is based on two potential mechanisms. The first being absorptive properties of the material and the second being dictated by structure. Through the absorption pathway, molecules absorb light of certain wavelengths, and thus the overall color of the material is manifested as a reflection of the non-absorbing wavelengths.⁵⁸ An example of this are dyes, which absorb wavelengths of light, resulting in visible colors to the human eye. Spiropyrans are commonly used as color indicators in polymeric materials.⁵⁹ In contrast, through the structural pathway, the color of a

material is dictated by the length scale of the structural repeating pattern of the material and its ability to interact with light. Some examples of this are butterfly wings or in some cases paints, which rely on micro or nanostructures to dictate color (**Figure 1.1**).⁶⁰

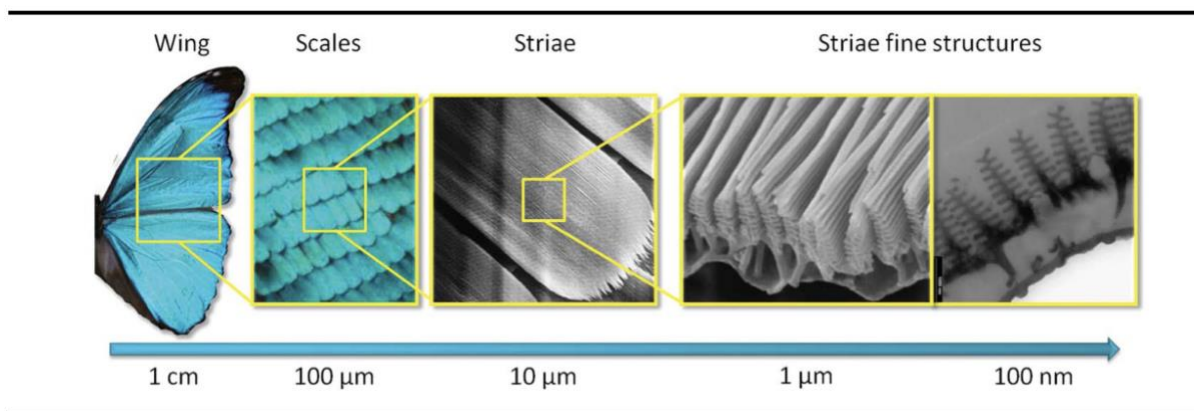


Figure 1.1: Examples of structurally colored materials. Image used from references.^{61,62}

The properties of structural color are desirable due to their robust and versatile nature. Structural colors do not photo bleach like absorptive colors can. There is also significant ability to modulate structural color by changing length scales, or repeating structure geometries. A variety of structurally color changing materials has been developed from coatings based on microstructures and colloids,^{2,60} to stretchable elastomers.^{63,64}

Cholesteric liquid crystals (CLCs) are a class of structurally colored materials with significant interest for optical applications. These materials often have high selectivity of wavelength reflected due to the homogeneity of the liquid crystalline mixture.^{65,66} Often these materials are liquids encased in glass cells. There is also a class of crosslinked CLCs known as CLC elastomers (CLCEs).^{67,68} Selectivity of the cholesteric alignment can be lost upon significant increases in crosslink density unless processed very precisely. With higher crosslink densities, these materials can be free-standing films, as opposed to their loosely crosslinked or non-crosslinked counterparts confined to glass cells. Upon doping an LC system with chiral liquid crystal mesogens, a handedness is induced in the alignment creating a helicoidal repeating

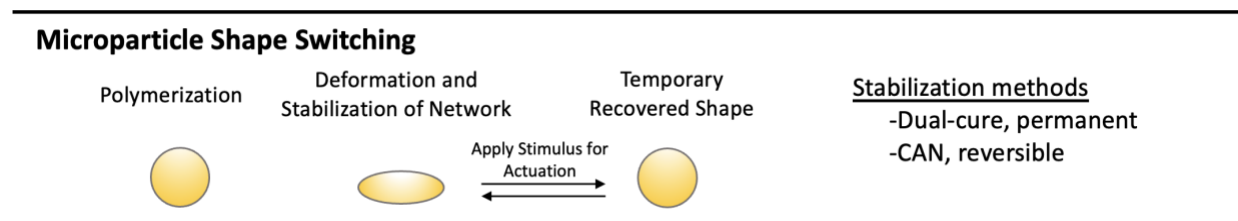
superstructure, or photonic crystal, that results in a Bragg reflection. The length scale of this repeating structure can be modulated a variety of ways to result in visible red and blue shifting of the wavelength reflected. Some methods include changes to dopant concentration,⁶⁹ electrical,⁷⁰ thermal,⁷¹ or mechanical stimuli.^{64,72}

A recurring theme in this thesis work is the design of reconfigurable materials. Many of these color changing materials are not programmable, but this work utilizes CANs to create tunable and controllable color switchable materials, or erasure of the reflective nature.

1.5 – Microparticles

1.5.1 – Shape Switching Microparticles

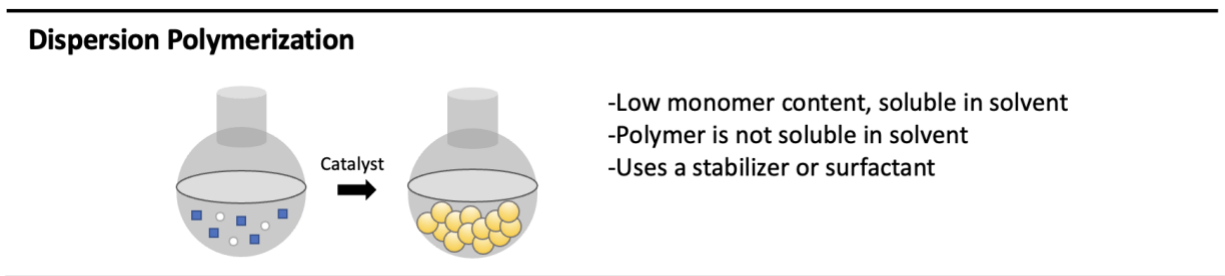
Significant focus is reserved for macroscopic shape changing materials, but microscopic materials have an exhaustive list of applications including drug delivery,³ cosmetics,⁷³ rheological,⁷⁴ and optical control.² Shape switching microparticles are achieved through a variety of polymerizations including emulsions,⁷⁵ dispersions,⁷⁶ or microfluidic setups.⁷⁷ Shape changing microparticles are achieved via anisotropy of their networks or mechanical properties.^{78,79,80} Often, microparticles are synthesized and either deformed pre- or post- polymerization, followed by a stabilization of the network (**Scheme 1.6**). This programming is permanent unless a CAN is employed to allow network reversibility post-polymerization.



Scheme 1.6: Microparticle programming and shape switching.

To actuate the microparticles a stimulus is then applied, akin to the macroscopic shape switching materials discussed in *Section 1.4*. Another class of shape switching microparticles utilizes the LC phase transitions to shift from ordered LC alignment to disorder, resulting in an overall shape change.⁷⁷ Significant work done by Wang et al. on clickable microparticles has paved the way for the research on CAN-microparticles in this thesis.^{81,82} The particles reported by Wang are not shape switching, but the research in this thesis expands upon the polymerization techniques used to generate them. An instance of CAN microparticles designed with an amorphous polymer network allow for reconfigurability into a new permanent shape, but do not switch shape.⁸³

The various polymerization methods to generate particles result in a variety of particle sizes and dispersities. This work focuses on the dispersion polymerization (**Scheme 1.7**), which provides a facile means to scale-up the yield of microparticles. The dispersion polymerization utilizes low concentration of monomer in a solvent, where the monomer is initially soluble. As the polymerization is catalyzed and proceeds forward, the polymer formed precipitates out of solution.⁸⁴ A surfactant is used in this process to stabilize microparticle formation. Variables to control microparticle size include, monomer solubility, monomer concentration, catalyst concentration, and surfactant concentration.



Scheme 1.7: Depiction of a dispersion polymerization to generate microparticles.

LC microparticles utilizing precipitation and dispersion polymerization methods have been reported, albeit without CANs functionality.^{85,86} Current shape switching microparticle systems

are programmed directly during polymerization or have singular programming, remaining permanent and cannot be recycled and reprogrammed. This work fills the gap between CANs microparticles and shape switching microparticles, to achieve reconfigurable shape switching microparticles.

1.5.2 – Microparticles to Generate Tunable Surfaces and Films

Microparticles are also of interest for their potential use in 3D printing applications. Designing CAN microparticles could enable selective deposition of particles and processing of materials to generate parts with spatially controlled mechanical properties. Direct write 3D printing techniques could be envisioned as a processing method for these materials.⁸⁷ Latexes are known for their coalescence process but yield degradable films.⁸⁸ Functionalizing microparticles with DCC enables interparticle bond exchange to result in covalently robust polymers, or potentially degradable as well, with some investigation done prior by Wang.⁸⁹ Sowan et al. demonstrated functionalization of Si nanoparticles to generate interfacial stress relaxation in composites.⁹⁰

Investigating CANs designed as a micro-network will yield valuable new accessible uses for microparticles. Microparticles that are reconfigurable post-polymerization increase the adaptability of the particles for the multiple purposes listed above and not just as a single use design.

1.6 – Summary

Here, the investigation of molecular self-assembly coupled with reversibly altering and programming the polymer network through the incorporation of DCC, expands new avenues and accessible applications for achieving macro and microscopic shape switching materials. A variety

of polymer networks with varying underlying alignment or lack-there-of is studied in this work. The work presented in this thesis investigates the design of tunable and re-writable materials. This is delineated in the following chapter and discussed as separate aims.

1.7 – References

- (1) Xie, M.; Hisano, K.; Zhu, M.; Toyoshi, T.; Pan, M.; Okada, S.; Tsutsumi, O.; Kawamura, S.; Bowen, C. Flexible Multifunctional Sensors for Wearable and Robotic Applications. *Advanced Materials Technologies* **2019**, *4* (3), 1800626. <https://doi.org/10.1002/admt.201800626>.
- (2) Belmonte, A.; Bus, T.; Broer, D. J.; Schenning, A. P. H. J. Patterned Full-Color Reflective Coatings Based on Photonic Cholesteric Liquid-Crystalline Particles. *ACS Applied Materials & Interfaces* **2019**, *11* (15), 14376–14382. <https://doi.org/10.1021/acsami.9b02680>.
- (3) Birnbaum, D. T.; Brannon-Peppas, L. Microparticle Drug Delivery Systems. In *Drug Delivery Systems in Cancer Therapy*; Brown, D. M., Ed.; Humana Press: Totowa, NJ, 2004; pp 117–135. https://doi.org/10.1007/978-1-59259-427-6_6.
- (4) Robert J. Young; Lovell, P. A. *Introduction to Polymers*, Third.; CRC Press, 2011.
- (5) Lee, T. Y.; Guymon, C. A.; Jönsson, E. S.; Hoyle, C. E. The Effect of Monomer Structure on Oxygen Inhibition of (Meth)Acrylates Photopolymerization. *Polymer* **2004**, *45* (18), 6155–6162. <https://doi.org/10.1016/j.polymer.2004.06.060>.
- (6) Paul C. Hiemenz; Lodge, T. P. *Polymer Chemistry*, 2nd ed.; Taylor and Francis Group, 2007.
- (7) Cramer, N. B.; Bowman, C. N. Kinetics of Thiol-Ene and Thiol-Acrylate Photopolymerizations with Real-Time Fourier Transform Infrared. *J. Polym. Sci. A Polym. Chem.* **2001**, *39* (19), 3311–3319. <https://doi.org/10.1002/pola.1314>.
- (8) O'Brien, A. K.; Cramer, N. B.; Bowman, C. N. Oxygen Inhibition in Thiol–Acrylate Photopolymerizations. *J. Polym. Sci. A Polym. Chem.* **2006**, *44* (6), 2007–2014. <https://doi.org/10.1002/pola.21304>.
- (9) Nair, D. P.; Podgórski, M.; Chatani, S.; Gong, T.; Xi, W.; Fenoli, C. R.; Bowman, C. N. The Thiol-Michael Addition Click Reaction: A Powerful and Widely Used Tool in Materials Chemistry. *Chemistry of Materials* **2014**, *26* (1), 724–744. <https://doi.org/10.1021/cm402180t>.
- (10) Hoyle, C. E.; Bowman, C. N. Thiol-Ene Click Chemistry. *Angewandte Chemie International Edition* **2010**, *49* (9), 1540–1573. <https://doi.org/10.1002/anie.200903924>.
- (11) McBride, M. K.; Worrell, B. T.; Brown, T.; Cox, L. M.; Sowan, N.; Wang, C.; Podgorski, M.; Martinez, A. M.; Bowman, C. N. Enabling Applications of Covalent Adaptable Networks. *Annual Review of Chemical and Biomolecular Engineering* **2019**, *10* (1), 175–198. <https://doi.org/10.1146/annurev-chembioeng-060718-030217>.
- (12) Podgórski, M.; Fairbanks, B. D.; Kirkpatrick, B. E.; McBride, M.; Martinez, A.; Dobson, A.; Bongiardina, N. J.; Bowman, C. N. Toward Stimuli-Responsive Dynamic Thermosets through Continuous Development and Improvements in Covalent Adaptable Networks (CANs). *Adv. Mater.* **2020**, *32* (20), 1906876. <https://doi.org/10.1002/adma.201906876>.

- (13) Kloxin, C. J.; Scott, T. F.; Adzima, B. J.; Bowman, C. N. Covalent Adaptable Networks (CANs): A Unique Paradigm in Cross-Linked Polymers. *Macromolecules* **2010**, *43* (6), 2643–2653. <https://doi.org/10.1021/ma902596s>.
- (14) Moad, G.; Rizzardo, E.; Thang, S. H. RAFT Polymerization and Some of Its Applications. *Chem. Asian J.* **2013**, *8* (8), 1634–1644. <https://doi.org/10.1002/asia.201300262>.
- (15) Fortman, D. J.; Brutman, J. P.; Cramer, C. J.; Hillmyer, M. A.; Dichtel, W. R. Mechanically Activated, Catalyst-Free Polyhydroxyurethane Vitrimers. *J. Am. Chem. Soc.* **2015**, *137* (44), 14019–14022. <https://doi.org/10.1021/jacs.5b08084>.
- (16) Otera, J. Transesterification. *American Chemical Society* **1993**, No. 93, 22.
- (17) Amamoto, Y.; Kamada, J.; Otsuka, H.; Takahara, A.; Matyjaszewski, K. Repeatable Photoinduced Self-Healing of Covalently Cross-Linked Polymers through Reshuffling of Trithiocarbonate Units. *Angew. Chem.* **2011**, *123* (7), 1698–1701. <https://doi.org/10.1002/ange.201003888>.
- (18) Christensen, P. R.; Scheuermann, A. M.; Loeffler, K. E.; Helms, B. A. Closed-Loop Recycling of Plastics Enabled by Dynamic Covalent Diketoenamine Bonds. *Nat. Chem.* **2019**, *11* (5), 442–448. <https://doi.org/10.1038/s41557-019-0249-2>.
- (19) Brutman, J. P.; Fortman, D. J.; De Hoe, G. X.; Dichtel, W. R.; Hillmyer, M. A. Mechanistic Study of Stress Relaxation in Urethane-Containing Polymer Networks. *J. Phys. Chem. B* **2019**, *123* (6), 1432–1441. <https://doi.org/10.1021/acs.jpcc.8b11489>.
- (20) Chen, X.; Dam, M. A.; Ono, K.; Mal, A.; Shen, H.; Nutt, S. R.; Sheran, K.; Wudl, F. A Thermally Re-Mendable Cross-Linked Polymeric Material. *Science, New Series* **2002**, *295* (5560), 1698–1702.
- (21) Denissen, W.; Winne, J. M.; Du Prez, F. E. Vitrimers: Permanent Organic Networks with Glass-like Fluidity. *Chem. Sci.* **2016**, *7* (1), 30–38. <https://doi.org/10.1039/C5SC02223A>.
- (22) Cash, J. J.; Kubo, T.; Bapat, A. P.; Sumerlin, B. S. Room-Temperature Self-Healing Polymers Based on Dynamic-Covalent Boronic Esters. *Macromolecules* **2015**, *48* (7), 2098–2106. <https://doi.org/10.1021/acs.macromol.5b00210>.
- (23) Kloxin, C. J.; Scott, T. F.; Bowman, C. N. Stress Relaxation via Addition–Fragmentation Chain Transfer in a Thiol-Ene Photopolymerization. *Macromolecules* **2009**, *42* (7), 2551–2556. <https://doi.org/10.1021/ma802771b>.
- (24) Bracher, P. J.; Snyder, P. W.; Bohall, B. R.; Whitesides, G. M. The Relative Rates of Thiol–Thioester Exchange and Hydrolysis for Alkyl and Aryl Thioalkanoates in Water. *Orig Life Evol Biosph* **2011**, *41* (5), 399–412. <https://doi.org/10.1007/s11084-011-9243-4>.
- (25) Michal, B. T.; Jaye, C. A.; Spencer, E. J.; Rowan, S. J. Inherently Photohealable and Thermal Shape-Memory Polydisulfide Networks. *ACS Macro Lett.* **2013**, *2* (8), 694–699. <https://doi.org/10.1021/mz400318m>.
- (26) Leung, D.; Bowman, C. N. Reducing Shrinkage Stress of Dimethacrylate Networks by Reversible Addition-Fragmentation Chain Transfer. *Macromol. Chem. Phys.* **2012**, *213* (2), 198–204. <https://doi.org/10.1002/macp.201100402>.
- (27) Photoinduced Plasticity in Cross-Linked Polymers | Science <https://science.sciencemag.org/content/308/5728/1615.long> (accessed 2019 -05 -03).
- (28) Ryu, J.; D’Amato, M.; Cui, X.; Long, K. N.; Jerry Qi, H.; Dunn, M. L. Photo-Origami—Bending and Folding Polymers with Light. *Appl. Phys. Lett.* **2012**, *100* (16), 161908. <https://doi.org/10.1063/1.3700719>.

- (29) Kloxin, C. J.; Scott, T. F.; Park, H. Y.; Bowman, C. N. Mechanophotopatterning on a Photoresponsive Elastomer. *Adv. Mater.* **2011**, *23* (17), 1977–1981. <https://doi.org/10.1002/adma.201100323>.
- (30) Cheng, C.; Bai, X.; Zhang, X.; Li, H.; Huang, Q.; Tu, Y. Self-Healing Polymers Based on a Photo-Active Reversible Addition-Fragmentation Chain Transfer (RAFT) Agent. *J Polym Res* **2015**, *22* (4), 46. <https://doi.org/10.1007/s10965-015-0691-9>.
- (31) Cargoët, M.; Diemer, V.; Snella, B.; Desmet, R.; Blanpain, A.; Drobecq, H.; Agouridas, V.; Melnyk, O. Catalysis of Thiol–Thioester Exchange by Water-Soluble Alkyldiselenols Applied to the Synthesis of Peptide Thioesters and SEA-Mediated Ligation. *J. Org. Chem.* **2018**, *83* (20), 12584–12594. <https://doi.org/10.1021/acs.joc.8b01903>.
- (32) Worrell, B. T.; McBride, M. K.; Lyon, G. B.; Cox, L. M.; Wang, C.; Mavila, S.; Lim, C.-H.; Coley, H. M.; Musgrave, C. B.; Ding, Y.; Bowman, C. N. Bistable and Photoswitchable States of Matter. *Nat Commun* **2018**, *9* (1), 2804. <https://doi.org/10.1038/s41467-018-05300-7>.
- (33) Wang, C.; Mavila, S.; Worrell, B. T.; Xi, W.; Goldman, T. M.; Bowman, C. N. Productive Exchange of Thiols and Thioesters to Form Dynamic Polythioester-Based Polymers. *ACS Macro Lett.* **2018**, *7* (11), 1312–1316. <https://doi.org/10.1021/acsmacrolett.8b00611>.
- (34) Podgórski, M.; Worrell, B. T.; Sinha, J.; McBride, M. K.; Bowman, C. N. Thermal Metamorphosis in (Meth)Acrylate Photopolymers: Stress Relaxation, Reshaping, and Second-Stage Reaction. *Macromolecules* **2019**, *52* (21), 8114–8123. <https://doi.org/10.1021/acs.macromol.9b01678>.
- (35) Brown, T. E.; Carberry, B. J.; Worrell, B. T.; Dudaryeva, O. Y.; McBride, M. K.; Bowman, C. N.; Anseth, K. S. Photopolymerized Dynamic Hydrogels with Tunable Viscoelastic Properties through Thioester Exchange. *Biomaterials* **2018**, *178*, 496–503. <https://doi.org/10.1016/j.biomaterials.2018.03.060>.
- (36) Worrell, B. T.; Mavila, S.; Wang, C.; Kontour, T. M.; Lim, C.-H.; McBride, M. K.; Musgrave, C. B.; Shoemaker, R.; Bowman, C. N. A User’s Guide to the Thiol-Thioester Exchange in Organic Media: Scope, Limitations, and Applications in Material Science. *Polym. Chem.* **2018**, *9* (36), 4523–4534. <https://doi.org/10.1039/C8PY01031E>.
- (37) Hubbard, A. M.; Mailen, R. W.; Zikry, M. A.; Dickey, M. D.; Genzer, J. Controllable Curvature from Planar Polymer Sheets in Response to Light. *Soft Matter* **2017**, *13* (12), 2299–2308. <https://doi.org/10.1039/C7SM00088J>.
- (38) Imran Khan M., Zagho M.M., Shakoor R.A. *Smart Polymer Nanocomposites. A Brief Overview of Shape Memory Effect in Thermoplastic Polymers.*; Springer, Cham, 2017.
- (39) Liu, Y.; Shaw, B.; Dickey, M. D.; Genzer, J. Sequential Self-Folding of Polymer Sheets. *Sci. Adv.* **2017**, *3* (3), e1602417. <https://doi.org/10.1126/sciadv.1602417>.
- (40) McBride, M. K.; Podgorski, M.; Chatani, S.; Worrell, B. T.; Bowman, C. N. Thermoreversible Folding as a Route to the Unique Shape-Memory Character in Ductile Polymer Networks. *ACS Appl. Mater. Interfaces* **2018**, *7*.
- (41) Chung, T.; Romo-Uribe, A.; Mather, P. T. Two-Way Reversible Shape Memory in a Semicrystalline Network. *Macromolecules* **2008**, *41* (1), 184–192. <https://doi.org/10.1021/ma071517z>.
- (42) Li, M.; Guan, Q.; Dingemans, T. J. High-Temperature Shape Memory Behavior of Semicrystalline Polyamide Thermosets. *ACS Appl. Mater. Interfaces* **2018**, *10*.

- (43) Meng, Y.; Yang, J.-C.; Lewis, C. L.; Jiang, J.; Anthamatten, M. Photoinscription of Chain Anisotropy into Polymer Networks. *Macromolecules* **2016**, *49* (23), 9100–9107. <https://doi.org/10.1021/acs.macromol.6b01990>.
- (44) Jin, B.; Song, H.; Jiang, R.; Song, J.; Zhao, Q.; Xie, T. Programming a Crystalline Shape Memory Polymer Network with Thermo- and Photo-Reversible Bonds toward a Single-Component Soft Robot. *Sci. Adv.* **2018**, *4* (1), eaao3865. <https://doi.org/10.1126/sciadv.aao3865>.
- (45) An, N.; Li, M.; Zhou, J. Predicting Origami-Inspired Programmable Self-Folding of Hydrogel Trilayers. *Smart Mater. Struct.* **2016**, *25* (11), 11LT02. <https://doi.org/10.1088/0964-1726/25/11/11LT02>.
- (46) Zheng, N.; Fang, Z.; Zou, W.; Zhao, Q.; Xie, T. Thermoset Shape-Memory Polyurethane with Intrinsic Plasticity Enabled by Transcarbamoylation. *Angew. Chem. Int. Ed.* **2016**, *55* (38), 11421–11425. <https://doi.org/10.1002/anie.201602847>.
- (47) White, T. J.; Broer, D. J. Programmable and Adaptive Mechanics with Liquid Crystal Polymer Networks and Elastomers. *Nature Materials* **2015**, *14* (11), 1087–1098. <https://doi.org/10.1038/nmat4433>.
- (48) Ube, T.; Kawasaki, K.; Ikeda, T. Photomobile Liquid-Crystalline Elastomers with Rearrangeable Networks. *Adv. Mater.* **2016**, *28* (37), 8212–8217. <https://doi.org/10.1002/adma.201602745>.
- (49) Ohm, C.; Brehmer, M.; Zentel, R. Liquid Crystalline Elastomers as Actuators and Sensors. *Adv. Mater.* **2010**, *22* (31), 3366–3387. <https://doi.org/10.1002/adma.200904059>.
- (50) K pfer, J.; Finkelmann, H. Nematic Liquid Single Crystal Elastomers. *Makromol. Chem., Rapid Commun.* **1991**, *12* (12), 717–726. <https://doi.org/10.1002/marc.1991.030121211>.
- (51) Yakacki, C. M.; Saed, M.; Nair, D. P.; Gong, T.; Reed, S. M.; Bowman, C. N. Tailorable and Programmable Liquid-Crystalline Elastomers Using a Two-Stage Thiol–Acrylate Reaction. *RSC Advances* **2015**, *5* (25), 18997–19001. <https://doi.org/10.1039/C5RA01039J>.
- (52) Ware, T. H.; McConney, M. E.; Wie, J. J.; Tondiglia, V. P.; White, T. J. Voxellated Liquid Crystal Elastomers. *Science* **2015**, *347* (6225), 982–984. <https://doi.org/10.1126/science.1261019>.
- (53) Kloxin, C. J.; Scott, T. F.; Adzima, B. J.; Bowman, C. N. Covalent Adaptable Networks (CANs): A Unique Paradigm in Cross-Linked Polymers. *Macromolecules* **2010**, *43* (6), 2643–2653. <https://doi.org/10.1021/ma902596s>.
- (54) Pei, Z.; Yang, Y.; Chen, Q.; Terentjev, E. M.; Wei, Y.; Ji, Y. Mouldable Liquid-Crystalline Elastomer Actuators with Exchangeable Covalent Bonds. *Nature Mater* **2014**, *13* (1), 36–41. <https://doi.org/10.1038/nmat3812>.
- (55) Wen, Z.; McBride, M. K.; Zhang, X.; Han, X.; Martinez, A. M.; Shao, R.; Zhu, C.; Visvanathan, R.; Clark, N. A.; Wang, Y.; Yang, K.; Bowman, C. N. Reconfigurable LC Elastomers: Using a Thermally Programmable Monodomain To Access Two-Way Free-Standing Multiple Shape Memory Polymers. *Macromolecules* **2018**, *51* (15), 5812–5819. <https://doi.org/10.1021/acs.macromol.8b01315>.
- (56) Wang, Z.; Tian, H.; He, Q.; Cai, S. Reprogrammable, Reprocessible, and Self-Healable Liquid Crystal Elastomer with Exchangeable Disulfide Bonds. *ACS Appl. Mater. Interfaces* **2017**, *9* (38), 33119–33128. <https://doi.org/10.1021/acsami.7b09246>.
- (57) Sun, D.; Zhang, J.; Li, H.; Shi, Z.; Meng, Q.; Liu, S.; Chen, J.; Liu, X. Toward Application of Liquid Crystalline Elastomer for Smart Robotics: State of the Art and Challenges. *Polymers* **2021**, *13* (11), 1889. <https://doi.org/10.3390/polym13111889>.

- (58) Bamfield, P.; Hutchings, M. *Chromic Phenomena - Technological Applications of Colour Chemistry*, 3rd ed.; Royal Society of Chemistry, 2018.
- (59) Zhang, H.; Chen, Y.; Lin, Y.; Fang, X.; Xu, Y.; Ruan, Y.; Weng, W. Spiropyran as a Mechanochromic Probe in Dual Cross-Linked Elastomers. *Macromolecules* **2014**, *47* (19), 6783–6790. <https://doi.org/10.1021/ma500760p>.
- (60) Datta, B. C.; Ortiz, C. Methods for Design and Fabrication of Bio-Inspired Nanostructures Exhibiting Structural Coloration. In *Advanced Fabrication Technologies for Micro/Nano Optics and Photonics XIII*; von Freymann, G., Blasco, E., Chanda, D., Eds.; SPIE: San Francisco, United States, 2020; p 33. <https://doi.org/10.1117/12.2544398>.
- (61) Nicole, L.; Laberty-Robert, C.; Rozes, L.; Sanchez, C. Hybrid Materials Science: A Promised Land for the Integrative Design of Multifunctional Materials. *Nanoscale* **2014**, *6* (12), 6267–6292. <https://doi.org/10.1039/C4NR01788A>.
- (62) Berthier, S. *Photonique Des Morphos*; Springer-Verlag: Paris, 2010.
- (63) Zhao, Q.; Finlayson, C. E.; Snoswell, D. R. E.; Haines, A.; Schäfer, C.; Spahn, P.; Hellmann, G. P.; Petukhov, A. V.; Herrmann, L.; Burdet, P.; Midgley, P. A.; Butler, S.; Mackley, M.; Guo, Q.; Baumberg, J. J. Large-Scale Ordering of Nanoparticles Using Viscoelastic Shear Processing. *Nat Commun* **2016**, *7* (1), 11661. <https://doi.org/10.1038/ncomms11661>.
- (64) Finkelmann, H.; Kim, S. T.; Muñoz, A.; Palffy-Muhoray, P.; Taheri, B. Tunable Mirrorless Lasing in Cholesteric Liquid Crystalline Elastomers. *Advanced Materials* **2001**, *13* (14), 1069–1072. [https://doi.org/10.1002/1521-4095\(200107\)13:14<1069::AID-ADMA1069>3.0.CO;2-6](https://doi.org/10.1002/1521-4095(200107)13:14<1069::AID-ADMA1069>3.0.CO;2-6).
- (65) Mulder, D. J.; Schenning, A. P. H. J.; Bastiaansen, C. W. M. Chiral-Nematic Liquid Crystals as One Dimensional Photonic Materials in Optical Sensors. *J. Mater. Chem. C* **2014**, *2* (33), 6695–6705. <https://doi.org/10.1039/C4TC00785A>.
- (66) Natarajan, L. V.; Wofford, J. M.; Tondiglia, V. P.; Sutherland, R. L.; Koerner, H.; Vaia, R. A.; Bunning, T. J. Electro-Thermal Tuning in a Negative Dielectric Cholesteric Liquid Crystal Material. *Journal of Applied Physics* **2008**, *103* (9), 093107. <https://doi.org/10.1063/1.2913326>.
- (67) Kizhakidathazhath, R.; Geng, Y.; Jampani, V. S. R.; Charni, C.; Sharma, A.; Lagerwall, J. P. F. Facile Anisotropic Deswelling Method for Realizing Large-Area Cholesteric Liquid Crystal Elastomers with Uniform Structural Color and Broad-Range Mechanochromic Response. *Advanced Functional Materials* **2020**, *30* (7), 1909537. <https://doi.org/10.1002/adfm.201909537>.
- (68) Varanytsia, A.; Nagai, H.; Urayama, K.; Palffy-Muhoray, P. Tunable Lasing in Cholesteric Liquid Crystal Elastomers with Accurate Measurements of Strain. *Scientific Reports* **2015**, *5* (1). <https://doi.org/10.1038/srep17739>.
- (69) Kim, D.-Y.; Lee, K. M.; White, T. J.; Jeong, K.-U. Cholesteric Liquid Crystal Paints: In Situ Photopolymerization of Helicoidally Stacked Multilayer Nanostructures for Flexible Broadband Mirrors. *NPG Asia Materials* **2018**, *10* (11), 1061–1068. <https://doi.org/10.1038/s41427-018-0096-4>.
- (70) White, T. J.; Bricker, R. L.; Natarajan, L. V.; Tondiglia, V. P.; Green, L.; Li, Q.; Bunning, T. J. Electrically Switchable, Photoaddressable Cholesteric Liquid Crystal Reflectors. *Optics Express* **2010**, *18* (1), 173. <https://doi.org/10.1364/OE.18.000173>.
- (71) Brannum, M. T.; Steele, A. M.; Venetos, M. C.; Korley, L. T. J.; Wnek, G. E.; White, T. J. Light Control with Liquid Crystalline Elastomers. *Advanced Optical Materials* **2019**, *7* (6), 1801683. <https://doi.org/10.1002/adom.201801683>.

- (72) Moirangthem, M.; Schenning, A. P. H. J. Full Color Camouflage in a Printable Photonic Blue-Colored Polymer. *ACS Applied Materials & Interfaces* **2018**, *10* (4), 4168–4172. <https://doi.org/10.1021/acsami.7b17892>.
- (73) Patravale, V. B.; Mandawgade, S. D. Novel Cosmetic Delivery Systems: An Application Update: Novel Cosmetic Delivery Systems. *International Journal of Cosmetic Science* **2008**, *30* (1), 19–33. <https://doi.org/10.1111/j.1468-2494.2008.00416.x>.
- (74) Mueller, S.; Llewellyn, E. W.; Mader, H. M. The Rheology of Suspensions of Solid Particles. *Proceedings of the Royal Society A: Mathematical, Physical and Engineering Sciences* **2010**, *466* (2116), 1201–1228. <https://doi.org/10.1098/rspa.2009.0445>.
- (75) Landfester, K. Miniemulsion Polymerization and the Structure of Polymer and Hybrid Nanoparticles. *Angewandte Chemie International Edition* **2009**, *48* (25), 4488–4507. <https://doi.org/10.1002/anie.200900723>.
- (76) Ho, C. C.; Keller, A.; Odell, J. A.; Ottewill, R. H. Preparation of Monodisperse Ellipsoidal Polystyrene Particles. *Colloid & Polymer Science* **1993**, *271* (5), 469–479. <https://doi.org/10.1007/BF00657391>.
- (77) Hessberger, T.; Braun, L.; Zentel, R. Microfluidic Synthesis of Actuating Microparticles from a Thiol-Ene Based Main-Chain Liquid Crystalline Elastomer. *Polymers* **2016**, *8* (12), 410. <https://doi.org/10.3390/polym8120410>.
- (78) Bhaskar, S.; Pollock, K. M.; Yoshida, M.; Lahann, J. Towards Designer Microparticles: Simultaneous Control of Anisotropy, Shape, and Size. *Small* **2010**, *6* (3), 404–411. <https://doi.org/10.1002/sml.200901306>.
- (79) Wischke, C.; Schossig, M.; Lendlein, A. Shape-Memory Effect of Micro-/Nanoparticles from Thermoplastic Multiblock Copolymers. *Small* **2014**, *10* (1), 83–87. <https://doi.org/10.1002/sml.201202213>.
- (80) Klinger, D.; Wang, C. X.; Connal, L. A.; Audus, D. J.; Jang, S. G.; Kraemer, S.; Killops, K. L.; Fredrickson, G. H.; Kramer, E. J.; Hawker, C. J. A Facile Synthesis of Dynamic, Shape-Changing Polymer Particles. *Angewandte Chemie International Edition* **2014**, *53* (27), 7018–7022. <https://doi.org/10.1002/anie.201400183>.
- (81) Wang, C.; Podgórski, M.; Bowman, C. N. Monodisperse Functional Microspheres from Step-Growth “Click” Polymerizations: Preparation, Functionalization and Implementation. *Mater. Horiz.* **2014**, *1* (5), 535–539. <https://doi.org/10.1039/C4MH00082J>.
- (82) Wang, C.; Zhang, X.; Podgórski, M.; Xi, W.; Shah, P.; Stansbury, J.; Bowman, C. N. Monodispersity/Narrow Polydispersity Cross-Linked Microparticles Prepared by Step-Growth Thiol–Michael Addition Dispersion Polymerizations. *Macromolecules* **2015**, *48* (23), 8461–8470. <https://doi.org/10.1021/acs.macromol.5b02146>.
- (83) Cox, L. M.; Sun, X.; Wang, C.; Sowan, N.; Killgore, J. P.; Long, R.; Wu, H.-A.; Bowman, C. N.; Ding, Y. Light-Stimulated Permanent Shape Reconfiguration in Cross-Linked Polymer Microparticles. *ACS Applied Materials & Interfaces* **2017**, *9* (16), 14422–14428. <https://doi.org/10.1021/acsami.7b02759>.
- (84) Kawaguchi, S.; Ito, K. Dispersion Polymerization. In *Polymer Particles*; Okubo, M., Ed.; Advances in Polymer Science; Springer Berlin Heidelberg: Berlin, Heidelberg, 2005; Vol. 175, pp 299–328. <https://doi.org/10.1007/b100118>.
- (85) Liu, X.; Xu, Y.; Heuts, J. P. A.; Debije, M. G.; Schenning, A. P. H. J. Monodisperse Liquid Crystal Network Particles Synthesized via Precipitation Polymerization. *Macromolecules* **2019**, *52* (21), 8339–8345. <https://doi.org/10.1021/acs.macromol.9b01852>.

- (86) Liu, X.; Pan, X. Programmable Liquid Crystal Elastomer Microactuators Prepared via Thiol-Ene Dispersion Polymerization. *Soft Matter* **2020**, *13* (45), 8368–8378. <https://doi.org/10.1039/C7SM01619K>.
- (87) Neumann, T. V.; Dickey, M. D. Liquid Metal Direct Write and 3D Printing: A Review. *Adv. Mater. Technol.* **2020**, *5* (9), 2000070. <https://doi.org/10.1002/admt.202000070>.
- (88) Chevalier, Y.; Pichot, C.; Graillat, C.; Joanicot, M.; Wong, K.; Maquet, J.; Lindner, P.; Cabane, B. Film Formation with Latex Particles. *Colloid Polym Sci* **1992**, *270* (8), 806–821. <https://doi.org/10.1007/BF00776153>.
- (89) Wang, C. Step-Growth Nano/Micro Polymer Networks. **2018**, 212.
- (90) Sowan, N.; Cox, L. M.; Shah, P. K.; Song, H. B.; Stansbury, J. W.; Bowman, C. N. Dynamic Covalent Chemistry at Interfaces: Development of Tougher, Healable Composites through Stress Relaxation at the Resin–Silica Nanoparticles Interface. *Adv. Mater. Interfaces* **2018**, *5* (18), 1800511. <https://doi.org/10.1002/admi.201800511>.

Chapter 2: Objectives

This thesis hypothesizes that by utilizing covalent adaptable networks and understanding fundamental molecular level self-assembly, re-writable and tunable dynamic materials are readily achieved. This investigation enabled generation of autonomously shape and color changing materials. This investigation will be implemented by achieving the following aims:

- *Aim 1: Investigating molecular level self-assembly to program and re-write tunable materials*
- *Aim 2: Designing reconfigurable color in materials linked to shape and underlying molecular alignment*
- *Aim 3: Translating CANs to micro-networks to enhance applications*

Aim 1: Investigating molecular level self-assembly to program and re-write tunable materials

This aim, initially begun in collaboration with Dr. McBride, investigates the incorporation of DCC into an LCE to relieve stress imparted on the polymer network through straining events, upon activation via light to ultimately achieve re-writable materials capable of actuation. The specific CAN used here implements addition-fragmentation chain-transfer (AFT) as the dynamic covalent chemistry. The AFT-LCE is programmed post-polymerization, which is ideal for versatility, and merely requires strain of the shape into its desired final shape, followed by irradiation with light. The light activated mechanism decouples bond exchange from the thermally stimulated LC phase transitions, required for actuation of the material. Heating the material above its LC phase transition or T_{NI} temporarily recovers the initial shape, resulting in an autonomously shape switching material. Irradiating the material with light above the phase transition temperature,

erases any programming done prior, and returns the AFT-LCE to its original starting shape, demonstrating re-writability.

Furthermore, to create an additional means of control, the material is embedded with a UV-absorbing compound to attenuate light enabling programming by controlling light penetration depth, creating a gradient of liquid crystal alignment, resulting in tunable actuation.

Aim 2: Designing reconfigurable color in materials linked to shape and underlying molecular alignment

This aim expands upon the first, incorporating a cholesteric dopant into the liquid crystal elastomer network. The incorporation of the cholesteric molecule induced a “cholesteric phase” in the LC alignment. This alignment results in a photonic structure which reflects light within the visible wavelength regime. Upon mechanically straining the material, the LC alignment is deformed and results in a blue shift in color, from a very visible red, through the spectrum to blue. Due to the latent DCC incorporated into the network from the previous aim’s material design, this cholesteric LCE (CLCE) is also programmed to maintain a variety of colors and patterns that are a result of strain and light irradiation. This programming is thermoreversible, temporarily restoring shape and color upon thermal cycling. Furthermore, these colors are permanently erased by irradiating the material above the T_{NI} , yielding a transparent, non-reflective and non-colored, polymer film.

Aim 3: Translating CANs to micro-networks to enhance applications

Aim 3.1 – Designing LCEMPs for one-way and two-way shape switching

Aim 3.2 – Designing AFT capable LCEMPs for rewritable and programmable two-way shape switching

Aim 3.3 – Designing CAN microparticles to create spatially controllable properties for applications in 3D printed materials

Aim 3.1 – Designing LCEMPs for one-way and two-way shape switching

Expanding on the previous aims demonstrating macroscopic shape control, liquid crystal elastomer microparticles (LCEMPs) were synthesized via a thiol-Michael dispersion. The basic mechanism for achieving shape switching geometries understood in *Aim 1* was applied to microscopic structures. It is important to first design and understand basic shape switching capabilities in LCEMPs before introducing DCC into the system. LCEMPs were designed without DCC. When the particles were compressed, the applied stress drove alignment to a temporary prolate shape. Upon heating past the T_{NI} , shape recovery back to spheres was achieved, demonstrating one-way shape switching. Building on this understanding, another set of LCEMPs were designed to contain an excess of acrylates in the network, capable of undergoing a 2nd stage reaction to permanently set a new shape employing the dual cure polymerization method. After compression, the particles pre-doped with photoinitiator underwent light exposure to crosslink the remaining acrylates and preserve the compressed shape. Cyclic heating and cooling autonomously switches the shape between spherical and prolate, respectively, demonstrating two-way shape switching. The two-way shape switching particles are not reprogrammable or recyclable.

Aim 3.2 – Designing AFT capable LCEMPs for rewritable and programmable two-way shape switching

AFT-capable LCEMPs were synthesized in the same manner as in *Aim 3.1*. Incorporating DCC into the network allows for access of rewritability of shapes, which enhances the capacity for application in drug delivery to rheological control, and optics. The microparticles containing the AFT exchangeable moiety were doped with photoinitiator and underwent deformation events at varying temperatures followed by light exposure to program these geometries with some geometries capable of autonomous shape switching upon thermal cycling. These AFT-LCEMPs were also capable of reconfiguration by irradiating the programmed particles above the T_{NI} , to erase any programming done prior. The AFT-LCEMPs are capable of reconfiguration and recycling.

Aim 3.3 – Designing CAN microparticles to create spatially controllable properties for applications in 3D printed materials

Amorphous CAN microparticles were also investigated to enable selective patterning of material properties with potential to enhance 3D printing applications. Thioester containing microparticles were designed with excess thiol, and upon addition of a base catalyst and clamping between glass slides, activating the thiol-thioester bond exchange between particles resulted in cohesive polymer films. This technology is similar to the latex coalescence process, albeit with the difference that the resulting polymer film is a covalently crosslinked network, capable of self-healing or further reconfiguration. Ideally, microparticles of varying mechanical properties could be selectively deposited and processed to result in a cohesive part with controllably spaced material properties.

Summary

This work systematically integrates CANs into polymer soft actuating materials. Chapter 3 discusses the design of a liquid crystalline CAN, to achieve programmable shapes capable of shape switching upon thermal cycling. This technology also enables erasure of programmed shapes, demonstrating reversibility. In Chapter 4, this technology is translated to a material that enables programming of color that is inherently linked to the underlying molecular assembly and macroscopic shape of the material. Chapters 5 and 6 discuss programmable non-CAN and CAN-LCEMPs, demonstrating the ability to translate these dynamic chemistries to the micro-scale. Chapter 7 examines CAN-microparticles containing a thioester network, to create polymer films from microparticles, with applications in additive manufacturing. Finally, Chapter 8 summarizes and draws conclusions about the work. This thesis spans a range of permanent and reversible programming from the macroscale to the micron scale that has not been achieved previously. The advances in this work are intended to expand CANs technology to achieve controllably adaptable soft materials post polymerization.

Chapter 3: Investigating molecular level self-assembly to program and re-write tunable materials

(Manuscript published - McBride, M. K.; Martinez, A. M.; Cox, L.; Alim, M.; Childress, K.; Beiswinger, M.; Podgorski, M.; Worrell, B. T.; Killgore, J.; Bowman, C. N. A Readily Programmable, Fully Reversible Shape-Switching Material. *Science Advances* **2018**, 4 (8), eaat4634. <https://doi.org/10.1126/sciadv.aat4634>.

Work here describes contributions made to this publication.)

A liquid crystal elastomer (LCE) containing a covalent adaptable network (CAN) allows for shape programmability post-polymerization, while the LC component allows for autonomous shape switching upon application of a thermal, phase changing stimulus. By utilizing dynamic covalent chemistry (DCC) afforded by the CAN, this approach enables bond rearrangement towards a thermodynamic equilibrium to set a new shape, simply by straining the elastomer and applying the activation stimulus for bond exchange. The DCC utilized herein is light initiated addition-fragmentation chain-transfer (AFT), which decouples the programming stimulus from the actuation stimulus. The thermal stimulus alters the LC phase behavior resulting in a macroscopic shape change. Furthermore, a UV-light absorbing compound is utilized to control the light penetration depth of the programming stimulus to set new geometries. These materials demonstrate re-writability affording the opportunity to program new shapes and erase these shapes thereafter, if desired.

3.1 – Introduction

Polymer based shape switching materials are highly examined due to their autonomous ability to change shape. Controlling shape enables an increased level of control over applications including optics,¹ wettability,² soft robotics,³ and drug delivery.⁴ These shape switching mechanisms are often activated via phase transitions, crystalline melting, glass transitions, or other

noncovalent intermolecular disruptions.^{5,6} Actuation can also result from chemical transitions such as pH changes or swelling and deswelling methods.^{7,8}

Liquid crystal elastomers (LCEs) are an attractive means to achieve shape switching polymeric materials. The disruption of liquid crystalline (LC) alignment while tethered to a polymer network generates a macroscopic shape change upon application of a stimulus. For thermotropic LCs, the temperature with which this transition occurs is known as the T_{NI} , or the transition from nematic and ordered to isotropic and disordered. Examples of shape switching LCEs include work done by Finkelmann and others, utilizing a dual cure polymerization technique to set the LC alignment.^{9,10} The LCE is initially loosely crosslinked and upon straining the material, the LCs are aligned, and a second polymerization stabilizes the alignment and shape. Thermal cycling induces the disruption of LC alignment and results in shape switching, but there is no reconfigurability thereafter. Other examples of shape switching LCEs utilize pre-alignment of LC mesogens prior to crosslinking.^{11,12} This method also results in a shape switching material, although it is not reconfigurable after the crosslinking step.

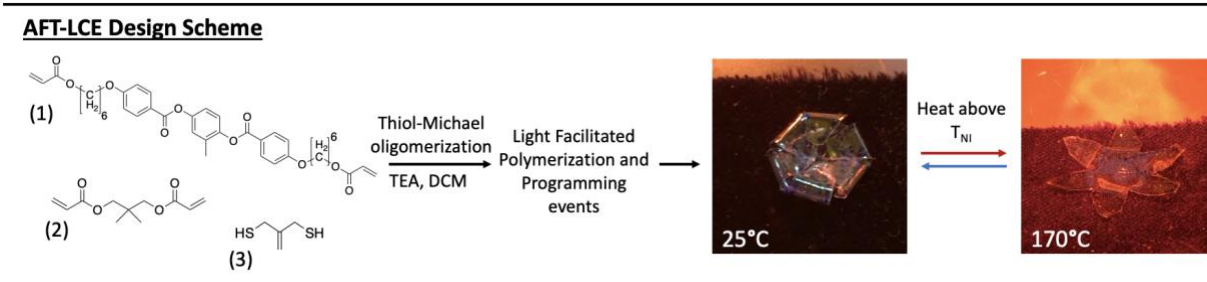
Another means of designing shape switching LCEs, is to incorporate dynamic covalent chemistry (DCC). DCC has garnered interest to enable reprogramming of materials. These chemistries designed as covalent adaptable networks (CANs) allow for a thermoset to transiently behave like a thermoplastic, by breaking and reforming covalent bonds upon application of a stimulus. There is an expansive library of CANs activated by a variety of stimuli including thermal,^{13,14} light,¹⁵ or chemoresponsive.¹⁶ By incorporating DCC into a network, it can be made programmable post-polymerization. A variety of thermally stimulated CAN-LCEs have been designed, but a thermally active CAN can limit the programming and shape switching process as the LCE phase behavior is also temperature dependent.^{17,18,19}

This work utilizes light facilitated DCC to decouple the thermally activated phase behavior of the LCs from the programming stimulus. Light activation also enables spatiotemporal control of programming. The DCC utilized is addition-fragmentation chain-transfer (AFT), which is a radical mediated reaction. Upon generation of a radical, this radical adds into the allyl sulfide functionality of the polymer backbone forming a thiyl radical, and a cascading bond exchange reaction occurs until the stimulus is removed, or initiator is depleted. Here, the programming and erasure of LC alignment is investigated to result in controllable complex shape switching structures demonstrating re-writability.

3.2 – Results and Discussion

Reported here is a light triggered LCE-based CAN. This combination affords at least two things: 1) Utilizing LCs enables shape switching and 2) Utilizing a CAN enables programmability post polymerization and reconfigurability or erasure of that programming. To implement DCC in an LCE network, first a base catalyzed thiol-Michael reaction was done with monomers to create a set of oligomers that are easily stored and utilized as desired. **Scheme 3.1** succinctly visualizes the process from synthesis to material programming. The monomers include the reactive liquid crystalline diacrylate RM82, the chain extender neopentyl glycol diacrylate (NPGDA), and the exchangeable monomer allyl dithiol (ADT), reacted in a 1:0.5:1.35 molar stoichiometry, as seen in **Scheme 3.1**. The specific CAN used here is mediated by the AFT reaction, achieved by embedding the ADT monomer into the backbone of the network. The oligomers were designed such that an acrylate excess allows for light activated acrylate homopolymerization, to generate crosslinked AFT-capable LCE films, upon pre-doping the resin mixture with a photoinitiator. To generate 3D deployable shapes, the AFT-LCE was programmed post-polymerization, which is

ideal for versatility, and merely requires strain of the shape into its desired final shape, followed by irradiation with light. The light activated mechanism decouples bond exchange from the thermally stimulated LC phase transitions, required for actuation of the material. Investigation by McBride et al. included how strain, temperature, and exposure time affect programming, and this work expands on how underlying alignment controls shape and actuation.²⁰



Scheme 3.1: AFT-LCE Design Scheme. Monomers for the AFT-LCE (1) Liquid Crystal, RM82, (2) NPGDA (3) CANs moiety, ADT. Thiol-Michael oligomerization done in DCM followed by a light facilitated acrylate homopolymerization. Light facilitated AFT programming done to result in a thermoreversible shape switching material.

Dynamic Mechanical Analysis (DMA) was used to determine the phase behavior of the LCE along with the glass transition (T_g) of 1°C (**Figure S3.1**), implying that a rubbery and easily deformable material exists at room temperature. Modulating the LC content by increasing the amount of NPGDA resulted in a shift and reduction of the LC phase transition. The programming scheme for the LCE is shown in **Figure 3.1a**, where an initially polymerized and polydomain LCE was strained to induce alignment along the direction of strain. With latent photoinitiator available after the initial polymerization, exposing the film to UV light activates the AFT exchange to relax the stress imparted by the straining event, towards a thermodynamic equilibrium, stabilizing this alignment and shape (**Figure 3.1b**). Upon heating above the T_{NI} , expansion perpendicular to the alignment director and contraction parallel to the director results in a macroscopic shape change

of the polymer film. Alignment following light-induced programming was confirmed by polarized optical microscopy (POM) (Figure 3.1c).

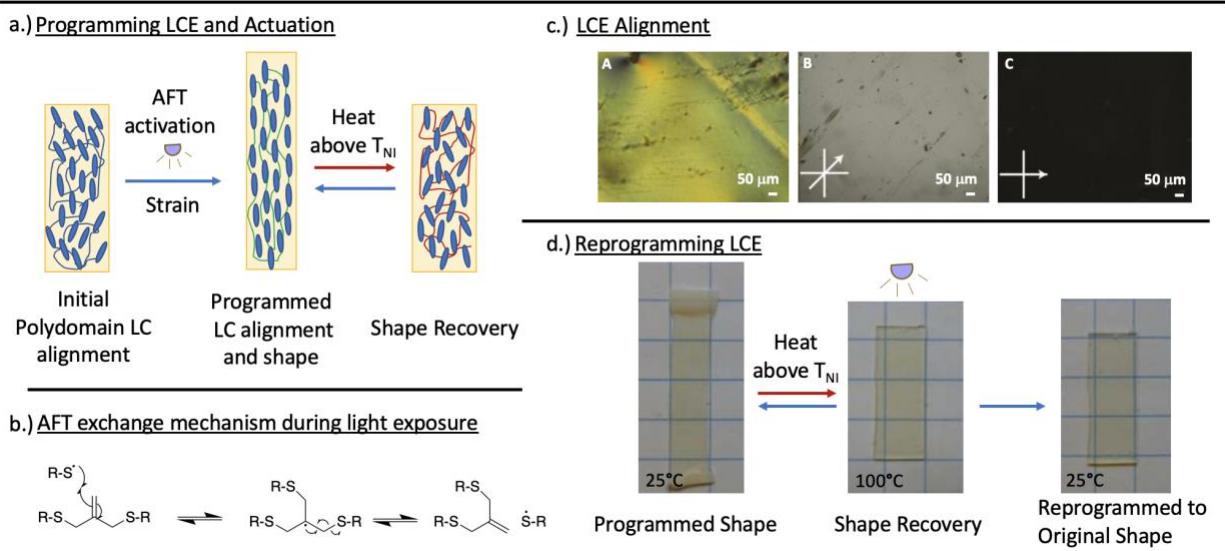


Figure 3.1: a.) Programming the LCE occurs by straining the material and irradiating with light. Heating the film returns it to its temporary starting shape. b.) AFT exchange mechanism c.) POM of LCE A – Before programming, B – After programming, 45 degrees to the polarizer, C – Aligned with the polarizer. d.) AFT-LCE reprogrammed by irradiating the film above the T_{NI} in its temporary recovered shape.

Panel A of Figure 3.1c illustrates the characteristic birefringence of a polydomain LCE. After programming the monodomain alignment, seen in panel B, the material crossed with the polarizer displayed light transmission and lack of the birefringence, indicative of the monodomain alignment. When the film is aligned with the polarizers, seen in panel C, light transmission is canceled, again confirming a monodomain alignment in the strain direction of the film. Finally, demonstrating the materials re-writability, a simple, secondary light exposure above the T_{NI} was required to erase the initially stabilized alignment (Figure 3.1d). The network after the first programming step was comparatively stress-free at room temperature, but upon heating above the T_{NI} , the entropy dominated contraction of the material returned it to a stressed state and thus

activation of AFT at this temperature acted to relieve that stress and erase the programming from the first step.

A systematic investigation was performed on the programming conditions of the AFT-LCE. Programming variables include temperature, strain, and light exposure. **Figure 3.2** investigates the modulation of these variables. **Figure 3.2a** and **b** report the final programmed shape of the LCE measured in the LC phase (**Figure 3.2a**) and the isotropic phase (**Figure 3.2b**). These films were programmed at 25°C, 67°C and 120°C. The temperatures chosen include the material in the LC phase, just near the phase transition indicated by DMA, and well above the T_{NI} . The LCE samples were strained to $45 \pm 10\%$ except for the 120°C samples, which were strained to $15 \pm 5\%$, and exposed to light for increasing amounts of time. Increasing the exposure time prolonged the time for covalent bond rearrangement to occur, which resulted in an increased final programmed strain measured in the LC phase. In parallel, increasing the temperature at which programming was done also increasingly affected the final programmed strain and thus shape measured in the LC phase. The temperature and light exposure duration with which programming is done alter the final resulting shape, with increased temperature allowing for more mobility during bond rearrangement and increased exposure allowing for prolonged rearrangement to occur.

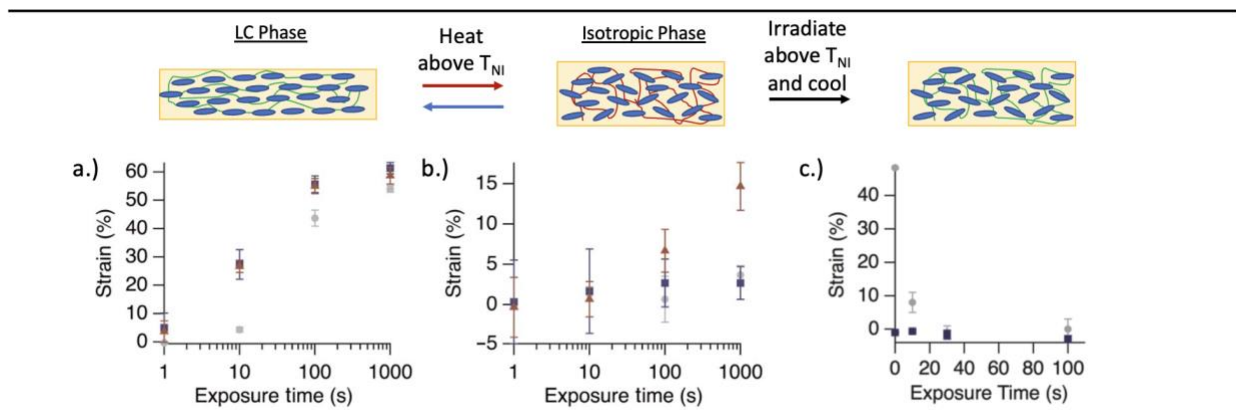


Figure 3.2: Strain measurements of the AFT-LCE programmed at varying light exposure durations measured in a.) the LC Phase at room temperature. b.) the isotropic phase at 120°C. c.) Erasing programming. Samples were initially programmed with 100 s, 365 nm, 30 mW/cm². They were then erased by heating to 100°C and irradiated with 320-500 nm 30 mW/cm². The LC (grey) and isotropic (blue) phase shape was then measured.

Programming done in the LC phase at 25°C did not have a significant effect on the isotropic shape. As reported by Terentjev et al., strain in the LC phase results in stress concentrated in the domain boundaries during the reorientation of mesogens towards the monodomain, which minimizes the free energy of the system.²¹ The soft elasticity in LCEs is also an indication of this, where stress does not increase during mesogen reorientation since it is being concentrated in domain boundaries instead of directly applied to the polymer network.²² The AFT programming in the LC phase more directly anneals out stress concentrated in the reoriented LC boundaries from a polydomain towards a monodomain. Programming above the T_{NI} had a significant effect on the final isotropic shape, with the LCE acting as a traditional elastomer in the isotropic phase. Behaving more as an amorphous elastomer, stress was more uniformly distributed throughout the network above the T_{NI} , thus programming more directly affected the entirety of the network and the resulting isotropic shape. **Figure S3.2** displays stress relaxation for the AFT-LCE at the three temperatures confirming the elastic behavior of the LCEs programmed at 67°C and 120°C before the light is turned on at 100 s.

Shape programming erasure was demonstrated by irradiating programmed samples above the T_{NI} , with significant shape recovery to the original shape reported in **Figure 3.2c**. Measurements were taken in the LC phase and isotropic phase. Irradiation above the T_{NI} relieves the stress built up in the network at high temperature and acts to erase any shape programming done prior to that exposure.

Strain was also investigated as a programming variable. LCEs were strained at 25°C to varying degrees and irradiated with light (**Figure S3.3**). The maximum applied strain was about 90%, but the resulting maximum strain measured after programming only reached about 60%. The inability to preserve 100% of the programming strain and exceed a final programmed strain of 60% is attributed to the network characteristics, with this value being near the end of the soft elasticity of the LCE (**Figure S3.4**). To increase the amount of maximum programmable strain, lowering the cross-linking density by increasing the oligomer length will subsequently increase the maximum programmable strain.

More complex shapes were generated by folding or bending materials into a desired shape and irradiating with light. Localized stress in folded regions is relaxed during light irradiation which introduces shape programming and thus autonomous shape memory as first seen by the flower in **Scheme 3.1** and further illustrated in **Figure 3.3**. A box is programmed simply by folding the LCE where the box hinges are desired. Irradiating the material with light relaxes the stress and programs the strained hinge regions (**Figure 3.3a**). The shape is then deployed via heating above the T_{NI} and can autonomously switch shape upon thermal cycling. As discussed above, prolonging or elevating programming conditions yields larger resultant deformations to the polymer network and thus final programmed shape. The box maintained 90-degree folds, but 180-degree folds are

realized by programming the flower at an elevated temperature of 40°C, and increased exposure time. (**Figure 3.3b**).

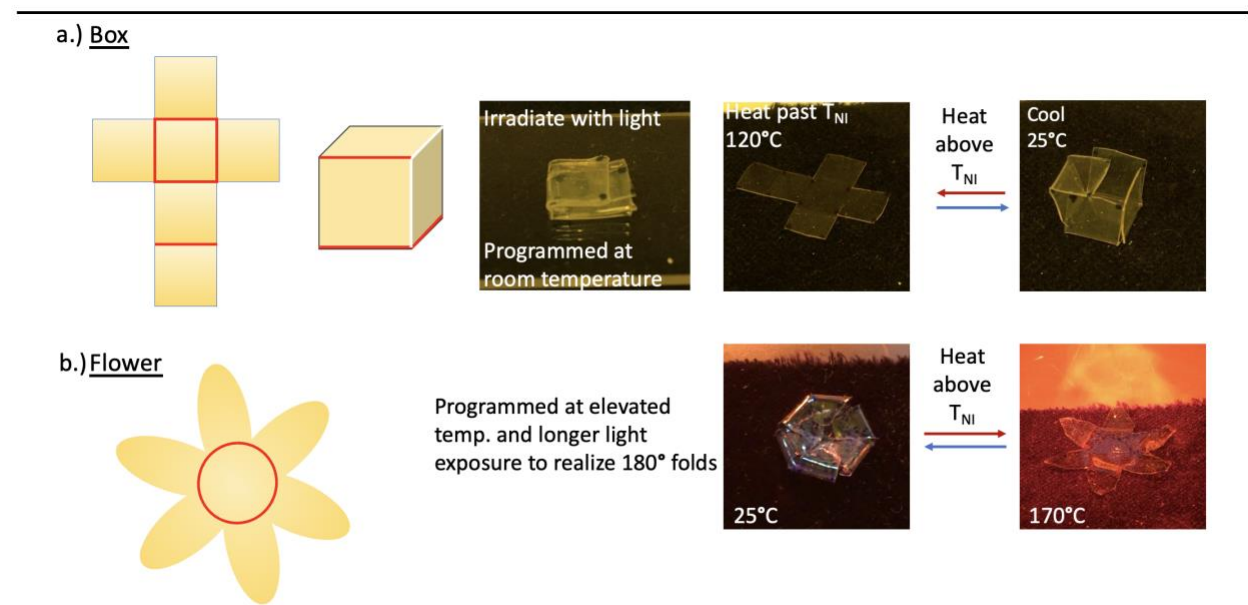


Figure 3.3: a.) Box shape programming at 25°C, 365 nm, 50mW/cm², 120 s. b.) Flower shape programming at 40°C, 365 nm, 50mW/cm², 200 s.

Concluding from the discussion above, programming above the T_{NI} is useful for altering not only the LC shape but the isotropic shape as well. A demonstration was done to showcase the dramatic shape alteration that could be achieved with this understanding. A rectangular LCE was folded and held between glass at 120°C (**Figure 3.4a**). The sample was then irradiated at this temperature and upon cooling, a tight 180-degree fold results (**Figure 3.4b**). Heating the free-standing film back above the T_{NI} deploys the shape, but full recovery to the flat starting shape does not occur and the isotropic shape has now been permanently altered (**Figure 3.4c**). This is in contrast to the programming of the flower shape prior, where programming at 40°C, below the T_{NI} , enhanced the folds, but still allowed for full shape recovery back to the flat starting shape during thermal cycling. The rectangular sample was irradiated with light above the T_{NI} , at 120°C which allowed for relaxation of the stress built up in the material at this temperature (**Figure 3.4d**).

Cooling the film back to 25°C, the bent shape persists, and this is the new permanent starting shape for the AFT-LCE (**Figure 3.4e**).

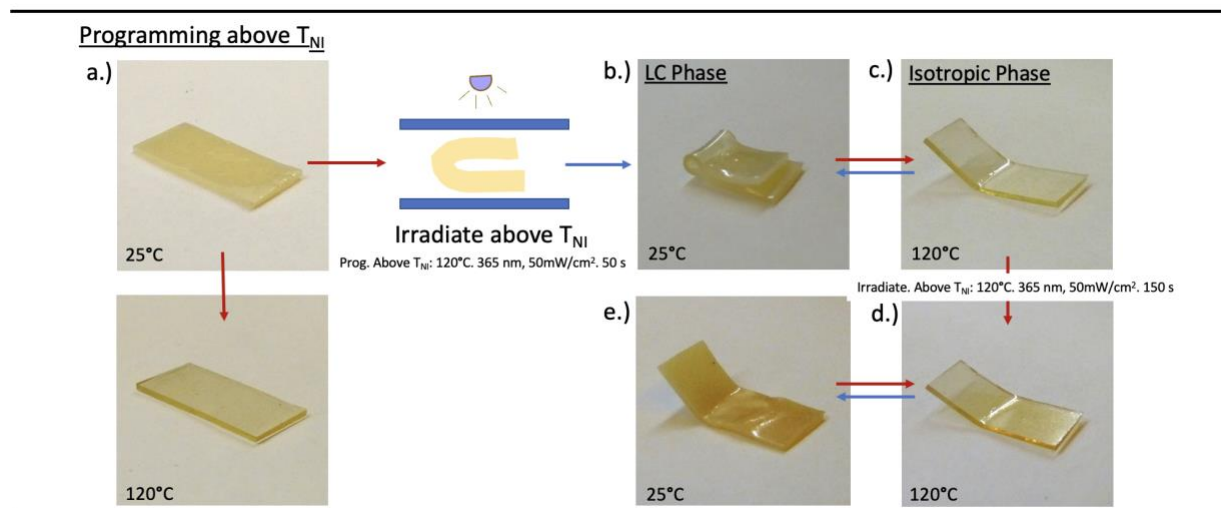


Figure 3.4: a.) LCE starting at 25°C (top) and heated above T_{NI} (bottom) b.) LCE viewed at 25°C, cooled after programming c.) LCE heated above the T_{NI} displaying a bent shape d.) LCE after irradiating at step c. e.) LCE cooled to 25°C displaying the new permanent starting shape.

To create an additional means of programming control, the material was embedded with a UV-absorbing compound, Tinuvin-328 (T-328), to attenuate light penetration through the thickness of the film and result in a through-plane gradient with respect to the liquid crystal alignment (**Figure 3.5a**). Out-of-plane buckling is commonly achieved via biased regions of LC alignment or non-uniform stresses throughout an elastomeric material.^{23,24,5,25} This same concept is utilized here where the AFT exchange is reduced through the thickness of the film due to light attenuation, creating a gradient of stabilized LC alignment and thus resulting in a 3D structure. This structure arises due to the non-uniform regions of stress the polymer network undergoes from the gradient of LC alignment tethered to the network. Employing a photomask further controls alignment programming. To achieve bending, the film is strained uniaxially and a photomask is placed over the region of the film where a hinge is desired. The outcome is illustrated in **Figure**

3.5b, where the desired folded region remains polydomain and unprogrammed, with monodomain alignment throughout the rest of the film. This programming technique is in contrast to the previous programming method of origami shapes where the bulk of the film remains polydomain and alignment is only achieved in the folds of the structure. **Figure 3.5c** demonstrates programmed twisting by having opposing alignment at each interface. The film is strained at opposing corners and irradiated with light on each side. Longer exposures enabled increased amounts of stress relaxation and network reorganization to occur and thus a final more exaggerated shape arises.

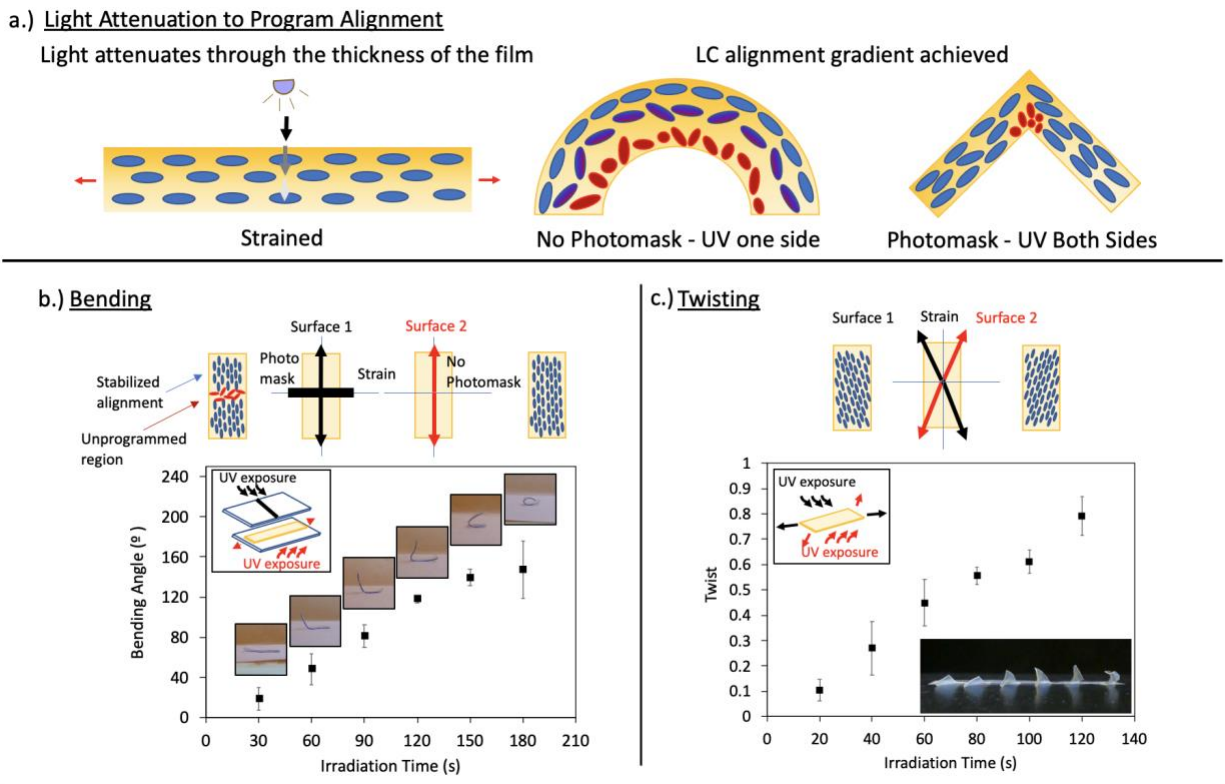


Figure 3.5: a.) Scheme for utilizing light attenuation to program LC alignment. b.) Bending LCE programmed by light attenuation. By increasing exposure time, network reorganization and alignment stabilization is increased resulting in enhanced 3D deformations. c.) Twisting LCE programmed in a similar manner.

The attenuation behavior is confirmed by the Beer-Lambert law ($A = \epsilon bC$), where A , absorption is equal to ϵ , the molar absorptivity multiplied by b , the path length and c , the concentration of the

absorptive molecule. The 250 μm thick LCE doped with 0.5 wt% T-328, yielded a calculated absorbance of 7.6, using the reported molar absorptivity of Tinuvin, which was $1476 \text{ M}^{-1}\text{mm}^{-1}$ at 347 nm. The value of molar absorptivity was not reported at the programming wavelength of 365 nm, so the molar absorptivity applied was simply used as an estimation to predict absorbance. UV light was significantly attenuated through the doped LCE at the programming wavelength, 365 nm, also confirmed by UV-vis (**Figure S3.5**).

More complex shapes were programmed utilizing this method. A saddle shape is achieved by straining the material in the long and short directions respectively and irradiating on each side. The competing strain on each interface of the saddle results in a negative Gaussian curvature and thus the saddle shape is realized (**Figure 3.6a**). **Figure 3.6b** and **c** display programming of a box and pyramid by utilizing photomasks, where the film is strained and the panels of the film are programmed to a monodomain. Due to placement of the photomask, the folds are essentially unprogrammed, maintaining their polydomain structure.

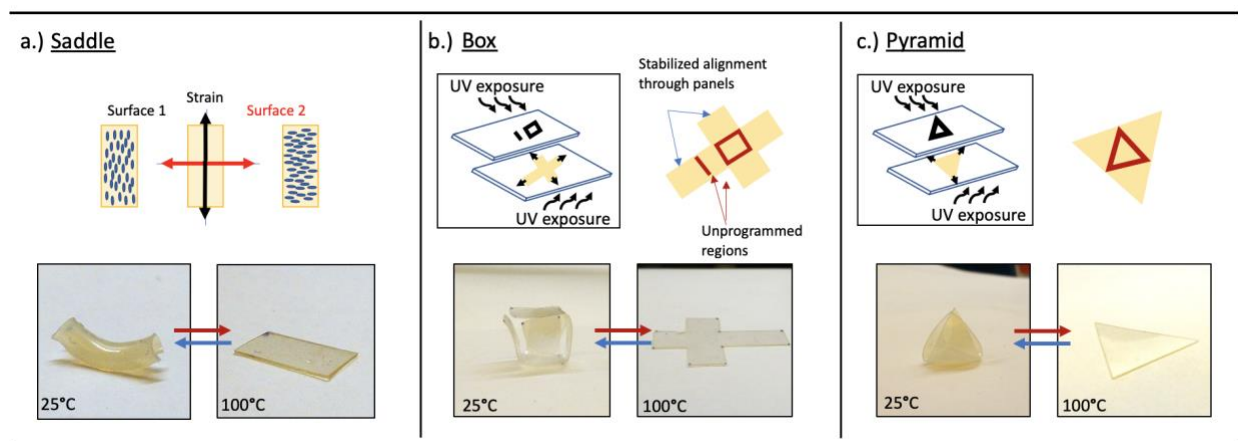


Figure 3.6: Programming the AFT-LCE in a variety of complex geometries using T-328 a.) Saddle. Using a photomask, programming a b.) Box and c.) Pyramid is achieved.

Heating and cooling cycles toggled the material between their initial flat and programmed shapes, respectively. Challenges recovering the desired shape were due to both the inherent

material properties and mechanics of the films as well as heat transfer considerations. The rubbery nature of the LCE makes it difficult for this monodomain stabilization to be self-supporting and alignment recovery to be uniform as the sample exceeds tens of millimeters in length and width.

3.3 – Conclusions

Here, we have demonstrated an LCE that is programmed into complex shapes post polymerization utilizing light activated AFT. This DCC is decoupled from the thermal LC phase transitions to actuate the material from the light facilitated programming of the polymer network. By understanding the underlying LC alignment, complex shapes are readily programmed. Investigating the programming stimuli such as temperature, strain, and exposure time enabled understanding and control of the final programmed and re-programmed shapes. Furthermore, utilizing a light absorber T-328, facilitates control of the light penetration depth to enable another means of programming and controlling LC alignment. Finally, AFT allows for re-programming of polymer shapes, and materials were returned to their initial starting shapes by irradiating materials above the T_{NI} , demonstrating reconfigurability.

3.4 – Experimental

Materials

1,1'-(2-Methyl-1,4-phenylene) ester 4-[[6-[(1-oxo-2-propen-1-yl) oxy]hexyl]oxy]-benzoic acid (RM82) was obtained from Wilshire Technologies. 3-Chloro-2-(chloromethyl)-1-propene, potassium ethyl xanthogenate, NPGDA, dichloromethane (DCM), and triethylamine (TEA) were purchased from Sigma-Aldrich. Ethylenediamine was obtained from TCI America. All chemicals were used as received unless otherwise noted.

Synthesis of allyl dithiol

2-Methylene-1,3-propanedithiol (allyl dithiol) was synthesized according to previously reported procedure (34). In a 1000-ml round-bottom flask with a stir bar, potassium ethyl xanthogenate (56.4 g, 352 mmol) was dissolved into ethanol (500 ml). 3-Chloro-2-(chloromethyl)-1-propene (18.5 ml, 160 mmol) was added dropwise, and the reaction was left overnight. The solids were then removed with filtration, and ethanol was removed using a rotary evaporator. Diethyl ether (200 ml) and water (100 ml) were added to the yellow residue, and the organic phase was removed and washed with water (2 \times , 100 ml), washed with brine (1 \times , 100 ml), and dried over sodium sulfate. The ether was removed under a vacuum, resulting in the protected allyl dithiol as a yellow low-viscosity liquid used without further purification in the next step. In a flame-dried, 50-ml round-bottom flask with an addition funnel under argon, the protected allyl dithiol (10 g, 33.8 mmol) was added over 30 min to anhydrous ethylenediamine (16 ml) held at 20°C. After 3 hours, the reaction mixture was slowly added to 200 g of ice and 32 ml of sulfuric acid (concentrated). The milky white solution was extracted with diethyl ether (2 \times , 200 ml). The organic phases were combined and extracted with 2 M sulfuric acid (2 \times , 100 ml) and brine (1 \times , 100 ml). The organic phase was then dried over sodium sulfate, filtered, and concentrated in vacuo, resulting in a slightly yellow low-viscosity liquid with an extremely foul odor. The allyl dithiol was distilled immediately before use (60°C, 0.1 mmHg, 2.6 g, 60% yield). Impurities were observed if allowed to sit overnight after purification. ¹H nuclear magnetic resonance (NMR) (400 MHz, CDCl₃, 25°C): 4.99 (broad singlet, 2H), 3.37 to 3.34 (multiplet, 4H), 1.48 (triplet, J = 8.15 Hz, 2H).

Purification of NPGDA

NPGDA was purified via flash chromatography. Column conditions were 10% ethyl acetate in hexanes using a Biotage Isolera One. Inhibitor, 4-methoxyphenol (MEHQ), was added in a 100–parts per million (ppm) concentration.

Synthesis of Diacrylate Oligomers

Diacrylate oligomers were synthesized via a base-catalyzed thiol- Michael addition in a manner similar to those previously reported (34). In an open 100-ml round bottom flask with a mechanical stir bar, butylated hydroxytoluene (9 mg, 1000 ppm), RM82 (6625 mg, 9.858 mmol), and NPGDA (1046 mg, 4.929 mmol) were dissolved into DCM (30 ml, 0.5 M), followed by the addition of allyl dithiol (1600 mg, 13.308 mmol). TEA (8.24 ml, 59.14 mmol) was added, and the reaction mixture was allowed to stir for 16 hours, followed by the removal of DCM and TEA in vacuo. The resulting viscous liquid was dissolved in DCM (200 ml) and washed with 1 M HCl (2×, 100 ml) and brine (1×, 100 ml), followed by drying with sodium sulfate and removal of DCM in vacuo, which produced a white semisolid resin. NMR was used to confirm the consumption of thiols and determine the average number of repeat units through end group analysis of acrylic protons compared to allylic allyl sulfide protons. A molar ratio of 1:0.5:1.35 (RM82/NPGDA/allyl dithiol) was used for all results shown unless explicitly stated. Note ADT was calculated as 0.9 x acrylate EQ.

Photopolymerization of polydomain films

Oligomers (400 mg) were dissolved in 4 ml of DCM. Photoinitiators (Irgacure 819, Irgacure 651, and Irgacure 2959) were dissolved in DCM (10 mg/ml) and added to the dissolved oligomers in

the appropriate proportions. Irgacure 819 and Irgacure 651 were added at 1.5 weight % (wt %) (6 mg, 600 ml) and 1 wt % (4 mg, 400 ml). Irgacure 2959 was added for multiple exposure experiments at 1 wt % (4 mg, 400 ml). The dissolved resin was then deposited onto a Rain-X-coated glass at 160°C on a hotplate and allowed the DCM to evaporate open to air (30 min) with occasional stirring. The resin was then pressed between two Rain-X-coated glass plates with 500-, 250-, or 140-mm plastic spacers and heated to 160°C on a hotplate for 5 min to erase residual stress. Photopolymerization was then performed at 110°C on a hotplate ($\pm 10^\circ\text{C}$ measured with a thermocouple) with 400- to 500-nm ($50 \text{ mW}/\text{cm}^2$) light (Exfo Acticure Hg Bulb) for 3 min. The resulting slightly yellow polymer network had a slight haze, confirming a polydomain structure. Thermal cycling led to a minimal shape change.

Measurement of strain after programming

LC and isotropic shape measurements were obtained by image analysis [ImageJ, National Institutes of Health (NIH)]. Two circular dots were marked on polydomain films (250-mm thickness, $3.15 \times 10 \text{ mm}$) approximately 2 mm apart. Images were taken using a Panasonic Lumix camera at room temperature (20°C , approximately room temperature) for LC strain (ϵ_0) and 120°C ($\pm 10^\circ\text{C}$ measured with a thermocouple) hotplate for isotropic strain (ϵ_0 ; isotropic and LC were approximately equal in all cases). The films were then placed in a stretching device and stretched to a predetermined length and irradiated with 320 to 500 nm ($50 \text{ mW}/\text{cm}^2$) for the prescribed amount of time. For samples irradiated at 67° and 120°C , an oven with a window was used to control the temperature. The temperature was measured with a thermocouple placed next to the sample, and the temperature was allowed to equilibrate for 30 min before exposure. The accuracy of the programming temperature measurement was estimated as $\pm 1^\circ\text{C}$. The samples were removed

from the stretching device, heated to 120°C on a hotplate, imaged for isotropic strain (eI,P), cooled to 20°C, and imaged for LC strain (eLC,P). Each data point was performed in triplicate, and SE was reported. All strains were reported relative to the initial “as-polymerized” shape of the LCE (e0).

DMA

Temperature scans (Tan delta and storage modulus) were run at 1 Hz, 3°C/min. Tests were run on an TA RSA-G2.

Optical and Polarized Microscopy

Optical and polarized optical microscopy (POM) were done with a Nikon Eclipse Ci

Programming with gradient light (T-328) (bending and folding)

Samples were made using a similar approach described above with the addition of Tinuvin-328 ultraviolet (UV) absorber in 0.5 wt% in the same manner as the photoinitiators. All films were 250 mm thick. Bending was achieved by irradiating one face of an LCE through a photomask (1-mm-thick line). Irradiation conditions: 25°C. 20% strain. 365 nm, 50mW/cm². each side. The sample was thermally cycled. Images of the final bent state were taken, and the bending angle was determined using ImageJ. Twisting was programmed straining the material at opposite corners and irradiating on each side. 15% strain. 365 nm, 50mW/cm². each side. Saddle was programmed straining the sample and irradiating on each side at the long length and short length of the rectangular sample respectively. 25°C. 35% strain. 365 nm, 50mW/cm². 120 s. each side. Box and Pyramid, utilizing a mask to block light at the hinges, samples were strained and irradiated on one

side with the mask, and the other side with no mask. 25°C. 20% strain. 365 nm, 50mW/cm². 120 s. each side.

3.5 – Acknowledgements

We acknowledge C. Yakacki for fruitful discussions. Certain commercial equipment, instruments, or materials are identified in this paper to specify the experimental procedure adequately. This identification does not imply recommendation or endorsement by National Institute of Standards and Technology, nor does it imply that the materials or equipment identified are necessarily the best available for the purpose. Funding: M.K.M. was funded by an NSF graduate fellowship (DGE 1144083), NSF CBET-1264298, NSF–Materials Research Science and Engineering Center DMR-1420736, NSF DMR-1310528, and NSF DMR- 1809841. Author contributions: M.K.M. and C.N.B. developed the idea and devised experiments. M.K.M., A.M.M., M.P., and B.T.W. performed experiments. L.C. and J.K. performed and interpreted nanoimprinting and AFM. M.K.M., A.M.M., M.A., and K.C. performed and interpreted diffraction data. M.B. performed shape memory experiments. Competing interests: The authors declare that they have no competing interests. Data and materials availability: All data needed to evaluate the conclusions in the paper are present in the paper and/or the Supplementary Materials. Additional data related to this paper may be requested from the authors.

3.6 – Supporting Information

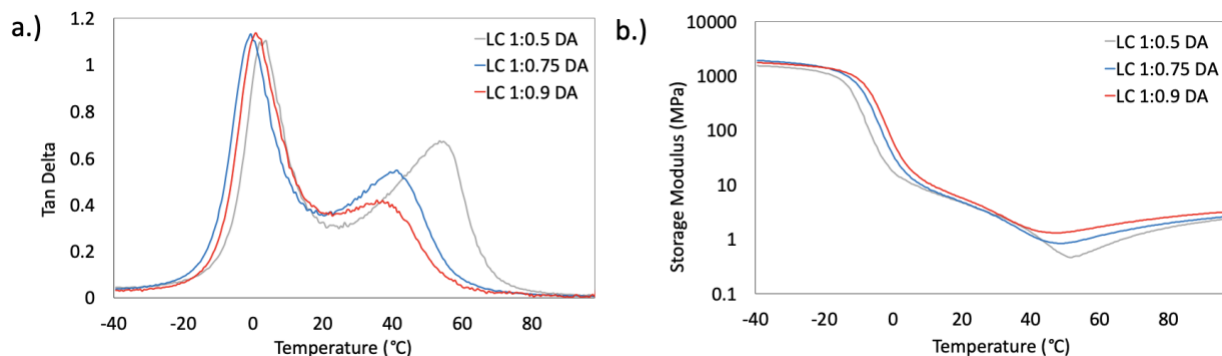


Figure S3.1: DMA for three LCE stoichiometries being RM82:NPGDA:ADT, displaying the modulation of NPGDA content, denoted diacrylate (DA), (full stoichiometry RM82:NPGDA:ADT at 0.9 x Acrylate EQ). Data displaying a change in the LC phase transitions as the concentration of LC monomer is changed a.) Tan Delta b.) Storage modulus.

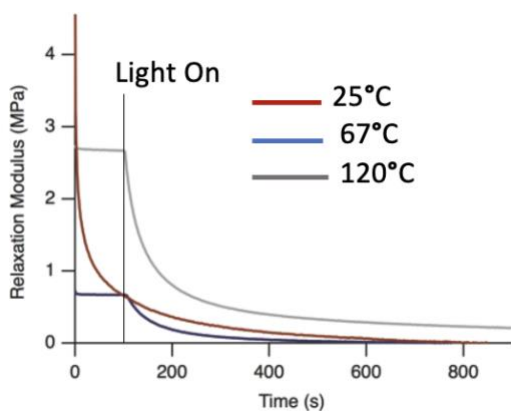


Figure S3.2: Stress relaxation behavior of LCE at 120°C (gray), 67°C (blue), and 25°C (red). Conditions: 10% strain, light on at 100 s (30 mW/cm², 320-500 nm).

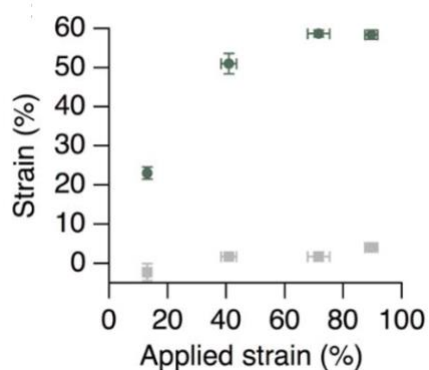


Figure S3.3: Strain measurements of the AFT-LCE programmed at varying strains in the LC Phase (green) and isotropic phase (grey).

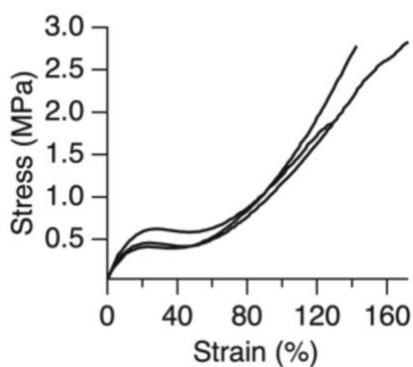


Figure S3.4: Strain to break experiments for 1:0.5:1.35 RM82/NPGDA/allyl dithiol. Conditions: 3.14×0.25×6 mm was stretched at 0.1 mm/s until slip or break on a TA RSA-G2. Experiment was run in triplicate.

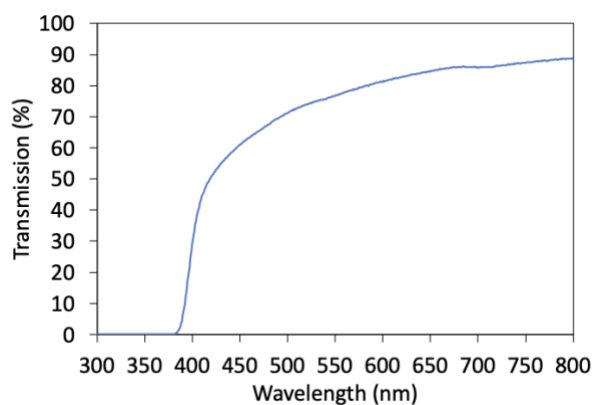


Figure S3.5: UV-vis for LCE doped with 0.5 wt% T328. Light attenuation is confirmed at the programming wavelength of 365 nm.

3.7 – References

- (1) Belmonte, A.; Bus, T.; Broer, D. J.; Schenning, A. P. H. J. Patterned Full-Color Reflective Coatings Based on Photonic Cholesteric Liquid-Crystalline Particles. *ACS Applied Materials & Interfaces* **2019**, *11* (15), 14376–14382. <https://doi.org/10.1021/acsami.9b02680>.
- (2) Wang, J.-N.; Liu, Y.-Q.; Zhang, Y.-L.; Feng, J.; Wang, H.; Yu, Y.-H.; Sun, H.-B. Wearable Superhydrophobic Elastomer Skin with Switchable Wettability. *Adv. Funct. Mater.* **2018**, *28* (23), 1800625. <https://doi.org/10.1002/adfm.201800625>.
- (3) Xie, M.; Hisano, K.; Zhu, M.; Toyoshi, T.; Pan, M.; Okada, S.; Tsutsumi, O.; Kawamura, S.; Bowen, C. Flexible Multifunctional Sensors for Wearable and Robotic Applications. *Advanced Materials Technologies* **2019**, *4* (3), 1800626. <https://doi.org/10.1002/admt.201800626>.
- (4) Birnbaum, D. T.; Brannon-Peppas, L. Microparticle Drug Delivery Systems. In *Drug Delivery Systems in Cancer Therapy*; Brown, D. M., Ed.; Humana Press: Totowa, NJ, 2004; pp 117–135. https://doi.org/10.1007/978-1-59259-427-6_6.
- (5) Liu, Y.; Genzer, J.; Dickey, M. D. “2D or Not 2D”: Shape-Programming Polymer Sheets. *Progress in Polymer Science* **2016**, *52*, 79–106. <https://doi.org/10.1016/j.progpolymsci.2015.09.001>.
- (6) Meng, Y.; Jiang, J.; Anthamatten, M. Shape Actuation via Internal Stress-Induced Crystallization of Dual-Cure Networks. *ACS Macro Lett.* **2015**, *4* (1), 115–118. <https://doi.org/10.1021/mz500773v>.
- (7) Han, Z.; Wang, P.; Mao, G.; Yin, T.; Zhong, D.; Yiming, B.; Hu, X.; Jia, Z.; Nian, G.; Qu, S.; Yang, W. Dual PH-Responsive Hydrogel Actuator for Lipophilic Drug Delivery. *ACS Appl. Mater. Interfaces* **2020**, *12* (10), 12010–12017. <https://doi.org/10.1021/acsami.9b21713>.
- (8) Lou, J.; Liu, Z.; Yang, L.; Guo, Y.; Lei, D.; You, Z. A New Strategy of Discretionarily Reconfigurable Actuators Based on Self-Healing Elastomers for Diverse Soft Robots. *Adv. Funct. Mater.* **2021**, *31* (11), 2008328. <https://doi.org/10.1002/adfm.202008328>.
- (9) K pfer, J.; Finkelmann, H. Nematic Liquid Single Crystal Elastomers. *Makromol. Chem., Rapid Commun.* **1991**, *12* (12), 717–726. <https://doi.org/10.1002/marc.1991.030121211>.
- (10) Portugall, M.; Ringsdorf, H.; Zentel, R. Synthesis and Phase Behaviour of Liquid Crystalline Polyacrylates. *Macromolecular Chemistry and Physics* **1982**, *183* (10), 2311–2321. <https://doi.org/10.1002/macp.1982.021831003>.
- (11) Ware, T. H.; McConney, M. E.; Wie, J. J.; Tondiglia, V. P.; White, T. J. Voxellated Liquid Crystal Elastomers. *Science* **2015**, *347* (6225), 982–984. <https://doi.org/10.1126/science.1261019>.
- (12) Kowalski, B. A.; Guin, T. C.; Auguste, A. D.; Godman, N. P.; White, T. J. Pixelated Polymers: Directed Self Assembly of Liquid Crystalline Polymer Networks. *ACS Macro Lett.* **2017**, *6* (4), 436–441. <https://doi.org/10.1021/acsmacrolett.7b00116>.
- (13) Fortman, D. J.; Brutman, J. P.; Cramer, C. J.; Hillmyer, M. A.; Dichtel, W. R. Mechanically Activated, Catalyst-Free Polyhydroxyurethane Vitrimers. *J. Am. Chem. Soc.* **2015**, *137* (44), 14019–14022. <https://doi.org/10.1021/jacs.5b08084>.
- (14) Otera, J. Transesterification. *American Chemical Society* **1993**, No. 93, 22.
- (15) Amamoto, Y.; Kamada, J.; Otsuka, H.; Takahara, A.; Matyjaszewski, K. Repeatable Photoinduced Self-Healing of Covalently Cross-Linked Polymers through Reshuffling of

- Trithiocarbonate Units. *Angew. Chem.* **2011**, *123* (7), 1698–1701. <https://doi.org/10.1002/ange.201003888>.
- (16) Christensen, P. R.; Scheuermann, A. M.; Loeffler, K. E.; Helms, B. A. Closed-Loop Recycling of Plastics Enabled by Dynamic Covalent Diketoenamine Bonds. *Nat. Chem.* **2019**, *11* (5), 442–448. <https://doi.org/10.1038/s41557-019-0249-2>.
- (17) Pei, Z.; Yang, Y.; Chen, Q.; Terentjev, E. M.; Wei, Y.; Ji, Y. Mouldable Liquid-Crystalline Elastomer Actuators with Exchangeable Covalent Bonds. *Nature Mater* **2014**, *13* (1), 36–41. <https://doi.org/10.1038/nmat3812>.
- (18) Curk, T.; Dobnikar, J.; Frenkel, D. Liquid Crystalline Epoxy Networks with Exchangeable Disulfide Bonds. *Soft Matter* **2016**, *12* (1), 35–44. <https://doi.org/10.1039/C5SM02144H>.
- (19) Wen, Z.; McBride, M. K.; Zhang, X.; Han, X.; Martinez, A. M.; Shao, R.; Zhu, C.; Visvanathan, R.; Clark, N. A.; Wang, Y.; Yang, K.; Bowman, C. N. Reconfigurable LC Elastomers: Using a Thermally Programmable Monodomain To Access Two-Way Free-Standing Multiple Shape Memory Polymers. *Macromolecules* **2018**, *51* (15), 5812–5819. <https://doi.org/10.1021/acs.macromol.8b01315>.
- (20) McBride, M. K.; Martinez, A. M.; Cox, L.; Alim, M.; Childress, K.; Beiswinger, M.; Podgorski, M.; Worrell, B. T.; Killgore, J.; Bowman, C. N. A Readily Programmable, Fully Reversible Shape-Switching Material. *Science Advances* **2018**, *4* (8), eaat4634. <https://doi.org/10.1126/sciadv.aat4634>.
- (21) Fridrikh, S. V.; Terentjev, E. M. Polydomain-Monodomain Transition in Nematic Elastomers. *Phys. Rev. E* **1999**, *60* (2), 1847–1857. <https://doi.org/10.1103/PhysRevE.60.1847>.
- (22) Ware, T. H.; Biggins, J. S.; Shick, A. F.; Warner, M.; White, T. J. Localized Soft Elasticity in Liquid Crystal Elastomers. *Nature Communications* **2016**, *7* (1). <https://doi.org/10.1038/ncomms10781>.
- (23) Kuenstler, A. S. Light-Induced Shape Morphing of Thin Films. *Interface Science* **2019**, 17.
- (24) Qin, L.; Gu, W.; Yu, Y. Photodeformable Liquid Crystalline Polymers LCPs. In *Polymers and Polymeric Composites: A Reference Series*; Palsule, S., Ed.; Springer Berlin Heidelberg: Berlin, Heidelberg, 2018; pp 1–29. https://doi.org/10.1007/978-3-642-37179-0_52-1.
- (25) Ma, S. J.; Mannino, S. J.; Wagner, N. J.; Kloxin, C. J. Photodirected Formation and Control of Wrinkles on a Thiol–Ene Elastomer. *ACS Macro Letters* **2013**, *2* (6), 474–477. <https://doi.org/10.1021/mz400166e>.

Chapter 4: Reconfigurable and Spatially Programmable Chameleon Skin-Like Material Utilizing Light Responsive Covalent Adaptable Cholesteric Liquid Crystal Elastomers

(Manuscript published - Martinez, A. M.; McBride, M. K.; White, T. J.; Bowman, C. N. Reconfigurable and Spatially Programmable Chameleon Skin-Like Material Utilizing Light Responsive Covalent Adaptable Cholesteric Liquid Crystal Elastomers. *Advanced Functional Materials* **2020**, 2003150. <https://doi.org/10.1002/adfm.202003150>.)

A mechanochromic, programmable, cholesteric liquid crystalline elastomer (CLCE) was fabricated, and after straining, resulting in a blue shift through the visible spectrum, was returned to its initial shape and color upon heating through its isotropic phase transition. Light initiated, radical-mediated, addition fragmentation chain transfer (AFT), facilitated permanent programming or erasure of thermoreversible shape and color by relaxing stress imparted on the strained network through reversible bond exchange. Thermoreversible strain was coupled with reversible color change and could be made permanent at any desired strain by light exposure and corresponding AFT activation, temporarily restoring nearly initial shape and color upon heating. The optical characteristics and photonic structure, inherently linked to the network, were measured as a function of strain, to confirm the reflection notch narrowing indicating that pre-polymerization alignment via shearing is poor thereby causing a broad spectrum of reflected light that narrows when the material is stretched. Beyond programming a new shape and color, the reflection notch was erased and separately, photopatterned to achieve dynamic color schemes that are toggled with heating and cooling, similar to that of a chameleon's camouflaging technique that has the ability to manipulate multiple colors in a single material, also with use for strain mapping.

4.1 – Introduction

Camouflage and synthetic mimics of it have been of interest for decades for applications in defense, textiles, and more. ^[1-3] The mechanism with which camouflage works is not always

simply a change in color but can include surface topography and structural changes as well.^[4] The chameleon is an ideal example of camouflaging capabilities that occur through structural changes that result in a color change to hide it from potential predators or allow for communication to other chameleons.^[5] One approach to forming synthetic analogues to camouflage and other optical transformations in materials uses liquid crystals (LCs) to modulate light either directly or through shape and dimensional changes including in applications for displays. Furthermore, chiral doped or cholesteric LCs (CLCs) are one example of a class of self-assembling photonic structures with the capacity to modulate color at the users discretion through varying stimuli such as temperature, light, or electricity, which is highly appropriate for applications in camouflage where color modulation is the premise.^[6-8] By adding a chiral monomer into a LC system, the handedness is transferred into the self-assembling LC structure, thereby making a repeating, photonic active structure known as the chiral nematic phase that reflects a corresponding wavelength of light designated as its reflection notch.^[9] CLC systems have been used for camouflage, optical applications, cosmetics, strain mapping, and tunable lasing.^[7,10-14]

Many color changing CLC systems are either loosely crosslinked or not crosslinked at all.^[6,8,15] The mechanisms through which these chiral nematic reflection notches are shifted include a variety of stimuli such as temperature, electric field, light, or strain.^[6-8,15] These techniques result in highly aligned CLC systems, achieving narrow reflection notches. The aforementioned systems undergo minor overall changes in shape to alter the repeating structure, or chiral nematic alignment known as the pitch, and are also limited to glass cells, making them less adaptable.^[16, 17] To circumvent this issue, Brannum *et al.* designed a crosslinked freely-standing cholesteric liquid crystal elastomer (CLCE) film that changes color via heating, which slightly increases the thickness of the sample and thus the pitch spacing, changing the wavelength

of light that the polymer reflects.^[18] For a more dramatic demonstration of strain changes linked to color change, Finkelmann *et al.* designed a PDMS dye doped CLCE that alters the wavelength transmitted through mechanical strain.^[13] Most recently, Kizhakidathazhath *et al.* used an anisotropic deswelling method to align a freely-standing CLCE film that uses uniaxial strain to dramatically deform the material and alter the visible reflection.^[19] Although this method produces robust, highly aligned elastomers, this method requires 24 hours of processing to occur, with 5 hours for the first polymerization stage, whereas the procedure reported here requires only manual shearing of the material to achieve the necessary alignment to obtain a reflective surface in minutes with polymerizations occurring within seconds using light irradiation to initiate an acrylate homopolymerization.

In a separate study not linked to light modulation, research has been done on programmable and reversible shape changing LCEs with several of these methods using covalent adaptable networks (CANs), for soft robotic applications or dynamic optical surfaces, which is advantageous to this research for control of the change in shape that is linked to color.^[20-22] The reversible shape changes in these LCEs occur due to the anisotropic alignment LCEs maintain, and by heating through the phase transitions to the isotropic phase, results in anisotropic expansion and contraction of the film.^[22] Crosslinking tethers the LC mesogens to the mechanical framework of the network translating molecular scale order to macroscopic shape to enable robust and repeatable shape changes, which are not achievable for loosely or non-crosslinked CLC systems. CANs LCEs enable permanently programmable and temporarily reversible shape changes which here are linked to color changes for the first time.

Here, these capabilities are expanded upon by linking control over color with shape change in a freely-standing elastomeric film by enabling it with the ability to permanently fix a new shape

and color or erase the color at the users' discretion using a light initiated AFT-based CAN CLCE. CANs provide the ability to reconfigure a crosslinked network post-polymerization through triggered bond rearrangements that relieve stress in the network and promote relaxation towards an equilibrium state and structure.^[23] The CANs-capable CLCE reported here is completely crosslinked and doped with a chiral LC monomer, having the advantage of being a freely-standing elastomeric film that is not limited by confinement in a glass cell, thereby improving its adaptability and flexibility. Mechanical strain causes a change in the arrangement of the LC structure and thus a color change from red to blue, much like a chameleon's skin which changes color due to expansion or contraction of the skin altering the spacing of the aligned biological structures on the skin's surface, which can also be used for strain mapping applications.^[5] Strain mapping has been demonstrated via CANs systems before, namely in a study done by Xie and coworkers on a non-LCE material, where a CAN-capable amorphous polymer was used to map strain to produce high resolution digital images.^[24] The CLCE reported is useful for strain mapping applications due to its high extensibility and furthermore, due to its dynamic covalent chemistry (DCC) character, the CLCE is capable of being spatially programmed to maintain the change in color and shape of the material achieved through strain with temporary reversal upon heating. The CLCE is thus selectively programmed to display complex optical and topographical patterns through photopatterning techniques.

While various technologies achieve robust and extensible films, these aforementioned methods have long processing times and are unable to be permanently reconfigured. The CLCE material reported here is processable in under an hour, utilizing a rapid light initiated polymerization that enables it to be permanently reconfigured to a new reflective wavelength or erased, again with light, providing spatiotemporal control. This approach is thus advantageous for

achieving adaptable materials that are reconfigured to a new desired color or to perform complex patterning that can later be erased if and when necessary.

4.2 – Results and Discussion

Previous freely-standing CLCE films have demonstrated control over color changes through thermal and mechanical strain, yet lack the ability to permanently reconfigure the optical characteristics as demonstrated here.^[13,18,19] We demonstrate both reversible color and shape change through transient application of strain and also permanent reconfiguration of color and shape through photoactivated AFT-based DCC.^[20] To achieve these outcomes, films were prepared with all the necessary elements; crosslinking, an LCE host, a chiral LC monomer, a radical photoinitiator, and incorporation of AFT-capable moieties throughout the network. For the film preparation the synthesis of LC diacrylate oligomers was achieved via a thiol-Michael addition reaction to incorporate the AFT chemistry into the backbone of the network. Next, to achieve a freely-standing CLCE, 4 wt% of the diacrylate chiral LC monomer, LC756, was mixed into a dichloromethane (DCM) solution of the oligomers, and photoinitiators, TPO (visible) and Irgacure 2959 (UV) to ensure homogenous mixing of the components (**Figure 4.1a**).

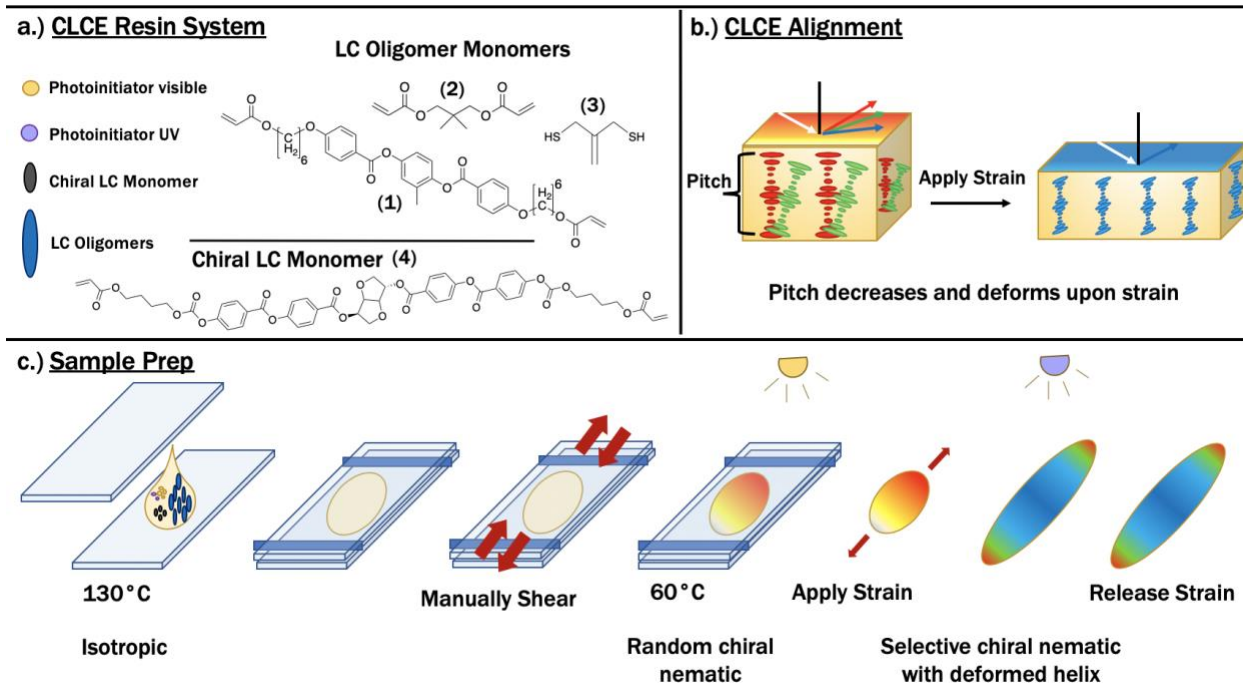


Figure 4.1: a.) Monomers used to prepare the CLCE: (1) RM82, (2) NPGDA, and (3) allyl dithiol were oligomerized as diacrylate functionalized oligomers and acrylate homopolymerized with chiral LC monomer (4) LC756. b.) Schematic of chiral nematic alignment in the film as the material is strained. Overall alignment improves along with a decrease and some deformation of the pitch. c.) Schematic of the polymerization and programming process. LC resin was repeatedly cooled and heated just below the T_{NI} while manual shearing between glass to align the monomers into the chiral nematic phase, polymerized with visible light and later programmed via straining and irradiating with UV light. Alignment follows Figure 1b depiction.

The chiral monomer is incorporated at necessary concentrations to transfer a biased chiral alignment to the LC oligomers to create a helicoidal superstructure that reflects visible light. The mixture was deposited onto a glass slide and heated to 130°C to remove the DCM and achieve a workable viscosity of the resin (**Figure 4.1c**). Important to note is that the method performed to align the LCs is due to the relatively high viscosity of the resin, which must be done manually instead of as typically performed in thin alignment cells ($< 50 \mu\text{m}$) used to align CLC systems. Other methods to achieve a helicoidal structure use anisotropic deswelling but this process takes $\sim 8+$ hours. ^[13,19,25] The approach reported here resulted in a CLCE film with thickness exceeding 50 μm , contributing to variability in alignment but increasing the directionality of observable

specular reflection. The resin was cooled between two glass slides to 60°C, between the broad chiral nematic phase transition temperature of 40°C and the transition from a chiral nematic to the isotropic phase (T_{NI}) at 70°C, as indicated by differential scanning calorimetry (DSC) measurements performed on the resin (**Figure S4.1**). At 60°C, the cell was gently sheared manually, uniaxially, and repeatedly heated and cooled around this temperature to enhance the alignment of the chiral nematic phase and obtain an apparently red, reflective surface, indicative of the presence of the chiral nematic phase. The resin system was photopolymerized using visible light to initiate an acrylate homopolymerization at about 57°C to stabilize the chiral nematic phase but resulted in haze due to the crosslinking and randomness in alignment. The CLCE has a T_g around 6.5°C, making for an easy to handle, elastomeric freely-standing film at room temperature, with extensibility up to 130% strain (**Figure S4.2a, b and Movie S4.1**). The film was removed from the glass and upon straining, the residual haze was reduced and the CLCE appeared visually blue due to reorientation of the chiral nematic phase with a generalized depiction shown in **Figure 4.1b**. Development and optimization of the techniques for producing this freely-standing CLCE film enabled the subsequent analysis and implementation of these films as elaborated in the following sections.

The freely-standing AFT capable CLCE, demonstrates significant extensibility with over 100% strain possible as seen in **Figures 4.2a and S4.2b**, and is advantageous for achieving dramatic color changes. **Figure 4.2b and c** display UV-vis measurements of the optical characteristics of the film, where contributions from the imperfectly aligned chiral nematic phase and spacing lead to reflection in the visible regime along with contributions to haze and scattering. The presence of the reflection notch, with the reported CLCE having a center minimum of 640 nm in the UV-vis, is indicative of the presence of the chiral nematic phase (**Figure 4.2b, c**).^[26]

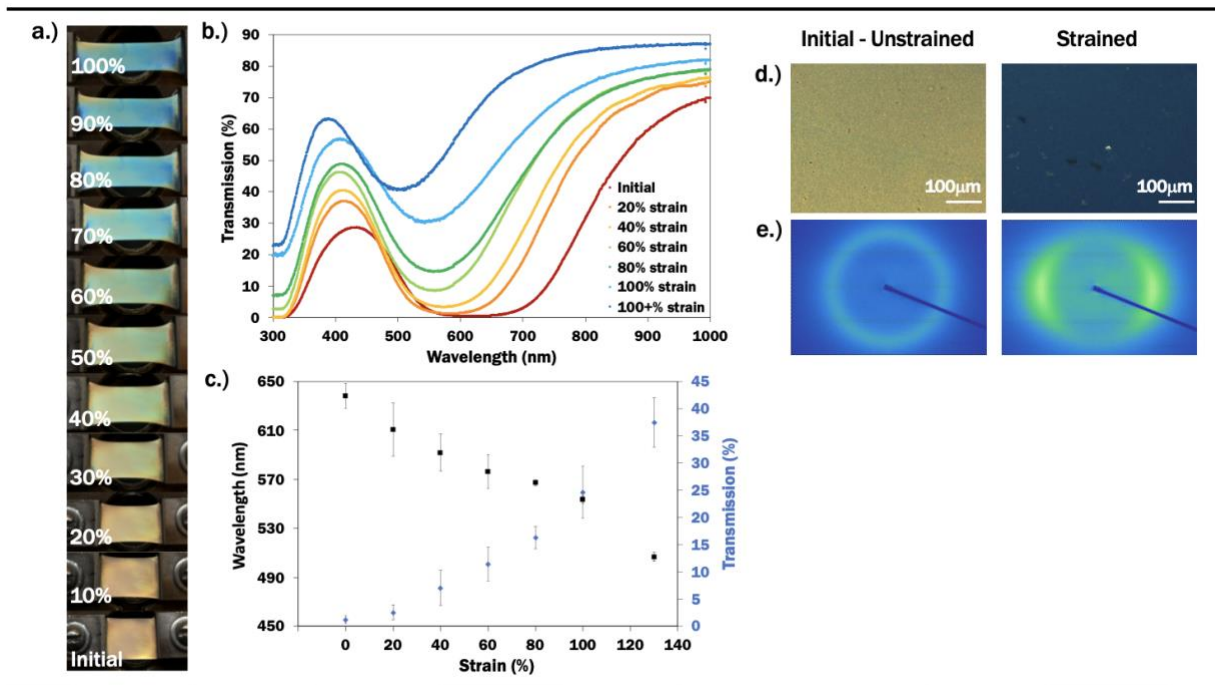


Figure 4.2: a.) Camera images of the CLCE being mechanically strained and corresponding b.) UV-Vis spectroscopy upon straining. c.) Wavelength of the film taken at the center minimum of the reflection notch at corresponding strain values. d.) Optical microscopy of the CLCE unstrained and strained. e.) WAXS on an unstrained film and then strained to 60% displaying chiral nematic alignment initially, then localization of intensity indicating a deformed chiral nematic.

As seen in **Figure 4.2b and c**, the reflection notch not only narrows and blue shifts from 640 nm to 500 nm when strained past 100% but also increases in transmission from 5% to 37%. A broad reflection notch is indicative of heterogeneities in the alignment and pitch spacing. Here, as the material is strained, the alignment and uniformity of the sample improve as seen through the narrowing of the notch.^[18,26] The CLCE displays the reflection notch and also has below 5% transmission of light so a control sample polymerized at the same conditions of the CLCE, but prepared without the chiral monomer, was analyzed by UV-vis. The a-chiral control displays a lack of the reflection notch and maintains below 5% transmission as initially polymerized and unstrained due to the polydomain alignment that forms during the photopolymerization (**Figure S4.3**).

Qualitative analysis on the domain structure and alignment was done using optical microscopy (OM), wide-angle X-Ray scattering (WAXS), and scanning electron microscopy (SEM). OM done on the CLCE gives evidence for the lack of a well-aligned chiral nematic phase evident in grain like texture (**Figure 4.2d**). Further investigation of the material via SEM on a cryo-microtomed sample as polymerized shows the CLCE does contain a chiral nematic phase as seen from the signature repeating lamellar-like structure imaged through the thickness of the film (**Figure S4.4**).^[12,18] WAXS done on the CLCE (**Figure 4.2e**) displays the initial isotropic halo expected for the chiral nematic phase. Upon uniaxial deformation, the localization of intensity is indicative of deviation from the periodic structure observed previously when CLCEs are uniaxially deformed.^[13,25,27-30] Mechanical deformation concurrently results in a reduction of the haze and improved transmission with the thinning of the material in the z direction. Furthermore, as the material is strained and the thickness decreases, this change causes a decrease in the pitch along with an unwinding of the helix of the chiral nematic phase, resulting in a blue shift or a narrowing of the reflection notch (**Figure 4.1b**).^[13,25,27-30] WAXS done on the same control discussed above (**Figure S4.5a**), shows minimal localization in the unstrained sample due to gentle shear-induced alignment used to mimic the procedure for the CLCE. Upon deformation, apparent reorientation of mesogens occurs in correlation to the localized intensity in the diffraction pattern, typical of an LC system with increased monodomain alignment (**Figure S4.5b**). Finally, comparing the stress-strain profiles of the CLCE and the control, it is apparent that the presence of the chiral monomer and thus the chiral nematic phase alters the soft elasticity the material exhibits when subjected to load (**Figure S4.2b**).^[22]

The CLCE was designed with the latent ability to perform bond exchange with light-activated AFT to enable reconfiguration of the network on demand with spatiotemporal control

afforded by light activation. An AFT capable species, the allyl dithiol, was incorporated into the backbone of the network to facilitate reversible bond exchange when activated (**Figure S4.6**). The AFT used here is initiated using light, selectively chosen for this system to decouple the temperature sensitive phase behavior of the LCs from the bond exchange activation. Uniaxial strain to 100% coupled with varying UV light exposure was performed at room temperature to program the LC order to varying extents. With increased exposure time and the corresponding continued activation of the DCC-induced relaxation of the sample towards equilibrium, the material's overall shape and color change are programmed to a greater degree, with the final programmed strain measured in both the LC phase at room temperature and the isotropic phase at high temperature (**Figure 4.3a, b**). The general response of AFT-capable LCEs to light programming was examined previously by McBride *et al.*, and these networks are expected to behave similarly though in the presence of a chiral monomer.^[20] The AFT exchange occurs only during radical generation while the light is turned on, allowing for spatiotemporal reconfiguration of the network during the exposure.

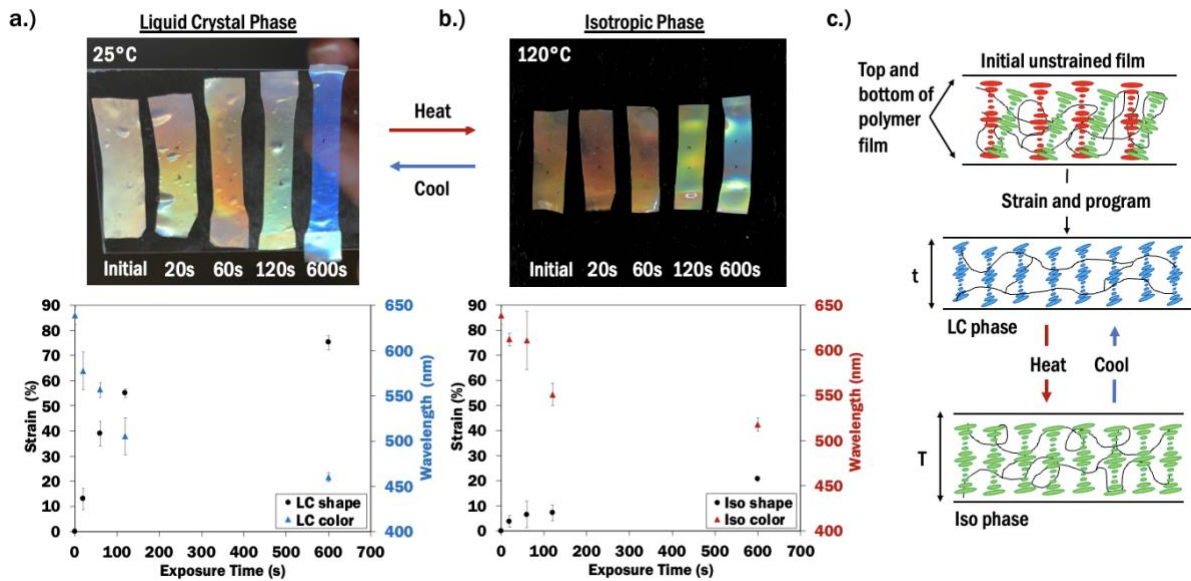


Figure 4.3: Values for CLCEs of the wavelength measured at the center minimum of the reflection notch and % strain from the initial length after programming, measured in the a.) LC phase and b.) Isotropic phase: programming done at 25°C, strained to 100%, exposed with light at 320-390 nm and 70 mW/cm² intensity for varying amounts of time (20 s, 60 s, 120 s, 600 s) and corresponding images. c.) Schematic of chiral nematic alignment before and after programming in the LC and isotropic phase with improvement to overall alignment but some deformation to the pitch.

The dependence of programmability on UV exposure conditions was investigated and used to manipulate the optical characteristics of the CLCE films. Measured in the LC phase at room temperature, the unstrained film starts with a center minimum reflection notch at 640 nm. The final center minimum in the reflection notch shifts to 577 nm, 556 nm, 505 nm, and 459 nm after exposure times of 20 s, 60 s, 120 s, and 600 s, respectively (**Figure 4.3a**). Increases in exposure time enable prolonged and more effective reconfiguration, resulting in a larger change in final strain and color as compared to the initially unstrained state. An overall wavelength shift of 181 nm was achieved from the initial film to the film exposed at the longest time of 600 s. After this exposure time of 600s, the permanent shape change achieved in the LC phase reaches a max of 75% strain as compared to the initial starting shape. When measured in the isotropic phase, after the max exposure time of 600s, the center minimum notch wavelength reaches 517 nm, and the

permanent shape change is only 20% strain. Here, the wavelength changes 123 nm from the initially unstrained state. It is important to note that an unexposed sample strained to 20% has a center minimum reflection notch at 611 nm, while after programming the reflection notch for 600 s, the programmed film measured in the isotropic phase having a 20% change in strain from the initial film is 100 nm lower, at 517 nm (**Figure 4.3b**). When the programmed film is heated to or above the isotropic temperature, the material reverts back in shape with only a 20% difference in strain from the initial, unprogrammed sample, but the color is still visually blue and does not revert back to an equivalent degree, with the color not directly correlating to the same strain/color profile of an initially polymerized film (**Figures 4.2a, b, c**). This behavior is an indication of the improvement and stabilization of the chiral nematic alignment from random to more selective along with stabilization of deviations to the periodic structure during AFT activation as seen in a generalized depiction in **Figure 4.3c**. It was concluded that extended exposures of the CLCE at the same strain increasingly programmed the shape and color of the material.

After quantitative measurements were performed on the reconfigured samples, qualitative observations were made using polarized OM (POM) on the structure of the LC phases. POM was used to assess LC alignment after UV exposure in comparison to the initial, unprogrammed film. The unprogrammed film displays nonuniformities in alignment as seen by a nonuniform color under POM and little change in birefringence upon viewing at 45 degrees (**Figure S4.7**). Observing the programmed CLCEs in the POM at 45 degrees to the polarizer shows the change in birefringence in comparison to the same CLCEs observed at 0 degrees, along with increased uniformity of color, supporting the conclusion that there is increased improvement and stabilization of the altered chiral nematic alignment as the CLCE is exposed for longer times under strain.

In addition to shifting the reflection notch and improving alignment by exposure in strained states at room temperature, erasing the reflection notch was achieved by activating AFT while the films were heated past the isotropic phase at 120°C where the LCE prefers a more random, isotropic configuration. Two sets of experiments were done; a set of samples kept between the glass slides they were polymerized in, and another set where the samples were removed from the glass as freely-standing films (Figures 4.4a, b). The samples were exposed to UV for varying amounts of time (10 s, 60 s, 600 s) at 120°C. The samples between glass, appeared to erase the reflection notch completely after 60 s of exposure, whereas the freely-standing films took 600 s of exposure to achieve the same erasure. Observing the UV-vis spectra, the reflection notch gradually disappears as the sample is exposed for longer times.

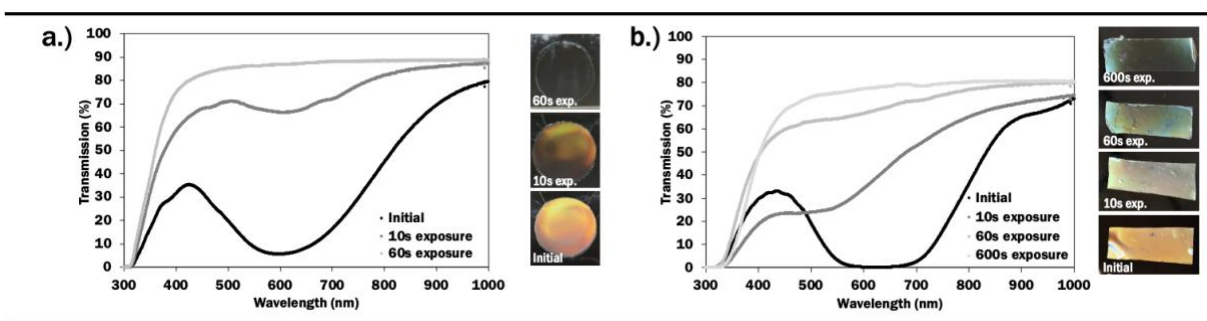


Figure 4.4: a.) UV-vis on erasing reflection band for samples fixed between glass, exposed with light at 320-390 nm and 70 mW/cm² intensity, at 120°C for varying amounts of time (10 s, 60 s) b.) Same experimental conditions done on free standing films (10 s, 60 s, 600 s).

After color reconfiguration and erasure were investigated, the cyclability of the material was examined. Concluding from the previous investigation, for both programming of and erasing of reflection notches by low and high temperature activation of the AFT process, domain boundaries are being eliminated resulting in increased transmission. A series of experiments were done to demonstrate the cyclability of the CLCE where **Step 1**: Initially unstrained films were measured in the UV-vis followed by **Step 2**: films were strained to 100% and irradiated for 180 s to program

a blue shift. **Step 3:** The films were then heated to the isotropic phase at 120°C, and exposed again for 10 s, programming the material back to a red shift. **Step 4:** The film was then strained again to 100%, with the associated blue shift, but transmission decreases during every step and will eventually result in a material with a completely erased reflection notch, no longer having a meaningful reflective nature (**Figures 4.5a, b**).

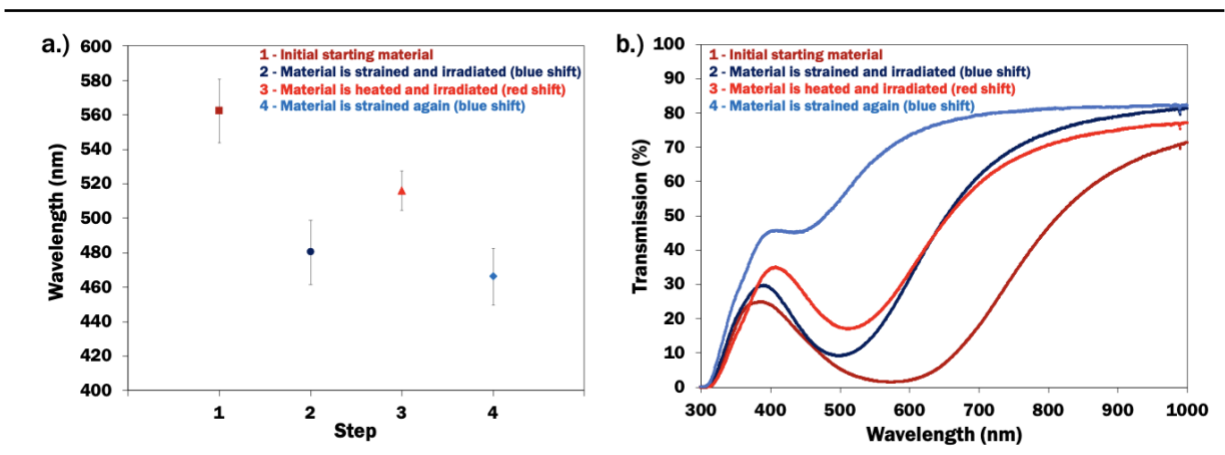


Figure 4.5: Demonstration of cycling back and forth between red and blue shifts. a.) Wavelength of the sample measured at the center minimum reflection notch of the curve done at each step and b.) the representative UV-vis curves for those values at each step.

The cyclability for programming or erasing of the CLCE is ultimately limited by the amount of photoinitiator in the system as well as the integrity of the remaining alignment capable of creating a meaningful reflective surface. The material demonstrates 1 full cycle of programming from red to blue and half a second cycle being able to program back towards red, with a significant reduction in the integrity of the reflection notch when strained back to blue.

Control over shape and color reconfiguration of the AFT capable CLCE was displayed which led to a series of photopatterning experiments done to demonstrate spatiotemporal control over the programmability of the material, resulting in complex patterns within the CLCE. Using a photomask with a striped pattern of varying line spacings, the CLCE was selectively patterned to

achieve apparently blue shifted lines and upon heating, the patterned regions red shift, but because of their inability to completely shift back, the lines appear a yellow/green color in contrast to the red un-patterned regions (**Figure 4.6a**). Image analysis (**Figure S4.8**) was done on the photopatterned samples from **Figure 4.6a** to demonstrate the level of spatial control that is achieved by photopatterning the DCC activation. Quantified regions of low and high intensities that correspond to the blue shifted exposed stripes and red unexposed regions. As expected, based on the mechanism of the DCC activation, on these scales, there is no loss in fidelity of the pattern during exposure and the spatial change in the behavior mimics the spatial pattern of the light exposure. Similarly, a chameleon skin display was created by patterning the CLCE with a uniquely shaped photomask to imitate the pattern of a chameleon's skin, where the pattern appears blue and yellow in the chameleon's "relaxed" state, but upon heating the material to its isotropic phase, appears green and red in the chameleon's "excited" state (**Figure 4.6b**).

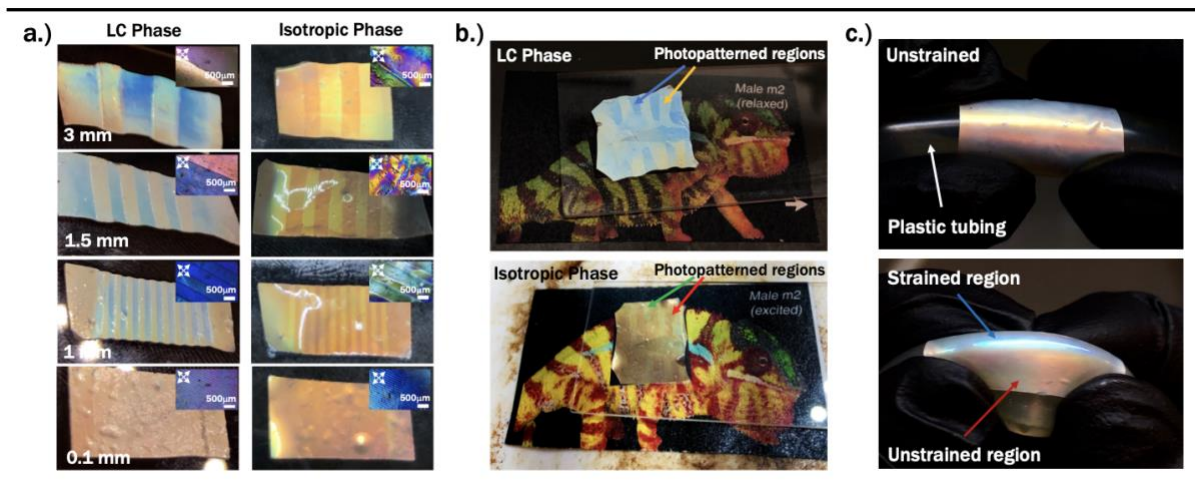


Figure 4.6: a.) Photo patterned lines of varying distances indicated in the bottom left corner of each photo, shown at room temperature in the LC phase and at 120°C in the isotropic phase. Cross-Polarized POM images are inset in the corners. b.) Photo patterned chameleon skin, (top) shown in the LC phase (25°C) and (bottom) shown in the isotropic phase (120°C). Chameleon background image used from Teyssier *et al.* [5] c.) The CLCE is wrapped around plastic tubing to demonstrate strain mapping when the tube is pulled with the top region of the film appearing blue under strain while the sides undergo little to no strain and remain red.

The material behaves just like a chameleon's skin which as discussed above, changes the spacing of the repeating structure to achieve different wavelengths of light reflected, making it helpful in situations where signaling or camouflage are necessary and need to become apparent at the user's discretion. Finally, a strain mapping demonstration was done by wrapping the CLCE around plastic tubing (**Figure 4.6c**). As the tube is bent and strained, the CLCE changes color in only the strained regions, giving valuable information as to where strain is being applied to an object the CLCE is wrapped around, and potentially how much strain is sustained. The strained regions of the film appear visibly blue while the unstrained regions remain red in color. **Figure S4.9** displays a 3D rendering of the optical response of the strained material's surface by image analysis done through measurements taken through the center of the film, moving from low intensity values in the blue shifted strained regions to high intensity values for the red colored unstrained regions, further demonstrating the potential for using this approach for analysis of the material's strain mapping capabilities. The CLCE is capable of not only achieving complex patterns, but can also be functional for strain mapping applications, amongst other uses even when permanent reconfigurations with AFT are not necessary.

4.3 – Conclusions

LCEs have demonstrated their unique and useful capabilities to preserve LC phase behavior with a polymer network for applications ranging from soft robotics to optics. Taking this technology a step further, the CLCE reported here is a visibly reflective, freely-standing extensible material, with the incorporation of DCC, thus allowing the user to permanently reconfigure the shape and ultimately the color or erasure of color from the material, and also enabling complex patterning. The color of the material was shown to be inherently linked to dimensional changes in

the LC structure from deformations to the network and is stabilized through activation of the DCC to reconfigure the network into an energetically favorable state. A level of temporary thermoreversibility has been demonstrated after programming along with one and a half programming cycles prior to loss of color integrity. The colored reflective integrity of the CLCE is also effectively shown to be erasable. The CLCE was patterned to mimic chameleon skin camouflage and also has use in textiles or dynamic optical applications. The CLCE is a freely-standing film, which further enhances the potential applications of the material as it is not confined to a glass cell like many other previously explored technologies, allowing the material to be conformable around complex structures to demonstrate its use in strain mapping applications amongst others.

4.4 – Experimental

Materials

1,4-Bis-[4-(6-acryloyloxyhexyloxy)-benzoyloxy]-2-methylbenzene (RM82) was purchased from Wilshire Technologies. Irgacure 2959 and LC756 were obtained from BASF. 3-Chloro-2-(chloromethyl)-1-propene, NPGDA, dichloromethane (DCM), Ethylenediamine, Diphenyl(2,4,6-trimethylbenzoyl) phosphine oxide (TPO), and triethylamine (TEA) were purchased from Sigma-Aldrich. Ethanol was purchased from Decon Laboratories Inc. Potassium ethyl xanthate was purchased from Bean Town Chemical. All chemicals were used as received unless otherwise noted.

Synthesis Steps for LC Oligomers (Synthesizing Allyl Dithiol)

2-Methylene-1,3-propanedithiol (allyl dithiol) was synthesized as previously reported in McBride *et. al.*^[20] Potassium ethyl xanthate (56.45 g, 352 mmol) was dispersed into 500 mL of ethanol in a 1000 mL round bottom flask with a stir bar. 3-Chloro-2-(chloromethyl)-1-propene (20 g, 160 mmol) was added dropwise and the reaction was allowed to stir overnight. Solids were removed with a filter funnel. Ethanol was removed via rotary evaporation. The product mixture was then dissolved with diethyl ether (100 mL) and water (200 mL). The organic layer was removed and washed with brine (100 mL). The organic layer was again removed and dried with sodium sulfate. Sodium sulfate was then filtered off and the ether was then rotavap'd off to yield the protected allyl dithiol as a yellow low viscosity liquid. In a sealed 100 mL round bottom with a stir bar, coupled to an addition funnel, purged of air and water and backfilled with argon, ethylenediamine (16.8 mL) was added. The protected allyl dithiol (10 g, 33.7 mmol) was then added to the ethylenediamine dropwise and allowed to react for 4 hours while kept at room temperature. After, the reaction mixture was slowly added to a mixture of sulfuric acid and of ice (64 mL, 400 mL). Diethyl ether was then added to the mix. The aqueous layer was decanted, setting the organic phase to the side, and the aqueous layer was washed with ether again to collect any more remaining product. The organic phases were combined and washed with 2 M sulfuric acid (200 mL). The organic phase was then washed with brine (2x, 200 mL) to remove any excess water. Sodium sulfate was added to further remove excess water. The sodium sulfate was then filtered off and the remaining ether rotavap'd. The solution was then distilled (60°C, 0.1 mmHg) to obtain the purified allyl dithiol. ¹H nuclear magnetic resonance (NMR) (400 MHz, CDCl₃, 25°C): 4.99 (broad singlet, 2H), 3.37 to 3.34 (multiplet, 4H), 1.48 (triplet, J = 8.15 Hz, 2H).

Synthesis Steps for LC Oligomers (Purifying NPGDA)

NPGDA was purified via flash chromatography. Column was set to 30% ethyl acetate, 70% hexanes using Biotage Isolera One. Inhibitor dibutylhydroxytoluene (BHT) was added at 100-ppm concentration.

Synthesizing LC Oligomers

Diacrylate liquid crystalline oligomers were synthesized via a catalyzed Thiol-Michael reaction as previously reported in McBride *et. al.* [20] RM82 (8.8 g, 13.15 mmol) was added to a 100 mL round bottom flask with a stir bar. 40 mL of DCM was added to dissolve the RM82. NPGDA (1.39 g, 6.57 mmol) was added to the flask. The BHT (0.012 g) inhibitor was added to the flask. The reaction was then catalyzed with TEA (8 g, 78.9 mmol). The reaction was then allowed to stir overnight with a loose plastic cap covering the opening of the flask. The reaction mixture was then rotavap'd to remove TEA. The mixture was then rinsed out 3x with DCM into a separatory funnel and then washed with 1 M HCL (100 mL). Washed with brine (2x, 100 mL) to remove excess water. Sodium sulfate was added to the organic phase to further remove any water. The DCM was then rotavap'd off and a viscous liquid remained. This was further dried over night at 40°C with air blowing over it, yielding an opaque resin. NMR was used to confirm the consumption of thiols using end group analysis of acrylate protons as compared to protons on the allyl moiety to determine repeat units. The molar ratio of components in this system are 1:0.5:1.35 RM82:NPGDA:Allyl Dithiol was used for all results shown.

CLCE Polymerization

To create the CLCE, a radical acrylate homopolymerization was done. The diacrylate oligomers were dissolved in DCM (100 mg/mL). Photoinitiators, TPO and 2959, were separately dissolved in DCM (10 mg/mL). The CLC monomer LC756 (4 wt%) (a diacrylate) was added directly to the dissolved oligomers. TPO and of 2959 (1.5 wt%, 1 wt%), were added to the oligomer solution. The solution was vortexed and deposited onto a RainX coated piece of glass where the solvent was then evaporated off at 130°C on a hotplate, leaving a clear viscous resin. A second piece of RainX coated glass was placed onto the material with 70 μ m spacers in between. The sample was then allowed to cool and manually sheared uniaxially (forwards and backwards), until a reflective surface was achieved upon cooling to 60°C, with repeated heating and shearing on the 60°C hotplate. The cell was then placed on the hotplate at 57°C and photopolymerized for 180 seconds on each side with a light intensity of 70 mW/cm² using a 400-500 nm filter and an Exfo Acticure Hg Bulb.

CLCE Characterization (Mechanical Characterization)

DMA: Mechanical analysis was run on a TSA RSA-G2. T_g scans were run at a ramp rate of 3°C/min at a frequency of 1 Hz. Stress strain tests were done at room temperature and strained at a rate of 0.1 mm/s. DSC: DSC was run on a TA DSC 2500. The resin was initially heated to erase thermal history, cooled, and the test was run from -40C to 140°C, ramped at 10°C/min, then cooled at the same rate to generate the reported curve.

CLCE Characterization (UV-Vis Measurements)

UV-Vis was run on a Thermo Fisher Scientific Evolution 300. Samples were measured with a Xenon lamp in absorbance between 300-1000 nm with a scan speed of 240 nm/min. A background was run and subtracted from the data. Data intervals were taken at 0.5 nm and a bandwidth of 2 nm. Data was then converted to Transmittance through the formula $[T = 10^{-A+2}]$. Quantitative measurements of the reflection notch were done by recording the center minimum value of the notch.

AFT Programming (Programming reflection notch)

The 100 μm thick polymerized film was strained 100% and exposed at room temperature for varying amounts of time (20s, 60s, 120s, 600s) with a light intensity of 70 mW/cm^2 using a 320-390 nm filter and an Exfo Acticure Hg Bulb. UV-vis was then run on each sample. Measurements of color and strain after programming: **Color** - Quantitative measurements of the reflection notch were done by recording the center minimum value of the notch. **Strain** - Two dots were placed at the center each film and the distance between them was measured prior to straining the sample. The sample was then strained to 100% and irradiated for varying amounts of time. After the irradiation the sample was thermally cycled and the distance between the dots was measured at room temperature in the LC phase and also at high temperature (120°C) in the isotropic phase.

AFT Programming (Erasing reflection notch)

As polymerized films between glass and free-standing films - The 100 μm thick polymerized film was placed on a hotplate at 120°C and irradiated for varying amounts of time (10s, 60s, 600s) with

a light intensity of 70 mW/cm² using a 320-390 nm filter and an Exfo Acticure Hg Bulb. UV-vis was then run on each sample.

AFT Programming (Red and Blue shift cycling display)

The 100 μm thick polymerized film underwent a series of steps with programming done at a light intensity of 70 mW/cm² using a 320-390 nm filter and an Exfo Acticure Hg Bulb. UV-vis was then run at each step. **Step 1:** Prepared initially unstrained films **Step 2:** Films were strained to 100% and irradiated for 180s to program a blue shift. **Step 3:** Films were then heated to the isotropic phase at 120°C and exposed again for 10s. **Step 4:** The film was then strained again to 100%.

AFT Programming (Photopatterning)

The 100 μm thick polymerized films were uniaxially stretched to 100% strain. A photomask was then placed over the film and it was then irradiated for 5 minutes at room temperature on one side with a light intensity of 70 mW/cm² using a 320-390 nm filter and an Exfo Acticure Hg Bulb. Measurements were done in ImageJ of the patterned profile for each film excluding the 0.1 mm spaced samples because the stripes were unable to be individually resolved. ImageJ was also used for strain mapping analysis.

X-ray Diffraction Measurements

WAXS was done on the CLCE and a control film containing no chiral monomer. WAXS was done with a Forvis Technologies instrument using a copper source ($\lambda = 1.5405 \text{ \AA}$). The detector was a Dectris Eiger R 1 M with a 0.075 x 0.075 mm² pixel size. The 250 μm thick polymerized films were scanned initially unstrained and then strained to 60% and scanned again.

SEM

Cryo-microtoming was done on the CLCE for SEM analysis with a Leica EM UC7 (cryo EM FC7) done at -80°C at NIST. Field Emission SEM (FESEM) was done with a JEOL JSM-740 1F on the microtomed samples.

4.5 – Acknowledgements

This work was completed with the financial support of NSF DMR 1809841. The authors gratefully acknowledge the use of facilities and instrumentation supported by the NSF MRSEC Grant DMR-1420736 performed by Vikina Martinez, the COSINC-CHR facility for use of their SEM at the University of Colorado at Boulder, the National Institute of Standards and Technology for the use of their cryo-microtome and Adrienne Blevins who operated the machine, a PhD student in Dr. Yifu Dings' lab at the University of Colorado at Boulder. The authors gratefully acknowledge Dr. Tim White's lab at the University of Colorado at Boulder, for the use of their DSC and discussion. The authors would like to acknowledge Dr. Lewis Cox of Montana State University and Carmen Martinez a PhD student at the University of New Mexico.

4.6 – Supporting Information

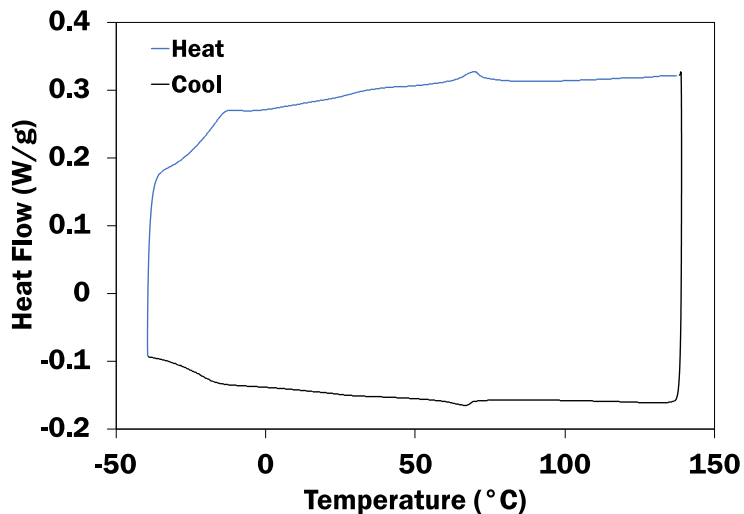


Figure S4.1: DSC on the cholesteric doped resin. Working temperature to shear resin between glass is done at 60°C, between the two-phase transitions, chiral nematic phase at 40°C and T_{NI} at 70°C.

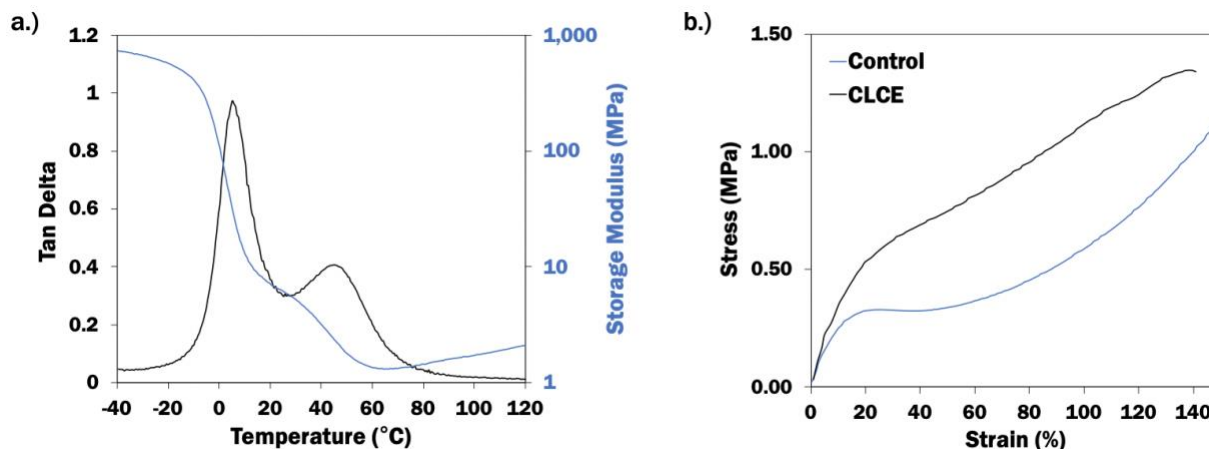


Figure S4.2: Analysis of CLCE mechanical properties a.) DMA T_g and storage modulus for the CLCE with a T_g around 6.5°C. b.) DMA Stress vs. Strain to break, showing how the CLCE has an altered strain profile due to the deformation of the chiral nematic phase.

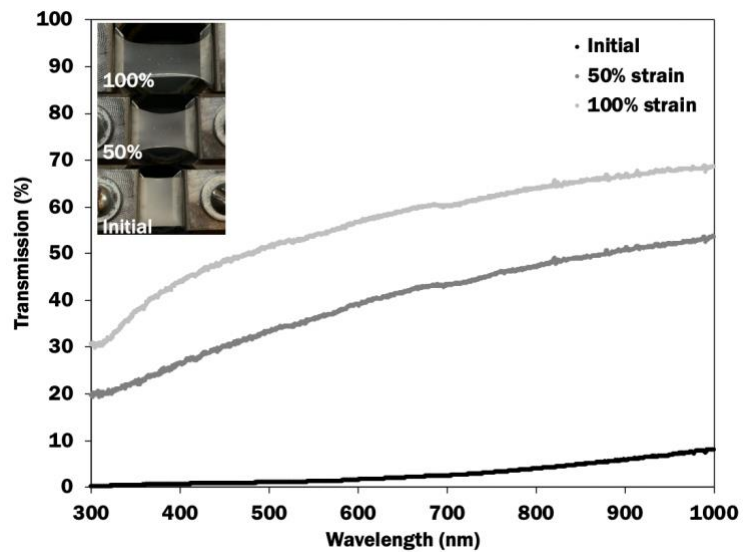


Figure S4.3: Control UV-Vis as the material is strained to 100%. Transmission improves as the material is strained.

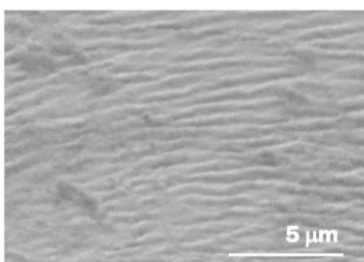
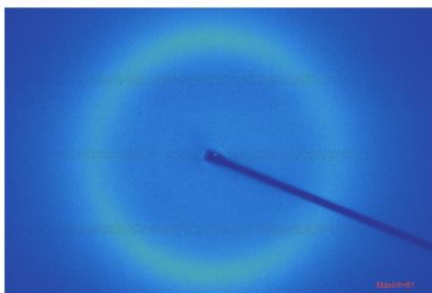


Figure S4.4: SEM on a cryo-microtomed unstrained and unprogrammed sample with imperfect lamellar orientation indicative of random alignment.

a.) Initial - Unstrained



b.) Strained 60%

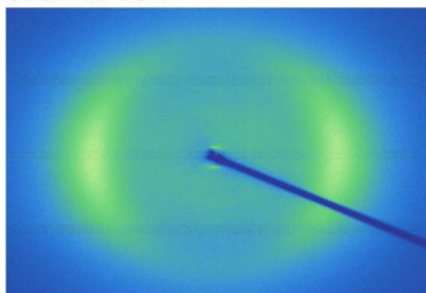


Figure S4.5: Control WAX for a.) unstrained material and b.) material strained to 60%. Weak localization of intensity at the top and bottom of the unstrained WAX diffraction pattern

confirming some alignment induced by slightly shearing the sample before polymerization. Straining the sample reorients mesogens to display a nematic with a biased ordering pattern.

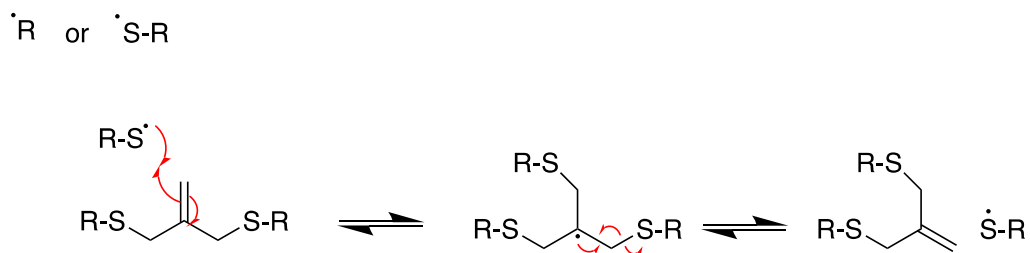


Figure S4.6: AFT exchange mechanism. A radical from the photoinitiator or a thiyl radical can induce bond exchange.

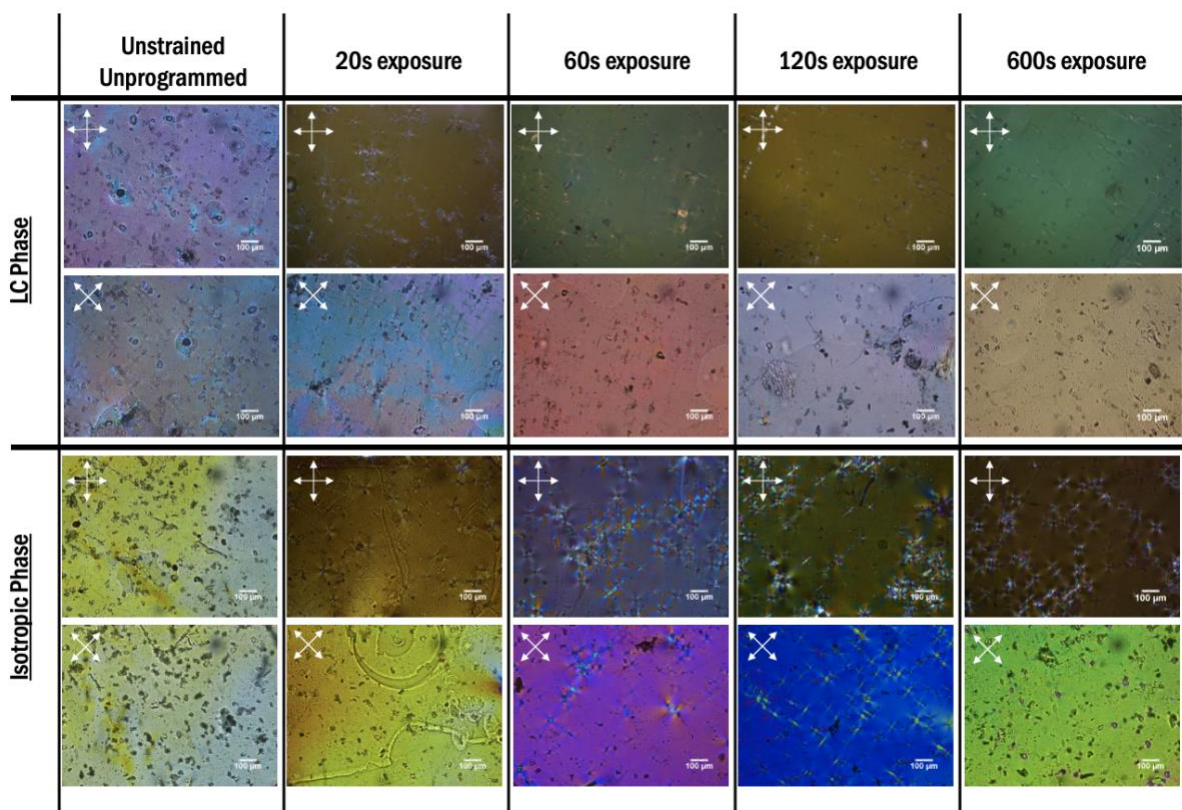


Figure S4.7: Polarized optical microscopy of the CLCE initially unprogrammed and unstrained, and programmed samples in the LC phase and Isotropic phase as indicated for varying exposure times (20 s, 60 s, 120 s, 600 s).

Movie S4.1: Uniaxial straining of CLCE

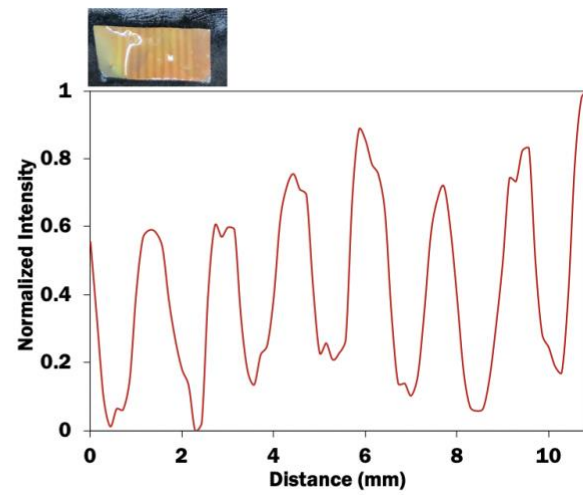
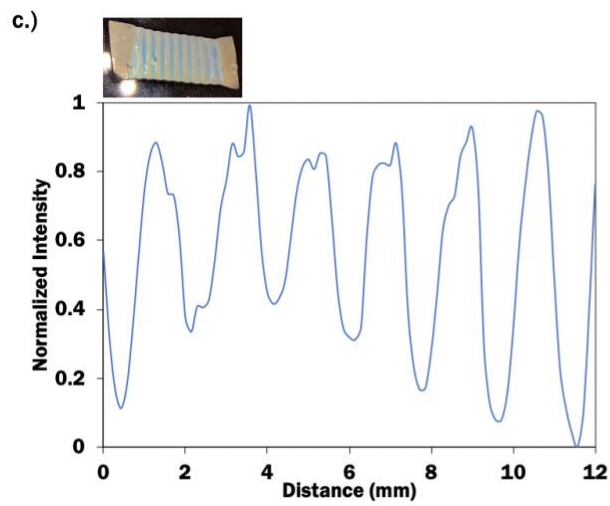
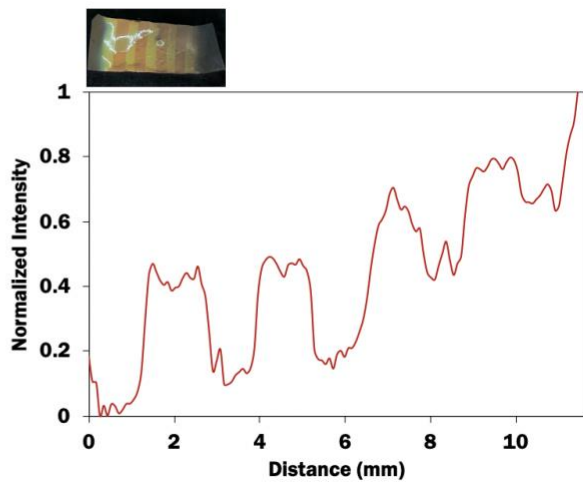
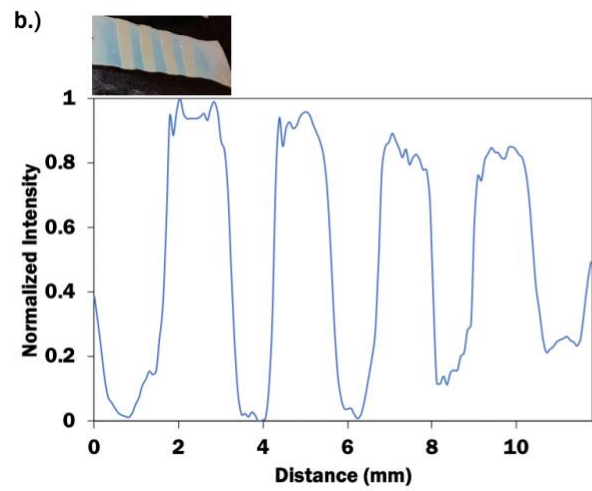
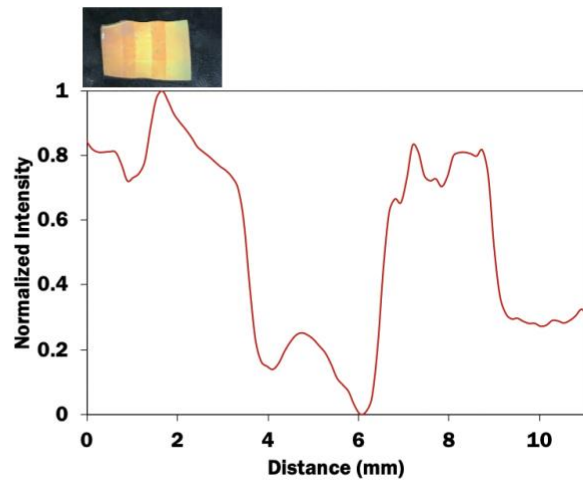
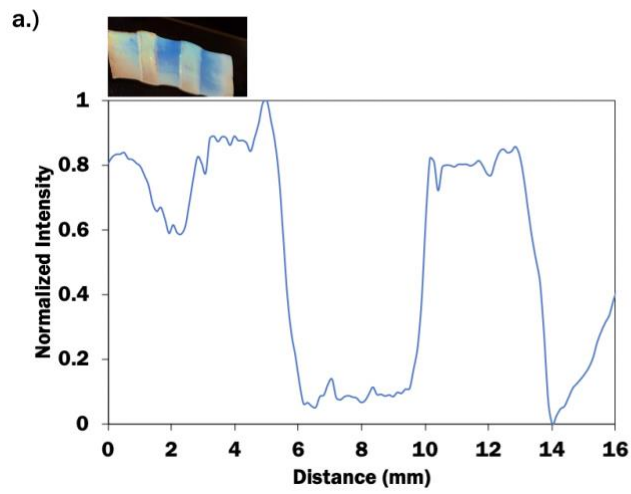


Figure S4.8: Image analysis done on photopatterned films measured in the (left-blue) LC phase, and (right-red) isotropic phase a.) 3 mm line spacing b.) 1.5 mm line spacing c.) 1 mm line spacing. Measurements in ImageJ were taken across the profile of each film from left to right recording the change of intensity vs. distance measured. Blue shifted regions were recoded to have a lower intensity value and the unexposed red regions recorded a higher intensity value, graphically displayed.

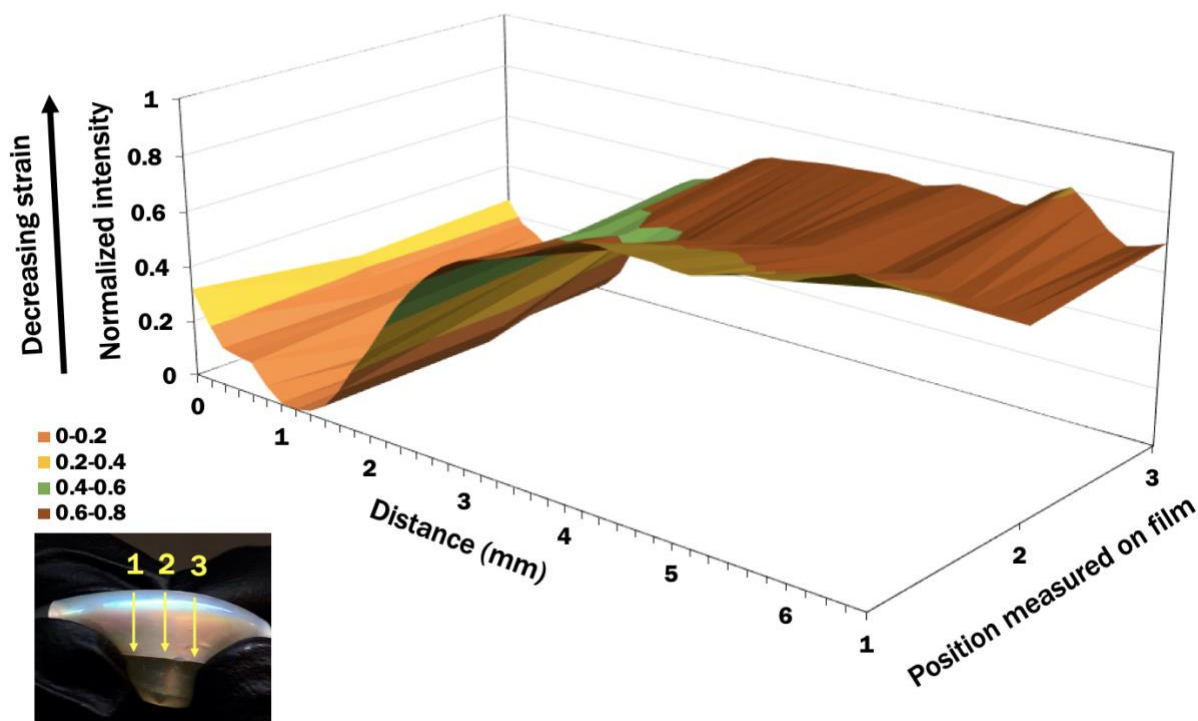


Figure S4.9: Image analysis done using ImageJ on the CLCE wrapped around a plastic tube and strained. Yellow arrows portray direction of measurement for three measurements done. The three measurements were taken down the center of the film, recording the intensity values across the measured region. Normalized intensity increases as strain on the material decreases and the color of the material shifts from blue, highly strained region, to red, unstrained region.

4.7 – References

- [1] Bienz, E. F, (Thermal Camouflage). *U.S. Patent*. 4,156,033. **1979**.
- [2] Han, T.; Bai, X.; Thong, J. T. L.; Li, B.; Qiu, C.-W. *Adv. Mater.* **2014**, *26*, 1731.
- [3] Yu, H.; Shao, S.; Yan, L.; Meng, H.; He, Y.; Yao, C.; Xu, P.; Zhang, X.; Hu, W.; Huang, W. *J Mater. Chem.* **2016**, *4*, 2269.
- [4] Ramsley, A. O. (Camouflage Patterns - Effects of Size and Color). *U.S. Army NATICK R&D*. Natick/TR-79/030. **1979**.
- [5] Teyssier, J.; Saenko, S. V.; van der Marel, D.; Milinkovitch, M. C. *Nat. Commun.* **2015**, *6*, 1.

- [6] Zhang, W.; Kragt, S.; Schenning, A. P. H. J.; de Haan, L. T.; Zhou, G. *ACS Omega* **2017**, *2*, 3475.
- [7] Kim, Y.; Tamaoki, N. *J. Mater. Chem.* **2014**, *2*, 9258.
- [8] White, T. J.; Bricker, R. L.; Natarajan, L. V.; Tondiglia, V. P.; Green, L.; Li, Q.; Bunning, T. J. *Optics Express* **2010**, *18*, 174.
- [9] Ge, J.; Yin, Y. *Angew.* **2011**, *50*, 1492.
- [10] Moirangthem, M.; Schenning, A. P. H. J. *ACS Applied Materials & Interfaces* **2018**, *10*, 4168.
- [11] Burton, E. R. (Color Changing Contact Lenses). *U.S. Patent*. US 8,542,325 B2. **2013**.
- [12] Kim, D.-Y.; Lee, K. M.; White, T. J.; Jeong, K.-U. *NPG Asia Materials* **2018**, *10*, 1061.
- [13] Finkelmann, H.; Kim, S. T.; Muñoz, A.; Palffy-Muhoray, P.; Taheri, B. *Adv. Mater.* **2001**, *13*, 1069.
- [14] Xie, M.; Hisano, K.; Zhu, M.; Toyoshi, T.; Pan, M.; Okada, S.; Tsutsumi, O.; Kawamura, S.; Bowen, C. *Adv. Mater. Tech.* **2019**, *4*, 1800626.
- [15] Kragt, A. J. J.; Broer, D. J.; Schenning, A. P. H. J. *Adv. Funct. Mater.* **2018**, *28*, 1704756.
- [16] White, T. J.; McConney, M. E.; Bunning, T. J. *J. Mater. Chem.* **2010**, *20*, 9832.
- [17] Mulder, D. J.; Schenning, A. P. H. J.; Bastiaansen, C. W. M. *J. Mater. Chem.* **2014**, *2*, 6695.
- [18] Brannum, M. T.; Steele, A. M.; Venetos, M. C.; Korley, L. T. J.; Wnek, G. E.; White, T. J. *Adv. Opt. Mater.* **2019**, *7*, 1801683.
- [19] Kizhakidathazhath, R.; Geng, Y.; Jampani, V. S. R.; Charni, C.; Sharma, A.; Lagerwall, J. P. F. *Adv. Funct. Mater.* **2020**, *30*, 1909537.
- [20] McBride, M. K.; Martinez, A. M.; Cox, L.; Alim, M.; Childress, K.; Beiswinger, M.; Podgorski, M.; Worrell, B. T.; Killgore, J.; Bowman, C. N. *Sci. Adv.* **2018**, *4*, 1.
- [21] Yakacki, C. M.; Saed, M.; Nair, D. P.; Gong, T.; Reed, S. M.; Bowman, C. N. *RSC Adv.* **2015**, *5*, 18997.
- [22] White, T. J.; Broer, D. J. *Nat. Mater.* **2015**, *14*, 1087.
- [23] Kloxin, C. J.; Scott, T. F.; Adzima, B. J.; Bowman, C. N. *Macromolecules* **2010**, *43*, 2643.
- [24] Zhang, G.; Peng, W.; Wu, J.; Zhao, Q.; Xie, T. *Nat. Commun.* **2018**, *9*, 1.
- [25] Cicuta, P.; Tajbakhsh, A. R.; Terentjev, E. M. *Phys. Rev.* **2004**, *70*, 011704.
- [26] Min Lee, K.; Tondiglia, V. P.; Godman, N. P.; Middleton, C. M.; White, T. J. *Soft Matter* **2017**, *13*, 5842.
- [27] Cicuta, P.; Tajbakhsh, A. R.; Terentjev, E. M. *Phys. Rev.* **2002**, *65*, 051704.
- [28] Stille, W. *Eur. Phys. J. Plus* **2009**, *28*, 57.
- [29] Warner, M.; Terentjev, E. M.; Meyer, R. B.; Mao, Y. *Phys. Rev. Lett.* **2000**, *85*, 2320.
- [30] Varanytsia, A.; Nagai, H.; Urayama, K.; Palffy-Muhoray, P. *Sci. Rep.* **2015**, *5*, 1.

Chapter 5: One- and Two-way Shape Switching Liquid Crystal Elastomer Microparticles

Liquid crystal elastomer microparticles (LCEMPs) reported here demonstrate one and two-way shape switching capabilities by modulating the network characteristics. The LCEMPs are generated via a thiol-Michael dispersion polymerization. One-way shape switching particles are designed with a stoichiometrically balanced ratio of monomers, while two-way shape switching particles utilize excess acrylate in the network structure to enable a second stage polymerization to set a new particle shape. Particles are compressed to induce alignment followed by thermal cycling to deploy the shape. The thermal phase transition inherent to liquid crystalline materials dictates the means for microparticle shape actuation. Controlling the shape and actuation of microparticles enhances their applications in drug delivery or optics.

5.1 – Introduction

Microparticles have been of interest to science for decades for their unique capabilities both as independent particles or as aggregates, for various applications including cosmetics, drug delivery, and optics.^{1,2,3} Research has been done on microparticles that have shape changing capabilities from thermal,⁴ electrical,⁵ or magnetic stimuli.⁶ Cox *et al.* developed a system to permanently program polystyrene particles to a flattened shape. This was achieved by incorporating a covalent adaptable network (CAN) to alter the static network and thus the permanent shape.⁷ Focusing on shape memory microparticles, specifically liquid crystal microparticles (LCMPs), have been studied for their unique capabilities to incorporate liquid crystalline (LC) properties into a microparticle system and have demonstrated their ability to

achieve shape changes due to manipulation of their LC alignment via thermal phase transitions.^{4,8,9,10,11}

There are various methods for generating LCMPs, including microfluidic devices which are not easily scalable systems,⁹ emulsions,¹⁰ or dispersions,¹² namely radical based precipitations.^{11,13} In 2001, Cairns et al. demonstrated success in making LCMPs using a radical based photopolymerization precipitation of LC particles.¹³ In 2004, Vennes et al. studied LCMPs via a precipitation method using radicals from a peroxide initiator. More recently in 2019 Schenning et. al developed a similar system via a photoinitiated radical based precipitation.^{14,15} These radical based systems are hindered by the presence of oxygen and the polymer properties of the material can be limited by the radical polymerization technique. Light based radical initiated polymerizations require an external light source which can be cumbersome or unavailable. Microfluidics and emulsifications have been prominent methods for generating shape changing liquid crystal elastomer microparticles (LCEMPs) but come with challenges in equipment needs or limited properties and processes.^{4,8,9,10,11}

Reported here is a facile and scalable thiol-Michael dispersion polymerization of one and two-way shape switching liquid crystal elastomer microparticles (LCEMPs). To achieve two-way shape switching, particles undergo a deformation step followed by light exposure to crosslink excess acrylates. In parallel, Schenning and coworkers most recently reported a thiol-Michael dispersion polymerization method to generate LCEMPs that undergo a light initiated radical based second stage polymerization to achieve two way shape changing LCEMPs.¹⁶ Work done by Bowman and coworkers describes a thiol-Michael dispersion polymerization to generate scalable microparticles.¹⁷ The dispersion polymerization reported here to generate the LCEMPs was done via the thiol-Michael addition polymerization reaction scheme using base to catalyze the reaction.

This method was chosen instead of radical based means demonstrated by aforementioned precipitation type methods of preparing LCMPs, which is advantageous due to: i.) its ability to be performed in oxygenated environments detrimental to radical based systems, and ii.) for the lack of the need of an external stimulus for initiation (lamp setups), which can be cumbersome or unavailable.¹⁷ This method is far simpler than a microfluidic setup required for other shape changing systems and only requires basic mechanical agitation to a reaction solution at ambient conditions. This polymerization method also expands the library of monomer combinations that can be used to achieve different mechanical properties. The crosslinked LCEMPs underwent deformation and shape recovery upon heating through their LC phase transition. One and two-way shape switching capabilities are advantageous for soft robotics, medicine, and cosmetics amongst other applications due to their ability to demonstrate meaningful actuation.

5.2 – Results and Discussion

Here, we demonstrate the facile polymerization of shape memory capable LCEMPs via a thiol-Michael dispersion polymerization. Previously reported dispersion methods utilize free-radicals to initiate their polymerizations, whereas the system reported here uses base as the catalyst, triethylamine (TEA), which is not oxygen sensitive or reliant on a light source like many radical based methods. Demonstrated is not only the one and two-way shape memory capabilities of the LCEMPs, but also the capability to easily alter stoichiometry with this thiol-Michael dispersion method to achieve particles with different material properties and/or size and behavior. Monomers as follows: liquid crystal RM82, chain extender propane dithiol (PDT), crosslinker pentaerythritol tetrakis(3-mercaptopropionate) (PETMP) and surfactant polyvinylpyrrolidone (PVP) were dissolved into solution at varying stoichiometries, and the reaction was started once TEA was

added to the solution and allowed to run overnight (**Figure 5.1a**). The stoichiometries analyzed are as follows: (PETMP:PDT:RM82): A (1:2:4), B (1:1:4), and C (1:0.5:4), with respect to moles. System A was designed with balanced molar stoichiometry, which produced observable LCCEMPs viewed under optical microscopy (OM) and displayed the characteristic birefringence of polydomain LC materials when viewed through polarized optical microscopy (POM) (**Figure 5.1b, c**). The particles on average are $13.0 \pm 4.2 \mu\text{m}$ in diameter and show polydispersity with a coefficient of variance (CV) of 33%. Upon heating the material past its isotropic phase transition (T_{NI}) to 120°C , the birefringence noticeably changes indicating the phase transition, which is important for shape memory actuation (**Figure 5.1d**). The stoichiometry is systematically altered to demonstrate the versatility of the dispersion polymerization with particle size, and property analysis investigation discussed below and summarized in **Table 5.1** along with particle size distributions recorded in **Figure S5.1**.

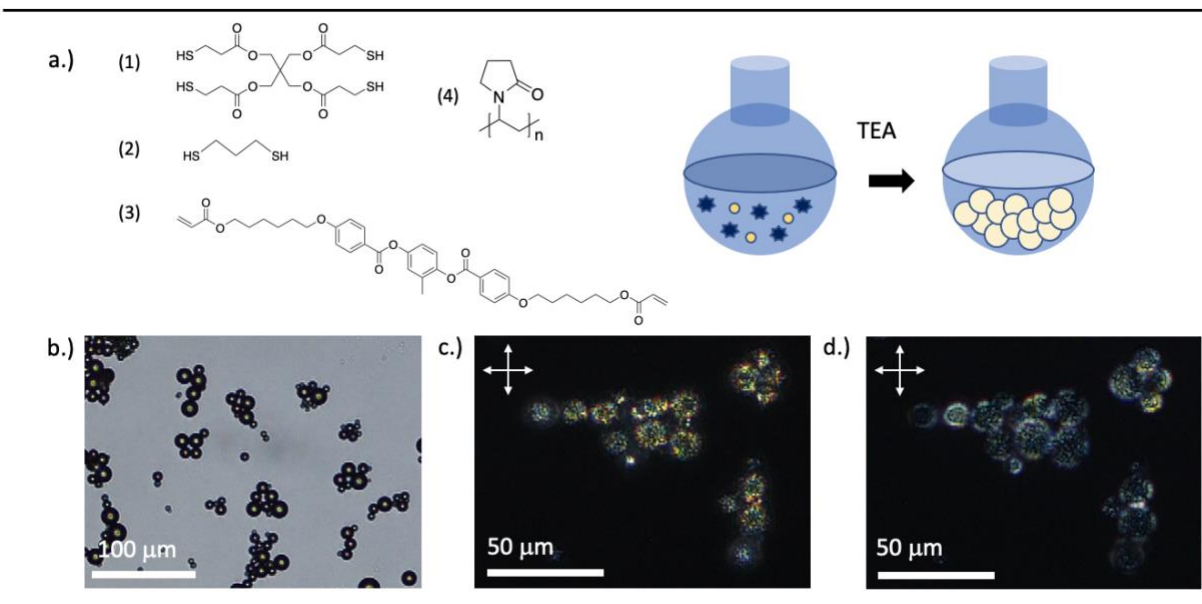


Figure 5.1: a.) Monomers and surfactant for dispersion polymerization (1) PETMP, (2) PDT, (3) RM82, (4) PVP surfactant, and TEA catalyst b.) OM of System A particles c.) POM of System A particles at room temperature d.) POM of System A particles at 120°C showing change in birefringence.

Summarized in **Table 5.1** are the material properties that change as a result of the reduction in PDT by half for each subsequent formulation along with the stoichiometric ratio (r) displaying a decrease from the balanced formulation having an r of 1. Reduction of PDT not only changes the crosslinking density but alters the liquid crystalline contribution and phase transition behavior. The gel point behavior of the system having two functionalities (fA and fB) was calculated using the Flory-Stockmayer equation (**equation 5.1**):¹⁷

$$P_{gel} = \frac{1}{\sqrt{r(f_A-1)(f_B-1)}} \quad (5.1)$$

P_{gel} is the probability of monomers that need to react to reach the gel point. P_{gel} increases with the reduction of PDT. As a result of this, it is expected that material properties will change while still maintaining a gelled network. Following this, analysis was done on the varying stoichiometries to elucidate the material properties reported in **Table 5.1**.

Table 5.1: For System A, B and C; monomer stoichiometry and polymer properties of particles. Where r is the ratio of thiol to acrylate, P_{gel} is the probability of gelation, Alignment is LC alignment determined by WAXS, D_n is average particle diameter, CV is coefficient of variance = (StDev/ D_n *100), and T_{NI} is the temperature for the LC phase transition from nematic to isotropic.

System	Stoichiometry			r	P_{gel}	Alignment	D_n (μ m)	CV	T_{NI} ($^{\circ}$ C)
	PETMP	PDT	RM82						
A	1	2	4	1	0.707	Polydomain	13.0 \pm 4.2	33%	117
B	1	1	4	0.75	0.756	Polydomain with possible secondary alignment	9.7 \pm 2.0	22%	115
C	1	0.5	4	0.625	0.784	Polydomain or possibly radial	9.4 \pm 3.7	39%	120

Figure **5.2a**, **b**, and **c** show the property analysis done on each system set of particle stoichiometry, including corresponding POM, wide angle X-ray scattering (WAXS), and differential scanning calorimetry (DSC). For each system, the apparent liquid crystallinity given by the birefringence is seen in the POM images shown in **Figure 5.2a**. It is evident from OM and

POM that varying the stoichiometry produces particles of varying size and aggregation, with relatively high coefficient of variance (CV) upwards of 20%, measured using ImageJ (**Table 5.1**). Particle diameter for Systems B and C were comparable and smaller than System A, at about 9.7 and 9.4 μm respectively. WAXS done on dried particles shown in **Figure 5.2b**, displays the LC alignment for each particle system. All systems display some polydomain characteristics. System B displays some smaller scale order. From POM, System C suggests a possible radial phase.¹⁸

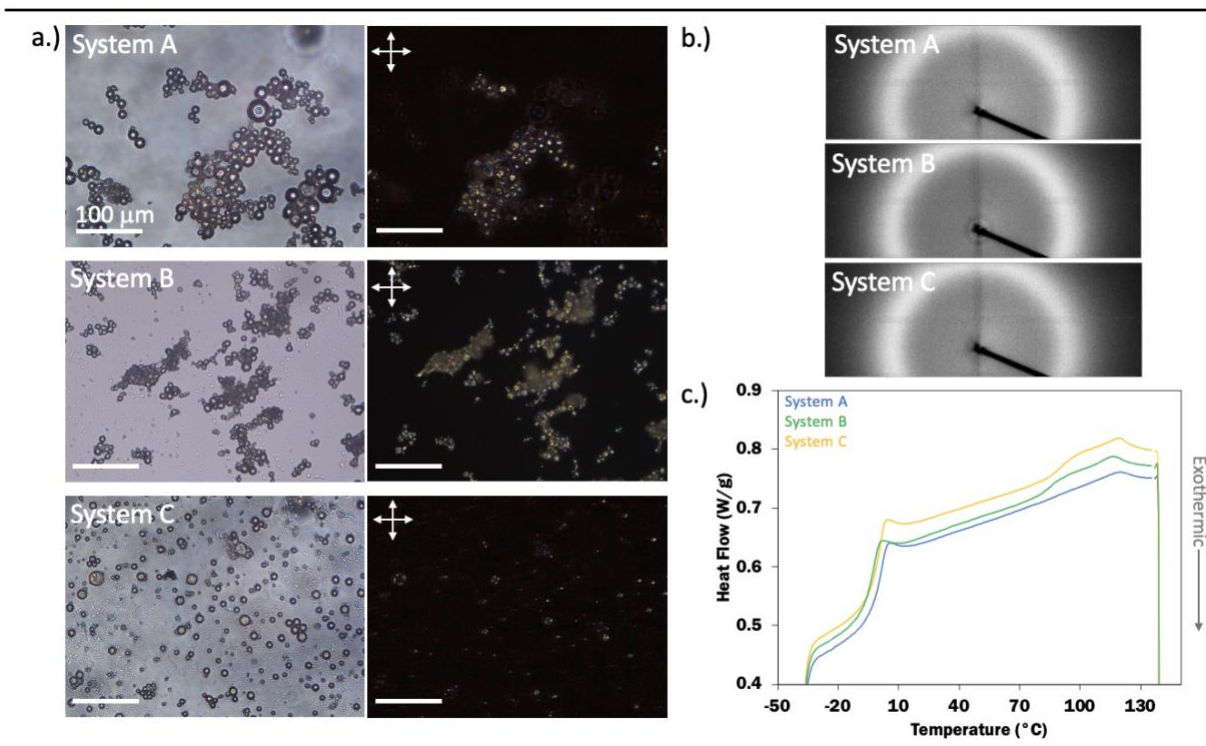


Figure 5.2: For all particle Systems A, B, and C a.) OM (left) and POM (right) with all scale bars representing 100 μm b.) WAXS c.) DSC traces.

Finally, the DSC traces shown in **Figure 5.2c**, display the glass transition temperature (T_g) and the T_{NI} for each system. The T_g for all three systems does not vary greatly, with a value around -3°C , indicating the particles are rubbery and easily manipulated at room temperature. System A displays a characteristic T_{NI} around 117°C . System B and C have noticeably broader phase transition regions. The T_{NI} for Systems B and C are about 115°C and 120°C respectively. The excess thiol

content stoichiometry of Systems B and C results in more heterogeneities in the network due to less crosslinking, allowing for a broadened thermal transition shown in the DSC traces. Following material property analysis, the shape memory capabilities were then evaluated.

The stoichiometrically balanced functional groups of System A effectively demonstrated one-way shape switching behavior. Following the scheme from **Figure 5.3a**, particles from System A were deposited onto a glass slide and solvent was allowed to evaporate at room temperature, followed by manual compression of the particles with a secondary piece of glass for 20 seconds. **Figure 5.3b** displays the particles under OM and POM before deformation at room temperature. After deformation at room temperature the particles exhibited a prolate shape with the manual compression imparting some directed LC alignment (**Figure 5.3c**). The change in birefringence also indicates a change in the underlying LC alignment from spherical to prolate. Upon removal of pressure the particles maintain their deformed shape, due to characteristic LC soft elasticity.¹⁹ The particles were then thermally cycled past their T_{NI} to 120°C and cooled back to room temperature, demonstrating shape recovery to a sphere (**Figure 5.3d**).

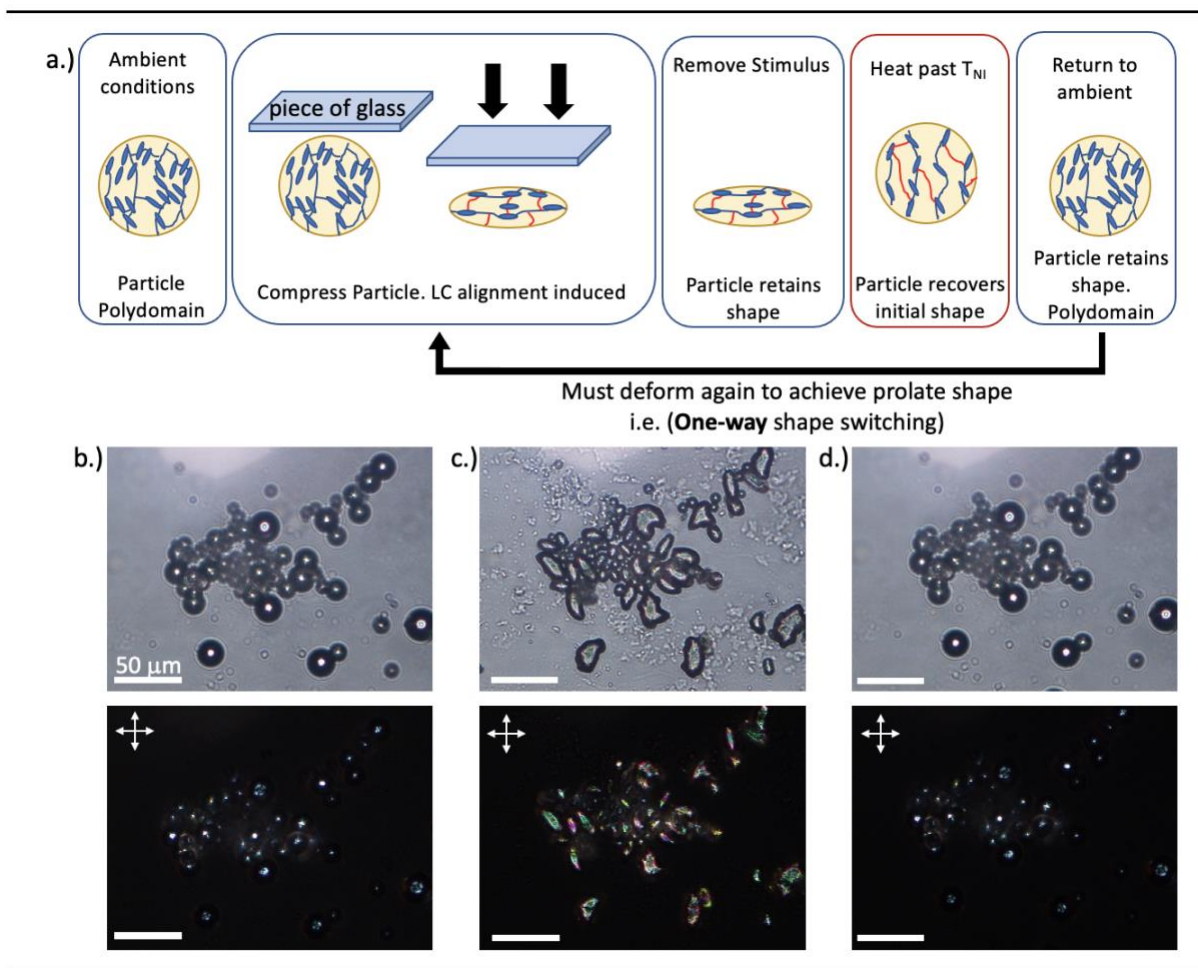


Figure 5.3: a.) Particle deformation and shape switching scheme. System A: One-way shape switching demonstration of LCEMPs top row OM and bottom row POM b.) Particles as polymerized initially at room temperature c.) Particles after manual compression at room temperature displaying prolate deformation d.) Particles after being thermally cycled from room temperature past their T_{NI} to 120°C and back to room temperature, displaying recovery of shape.

To demonstrate two-way shape switching, particles of System C, with a network containing 60% excess acrylates, were swollen with photoinitiator. Following the same deformation procedure from above, the particles were compressed, maintaining their shape after removal of pressure, followed by irradiation with light to crosslink the excess acrylates, which preserve the compressed shape (**Figure 5.4a**). Upon thermal cycling, the particles toggle between their low temperature programmed shape and a high temperature spherical shape.

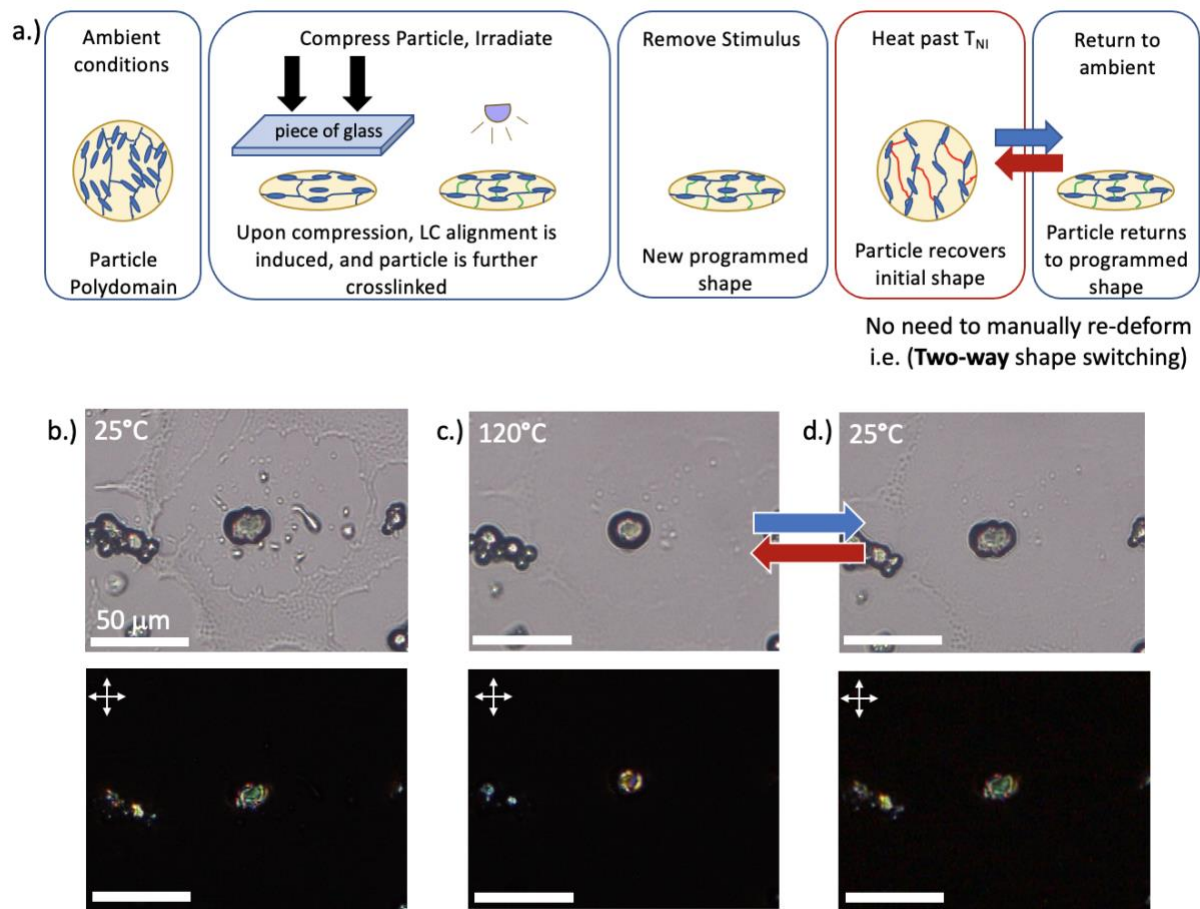


Figure 5.4: a.) Particle programming and shape switching scheme. System C: Two-way shape switching demonstration of LCCEMPs top row OM and bottom row POM b.) Particle after being compressed and irradiated at room temperature c.) Particle in a temporary recovered shape above the T_{NI} at 120°C d.) Particle returned to room temperature demonstrating recovery to programmed shape.

Figure 5.4b displays the particle after programming at room temperature. **Figure 5.4c** and **d** display the two-way shape switching achieved by thermally cycling the programmed particle. This programming is not reversible.

5.3 – Conclusions

This study reports a facile means to polymerize one and two-way shape switching capable LCEMPs through a single stage thiol-Michael addition dispersion polymerization. Systematically altering the stoichiometry demonstrated tunable changes in material properties, and transition temperatures to actuate shape switching. The LCEMPs reported here were manually compressed into a deformed shape with System A achieving one-way shape switching, while System C underwent a two-stage polymerization process to achieve two-way shape switching. Shape switching LCEMPs have applications in soft robotics, cosmetics, drug delivery, and surface cleanings.

5.4 – Experimental

Materials

1,4-Bis-[4-(6-acryloyloxyhexyloxy)-benzoyloxy]-2-methylbenzene (RM82) was purchased from Wilshire Technologies. Polyvinylpyrrolidone (PVP), Pentaerythritol tetrakis(3-mercaptopropionate) (PETMP), triethylamine (TEA), dichloromethane (DCM), and methanol were purchased from Sigma-Aldrich. Propanedithiol (PDT) was purchased from TCI.

Preparation of LCEMPs

The preparation of the LCEMP sets is the same for each with only changes to monomer stoichiometry. System A was prepared as follows: With a stir bar continuously stirring to mix the system, 0.037 g of PVP (15 wt% to monomer) was dissolved in 6.98 mL of DCM. 0.165 g of RM82 was then dissolved in the solution. 14.33 mL of MeOH (45 wt% DCM/55 wt% MeOH) was mixed into the solution and checked to ensure the monomer RM82 remained dissolved. 0.0125

mL of PDT was dissolved in the solution followed by 0.0234 mL of PETMP (1 wt% monomer in solvent). 0.032 mL of the catalyst TEA (10 wt% to monomer) was then added to the reaction and the reaction was left overnight. The mixture turns turbid after about 15 minutes. The following day the product was centrifuged at 3000 RPM for 2 min and washed 3X with the same MeOH/DCM mixture. The particles were allowed to dry at ambient conditions and stored in a freezer. The stoichiometric ratios for the systems are as follows: PETMP:PDT:RM82 A(1:2:4) B(1:1:4) C(1:0.5:4).

Image Analysis of LCEMPs

ImageJ analysis was done on 50 particles of each formulation to determine average particle diameter and coefficient of variance. Optical and polarized microscopy (POM) were done with a Nikon Eclipse Ci.

X-Ray Diffraction Measurements

WAXS was run on dry particles. Scans was done with a Forvis Technologies instrument using a copper source ($\lambda = 1.5405 \text{ \AA}$). The detector was a Dectris Eiger R 1 M with a $0.075 \times 0.075 \text{ mm}^2$ pixel size.

DSC

The particles were initially heated to erase thermal history, cooled at a rate of $5^\circ\text{C}/\text{min}$ from 140°C to 20°C , and finally heated at a rate of $20^\circ\text{C}/\text{min}$ to 140°C to generate the reported curves. DSC was run on a TA DSC 2500.

Programming LCEMPs

One-way shape switching: After washing, particles were suspended in the MeOH/DCM solvent mixture and deposited onto a glass microscope slide on the benchtop. After solvent evaporation, a small piece of a microscope slide was used to compress a region of the deposited sample. The sample was then observed under OM and POM. The sample was heated above the phase transition temperature to 120°C and then cooled back to room temperature. Two-way shape switching: Harvested particles were swollen over night with 5 wt% initiator I-819 in DCM. The particles were drop cast and compressed with a piece of microscope slide. The particles were then irradiated with 400-500 nm light at 50 mW/cm² for 5 min. Upon thermal cycling past 120°C, the particles demonstrated reversible shape switching.

5.5 – Acknowledgments

This work would like to acknowledge Russell Riley for experimental work, and Nicholas Bongiardina for scientific discussion. This work was completed with the financial support of NSF DMR 1809841. The authors gratefully acknowledge the use of facilities and instrumentation supported by the NSF MRSEC Grant DMR-1420736 performed by Vikina Martinez. The authors gratefully acknowledge Dr. Tim White's lab at the University of Colorado at Boulder, for the use of their DSC.

5.6 – Supporting Information

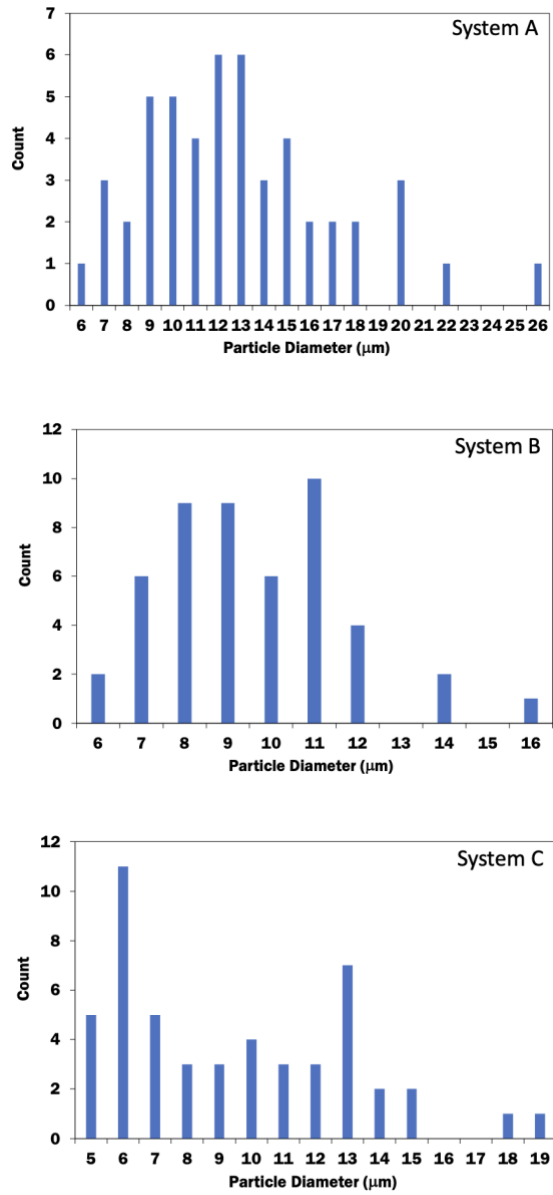


Figure S5.1: Particle size distribution for system A, B, and C

5.7 – References

- (1) Patravale, V. B.; Mandawgade, S. D. Novel Cosmetic Delivery Systems: An Application Update: Novel Cosmetic Delivery Systems. *International Journal of Cosmetic Science* **2008**, *30* (1), 19–33. <https://doi.org/10.1111/j.1468-2494.2008.00416.x>.
- (2) Birnbaum, D. T.; Brannon-Peppas, L. Microparticle Drug Delivery Systems. In *Drug Delivery Systems in Cancer Therapy*; Brown, D. M., Ed.; Humana Press: Totowa, NJ, 2004; pp 117–135. https://doi.org/10.1007/978-1-59259-427-6_6.
- (3) Belmonte, A.; Bus, T.; Broer, D. J.; Schenning, A. P. H. J. Patterned Full-Color Reflective Coatings Based on Photonic Cholesteric Liquid-Crystalline Particles. *ACS Applied Materials & Interfaces* **2019**, *11* (15), 14376–14382. <https://doi.org/10.1021/acsami.9b02680>.
- (4) Marshall, J. E.; Gallagher, S.; Terentjev, E. M.; Smoukov, S. K. Anisotropic Colloidal Micromuscles from Liquid Crystal Elastomers. *Journal of the American Chemical Society* **2014**, *136* (1), 474–479. <https://doi.org/10.1021/ja410930g>.
- (5) Kishi, R.; Osada, Y. Reversible Volume Change of Microparticles in an Electric Field. *Journal of the Chemical Society, Faraday Transactions 1: Physical Chemistry in Condensed Phases* **1989**, *85* (3), 655. <https://doi.org/10.1039/f19898500655>.
- (6) Uto, K.; Ebara, M. Magnetic-Responsive Microparticles That Switch Shape at 37 °C. *Applied Sciences* **2017**, *7* (11), 1203. <https://doi.org/10.3390/app7111203>.
- (7) Cox, L. M.; Sun, X.; Wang, C.; Sowan, N.; Killgore, J. P.; Long, R.; Wu, H.-A.; Bowman, C. N.; Ding, Y. Light-Stimulated Permanent Shape Reconfiguration in Cross-Linked Polymer Microparticles. *ACS Applied Materials & Interfaces* **2017**, *9* (16), 14422–14428. <https://doi.org/10.1021/acsami.7b02759>.
- (8) Hessberger, T.; Braun, L.; Zentel, R. Microfluidic Synthesis of Actuating Microparticles from a Thiol-Ene Based Main-Chain Liquid Crystalline Elastomer. *Polymers* **2016**, *8* (12), 410. <https://doi.org/10.3390/polym8120410>.
- (9) Ohm, C.; Serra, C.; Zentel, R. A Continuous Flow Synthesis of Micrometer-Sized Actuators from Liquid Crystalline Elastomers. *Advanced Materials* **2009**, *21* (47), 4859–4862. <https://doi.org/10.1002/adma.200901522>.
- (10) Haseloh, S.; Ohm, C.; Smallwood, F.; Zentel, R. Nanosized Shape-Changing Colloids from Liquid Crystalline Elastomers. *Macromolecular Rapid Communications* **2011**, *32* (1), 88–93. <https://doi.org/10.1002/marc.201000324>.
- (11) Yang, Z.; Huck, W. T. S.; Clarke, S. M.; Tajbakhsh, A. R.; Terentjev, E. M. Shape-Memory Nanoparticles from Inherently Non-Spherical Polymer Colloids. *Nature Materials* **2005**, *4* (6), 486–490. <https://doi.org/10.1038/nmat1389>.
- (12) Vennes, M.; Martin, S.; Gisler, T.; Zentel, R. Anisotropic Particles from LC Polymers for Optical Manipulation. *Macromolecules* **2006**, *39* (24), 8326–8333. <https://doi.org/10.1021/ma0613279>.
- (13) Cairns, D. R.; Sibulkin, M.; Crawford, G. P. Switching Dynamics of Suspended Mesogenic Polymer Microspheres. *Applied Physics Letters* **2001**, *78* (18), 2643–2645. <https://doi.org/10.1063/1.1367292>.
- (14) Vennes, M.; Zentel, R. Liquid-Crystalline Colloidal Particles. *Macromolecular Chemistry and Physics* **2004**, *205* (17), 2303–2311. <https://doi.org/10.1002/macp.200400296>.

- (15) Liu, X.; Xu, Y.; Heuts, J. P. A.; Debije, M. G.; Schenning, A. P. H. J. Monodisperse Liquid Crystal Network Particles Synthesized via Precipitation Polymerization. *Macromolecules* **2019**, *52* (21), 8339–8345. <https://doi.org/10.1021/acs.macromol.9b01852>.
- (16) Liu, X.; Pan, X. Programmable Liquid Crystal Elastomer Microactuators Prepared via Thiol-Ene Dispersion Polymerization. *Soft Matter* **2020**, *13* (45), 8368–8378. <https://doi.org/10.1039/C7SM01619K>.
- (17) Wang, C.; Zhang, X.; Podgórski, M.; Xi, W.; Shah, P.; Stansbury, J.; Bowman, C. N. Monodispersity/Narrow Polydispersity Cross-Linked Microparticles Prepared by Step-Growth Thiol–Michael Addition Dispersion Polymerizations. *Macromolecules* **2015**, *48* (23), 8461–8470. <https://doi.org/10.1021/acs.macromol.5b02146>.
- (18) Wang, X.; Xu, M.; Ren, H.; Wang, Q. A Polarization Converter Array Using a Twisted-Azimuthal Liquid Crystal in Cylindrical Polymer Cavities. *Opt. Express* **2013**, *21* (13), 16222. <https://doi.org/10.1364/OE.21.016222>.
- (19) Ware, T. H.; Biggins, J. S.; Shick, A. F.; Warner, M.; White, T. J. Localized Soft Elasticity in Liquid Crystal Elastomers. *Nature Communications* **2016**, *7* (1). <https://doi.org/10.1038/ncomms10781>.

Chapter 6: Permanent and Reversibly Programmable Shapes in Liquid Crystal Elastomer Microparticles Capable of Shape Switching

(Manuscript published - Martinez, A. M.; Cox, L. M.; Killgore, J. P.; Bongiardina, N. J.; Riley, R. D.; Bowman, C. N. Permanent and Reversibly Programmable Shapes in Liquid Crystal Elastomer Microparticles Capable of Shape Switching. *Soft Matter* **2020**, *17* (3), 467–474. <https://doi.org/10.1039/D0SM01836H>.)

Reversibly programmable liquid crystal elastomer microparticles (LCEMPs), formed as a covalent adaptable network (CAN), with an average diameter of $7 \pm 2 \mu\text{m}$, were synthesized via a thiol-Michael dispersion polymerization. The particles were programmed to a prolate shape via a photoinitiated addition-fragmentation chain-transfer (AFT) exchange reaction by activating the AFT after undergoing compression. Due to the thermotropic nature of the AFT-LCEMPs, shape switching was driven by heating the particles above their nematic-isotropic phase transition temperature (T_{NI}). The programmed particles subsequently displayed cyclable two-way shape switching from prolate to spherical when at low or high temperatures, respectively. Furthermore, the shape programming is reversible, and a second programming step was done to erase the prolate shape by initiating AFT at high temperature while the particles were in their spherical shape. Upon cooling, the particles remained spherical until additional programming steps were taken. Particles were also programmed to maintain a permanent oblate shape. Additionally, the particle surface was programmed with a diffraction grating, demonstrating programmable complex surface topography via AFT activation.

6.1 – Introduction

Microparticles have been the subject of significant research efforts due to their incorporation into a wide range of applications including cosmetics, drug therapy, optics, and adsorption, amongst others.¹⁻⁵ Numerous methodologies exist for generating microparticles and a key objective in related research has been overcoming the static nature of microparticle geometry.

Shape changing microparticles are of growing interest since dynamic control over geometry facilitates integration into a wider range of applications demanding optical dynamics, tunable adhesion, rheological control, and micromechanical actuation.⁶⁻⁹

Beyond typical one-way shape switching phenomena, two-way shape switching materials are desirable for their inherent ability to change between different shapes without requiring repeated, direct mechanical deformation events. Shape switching microparticles often rely on pre-alignment, or biased regions of mismatched properties, to achieve shape changes upon application of a stimulus.¹⁰⁻¹² A common method to generate shape switching particles is to embed them in a film and strain that film, which deforms the particles. Such a strain is often followed by a secondary programming process, possibly involving additional reactions, to stabilize this shape.^{10,13,14} Although this method is effective for achieving shape switching particles, harvesting the programmed particles for desired application involves additional steps to embed particles in a matrix and subsequently remove the matrix and recover the programmed particles.

Recently, the unique optical and phase changing properties of liquid crystals (LCs) have been integrated into liquid crystal microparticle (LCMP) systems.¹⁵⁻¹⁸ LCMPs demonstrating two-way shape switching behavior have been investigated, but the fabrication methods have challenges in scalability, or generate nanoparticles with size-limitations.¹⁹⁻²² Some demonstrations of two-way shape switching liquid crystal elastomer microparticles (LCEMPs) use radical based polymerizations mediated by microfluidic set-ups to generate particles with pre-alignment of the LC mesogens, enabling inherent shape switching capabilities.^{16,23,24} In LCEMPs, a physical pre-alignment of mesogens tethered to a polymer network define one of two accessible particle geometries. When the particles are heated past their nematic-isotropic phase transition temperature (T_{NI}), the polymer network contracts parallel to the alignment director and expands perpendicular

to the alignment director, thus accessing the second geometry. Temperature modulation enables repeated switching between geometries, resulting in a two-way shape switching capable material.^{25,26} These LCEMPs are crosslinked materials, yet microfluidic systems have challenges with regard to scaling up. Recently, Schenning and coworkers reported a facile dispersion polymerization method to generate scalable, programmable LCEMPs.¹⁰ Their method utilizes a thiol-Michael dispersion polymerization, which eliminates the need for microfluidic equipment or the oxygen controlled environments radical based polymerizations require.²⁷⁻²⁹ To program these LCEMPs, Schenning and coworkers deform the particles embedded in a film, aligning the LC mesogens into a new prolate or oblate particle shape. Next, they use a second stage polymerization to alter the chemical composition, thus permanently crosslinking these particles into the deformed shape below the T_{NI} , an approach which has previously been demonstrated in bulk liquid crystal elastomers (LCEs).²⁶ Temporary recovery of the original spherical shape is achieved by heating past the T_{NI} . This system is the most viable approach to a scalable system achieving switchable particle geometries but requires particle crosslink density to be permanently altered during shape programming, which lacks a capacity for re-programmability.

6.2 – Results & Discussion

Reported here is a facile means to generate and program LCEMPs comprised of a covalent adaptable network (CAN) into permanent or reprogrammable shapes, achieving two-way shape switching capabilities. By employing a CAN, a typical static polymer network is rendered dynamic upon application of the appropriate stimulus.^{30,31} The dynamic network acts to relieve stress, imparted through a straining event, by reconfiguring the network and allowing it to trend towards a thermodynamic equilibrium through exchangeable crosslinks. A variety of stimuli exist for

network reconfiguration of CAN-based LCE materials, including thermal activation of vitrimers; however, in the work reported here, light activation is used to decouple the thermotropic LC phase transition from the programming stimulus.^{32,33} A reversibly programmable and two-way shape switching mechanism has been demonstrated in a light activated CAN-based bulk LCE, as reported by McBride et al., but this mechanism has not previously been demonstrated in micron-scale LC particles.³⁴ Furthermore, Non-LC CAN-based particles have been reported that do not switch shape, unlike the system reported here that has two-way shape switching capabilities due to the LCE character of the particles.³⁵ Reported here, a thiol-Michael dispersion polymerization is used to generate CAN-based LCEMPs, which alleviates the aforementioned challenges of scale-up and oxygen sensitivity identified in microfluidic and radical-based precipitation polymerizations. The CAN mechanism utilized is mediated by a light initiated addition-fragmentation chain-transfer (AFT) reaction, where the crosslink density of the network remains unchanged throughout the duration of the programming steps following polymerization.^{30,31} Once AFT-LCEMPs are programmed to a new shape, the original spherical shape of the particle is recovered and/or further altered in subsequent programming steps, limited only by the amount of photoinitiator available in the system. Particles were also programmed to have a complex surface topography.

The AFT-LCEMPs reported here were generated by thiol-Michael dispersion polymerization. The monomers used to generate the AFT-LCEMPs include the following: a polymerizable diacrylate liquid crystal RM82, a tetra-thiol crosslinker pentaerythritol tetrakis (3-mercaptopropionate) (PETMP), an exchangeable moiety the allyl dithiol (ADT), and the surfactant polyvinylpyrrolidone (PVP) (**Figure 6.1a**). The AFT exchange reaction chosen requires an exchangeable moiety, in this system, the allyl sulfide functionality that is achieved by the ADT monomer. By embedding this exchangeable moiety in the network backbone, the covalent

crosslinks are altered from static to dynamic upon photoinitiation of a radical species, which generates a cascading bond exchange reaction facilitated by the allyl sulfide functionality of the exchangeable moiety during light exposure to relieve stress in the network, while maintaining the crosslink density during the exchange reaction (**Figure 6.1b**).^{30,31}

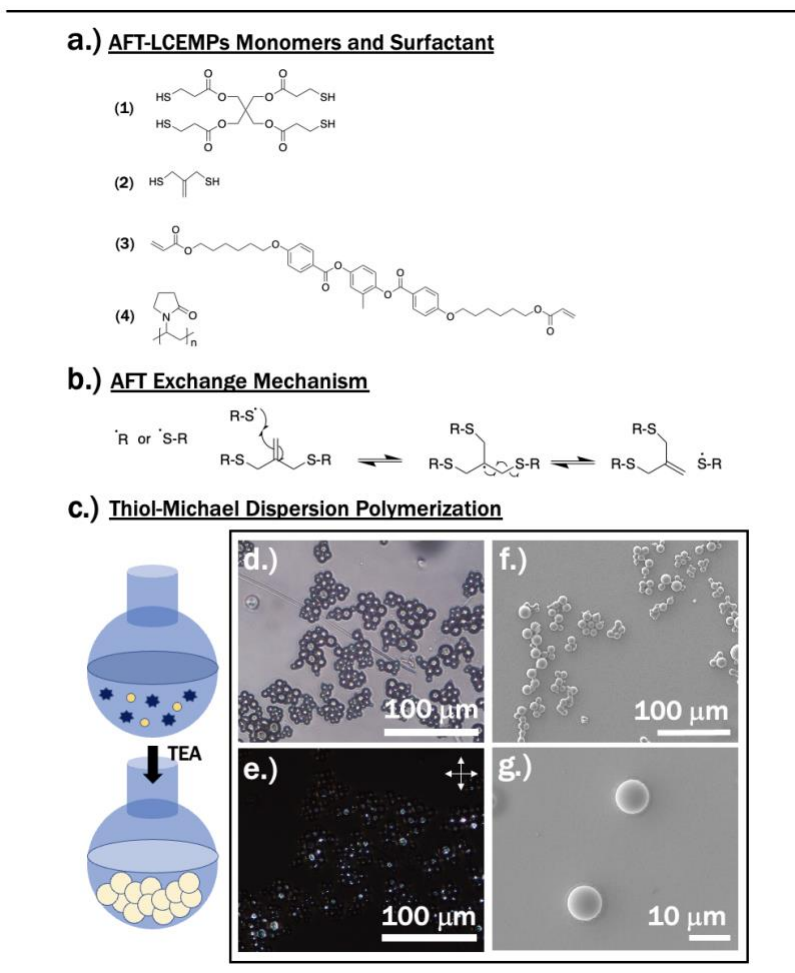


Figure 6.1: a.) Monomers and surfactant for the thiol-Michael dispersion polymerization (1) PETMP, (2) ADT the AFT moiety, (3) RM82, (4) PVP surfactant b.) AFT exchange mechanism. Crosslink density is maintained due to the exchange type mechanism where a radical adds into the exchangeable moiety before a sulfide bond is broken. c.) Thiol-Michael dispersion polymerization scheme with catalyst TEA added to start the reaction. AFT-LCEMPs as polymerized d.) Optical microscopy e.) Polarized optical microscopy f.) g.) SEM.

The monomers were added to a MeOH/DCM mixture, with a slight excess of the thiol crosslinker, in the following monomer ratios; PETMP:ADT:RM82 1.05:2:4. A slight excess of the thiol

crosslinker was used to increase the acrylate conversion so as to eliminate acrylate polymerization in the second step, which requires light initiation of a radical species to start the bond exchange reaction for shape programming. Secondary acrylate polymerizations are used in dual cure methods from aforementioned programming techniques, but here the reaction mechanism for programming relies on covalent bond exchange instead of a secondary polymerization. PVP was used to stabilize microparticle formation and finally, triethylamine (TEA) was added to catalyze the thiol-Michael reaction, which was allowed to run overnight (**Figure 6.1c**).

This polymerization yielded AFT-LCEMPs with an average diameter (D_n) of $7 \pm 2 \mu\text{m}$ and a coefficient of variance (CV) of 31 %, as calculated by equation (6.1),

$$CV\% = \frac{SD}{D_n} * 100 \quad (6.1)$$

where the standard deviation (SD) is divided by D_n . Particle size distribution is reported in further detail by the bar graph included in **Figure S6.1**. A glass transition (T_g) of $-8.5 \text{ }^\circ\text{C}$ was determined by differential scanning calorimetry (DSC) on dried particles, indicating that the material is rubbery at room temperature and well-suited for manual deformation (**Figure S6.2**). DSC also indicated a T_{NI} of $115 \text{ }^\circ\text{C}$. After the polymerization was complete, the particles were washed and observed under optical microscopy (OM) and polarized optical microscopy (POM), displaying the characteristic birefringence of polydomain LC alignment (**Figure 6.1d,e**). Scanning electron microscopy (SEM) was also performed on the as-polymerized particles, seen in **Figure 6.1f and g**. The AFT-LCEMPs were then programmed to have two-way shape switching capabilities.

To program the two-way shape switching of the AFT-LCEMPs, particles were processed following the programming scheme seen in **Figure 6.2a**. First, particles were deposited on a glass slide and compressed manually by a second piece of glass (superstrate) at room temperature, resulting in a prolate shape (**Figure 6.2b, S6.3**). This shape is often seen in actuatable LCEMPs

due to the directed re-orientation of LC mesogens by the deformation mechanism.^{10,16} Observed in the corresponding POM images is the change in birefringence from spherical particles, exhibiting a consistent blue hue (**Figure 6.1e**), to the prolate shaped particles, exhibiting significant variation of color (**Figure 6.2b, S6.4a**), indicating the change in LC alignment associated with the change in shape. Birefringence disappears as prolate particles are angled 45 degrees to the cross-polarizers, indicating a skewed alignment along the long axis of the particle, with some remaining birefringence seen near the tips where alignment is constrained by particle geometry (**Figure S6.4b**). There are several factors which may contribute to the deformed particle shape including crosslink density, particle size, and LC phase that are not systematically explored here and remain open questions regarding the degrees of control afforded by these AFT-LCEMPs.

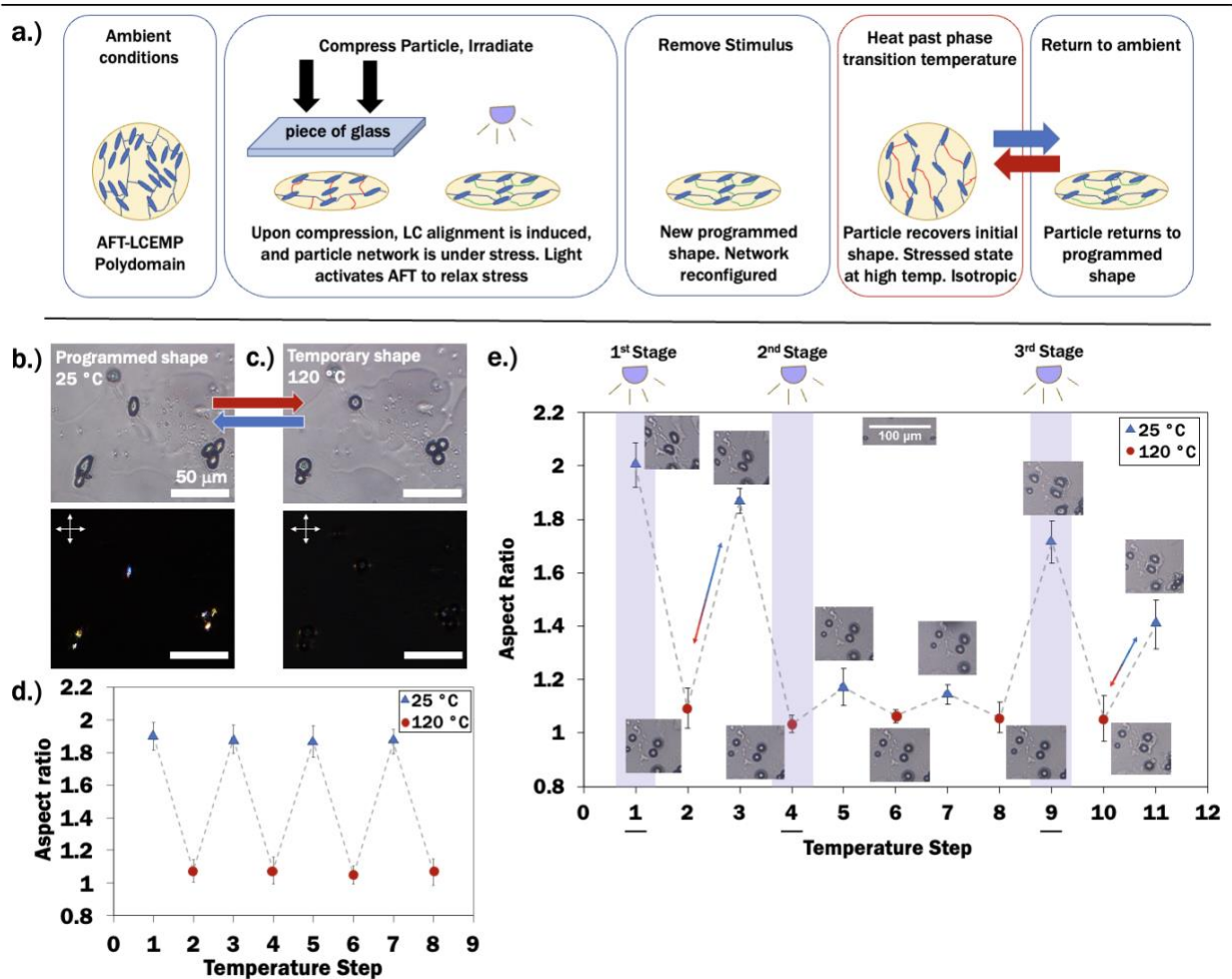


Figure 6.2: a.) Schematic of programming particles and shape switching behavior of particles after programming. b.) Particles after programming displaying a prolate shape at room temperature (top) OM (bottom) POM c.) Particles at 120 °C recovering their temporary spherical shape and appearing almost fully isotropic in POM with birefringence almost completely gone. d.) Aspect ratio plot for particles undergoing temperature cycles and switching shape from prolate to spherical. Dashed line for ease of viewing. e.) Aspect ratio plot of particles undergoing three programming steps: **1st Stage** - Particles pictured after compression and irradiated with light, programmed to the prolate shape at Temp. Step 1. Particles cycle shape between Temp. Step 2 and 3. **2nd Stage** - Particles undergo a re-programming step, light exposure at high temperature, back to the spherical shape at Temp. Step 4. **3rd Stage** - Particles undergo a final programming step, particles pictured after compression and irradiated with light, programmed back to the prolate shape at Temp. Step 9. Particles cycle shape between Temp. Step 10 and 11. Dashed line for ease of viewing.

Next, the glass used for compression was removed and the particles were found to maintain their deformed shape due to soft elasticity arising from the LC mesogen reorientation.³⁶ A bulk

LCE analog was fabricated to generate a stress-strain profile representative of the particle material properties (**Figure S6.5**). The soft elasticity is exhibited by the decrease in stress starting at about 35 % strain, indicative of the LC mesogen reorientation. It is also important to note that the stress-strain profile for a spherical particle might be somewhat altered due to shape confinement in contrast to the rectangularly shaped bulk LCE analog used for analysis. The AFT reaction acts to relieve stress on the crosslinks generated from the strain deformation event, which in this study is compression of the particle network. Compression at room temperature shifts the polydomain LC mesogen alignment towards a global alignment, yielding the observed prolate particle shape.

After compression, the sample is irradiated with low wavelength light, used to initiate the AFT exchange reaction via the photoinitiator 2,2-dimethoxy-2-phenylacetophenone (DMPA) and/or Irgacure 819 as indicated in the supporting information (SI), which are swollen into the particle after polymerization. Two initiators with different absorbance profiles were used to increase the amount of accessible initiator for programming cycles. The bond exchange facilitated by AFT relaxes the stresses applied to the particle, and this new LC alignment is stabilized without altering the crosslink density due to the exchange-based relaxation mechanism.^{30,31} Using light to initiate the exchange reaction decouples this programming step from the temperature dependent LC phase behavior of the particles, giving control over the conditions under which programming and actuation occur. Following this programming step, the particles were heated past their T_{NI} of 115 °C to 120 °C, and the original spherical shape was recovered (**Figure 6.2c, S6.6b**). A near-isotropic phase is confirmed by corresponding POM images with nearly complete absence of birefringence. Due to the programmed LC alignment at room temperature in the LC phase, as the particles move through their LC phase transition to the isotropic phase, they experience a contraction parallel to the aligned director, and expansion perpendicular to the director, returning

them to a spherical shape, which is characteristic of shape changing LCEs.^{25,34} Upon cooling back to the LC phase at room temperature, the particles return to their prolate programmed shape (**Figure 6.2b, S6.6a**).

Thermally cycling the programmed particles reliably cycles the particles through a prolate shape in the low-temperature LC phase to a spherical shape in the high-temperature isotropic phase (**Figure 6.2b,c**), as quantified by the aspect ratio. Aspect ratio, or the ratio of an object's length to its width, was measured from OM using ImageJ to analyze the change in shape from the prolate shape in the LC phase to the spherical shape in the isotropic phase, upon thermally cycling the particles multiple times after programming (**Figure 6.2d**). The aspect ratio was calculated using the following equation:

$$A_R = \frac{d_2}{d_1} \quad (6.2)$$

where d_1 represents the particle short axis and d_2 represents the particle long axis.²⁰ After programming and thermal cycling, the particles measured in the LC phase achieved an average aspect ratio of 1.89 with 90 ± 4 % shape fixity, which describes the relatively high aspect ratio of the prolate shape observed in OM and SEM. Particles measured in the isotropic phase displayed an average aspect ratio of 1.1 with 95 ± 4 % shape recovery from an un-programmed spherical particle, corresponding to the spherical shape they temporarily exhibit. In comparison, initially polymerized un-programmed particles exhibit an average aspect ratio of 1.

A variety of control experiments were performed to establish that AFT programming in this study relies on the presence of the AFT moiety, and photoinitiator coupled with light exposure to activate the exchange. In the first control, AFT-LCEMPs were not swollen with photoinitiator, but were still compressed to a prolate shape, irradiated with light, and thermally cycled past the T_{NI} . These AFT-LCEMPs returned to their initial spherical shape with the aspect ratio returning to

1, demonstrating the need for photoinitiator to program the prolate shape (**Figure S6.7a,b**). In parallel, non-AFT capable LCEMPs were swollen with photoinitiator, compressed to the prolate shape, irradiated with light, and thermally cycled past the T_{NI} , again returning to their initial spherical shape with an aspect ratio of 1, demonstrating the need for the AFT moiety (**Figure S6.7c,d**). In an additional control, no light exposure and no photoinitiator were used, but the particles were compressed to the prolate shape and thermally cycled past the T_{NI} , returning to their initial spherical shape, both returning to an aspect ratio of 1, demonstrating the need of photoinitiator coupled with light exposure for programming (**Figure S6.8a,b and c,d**). Shape recovery back to an aspect ratio of 1 eliminates the possibility of substrate adhesion being an issue for prolate to spherical shape recovery on glass substrates. All controls, regardless of initiator content, were pre-irradiated with light to ensure any excess acrylate and thiol were reacted and thus controls were started under the same conditions (**Figure S6.9**).

To demonstrate the re-programmability of the AFT-LCEMPs, a 3-stage programming series was performed. Particles underwent the same programming procedure described above to achieve the reversible prolate-to-spherical shape switching, designated by the 1st Stage at Temperature Step 1 of **Figure 6.2e**. The particles pictured at Temperature Step 1 of **Figure 6.2e** have been compressed and irradiated with light at room temperature. The programmed particles are thermally cycled past their T_{NI} , with the corresponding particle images from Temperature Step 2 and 3 (**Figure 6.2e**) being the new switchable prolate and spherical shapes, respectively. The prolate shape has an average aspect ratio of 1.87, with a shape fixity of 93 ± 2 % from the initial compressed prolate shape.

The programmed prolate shaped particles then underwent light exposure at high temperature, to erase the prolate shape and return to a permanent spherical shape, as performed in

the 2nd Stage at Temperature Step 4 (**Figure 6.2e, S6.10**). In the 1st Stage, programming to the prolate shape, the network was reconfigured such that it is in a nearly stress-free thermodynamic equilibrium at room temperature. Upon heating past the LC phase transition to 120 °C, the movement of LC mesogens and polymer chains back to an entropically driven sphere puts stress on the reconfigured network. The particles at high temperature were exposed to light to reprogram this spherical shape by allowing relaxation of the stress generated in the network at high temperature. Upon cooling back to room temperature, the particles maintained the spherical shape with an average aspect ratio of 1.1 and 88 ± 5 % spherical shape recovery as compared to an initially polymerized un-programmed spherical particle, as displayed at Temperature Steps 5 and 7 (**Figure 6.2e**). Cooling and heating cycles shown at Temperature Steps 4 through 8 (**Figure 6.2e**) demonstrate significant recovery of the spherical shape after stress relaxation, although not 100 %, which is attributed to insufficient stress relaxation to completely erase the prolate shape, resulting from either the depletion of the necessary photoinitiator or insufficient light exposure.

To demonstrate one more programming iteration, the re-programmed spherical particles underwent a final programming event, back to a prolate shape, by manual compression and light irradiation at room temperature, performed in the 3rd Stage at Temperature Step 9 (**Figure 6.2e, S6.11**). After thermal cycling past the T_{NI} , displayed at Temperature Step 11 (**Figure 6.2e**), the particles exhibited an average aspect ratio of 1.4, with 82 ± 2 % shape fixity from the initially compressed prolate shape at Temperature Step 9 (**Figure 6.2e**). This new prolate shape consistently cycles shape between the aspect ratios recorded at Temperature Steps 10 and 11 (**Figure 6.2e**).

Variables contributing to the programmability of the particles include photoinitiator concentration, achievable applied strain, temperature, and duration of light exposure, which were

not systematically studied here. This behavior has been studied in bulk AFT-LCEs reported by McBride et al., and little deviation from that qualitative behavior would be expected in these microparticles.³⁴ The strain applied to the particles varied from 20 % to 40 % strain, a result of particle size polydispersity, so the fixity is reported for the particles from their initial deformed shape to their new permanent shape after thermally cycling, with an effort to analyze particles of similar sizes and strains. About 67 ± 1 % of particles casted were successfully deformed and programmed, while 32 ± 3 % remained un-deformed and un-programmed due to lack of contact with the superstrate, with these particles being 4 microns or smaller. There was no noticeable threshold on size dependence for shape switching capabilities, with the limiting factor being particle contact with the superstrate to result in deformation.

To access more particle geometries, AFT-LCEMPs were programmed by nanoimprint lithography (NIL). NIL allows for controlled heating and light irradiation during compression. NIL was used to achieve a permanent oblate shape configuration. Particles swollen with photoinitiator were deposited on silicon, heated past their T_{NI} to 140 °C, and subjected to compression with a flat glass superstrate at this high temperature, yielding an oblate shape. The particles being in their isotropic phase, now deform into an oblate shape with LC mesogens and polymer chains having more mobility to deform at high temperature. The particles were exposed to light at high temperature under compression to activate the AFT bond exchange and were then cooled to ambient, achieving a permanent oblate shape (**Figure 6.3a**). Atomic Force Microscopy (AFM) was done to confirm the height profile and aspect ratio of the particles, with a 15:3 length to height ratio (**Figure 6.3b**).

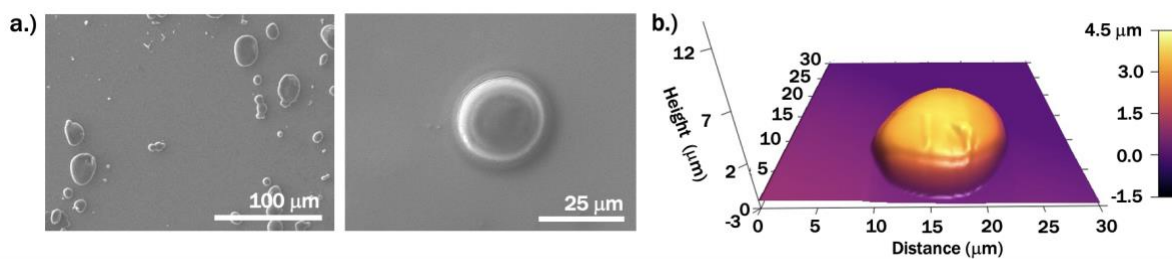


Figure 6.3: a.) SEM of particles after undergoing NIL, run with a flat superstrate under compression at 140 °C to program a permanent oblate shape b.) AFM of an oblate programmed particle displaying the flat particle aspect ratio of 15:3 length to height ratio.

Furthering the application possibilities of AFT-LCEMPs for photonics or rheological control, particles were programmed to have a switchable complex surface topography, aided by the AFT exchange. The particle surface was patterned with a line grating by NIL, substituting the flat superstrate for one with a diffraction grating of 833 nm periodicity. Undergoing compression at 140 °C during light exposure, with 5-micron spacers dispersed on the substrate surface to control compression, the particles yield a line-patterned surface topography at high temperature, as determined by AFM (**Figure 6.4a**). AFM of a particle cross-section indicates that the imprinting yields about 150 ± 60 nm deep surface features, which is about 75 % of the depth of the 200 nm deep grooves in the mold (**Figure S6.12**). Due to the curved particle shape, the average pattern depth was calculated from measurements taken towards the center of the particle surface. Upon cooling below the T_{NI} to 35 °C, the patterned surface is disrupted (**Figure 6.4b**). Heating the particles above the T_{NI} recovers the imprinted pattern, creating a switchable complex surface (**Figure 6.4c**). Alternately, imprinting done without spacers yields a complex surface topography below the T_{NI} (**Figure S6.13**).

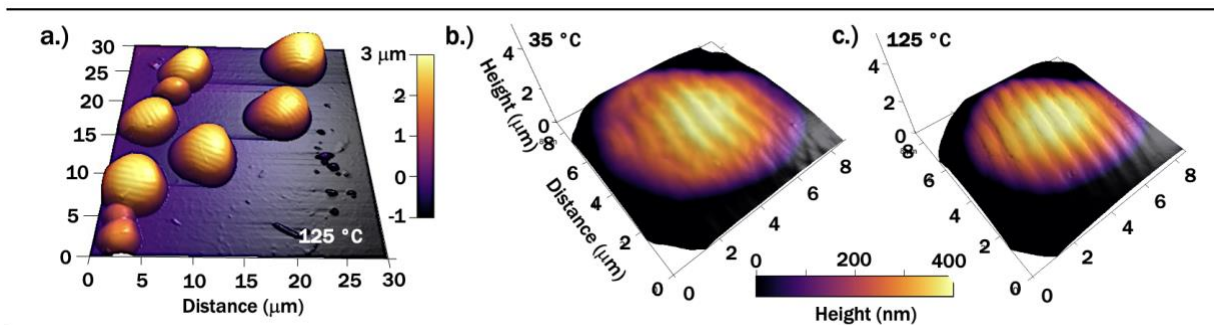


Figure 6.4: a.) AFM of multiple particles imaged at 125 °C displaying the patterned surface topography incurred by NIL programming, compressed at 140 °C using a diffraction grating mold as the superstrate. b.) AFM of a particle surface imaged at 35 °C displaying pattern disruption c.) AFM of the same particle surface imaged at 125 °C displaying pattern recovery. Axes for b.) and c.) are in μm as indicated by b.).

NIL has been studied on AFT capable materials, specifically on bulk AFT-LCEs as reported by McBride et al., and separately on non-LC AFT-particles as reported by Cox et al., but has not been reported for AFT-LCEMPs before.^{34,35} Influences which may contribute to controlling the surface topography are material properties including particle size and shape, chemical composition, temperature, irradiation, and applied strain. Complex surface topography of microparticles often occurs during polymerization, modulated by polymerization conditions, monomer content, or deswelling, whereas in this study, the surface topography is modified post-polymerization at the users' discretion.^{17,37,38} These complex surface topographies are advantageous for photonics and controlling surface adhesion or rheological behavior.

6.3 – Conclusions

Reported here is a facile and scalable means to achieve reversibly programmable AFT-LCEMPs via a thiol-Michael dispersion polymerization. Undergoing a light-initiated programming event, the particles were programmed to be two-way shape switching capable by irradiating particles that had been compressed into a prolate shape with light to initiate AFT bond

exchange. This exchange relieved stress in the network to achieve a low temperature prolate shape. Upon heating and cooling, these particles cyclically transitioned between spherical and prolate, respectively. Furthermore, these two-way shape switching particles were shown to be reversibly programmable by irradiating the particles at high temperature, while in their temporary spherical shape, to return them to their original permanent spherical shape. The particles were also programmed to achieve a permanent oblate shape, and separately, the surface was programmed with a switchable diffraction grating, demonstrating control over the surface topography. The particles are reusable due to their AFT re-programmability and can be re-swollen with photoinitiator to facilitate additional programming events. These AFT-LCEMPs have potential applications in micro-actuation, photonics, or surface control, which can be made adaptable at the users' discretion.

6.4 – Experimental

Materials

1,4-Bis-[4-(6-acryloyloxyhexyloxy)-benzoyloxy]-2-methylbenzene (RM82) was purchased from Wilshire Technologies. Pentaerythritol tetrakis(3-mercaptopropionate) (PETMP) and triethylamine (TEA), dichloromethane (DCM), polyvinylpyrrolidone (PVP), 2,2-dimethoxy-2-phenylacetophenone (DMPA), and methanol were purchased from Sigma-Aldrich. Propane dithiol (PDT) was purchased from TCI. Irgacure 819 was purchased from IGM resins. 5-micron glass rod spacers were purchased from Nippon Electric Glass Co., Ltd. Diffraction grating substrate was purchased from LightSmyth Technologies, Inc.

Allyl dithiol (ADT) synthesis

Prepared as reported by Martinez et al. – A. Martinez, M. McBride, T. White, C. Bowman, *Adv. Funct. Mater.* 2020, **30**, 35, 2003150.

Preparation of AFT-LCEMPs

The AFT-LCEMPs were prepared as follows: Reaction concentration was 1 mass % of monomers to solvent. Monomer molar ratio PETMP:ADT:RM82 1.05:2:4. With a stir bar continuously stirring to mix the system, 0.035 g (15 mass % to monomers) of PVP was dissolved in 6.73 mL of DCM. 0.157 g of RM82 was then dissolved in the solution. 13.8 mL of MeOH was added to the solution. 0.014 g of ADT was dissolved in the solution followed by 0.03 g of PETMP. 0.031 mL (10 mass % to monomers) of the catalyst TEA was then added to the reaction. The mixture turns turbid after about 15 minutes and was allowed to run overnight. The following day the product was centrifuged at 3000 RPM for 2 min and washed three times with the same MeOH/DCM mixture. Particles were stored dry in the freezer. A yield of 40 % was achieved. A 0.2 g batch of starting material yields about 0.08 g of particles. Control experiments done with non-AFT capable LCEMPs were prepared in a stoichiometric ratio of thiols to acrylates at a 1:2:4 (PETMP:PDT:RM82) monomer molar ratio, using propane dithiol instead of the ADT monomer.

Preparation of bulk LCE analog for stress-strain profile

Monomers PETMP:Propane dithiol (ADT analog):RM82 were mixed in a stoichiometric ratio of thiols to acrylates at a 1:2:4 monomer molar ratio, in 1 mL of DCM (40 mass % RM82 to DCM). 3.5 mass % to monomers of TEA was added, and the resin was then filled between two pieces of

glass with 0.5 mm spacers. The resin was allowed to react overnight at 40 °C to ensure monomer RM82 remained dissolved.

Characterization of AFT-LCEMPs

Differential scanning calorimetry (DSC): The dry particles were initially heated to erase thermal history, cooled at 5 °C/min to -40 °C and the test was run from -40 to 140 °C, ramped at 20 °C/min, to generate the reported curve. DSC was run on a TA DSC 2500.

Stress-Strain profile: Stress–strain tests were done at room temperature and strained at a rate of 0.1 mm/s on rectangular samples with dimensions 13.65 mm x 4.4 mm x 0.57 mm. This results in a volume of ~34.2 mm³ with a weight of 0.05 grams. In comparison, about 0.03 to 0.05 grams of microparticles are needed to create this same volume. Tests were run on a TA RSA-G2.

Fourier transform infrared spectroscopy (FTIR): Attenuated Total Reflectance (ATR) - FTIR was done on dried particles. ATR-FTIR was run on a Thermo Fischer Scientific Nicolet iS50 FT-IR.

Image Analysis: ImageJ was used to measure particle shape to determine coefficient of variance (150 particles analyzed) and aspect ratio from optical microscope (OM) images. For prolate programming aspect ratio measurements, 30 particles were analyzed. Out of 180 particles analyzed, 67 ± 1 % of particles casted were successfully deformed and programmed, while 32 ± 3 % remained un-deformed and un-programmed due to lack of contact with the superstrate, with these particles being 4 microns or smaller. OM and polarized optical microscopy (POM) were done with a Nikon Eclipse Ci. Field emission scanning electron microscopy (FESEM) was done with a JEOL JSM-740 1F.

AFM: Particle morphology was characterized by intermittent contact atomic force microscopy. Specialized cantilevers with a visible tip (ATEC-FMAu, Nanosensors, nominal spring constant

2.8 N/m) were used to align imaging with particles of interest. Particles were imaged at a setpoint amplitude equal to 50 % of the free amplitude. Samples were placed on a custom low-expansion, low-drift hot plate inside the atomic force microscope (Cypher S, Oxford Instruments) and controlled to either 35 °C or 125 °C, as indicated.

Programming AFT-LCEMPs

Switchable prolate shape programming (Figure 6.2b,c,d): After washing, particles were dissolved in DCM with 5 mass % DMPA and left to swell overnight. Particles were then deposited onto a glass microscope slide on the benchtop. After solvent evaporation, a small piece of a microscope slide was used to compress a region of the deposited sample, and subsequently removed. The sample was then irradiated with 365 nm light at an intensity of 70 mW/cm², for 120 s. The sample was observed under OM and POM and heated above to 120 °C and then cooled back to room temperature.

Erasure of the prolate shape to permanent spherical shape (Figure S6.10): Particles from programming done in the above procedure were heated to 120 °C and irradiated with 365 nm light at an intensity of 70 mW/cm² for 5 min. They were then cooled to room temperature and observed under OM.

3-Stage programming series (Figure 6.2e, S6.11): Particles were dissolved in DCM with photoinitiators Irg-819 and DMPA (5 mass % of each) and left to swell overnight. Particles were cast on a glass slide and underwent - 1st Stage programming with 400 to 500 nm light at an intensity of 70 mW/cm² for 60 s. 2nd Stage programming; heating to 120°C and irradiated with 400 to 500 nm light at an intensity of 70 mW/cm² for 5 min. 3rd Stage programming; at room temperature

were compressed and irradiated with 365 nm light at an intensity of 70 mW/cm² for 10 min and observed under OM. Lamp for programming: Exfo Acticure Hg Bulb with noted filter.

Nanoimprint Lithography (NIL): Oblate shape programming – Particles were dissolved in DCM with photoinitiators Irg-819 and DMPA (2.5 mass % of each) and left to swell overnight. They were then dip coated onto a silicon chip. A glass superstrate was placed on top of the coated Si substrate to ensure light transmission for programming. The samples were run at 140 °C, 2 MPa, while exposed to 300 to 400 nm light at an intensity of 20 mW/cm² for 2 min. After light exposure, the samples were released from pressure and cooled. **Diffraction grating programming** – Particles were dissolved in DCM with photoinitiators Irg-819 and DMPA (2.5 mass % of each) and left to swell overnight. 5-micron rod shaped spacers were then dispersed in the mixture. Particles were dip coated onto a glass substrate. A silicon superstrate containing a diffraction grating with a line pattern (833 period, 416 nm line, 200 nm groove depth) was placed beneath the coated glass substrate and the samples were run at 140 °C, 1 MPa, while exposed to 300 to 400 nm light at an intensity of 20 mW/cm² for 2 min. After light exposure, the samples were released from pressure and cooled. NIL was done with an Eitre 3, Obducat imprinter machine. The low temperature diffraction grating was imprinted by performing the same steps without the 5-micron spacers.

Glass and silicon substrates for NIL were prepared as follows: 5 min sonication in soap and water. 5 min sonication in isopropyl alcohol. Rinse with IPA and blow dry.

Controls

All particles were cast on a glass slide and pre-irradiated with 365 nm light at an intensity of 70 mW/cm² for 30 s. Non-AFT capable particles replace the ADT monomer with a non-exchangeable monomer, propane dithiol.

Control 1 – light exposed: AFT-LCEMPs not containing photoinitiator, and non-AFT capable LCEMPs prior swollen in DCM with 5 mass % DMPA, were compressed at room temperature, irradiated with 365 nm light at an intensity of 70 mW/cm² for 30 s, heated to 120 °C, and returned to room temperature displaying spherical shape recovery.

Control 2 – no light exposure, no photoinitiator: AFT-LCEMPs and non-AFT capable LCEMPs were compressed at room temperature, heated to 120 °C, and returned to room temperature displaying spherical shape recovery.

6.5 – Acknowledgements

This work was completed with the financial support of NSF DMR 1809841 and NIH grant 1 F31 DE027861-01A1. The authors gratefully acknowledge Professor Timothy White's lab, Tayler Hebner, and Kyle Schlafmann, for use of their DSC at the University of Colorado, Boulder. The authors gratefully acknowledge Professor Yifu Ding's lab and Adrienne Blevins, for use of their nanoimprinter at the University of Colorado, Boulder. The authors gratefully acknowledge the COSINC-CHR facility and Dr. Tomoko Borsa, for use of the FESEM at the University of Colorado, Boulder. Certain commercial equipment, instruments, or materials are identified in this paper in order to specify the experimental procedure adequately. Such identification is not intended to imply recommendation or endorsement by NIST. Contribution of NIST, an agency of the U.S. government; not subject to copyright.

6.6 – Supporting Information

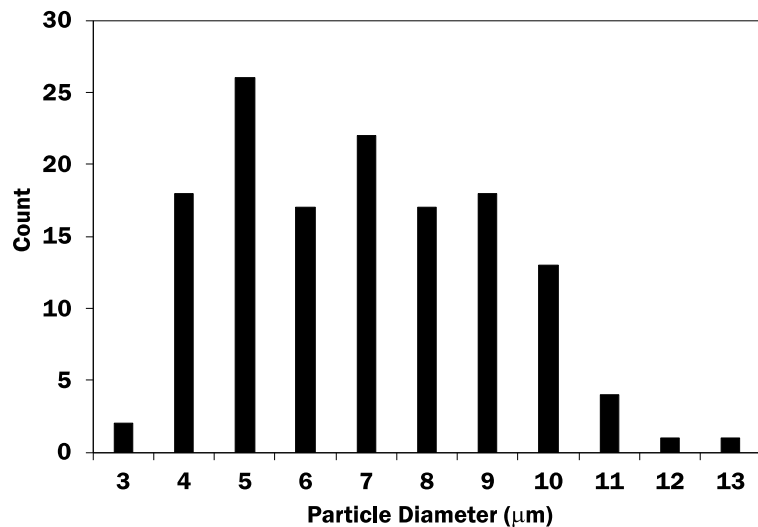


Figure S6.1: Bar graph detailing particle size dispersity for the reported system.

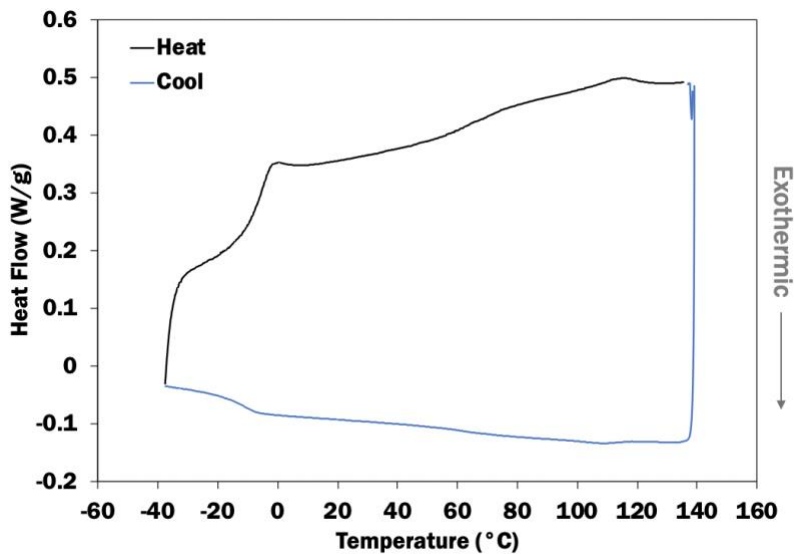


Figure S6.2: Differential scanning calorimetry for the AFT-LCEMPs.

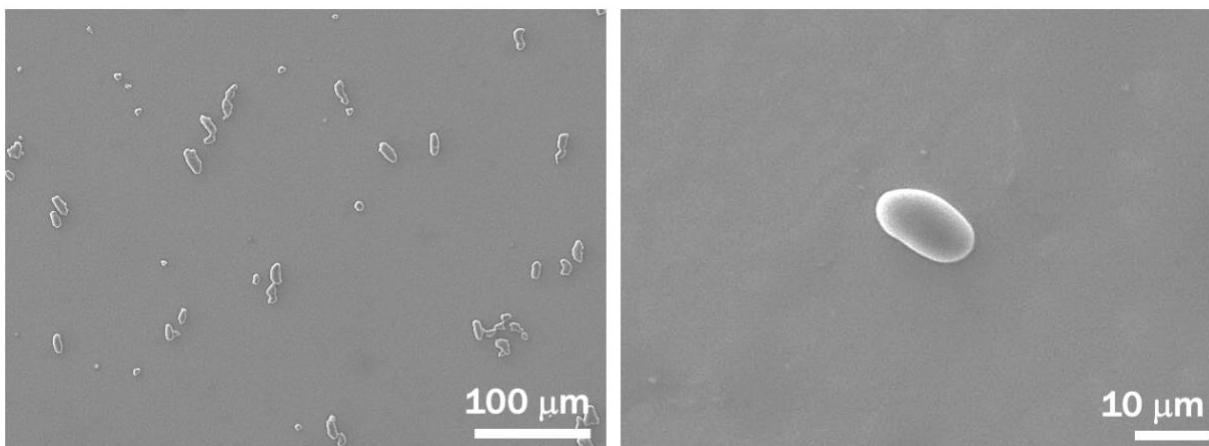


Figure S6.3: Scanning electron microscopy (SEM) of particles after programming displaying a prolate shape.

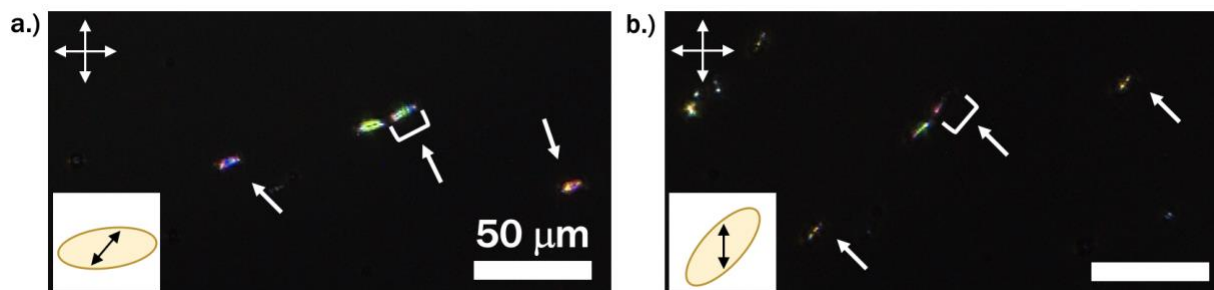


Figure S6.4: Compressed AFT-LCEMPs under POM. Inset represents a microparticle and the LC alignment director within. a.) Particles aligned with polarizers displaying a skewed alignment along the particle long axis b.) Particles 45 degrees to polarizers displaying a disappearance of birefringence.

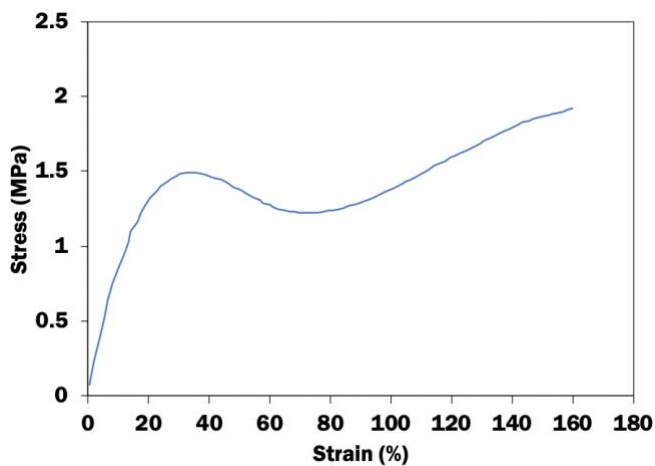


Figure S6.5: Stress-Strain profile for bulk LCE analog of the LCEMPs. Data taken until sample slipped or broke.

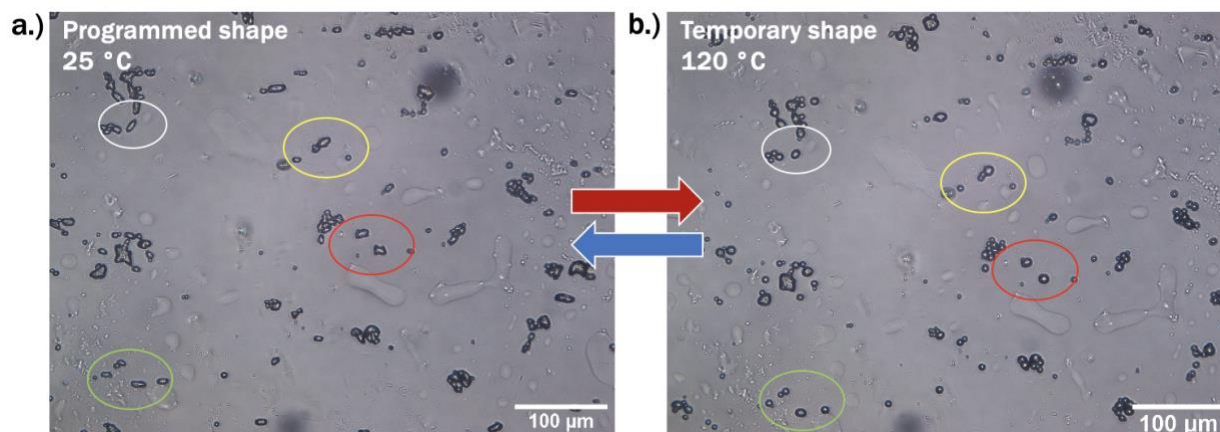


Figure S6.6: Particles after programming. a.) Programmed particles display a permanent prolate shape. b.) Particles recover temporarily to their initial shape when heated above their T_{NI} .

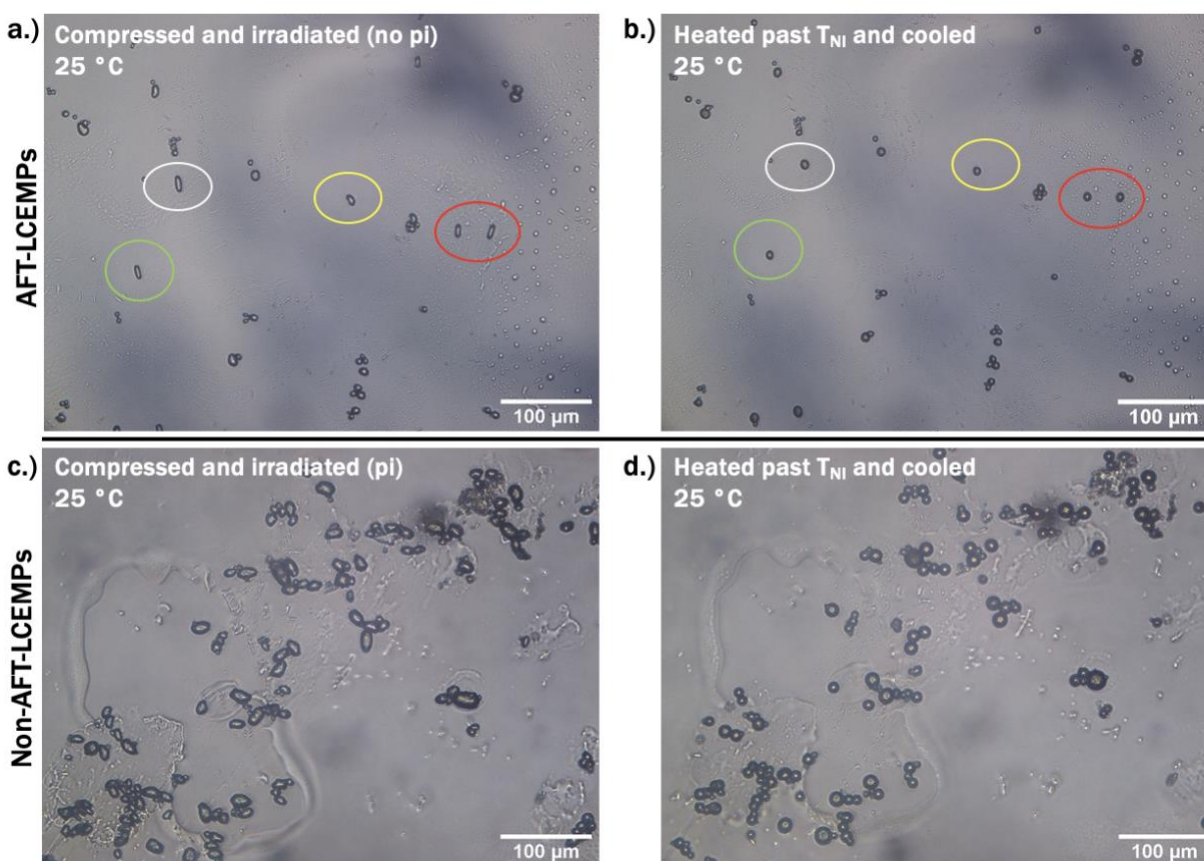


Figure S6.7: Control 1: light exposed - Particles were pre-irradiated with UV light for 30 s to ensure any excess acrylates and thiols were reacted. AFT-LCEMPs without photoinitiator (no pi) a.) Particles were compressed and exposed to light for 30 s. b.) Particles were heated past the T_{NI} and returned to room temperature displaying the recovered original spherical shape. Non-AFT

capable LCEMPs swollen with photoinitiator (pi) c.) Particles were compressed and exposed to light for 30 s. b.) Particles were heated past the T_{NI} and returned to room temperature displaying the recovered original spherical shape.

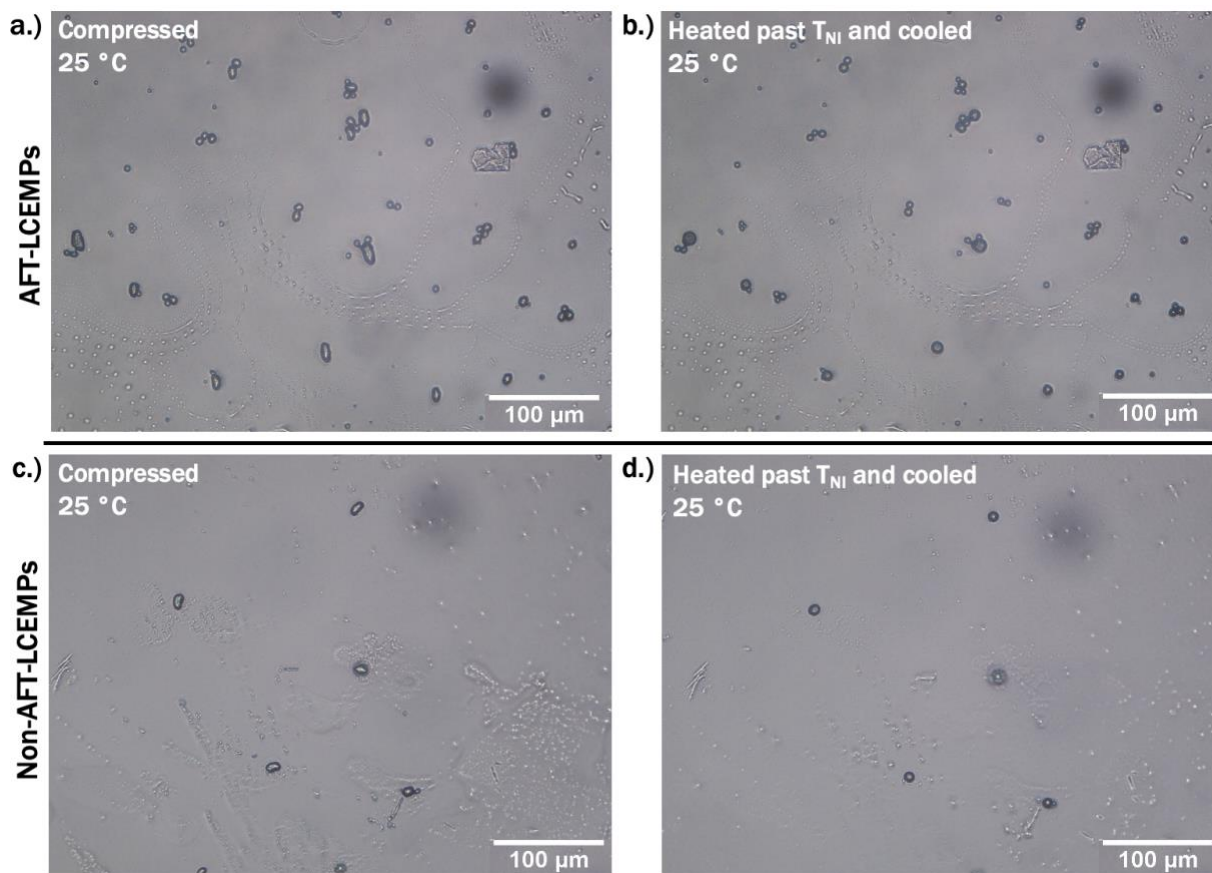


Figure S6.8: Control 2: no photoinitiator, no light exposure - Particles were pre-irradiated with UV light for 30 s to ensure any excess acrylates and thiols were reacted. AFT-LCEMPs without photoinitiator a.) Particles were compressed at room temperature. b.) Particles were heated past the T_{NI} and returned to room temperature displaying the recovered original spherical shape. Non-AFT capable LCEMPs without photoinitiator c.) Particles were compressed at room temperature. d.) Particles were heated past the T_{NI} and returned to room temperature displaying the recovered original spherical shape.

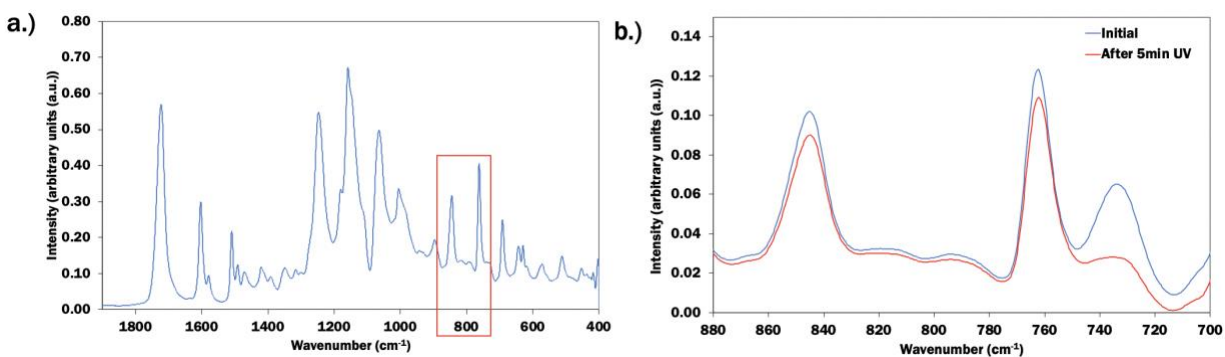


Figure S6.9: Fourier Transform Infrared Spectroscopy for a.) Dried AFT-LCEMPs not containing photoinitiator b.) Zoomed in on the faint acrylate region at 800 to 830 cm^{-1} .

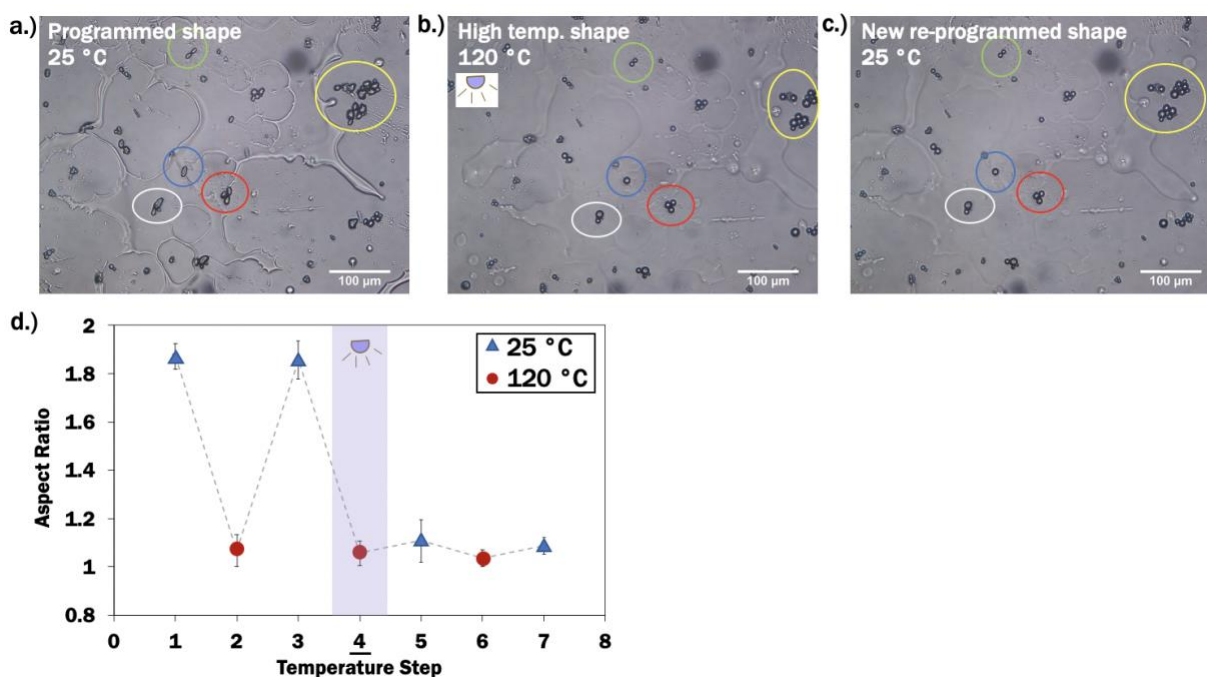


Figure S6.10: Particles undergoing reverse programming. a.) Programmed particles display a permanent prolate shape. b.) Particles recover temporarily to their initial shape when heated above their T_{NI} and are exposed to light again c.) Particles are cooled back to room temperature displaying their re-programmed permanent spherical shape. d.) Aspect ratio for particles during temperature steps demonstrating the initial prolate shape is re-programmed to a permanent sphere. Dotted line for ease of viewing.

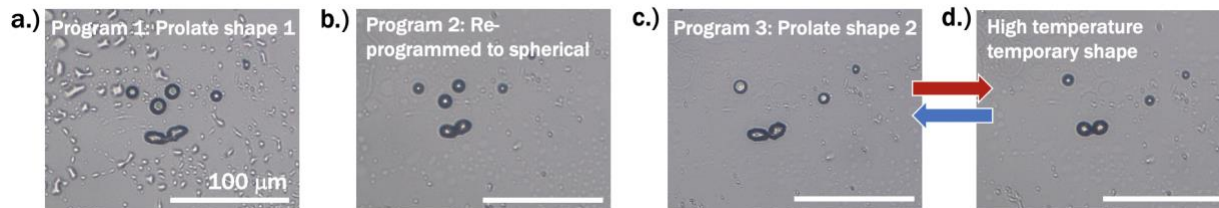


Figure S6.11: Particles undergoing 1st through 3rd Stage programming. Particles were initially swollen with Irg-819 and DMPA a.) Programmed particles display a permanent prolate shape. b.) Particles recover temporarily to their initial spherical shape when heated above their T_{NI} and are exposed to light again at high temperature, followed by cooling to room temperature, maintaining a spherical shape c.) Particles are compressed and exposed to light again to re-program the prolate shape. d.) Particles are heated above the T_{NI} and are cooled back to room temperature to recover the prolate shape and demonstrate shape switching. The shape can be toggled between prolate and spherical by thermally cycling past the T_{NI} .

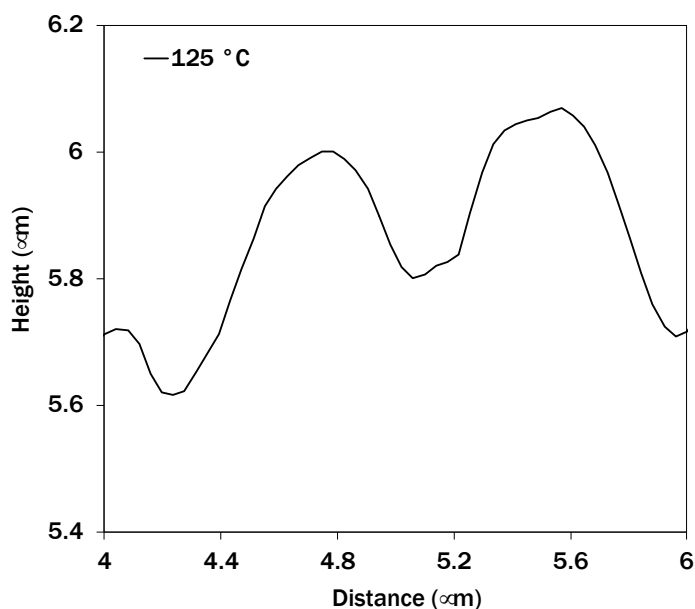


Figure S6.12: Zoomed in AFM cross-section of a single particle surface after undergoing NIL programming with a diffraction grating mold utilizing spacers, imaged at 125 °C displaying pattern profile. Axes in microns.

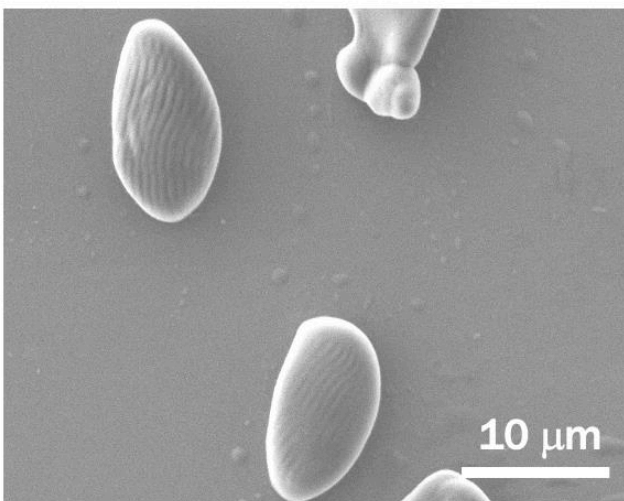


Figure S6.13: SEM of particles after NIL programming at high temperature with a diffraction grating mold, without the use of spacers, yielding a complex surface topography.

6.7 – References

- (1) Patravale, V. B.; Mandawgade, S. D. Novel Cosmetic Delivery Systems: An Application Update: Novel Cosmetic Delivery Systems. *International Journal of Cosmetic Science* **2008**, *30* (1), 19–33. <https://doi.org/10.1111/j.1468-2494.2008.00416.x>.
- (2) Birnbaum, D. T.; Brannon-Peppas, L. Microparticle Drug Delivery Systems. In *Drug Delivery Systems in Cancer Therapy*; Brown, D. M., Ed.; Humana Press: Totowa, NJ, 2004; pp 117–135. https://doi.org/10.1007/978-1-59259-427-6_6.
- (3) Xia, Y.; Gates, B.; Yin, Y.; Lu, Y. Monodispersed Colloidal Spheres: Old Materials with New Applications. *Advanced Materials* **2000**, *12* (10), 693–713. [https://doi.org/10.1002/\(SICI\)1521-4095\(200005\)12:10<693::AID-ADMA693>3.0.CO;2-J](https://doi.org/10.1002/(SICI)1521-4095(200005)12:10<693::AID-ADMA693>3.0.CO;2-J).
- (4) van Kuringen, H. P. C.; Mulder, D. J.; Beltran, E.; Broer, D. J.; Schenning, A. P. H. J. Nanoporous Polymer Particles Made by Suspension Polymerization: Spontaneous Symmetry Breaking in Hydrogen Bonded Smectic Liquid Crystalline Droplets and High Adsorption Characteristics. *Polymer Chemistry* **2016**, *7* (29), 4712–4716. <https://doi.org/10.1039/C6PY00865H>.
- (5) Bhaskar, S.; Pollock, K. M.; Yoshida, M.; Lahann, J. Towards Designer Microparticles: Simultaneous Control of Anisotropy, Shape, and Size. *Small* **2010**, *6* (3), 404–411. <https://doi.org/10.1002/smll.200901306>.
- (6) Cox, L. M.; Killgore, J. P.; Li, Z.; Long, R.; Sanders, A. W.; Xiao, J.; Ding, Y. Influences of Substrate Adhesion and Particle Size on the Shape Memory Effect of Polystyrene Particles. *Langmuir* **2016**, *32* (15), 3691–3698. <https://doi.org/10.1021/acs.langmuir.6b00588>.
- (7) Mueller, S.; Llewellyn, E. W.; Mader, H. M. The Rheology of Suspensions of Solid Particles. *Proceedings of the Royal Society A: Mathematical, Physical and Engineering Sciences* **2010**, *466* (2116), 1201–1228. <https://doi.org/10.1098/rspa.2009.0445>.
- (8) Uto, K.; Ebara, M. Magnetic-Responsive Microparticles That Switch Shape at 37 °C. *Applied Sciences* **2017**, *7* (11), 1203. <https://doi.org/10.3390/app7111203>.

- (9) Marshall, J. E.; Gallagher, S.; Terentjev, E. M.; Smoukov, S. K. Anisotropic Colloidal Micromuscles from Liquid Crystal Elastomers. *Journal of the American Chemical Society* **2014**, *136* (1), 474–479. <https://doi.org/10.1021/ja410930g>.
- (10) Liu, X.; Pan, X.; Debije, M.; Huets, J.; Mulder, D.; Schenning, A. Programmable Liquid Crystal Elastomer Microactuators Prepared via Thiol-Ene Dispersion Polymerization. *Soft Matter* **2020**, *13* (45), 8368–8378. <https://doi.org/10.1039/C7SM01619K>.
- (11) Klinger, D.; Wang, C. X.; Connal, L. A.; Audus, D. J.; Jang, S. G.; Kraemer, S.; Killops, K. L.; Fredrickson, G. H.; Kramer, E. J.; Hawker, C. J. A Facile Synthesis of Dynamic, Shape-Changing Polymer Particles. *Angewandte Chemie International Edition* **2014**, *53* (27), 7018–7022. <https://doi.org/10.1002/anie.201400183>.
- (12) Wischke, C.; Schossig, M.; Lendlein, A. Shape-Memory Effect of Micro-/Nanoparticles from Thermoplastic Multiblock Copolymers. *Small* **2014**, *10* (1), 83–87. <https://doi.org/10.1002/smll.201202213>.
- (13) Ho, C. C.; Keller, A.; Odell, J. A.; Ottewill, R. H. Preparation of Monodisperse Ellipsoidal Polystyrene Particles. *Colloid & Polymer Science* **1993**, *271* (5), 469–479. <https://doi.org/10.1007/BF00657391>.
- (14) Rešetič, A.; Milavec, J.; Zupančič, B.; Domenici, V.; Zalar, B. Polymer-Dispersed Liquid Crystal Elastomers. *Nature Communications* **2016**, *7* (1). <https://doi.org/10.1038/ncomms13140>.
- (15) Belmonte, A.; Bus, T.; Broer, D. J.; Schenning, A. P. H. J. Patterned Full-Color Reflective Coatings Based on Photonic Cholesteric Liquid-Crystalline Particles. *ACS Applied Materials & Interfaces* **2019**, *11* (15), 14376–14382. <https://doi.org/10.1021/acsami.9b02680>.
- (16) Ohm, C.; Serra, C.; Zentel, R. A Continuous Flow Synthesis of Micrometer-Sized Actuators from Liquid Crystalline Elastomers. *Advanced Materials* **2009**, *21* (47), 4859–4862. <https://doi.org/10.1002/adma.200901522>.
- (17) Yu, H.; Liu, H.; Kobayashi, T. Fabrication and Photoresponse of Supramolecular Liquid-Crystalline Microparticles. *ACS Applied Materials & Interfaces* **2011**, *3* (4), 1333–1340. <https://doi.org/10.1021/am2001289>.
- (18) Ryabchun, A.; Bobrovsky, A. Photocontrollable Deformations of Polymer Particles in Elastic Matrix. *Advanced Optical Materials* **2019**, *7* (24), 1901486. <https://doi.org/10.1002/adom.201901486>.
- (19) Vennes, M.; Zentel, R. Liquid-Crystalline Colloidal Particles. *Macromolecular Chemistry and Physics* **2004**, *205* (17), 2303–2311. <https://doi.org/10.1002/macp.200400296>.
- (20) Yang, Z.; Huck, W. T. S.; Clarke, S. M.; Tajbakhsh, A. R.; Terentjev, E. M. Shape-Memory Nanoparticles from Inherently Non-Spherical Polymer Colloids. *Nature Materials* **2005**, *4* (6), 486–490. <https://doi.org/10.1038/nmat1389>.
- (21) Haseloh, S.; Ohm, C.; Smallwood, F.; Zentel, R. Nanosized Shape-Changing Colloids from Liquid Crystalline Elastomers. *Macromolecular Rapid Communications* **2011**, *32* (1), 88–93. <https://doi.org/10.1002/marc.201000324>.
- (22) Haseloh, S.; Zentel, R. Synthesis of Liquid-Crystalline Colloids in Nonpolar Media and Their Manipulation in Electric Fields. *Macromolecular Chemistry and Physics* **2009**, *210* (17), 1394–1401. <https://doi.org/10.1002/macp.200900122>.
- (23) Hessberger, T.; Braun, L.; Zentel, R. Microfluidic Synthesis of Actuating Microparticles from a Thiol-Ene Based Main-Chain Liquid Crystalline Elastomer. *Polymers* **2016**, *8* (12), 410. <https://doi.org/10.3390/polym8120410>.

- (24) Fleischmann, E.-K.; Forst, F. R.; Köder, K.; Kapernaum, N.; Zentel, R. Microactuators from a Main-Chain Liquid Crystalline Elastomer via Thiol–Ene “Click” Chemistry. *Journal of Materials Chemistry C* **2013**, *1* (37), 5885. <https://doi.org/10.1039/c3tc30272e>.
- (25) White, T. J.; Broer, D. J. Programmable and Adaptive Mechanics with Liquid Crystal Polymer Networks and Elastomers. *Nature Materials* **2015**, *14* (11), 1087–1098. <https://doi.org/10.1038/nmat4433>.
- (26) Yakacki, C. M.; Saed, M.; Nair, D. P.; Gong, T.; Reed, S. M.; Bowman, C. N. Tailorable and Programmable Liquid-Crystalline Elastomers Using a Two-Stage Thiol–Acrylate Reaction. *RSC Advances* **2015**, *5* (25), 18997–19001. <https://doi.org/10.1039/C5RA01039J>.
- (27) Liu, X.; Xu, Y.; Heuts, J. P. A.; Debije, M. G.; Schenning, A. P. H. J. Monodisperse Liquid Crystal Network Particles Synthesized via Precipitation Polymerization. *Macromolecules* **2019**, *52* (21), 8339–8345. <https://doi.org/10.1021/acs.macromol.9b01852>.
- (28) Wang, C.; Zhang, X.; Podgórski, M.; Xi, W.; Shah, P.; Stansbury, J.; Bowman, C. N. Monodispersity/Narrow Polydispersity Cross-Linked Microparticles Prepared by Step-Growth Thiol–Michael Addition Dispersion Polymerizations. *Macromolecules* **2015**, *48* (23), 8461–8470. <https://doi.org/10.1021/acs.macromol.5b02146>.
- (29) Durham, O. Z.; Shipp, D. A. Polymer Colloids from Step-Growth Thiol-X Polymerizations. *Polymer Reviews* **2020**, 1–26. <https://doi.org/10.1080/15583724.2020.1743307>.
- (30) McBride, M. K.; Worrell, B. T.; Brown, T.; Cox, L. M.; Sowan, N.; Wang, C.; Podgorski, M.; Martinez, A. M.; Bowman, C. N. Enabling Applications of Covalent Adaptable Networks. *Annual Review of Chemical and Biomolecular Engineering* **2019**, *10* (1), 175–198. <https://doi.org/10.1146/annurev-chembioeng-060718-030217>.
- (31) Kloxin, C. J.; Scott, T. F.; Adzima, B. J.; Bowman, C. N. Covalent Adaptable Networks (CANs): A Unique Paradigm in Cross-Linked Polymers. *Macromolecules* **2010**, *43* (6), 2643–2653. <https://doi.org/10.1021/ma902596s>.
- (32) Hanzon, D. W.; Traugott, N. A.; McBride, M. K.; Bowman, C. N.; Yakacki, C. M.; Yu, K. Adaptable Liquid Crystal Elastomers with Transesterification-Based Bond Exchange Reactions. *Soft Matter* **2018**, *14* (6), 951–960. <https://doi.org/10.1039/C7SM02110K>.
- (33) Saed, M. O.; Gablier, A.; Terentejv, E. M. Liquid Crystalline Vitrimers with Full or Partial Boronic-Ester Bond Exchange. *Advanced Functional Materials* **2020**, *30* (3), 1906458. <https://doi.org/10.1002/adfm.201906458>.
- (34) McBride, M. K.; Martinez, A. M.; Cox, L.; Alim, M.; Childress, K.; Beiswinger, M.; Podgorski, M.; Worrell, B. T.; Killgore, J.; Bowman, C. N. A Readily Programmable, Fully Reversible Shape-Switching Material. *Science Advances* **2018**, *4* (8), eaat4634. <https://doi.org/10.1126/sciadv.aat4634>.
- (35) Cox, L. M.; Sun, X.; Wang, C.; Sowan, N.; Killgore, J. P.; Long, R.; Wu, H.-A.; Bowman, C. N.; Ding, Y. Light-Stimulated Permanent Shape Reconfiguration in Cross-Linked Polymer Microparticles. *ACS Applied Materials & Interfaces* **2017**, *9* (16), 14422–14428. <https://doi.org/10.1021/acsami.7b02759>.
- (36) Ware, T. H.; Biggins, J. S.; Shick, A. F.; Warner, M.; White, T. J. Localized Soft Elasticity in Liquid Crystal Elastomers. *Nature Communications* **2016**, *7* (1). <https://doi.org/10.1038/ncomms10781>.
- (37) Yu, H.; Dong, C.; Zhou, W.; Kobayashi, T.; Yang, H. Wrinkled Liquid-Crystalline Microparticle-Enhanced Photoresponse of PDLC-Like Films by Coupling with Mechanical Stretching. *Small* **2011**, *7* (21), 3039–3045. <https://doi.org/10.1002/sml.201101098>.

- (38) Liu, J.; Liu, Y.; Xue, Y.; Ren, Y.; Fan, X.; Wang, R.; Zhang, H.; Zhang, B.; Zhang, Q. Fabrication and Characterization of Controllable Wrinkled-Surface Polymer Microparticles. *Journal of Materials Science* **2019**, *54* (7), 5852–5864. <https://doi.org/10.1007/s10853-018-2421-2>.

Chapter 7: Tunable Surfaces and Films from Thioester Containing Microparticles

(Manuscript in preparation for submission early 2022)

Reported here, thioester containing microparticles formed from a covalent adaptable network (CAN) were designed with 40% excess thiol to enable thiol-thioester exchange to facilitate the formation of cohesive films from the particles. A thiol-Michael dispersion polymerization was done to generate thioester containing microparticles with a diameter of $4.0 \pm 0.4 \mu\text{m}$. The particles were then swollen with base at varying concentrations to activate the thiol-thioester exchange and subsequently compressed between two glass slides. Resultant films were characterized over time with profilometry and atomic force microscopy (AFM) to infer particle coalescence at different catalyst loadings and times. Tensile tests were performed confirming the structural integrity of the particle-based films. Furthermore, microparticles were welded to a non-dynamic network demonstrating feasibility in potential applications to generate materials containing differing mechanical properties. Being able to control the functionality of particles and thus mechanical properties of the resultant films, is also important for applications in coatings, adhesives and 3D printing where spatial patterning or selective material property control is needed.

7.1 – Introduction

Selective control over material composition is important in a multitude of applications including 3D printing,¹ biological applications,² and composites.³ The precision and selectivity with which materials can be controllably deposited is a significant challenge in controlling these properties. An example of selective deposition is direct write 3D printing, which is capable of depositing materials with micron-scale resolution.⁴ Investigating the chemistries for the writing “ink” in these processes is important to understanding and controlling resultant network hetero- or

homogeneity. Often, interfaces between materials of varying composition result in failure. Traditionally, interfacial welding is a chemical process, achieved between two materials of the same or differing chemistries, where a reaction takes place to covalently bond materials together. Self-healing at these interfaces often restores the integrity or capability of the chemistry(ies) chosen. Distinctly, the latex coalescence process can be thought about as a mechanical interfacial welding process, with increased physical entanglements of polymer chains resulting in linear polymeric films.⁵ Particle coalescence of linear or branched polymers has been studied with the resulting materials demonstrating homogenous properties. Although, the non-crosslinked characteristics of these materials make them degradable. Instances of coalesced crosslinked particles have been demonstrated but have difficulty reaching a homogenous network structure. One processing method includes vulcanization of rubber particles.^{6,7}

Covalent adaptable networks (CANs) have been at the forefront of chemistries used to address issues of homogeneity, intermolecular network exchange, self-healing, and reprocessability. As typically demonstrated in bulk films, interfacial welding is widely used as a demonstration for CAN capabilities.^{8,9} A variety of dynamic covalent chemistries (DCCs) have been demonstrated to promote self-healing or be capable of interfacial welding including Diels-Alder,^{10,11} addition-fragmentation chain-transfer,^{12,13} and transesterification.^{14,15} With this understanding, CANs have become an attractive means to control resultant material properties to address interfacial complexities for the applications listed prior. Some of these DCCs including dynamic disulfide chemistries,¹⁶ thiol-thioester exchange,¹⁷ addition-fragmentation chain-transfer,¹⁸ and transesterification-based epoxies.¹⁹ Some reports have demonstrated successful annealing of polymer particles into a coalesced film. Huang *et al.* utilized boronic ester exchange as a DCC in polymer microparticles coated with carbon nanotubes to create a cohesive network

structure with embedded functionality.²⁰ Another report by Lu and coworkers utilized the transesterification reaction to study the coalescence of vitrimer particles of different sizes, concluding particles of smaller dimension result in materials with higher mechanical properties.²¹

By incorporating CANs, networks are able to realize homogenous properties. CANs also enable re-processability or recyclability depending on the chemistry and conditions. Combining the advantages of particle coalescence with a CAN, there is potential to achieve homogeneity in crosslinked structures. CAN-particles utilized as a writing ink also have the advantage of selective deposition and structural integrity after deposition, where many liquid resins do not. Here, interfacial coalescence of CAN-microparticles containing a thioester network capable of thiol-thioester exchange is demonstrated. The network is designed with free thiols, which exchange with the thioester backbone, with this mechanism being base catalyzed. By activating the DCC within the CAN, particles are transformed into robust polymer films with comparable mechanical integrity to polymer films made directly from monomers. The mechanism for coalescence is driven by inter-particle bond exchange. By selectively varying the catalyst loading and processing time, control over the particle coalescence to a film is demonstrated and evaluated with UV-visible spectroscopy (UV-vis), optical microscopy, profilometry, and atomic force microscopy (AFM). Furthermore, we demonstrate the ability to create a cohesive polymer film with selectively deposited particles resulting in spatially controlled mechanical properties.

7.2 – Results and Discussion

Here, amorphous crosslinked microparticles are designed and synthesized with a CAN achieving selectively controllable bond exchange to activate particle coalescence resulting in crosslinked film formation. The particles include catalyst activated thiol-thioester exchange, with

excess thiols designed into the network. To generate crosslinked particles capable of thiol-thioester exchange, a thiol-Michael dispersion polymerization was done in MeOH utilizing PETMP and the thioester diacrylate monomer (TEDA) at a 1.4 to 2 monomer molar ratio, leaving a 40% excess of thiol (**Figure 7.1a**). Polyvinylpyrrolidone (PVP) was added at 50 wt% with respect to monomers to stabilize microparticle formation. Triethylamine (TEA) was used to catalyze the polymerization at 10 wt% with respect to monomers. TEA also catalyzes the thiol-thioester exchange. Microparticles had an average diameter (D_n) of $4.0 \pm 0.4 \mu\text{m}$ with a coefficient of variance (CV) of 10% as determined by ImageJ analysis of optical microscopy (**Figure 7.1b**). Particle size distribution is reported in **Figure S7.1**. Dynamic scanning calorimetry (DSC) was done to determine the glass transition (T_g) of the particle network to be -22°C (**Figure S7.2**). Fourier-transform infrared spectroscopy (FTIR) was run on dry particles to confirm the presence of residual, unreacted thiol and practically complete consumption of the acrylates as seen in **Figure S7.3**.

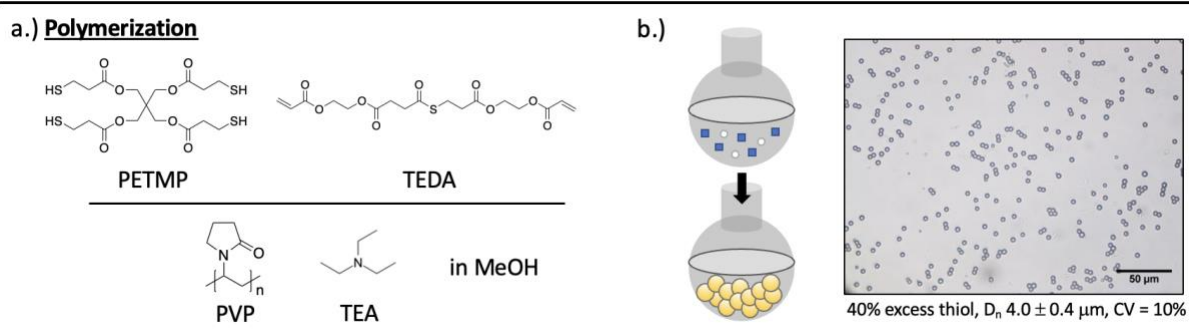


Figure 7.1: a) Monomers and reaction constituents for the thiol-Michael dispersion polymerization b) Optical microscopy of thioester containing microparticles.

The particle casting and coalescence process is illustrated in **Figure 7.2a**, where particles are cast on a substrate, and upon addition of the appropriate stimuli, the result is a homogenous covalent network. To demonstrate coalescence, dry particles were cast on a glass slide at room

temperature. Particles were then swollen with liquid base, N,N,N',N'',N''-pentamethyldiethylenetriamine (PMDETA), as the catalyst for the thiol-thioester exchange. The initial polymerization was done with TEA, but due to PMDETA's higher boiling point, this catalyst was chosen to swell into particles to mitigate evaporation over sample processing times. In the presence of free thiols, the base deprotonates the free thiol to generate a thiolate anion that is then able to add into the thioester carbonyl (**Figure 7.2b**). This reaction then enables bond exchange where the bond to another sulfide is broken, regenerating the thiolate anion, and the reaction persists so long as the base catalyst is present. This behavior results in inter-particle bond exchange and thus coalescence into a homogenous polymer film. The particles were compressed between two pieces of glass, maintained at ambient conditions, and monitored over time, resulting in free standing polymer films with a thickness of about 150 microns after 24 hours (**Figure 7.2c**).

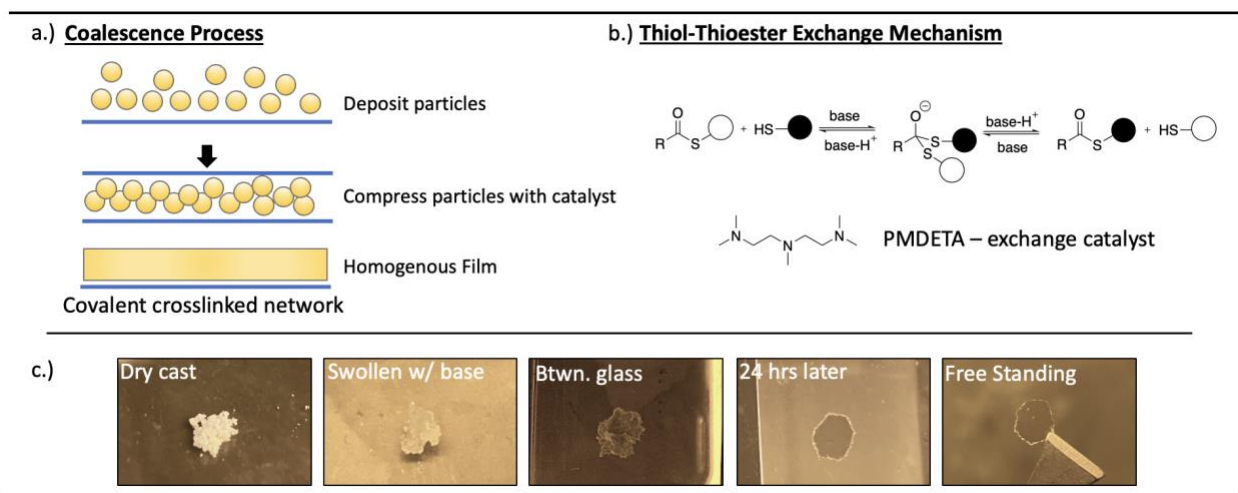


Figure 7.2: a) Schematic of the particle deposition and coalescence process b) Mechanism for the thiol-thioester exchange. c) Images from the actual particle casting and coalescence process over time.

The concentration of base added was 5, 10, or 20 wt% relative to the monomers to control the timescale with which bond exchange and coalescence occurred. Optical microscopy was performed to observe the coalescence process over time at the three catalyst loadings seen in **Figure 7.3**, including corresponding images of the polymer films (**Figure S7.4**). Time points

include the particles initially just after swelling with base, 1 hour, 6 hours, and 24 hours, after swelling. Distinct particle boundaries are observed, although in many regions, resolution of every individual particle cannot be achieved due to their contact with the glass and each other in the swollen state. Visually, over time, there is a reduction of visible particle boundaries with the coalescence of the individual polymer networks. A control was run for 24 hours without the addition of base, to confirm a lack of particle coalescence (**Figure S7.5**).

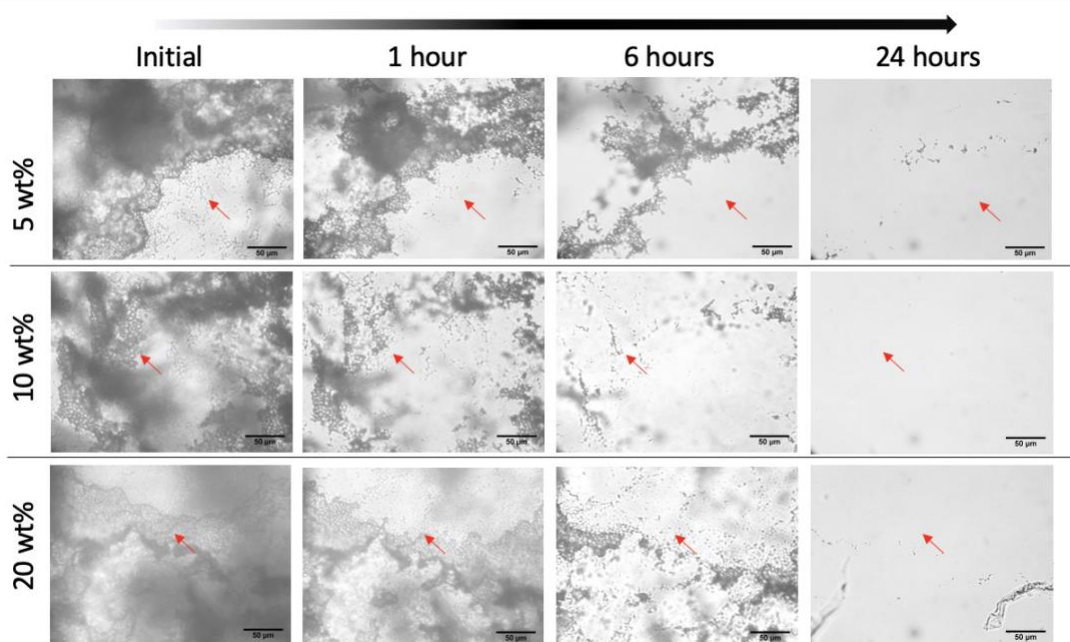


Figure 7.3: Optical microscopy of the particle coalescence process over time at varying concentrations of base: 5, 10, and 20 wt% loading. Imaged immediately after swelling, 1 hour, 6 hours, and 24 hours after swelling displaying particle coalescence through the bulk of the film over time. A red arrow has been placed in the same position for each catalyst loading as a reference to monitor particle coalescence.

In samples containing base, optical transparency improves over time due to coalescence, which was observed by eye and by optical microscopy (**Figure 7.4a**). This increase in transparency was also confirmed by UV-vis (**Figure 7.4b**). Transmission was reported at a wavelength of 600 nm.

Complete UV-vis spectra are available in **Figure S7.6**. Over time, transmission increases until about 3 days. There is very little increase in transmission from 3 days to 7 days, indicating the coalescence process has reached near completion, optically, by the third day. Particle coalescence at the 10 and 20 wt% catalyst loadings had comparatively similar behavior, but the 5 wt% loading was slower and did not achieve the same final transmission value as the 10 and 20 wt% loadings, by the seventh day. UV-vis was run for the control not containing base, with no change to the spectrum from the initial time point to 24 hours later, confirming a lack of particle coalescence without the presence of the exchange catalyst (**Figure S7.7**). These optical characterizations measure the behavior through the thickness of the material while surface measurements are presented later. It is important to note that samples cannot be reproduced exactly in regard to particle distribution during casting and swelling, with variable contact points during compression, so some variability is expected in results, with the overarching conclusion that addition of base does induce particle coalescence.

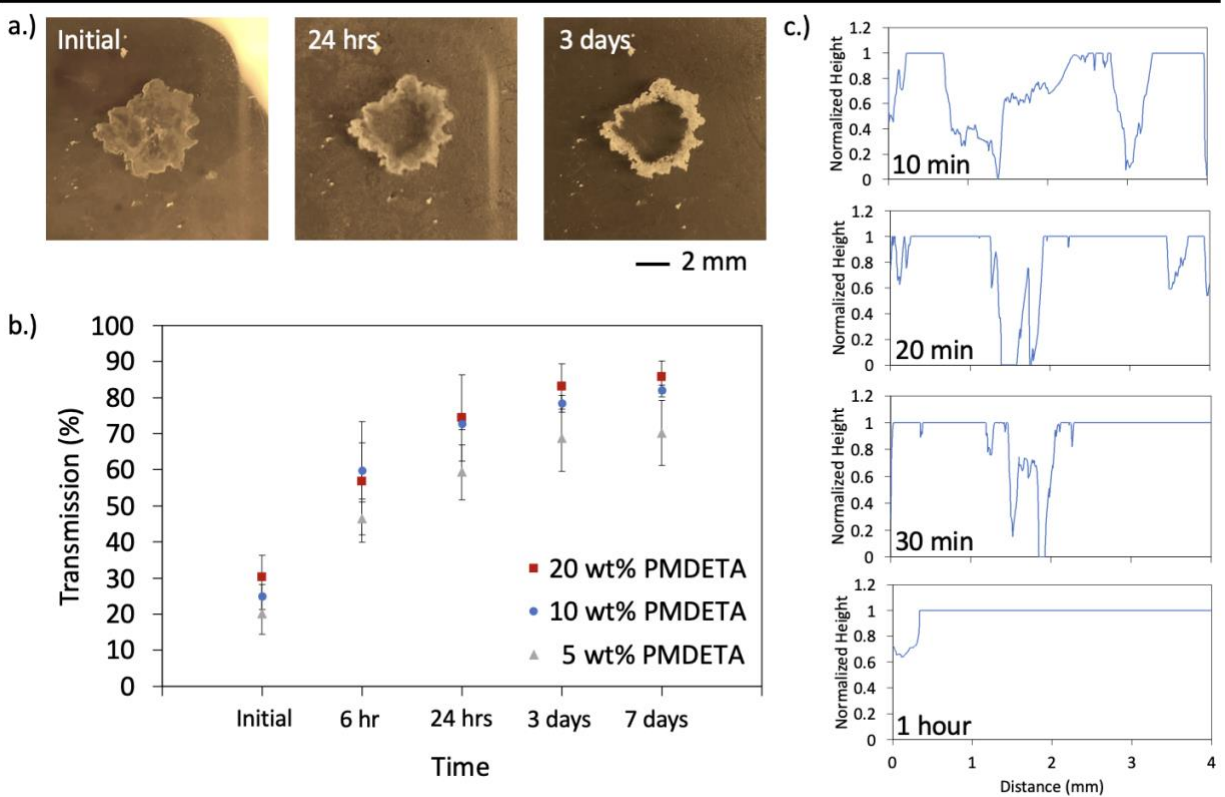


Figure 7.4: a) Images of films undergoing particle coalescence over time b) UV-vis for particle coalescence over time at 5, 10, and 20 wt% catalyst loadings reported at 600 nm. c) Profilometry for the 20 wt% catalyst loading at time increments of 10, 20, 30 min, and 1 hour.

To confirm control of the time scale of bond exchange and coalescence via modulation of the catalyst concentration, stress relaxation experiments were performed on bulk polymer films made from monomers, as an analog to replicate the particle bond exchange. Bulk films were polymerized neat utilizing the same monomer stoichiometry used for the particle formulation of 1.4:2 PETMP to TEDA. To mirror the particle polymerization process, the reaction was catalyzed with TEA and allowed to react overnight. TEA was evaporated from the films and the films were subsequently swollen with indicated amounts of the exchange catalyst, PMDETA, prior to testing. DSC was run to confirm the network of the bulk film was representative of the particle network, with the T_g of the bulk film being -21°C , recalling that the T_g of the particles was -22°C (**Figure**

S7.2). Stress relaxation was performed on rectangular films strained to 5% in tension at ambient conditions. The results in **Figure S7.8** conclude that increasing the content of the base increases the rate at which stress relaxation occurs, which was also investigated previously from thiol-thioester exchange studies done by Worrell et al.²² A control was run at ambient conditions without any base to confirm stress relaxation does not occur in this formulation without the presence of base, and also confirming the base evaporation step is successful. The 20 wt% base concentration was chosen as the representative system to perform further characterization experiments due to its rapid relaxation behavior determined by bulk film stress relaxation tests, although in optical microscopy and UV-vis, particle coalescence at the 10 and 20 wt% catalyst loadings, as mentioned prior, had comparatively similar behavior.

Profilometry was performed to measure changes in the surface topography of the particle coalescence over time at the 20 wt% catalyst concentration (**Figure 7.4c**). Samples were prepared in the same manner as for the optical experiments. To perform surface scans, the sample was removed from between the glass slides, and the base was evaporated off at 70°C for 6 minutes before scanning, so the liquid base did not confound the probe measurements. The sample was scanned, base was then re-added to the sample, and it was sealed between glass again until the next scanning time point. The same sample was used for testing the 10, 20, and 30 minute timepoints, following the procedure listed above, but a new sample was used to test the 1 hour time point. Opening and closing of the sample has the capacity to disturb the coalescence behavior, so for the longest timepoint, a pristine sample was used. Profilometry showed the reduction of surface features measured over time on the order of millimeters to microns. At 1 hour, films reached a relatively flat surface, although in optical microscopy particle coalescence was occurring up until 24 hours, and in the UV-vis, transmission continued to change through the bulk of the material for

up to about 3 days (**Figure 7.4, S7.6**). These results indicate that stresses at the particle and glass interface are likely much higher than through the bulk and results in faster relaxation time scales.²³ It is important to note, that as reported in literature, elevated temperatures can enhance stress relaxation.²² During the evaporation step, it is likely stress relaxation is enhanced, although, the particles are no longer being compressed between glass. To determine that this issue was not significant, control UV-vis experiments were performed where a sample was still clamped between glass and heated to 70°C for 6 min to replicate the temperature and duration of heating for the profilometry experiments. No significant change was seen in the spectrum from before and after heating at the 30 minute time point (**Figure S7.9a**). The same sample after sitting for 1 hour was heated to 100°C for 10 minutes. There was a slight increase of transmission, but it was also noticed that the base was being removed from the film (**Figure S7.9b**). Heating the sample at 100°C confirmed that processing at too high of temperatures results in depletion of the base, which would ultimately result in retardation of bond exchange and polymer coalescence once a significant amount of the catalyst is removed. These controls confirm that the heating steps taken to remove base for profilometry measurements are not significantly enhancing stress relaxation or confounding measurements. Profilometry data overall confirmed that particle surface features reduce to flat surfaces on a shorter time scale than coalescence through the bulk of the material. It also confirms the main phenomenon of this study that particles are coalescing into films.

AFM was performed at the surface of the particle coalescence process at the glass-particle interface, to determine homogeneity of the network modulus. Optical characterization gave qualitative information about particle coalescence and quantitative light transmission information through the film thickness. Profilometry was limited to measuring surface topography, although it was able to scan shorter time points than AFM, with the surface topography being too great to scan

until later time points. AFM was used to measure the surface modulus changes over time after the addition of the base catalyst. Samples were made and measured mirroring the process used for profilometry at 20 wt% base. AFM confirmed that surface topography was relatively flat at 1 hour, with tens of nanometers length scale changes still occurring on the surface up to 3 days (**Figure S7.10**). It is important to note, that although optical characterization suggests homogeneity at 3 days, the modulus map seen in **Figure 7.5a** still displays a measurable interface in the modulus between particles at this time point. Total coalescence and modulus homogeneity is not yet achieved until about 7 days (**Figure 7.5b**). The particle coalescence process predicted by Long *et al.* in a modeling study of vitrimer particle coalescence behavior, reports that interfaces between particles undergo regimes of elevated stress as compared to the bulk particle, and eventually result in coalescence.²⁴ Initially, crosslink density may be low between particles, but at sufficient lengths of time, the increase in crosslinking across the interface results in modulus values near that of the bulk particle and ultimately results in a homogenous surface. It is also important to recall that coalescence behavior at the glass-particle interface occurs on a faster timescale than through the bulk, so the modulus through the bulk may not be homogenous at the same time as the surface.

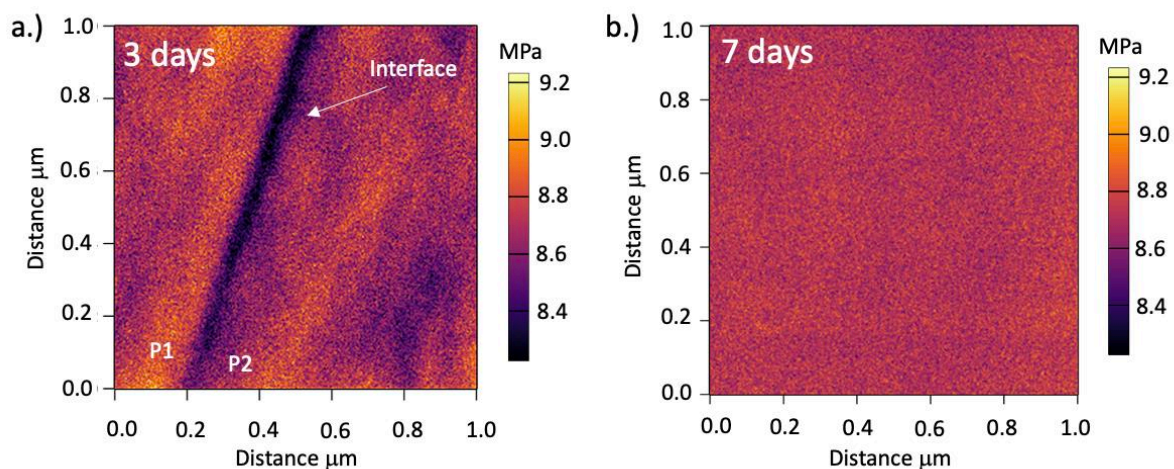


Figure 7.5: AFM modulus map for an interface between two particles (P1 and P2) at a) 3 days and b) 7 days of compression.

Interestingly, at 24 hours and up to about 7 to 10 days, the sample, visible by eye, has a noticeably heterogenous appearance through the thickness, having an almost “stained glass” appearance (**Figure S7.11**). UV-vis reports relatively unchanging transmission after 3 days although the texture is still visible at 3 days (**Figure 7.4, S7.6**). It has been determined by profilometry and AFM, that the surface is relatively flat at this timepoint, so this phenomenon is likely occurring through the bulk.

Uniaxial tensile tests were performed on dog-bone shaped films prepared from particles via the coalescence process and compared with films formed by bulk polymerizations from monomer, to compare the integrity of the films generated by the particle coalescence process (**Figure 7.6**). Thioester containing particles were cast into a rectangular shape and 20 wt% base was added. The sample was then compressed between glass and allowed to coalesce, with samples setting at two timepoints, 3 and 7 days. At each time point, the samples were then thermally treated to remove base and halt any dynamic processes thereafter. After 3 and 7 days of particle coalescence, there are no further transmission changes, with a near identical spectrum to the

monomer-films (**Figure S7.12**). For the monomer-film polymerizations, PETMP and TEDA were mixed with TEA to catalyze the reaction and immediately cast and compressed between glass. The reaction proceeded overnight, and the following day TEA was evaporated from the films. All samples for tensile testing no longer contained base.

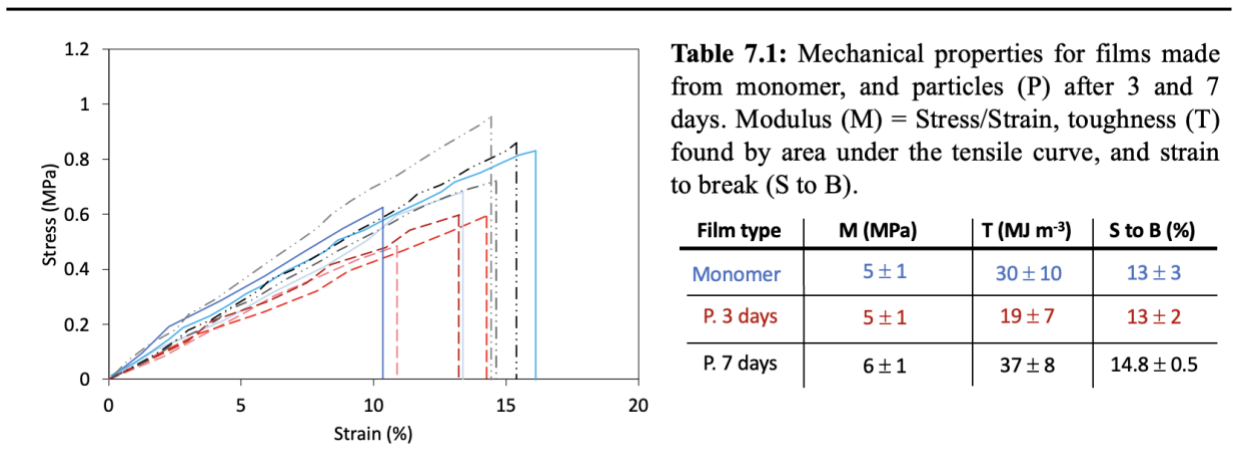


Figure 7.6: Tensile tests for films prepared from monomer (blue + repeats), particles after 3 days (red, dashed + repeats), particles after 7 days (black, long dash + repeats).

After 3 days of coalescence time, the modulus and toughness reported in **Table 7.1** are 5 ± 1 MPa and 19 ± 7 MJ/m³ respectively, with the modulus being the same as the monomer-film, but the toughness being lower. Modulus and toughness for the monomer-film were measured to be 5 ± 1 MPa and 30 ± 10 MJ/m³. After 7 days of coalescence, the particle-films appeared to have comparable mechanical properties to that of the films made from monomer with the modulus and toughness of the particle-films being 6 ± 1 MPa and 37 ± 8 MJ/ m³ respectively. The mechanical properties are comparable and within error, concluding that the films made from particles do not result in compromised integrity after 7 days of coalescence time, in comparison to their counterpart made directly from monomer. From this analysis it is determined that thioester containing microparticles are able to achieve comparable mechanical properties in comparison to bulk

polymerized films. Particle-films also have the advantage of annealing out defects over the longer processing time than the monomer-films.

A second network was developed not containing the thioester backbone but was designed with excess thiols. The network is not dynamically active, but it can participate in bond exchange with the particle network through the availability of the excess thiols. The second network was designed with a 1:2 monomer molar ratio of 2,4,6-triallyloxy-1,3,5-triazine (TAT) and hexane dithiol (HDT), achieving a 33% excess of thiols and a T_g of -55°C (**Figure S7.13**). A thiol-ene polymerization reaction was done to form the network by mixing in photoinitiator with the two monomers and irradiating the resin with light. The secondary network and thioester containing microparticles were coupled via interfacial thiol-thioester exchange (**Figure 7.7**). Particles were cast overlapping a rectangular film comprised of the secondary network (2nd Net.) and base was added to induce bond exchange with the film.

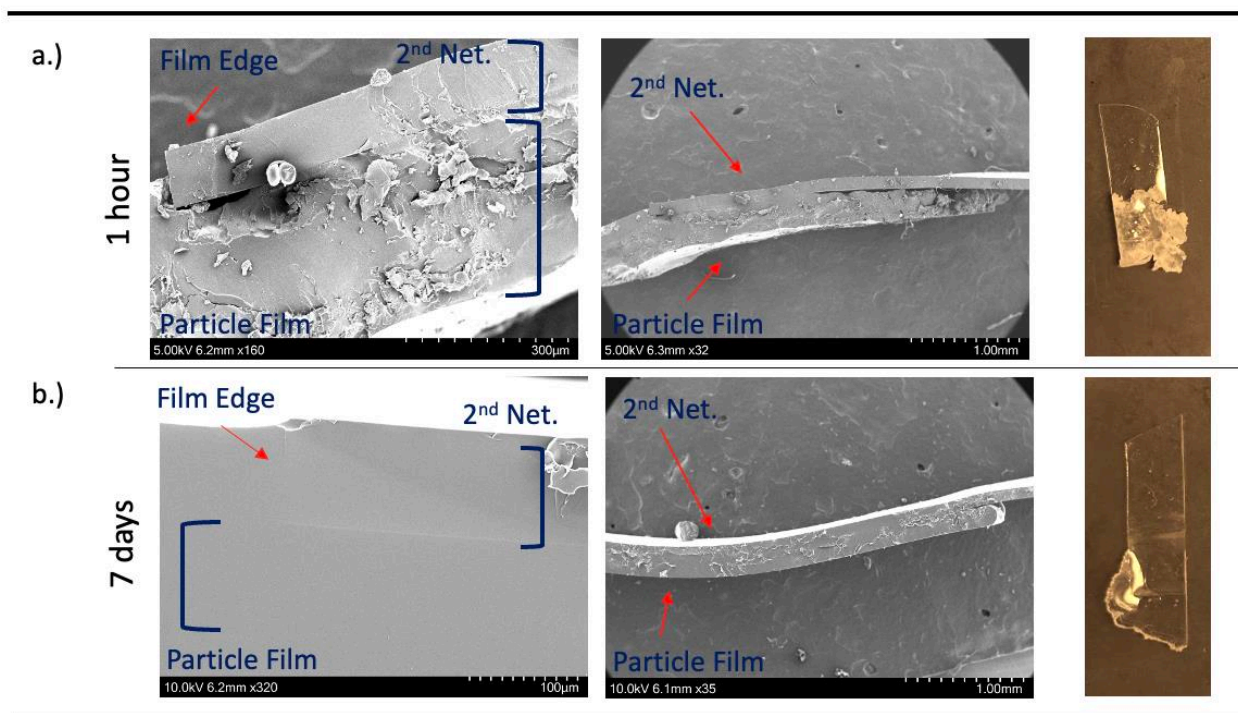


Figure 7.7: SEM for particles welding to the secondary network (2nd Net.) at a) 1 hour, showing a visible interface between the films, and b) 7 days, with a nearly indiscernible interface between

films. The film made from the secondary network is positioned in the top of each photo and the film made from particles is on the bottom. To the right is an image of the joined polymer films at the corresponding weld times with the secondary network to the top of the image, and the particle film towards the bottom.

Scanning electron microscopy (SEM) was performed on the sample after 1 hour and 7 days of compression to confirm welding between particles and the film. At 1 hour, there are very noticeable voids between the secondary network and the particle layer (**Figure 7.7a**). At 7 days the two interfaces are almost indiscernible, but at higher magnification, there is still a faintly visible interface (**Figure 7.7b**). The secondary network was designed to demonstrate the compatibility of CAN particles with networks of differing chemistries.

Another demonstration was performed, where the thioester particles were selectively deposited along two rectangular strips of the secondary network (**Figure 7.8**). Base was added to the particles, the materials were then compressed between glass, and allowed to coalesce for 3 days.

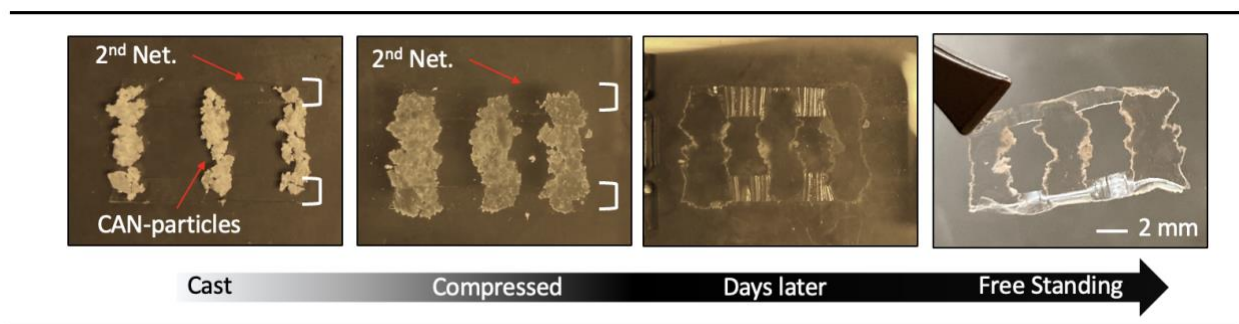


Figure 7.8: Images of particles being welded to the secondary network in a complex geometry. The particles are initially cast, compressed with base added, and allowed to coalesce and weld over time, resulting in a free-standing polymer film.

After the particles were allowed to coalesce and weld over time, a free-standing polymer “part” is achieved. There is noticeable deformation to the part due to shrinkage stress, which could be

alleviated if the secondary network was designed as a CAN, enabling stress relaxation throughout the entirety of both networks and welding sites.

Moving forward with this technology, different sets of microparticles with varying mechanical properties, could be selectively deposited and coalesced together to control resultant mechanical properties within one material. Also, it would be interesting to study the coalescence behavior on shorter timescales if at all achievable, specifically using AFM to map the modulus changes on earlier time scales.

7.3 – Conclusions

Thioester containing microparticles were synthesized via a thiol-Michael dispersion method. This yielded particles capable of interparticle dynamic covalent bond exchange. The particles designed with an excess of thiol were compressed after the addition of a base catalyst, which resulted in coalescence into homogenous polymer films. Optical and surface analyses measured and confirmed the particle coalescence into homogenous polymer films. Uniaxial tensile tests were performed to compare films made from monomer to films made from particles, with the results concluding that there is no compromise to the network integrity after particle coalescence. Mechanical properties of the particle-films are comparable to monomer-films. Furthermore, welding of the particles to a secondary non-CAN network, also containing excess thiols, demonstrated the ability for this technology to be utilized for selective particle deposition to result in spatial control of material properties in a resulting polymer film.

7.4 – Experimental

Materials

Pentaerythritol tetrakis(3-mercaptopropionate) (PETMP) and triethylamine (TEA), polyvinylpyrrolidone (PVP), 2,4,6-triallyloxy-1,3,5-triazine (TAT), hexane dithiol (HDT), and Methanol were purchased from Sigma-Aldrich. Irgacure-819 was purchased from iGM resins. Binder clips were purchased from Staples and used brand new.

Thioester Diacrylate (TEDA) Synthesis

Synthesis largely followed after that reported and developed by Worrell et al.²⁵

Microparticle polymerization

Microparticle polymerization was performed as follows with a monomer molar ratio of 1.4:2 PETMP to TEDA to yield a network with excess thiol. 0.09935 g of PVP (50 wt% to monomers) was dissolved in 3.14 mL (2.48 g) of MeOH (8 wt% monomers to solvent). 0.0913 g (0.0713 mL) of PETMP was dissolved. 0.1074 g (0.100 mL) of TEDA was dissolved. The mixture was stirred, and TEA was then added to start the reaction at 0.01987 g (0.0274 mL at 10 wt% to monomers). The reaction ran for 1 hour and was then quenched with 10% excess of acetic acid for 30 minutes. The mixture was centrifuged at 3000 RPM for 2 minutes, pouring off the clear supernatant, and subsequently washed and centrifuged 3X with MeOH at 3X the volume and spun at the same conditions. MeOH was largely poured off, and the remaining solvent was allowed to evaporate at ambient conditions for two days. The dry particles were then stored in the freezer (-18°C). The polymerization resulted in a yield of about 90%.

300 particles chosen randomly were analyzed via optical microscope images with ImageJ to determine average diameter (D_n) and coefficient of variance (CV). CV was calculated as $CV\% = (SD/D_n * 100)$, where SD = standard deviation. Optical microscopy was done with a Nikon Eclipse Ci.

Bulk film polymerization (particle coalescence) from particles

Done at ambient conditions. Particles were cast on a glass slide. Indicated amounts of PMDETA liquid base were added to the particles. Ex: 10 mg of particles cast, 5 wt% base – 0.5 mg of base added, 10 wt% base – 1 mg of base added, 20 wt% base – 2 mg of base added. The particles were then compressed between two pieces of glass using binder clips and 100-micron spacers. Using 10 mg of particles repeatedly resulted in 150-micron films despite the spacer thickness used.

Bulk film polymerization from monomer

At a 1.4:2 PETMP to TEDA monomer molar ratio, 0.1369 g of PETMP (0.10698 mL) was mixed with 0.1611 g of TEDA (0.150 mL). 0.00894 g of TEA was added (0.0123 mL at 3 wt% to monomers) and the mixture was cast and compressed between glass slides utilizing indicated spacers to control thickness. The films were allowed to react overnight. To remove the TEA, the films were held at 70°C in a vacuum oven overnight and the following day placed on a hot plate at 100°C for ~2 hrs. while vacuum was pulled, to remove any remaining TEA, until the mass of the film no longer changed (indicating TEA removal).

Secondary network for welding demonstration

1:2 monomer molar ratio of 2,4,6-triallyloxy-1,3,5-triazine (TAT) and hexane dithiol (HDT) were mixed with 1 wt% photoinitiator Irgacure-819. The mixture was cast and compressed between glass using 100-micron spacers. The resin was irradiated with 400-500 nm light at 70mW/cm² for 2 minutes. Two-piece welding demo: A piece of the secondary network was cut. 10 mg of particles were cast overlapping and extending beyond the secondary network. 20 wt% PMDETA was added to the particles and the materials were clamped between glass and coalesced for 1 hour and a second sample for 7 days. Complex shape demo: Two strips of the secondary network were laid out. 30 mg of particles were split into three regions and 20 wt% of PMDETA was added to the particles. The materials were then clamped between glass and allowed to coalesce for 3 days.

SEM

SEM was performed on a Hitachi SU3500.

Ultra-violet Visible Spectroscopy (UV-vis)

UV-vis was run on a Thermo Fisher Scientific Evolution 300. Samples were measured with a Xenon lamp in transmittance between 200 and 1000 nm with a scan speed of 240 nm min⁻¹. Data intervals were taken at 1 nm and a bandwidth of 2 nm. A background was run and subtracted from the data.

Profilometry

Samples were prepared as described in (particle coalescence) section. Samples were then opened at each time point (10 min, 20 min, 30 min) and the base was evaporated at 70°C for 6 min. The

samples were then scanned. Samples were reswollen with appropriate amounts of base and clamped again until the next time point was reached, and the same steps were followed to take measurements. For the 1-hour sample, this sample was allowed to sit unopened for 1 hour and then scanned. Scan speed 100 s. Scans run on a Dektak 6m profilometer.

Atomic Force Microscopy (AFM)

Atomic force microscopy (AFM) analyses were performed with an Asylum Research Cypher S force microscopy system with an etched silicon tip (Tap300Al-G, 40 N/m spring constant, BudgetSensors, Sofia, Bulgaria). Fast force mapping (FFM) scans were performed at 250 Hz with a peak force of 300 nN. FFM force curves were analyzed using a Hertzian contact mechanics model to generate a maps modulus gradation at particle interfaces with sub-20 nanometer spatial resolution.

FTIR

Attenuated Total Reflectance (ATR) - FTIR was done on dried particles. 32 scans with a resolution of 4. ATR-FTIR was run on a Thermo Fischer Scientific Nicolet iS50 FT-IR.

DSC

The samples (particles or bulk film) were initially heated to 70°C to erase thermal history, cooled at 5 °C/min to -70°C and the test was run from -70 to 70°C, ramped at 10°C/min, to generate the reported curve. DSC was run on a TA DSC 2500.

DMA

Tests were run on an TA RSA-G2.

Stress Relaxation

Bulk films made from monomers were used. Indicated amounts of liquid base PMDETA were swollen into the films post-polymerization. 5 wt% strain was exacted on the films and run for 2 hours at ambient conditions. *Control*: Bulk films from monomer with base evaporated out as described above were run at the same conditions. 100-micron thick films.

Stress-Strain

Bulk films made from monomer: Procedure as listed above utilizing 400-micron spacers. *Bulk films made from particles*: Films were prepared as discussed above and allowed to process for 3 and 7 days. To remove the base, the films were held at 70°C in a vacuum oven overnight and the following day placed on a hot plate at 100°C for ~2 hrs. while vacuum was pulled, to remove any remaining base, until the mass of the film no longer changed (indicating base removal). Dog-bone dimensions for all samples were approximately 12.47 mm x 2.5 mm x 0.37 mm (lxwxt). Samples were strained at 0.1 mm/s at ambient conditions and run in triplicate for each polymer film type. Young's Modulus was calculated as the slope of the tensile curve (Stress/Strain). Toughness was found using the trapezoid rule to find the area under the tensile curve.

7.5 – Acknowledgements

The authors would like to thank Lewis Cox, Amir Darabi-Noferesti, and Nicholas Bongiardina for contributions to this chapter. This work was completed with the financial support of National Science Foundation (NSF) DMR 1809841, NIH grant 1 F31 DE027861-01A1, and NSF funding under grant number CMMI-2038512. The authors would like to thank the CU Boulder COSINC-FAB facility for use of their profilometer. The authors would like to thank CU Boulder COSINC-

CHR facility for use of their SEM. The authors would like to thank Professor Tim White's lab, for use of their DSC.

7.6 – Supporting Information

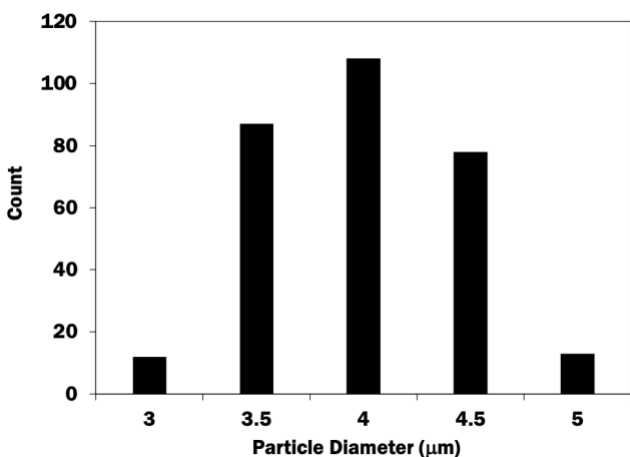


Figure S7.1: Particle size distribution for the thioester containing microparticles.

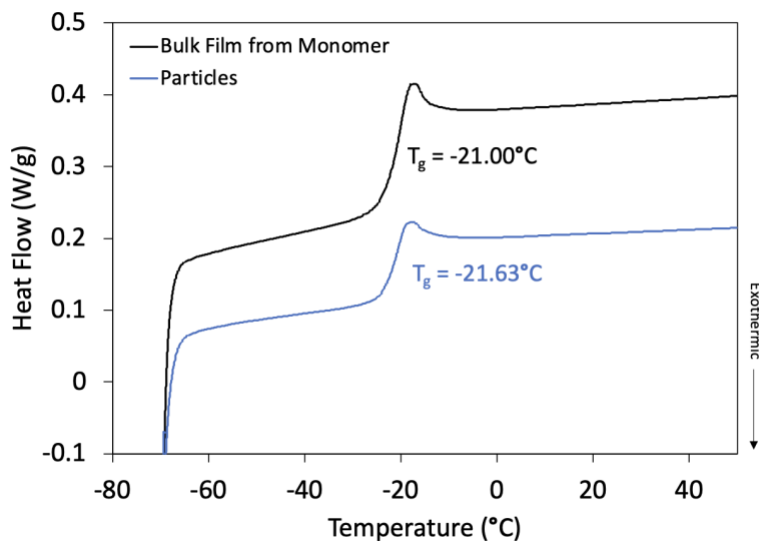


Figure S7.2: DSC traces for microparticles and bulk film made from monomer.

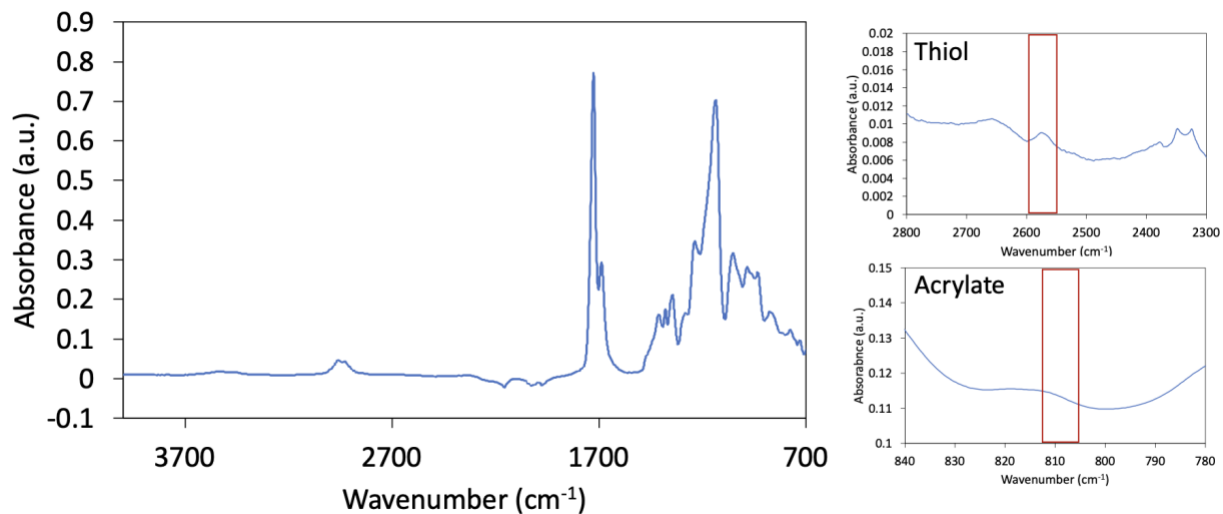


Figure S7.3: FTIR for thioester containing particles with 40% excess thiol.

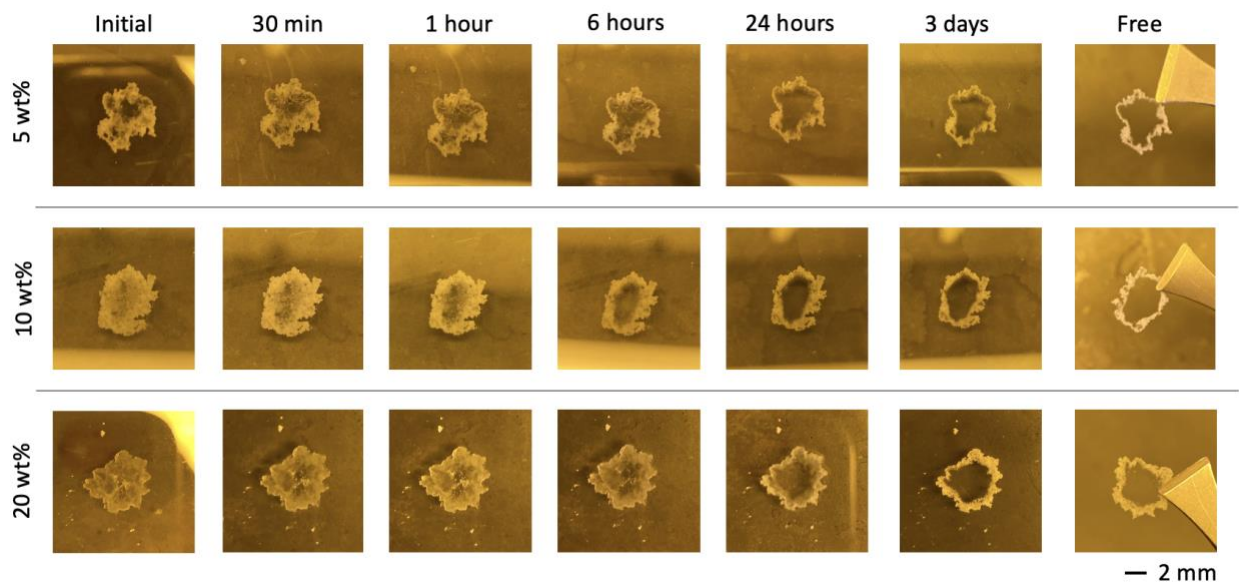


Figure S7.4: Images of particles coalescing into films for the designated catalyst loadings (5, 10, and 20 wt% PMDETA).

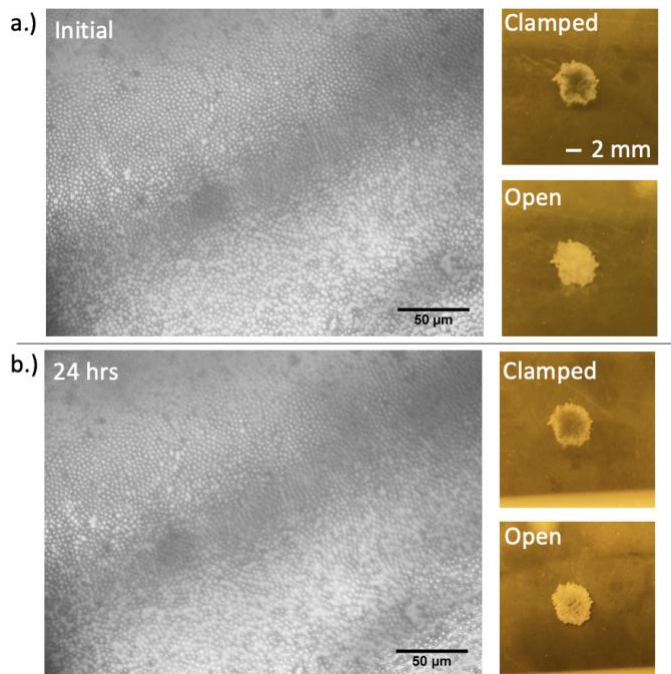


Figure S7.5: Optical microscopy paired with camera images of control experiment; particles not swollen with base a) Initial time point b) After 24 hours. Camera images show particles clamped between glass (top) and open and un-clamped (bottom).

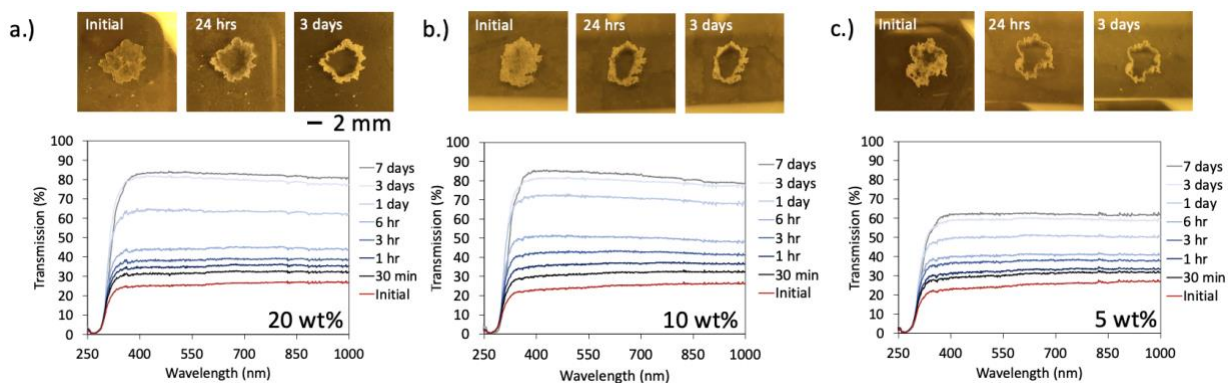


Figure S7.6: Camera images (top) of particle coalescence over time at the designated catalyst loadings a) 20 b) 10 and c) 5 wt% PMDETA and corresponding UV-vis spectra (bottom).

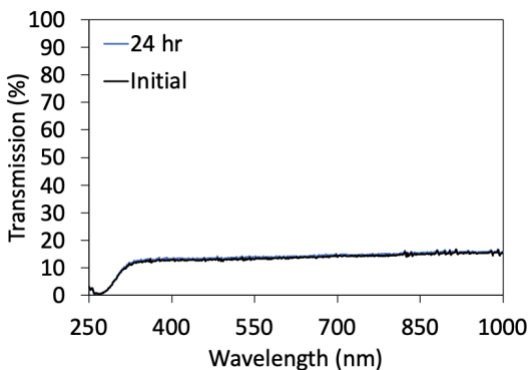


Figure S7.7: UV-vis spectra for control experiment of thioester particles not swollen with base.

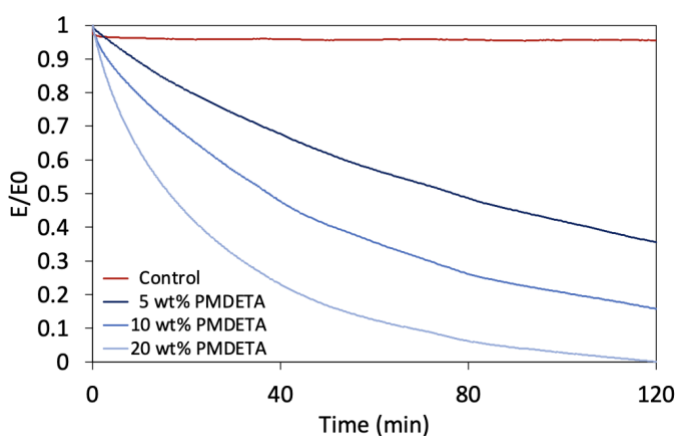


Figure S7.8: Stress strain profiles for bulk films made from monomer at different PMDETA catalyst loadings, demonstrating control of stress relaxation rate. The control contains no base.

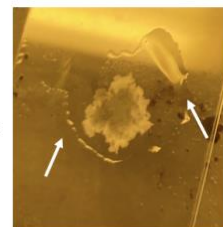
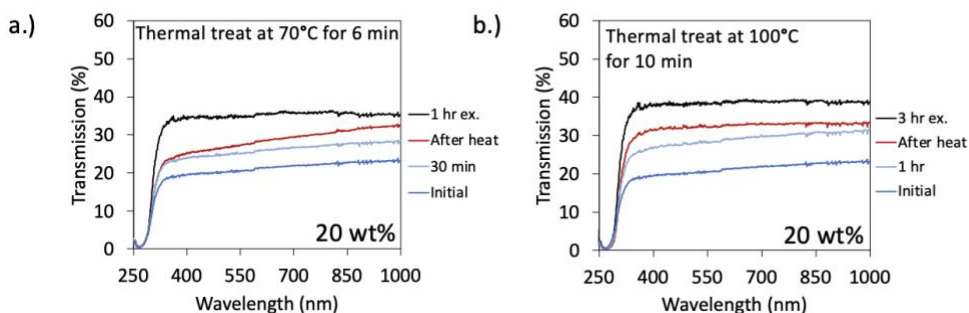


Figure S7.9: UV-vis for samples after thermal treatments. Thermal treatment after a) 30 min. of coalescence treated at 70°C for 6 min. b) 1 hour of coalescence treated at 100°C for 10 min. Image to the right displaying evaporation of base from the polymer film at the elevated processing

conditions. Black curves are representative data for 1 hr. and 3 hr. spectra as an example to demonstrate insignificant shift in UV-vis after heating.

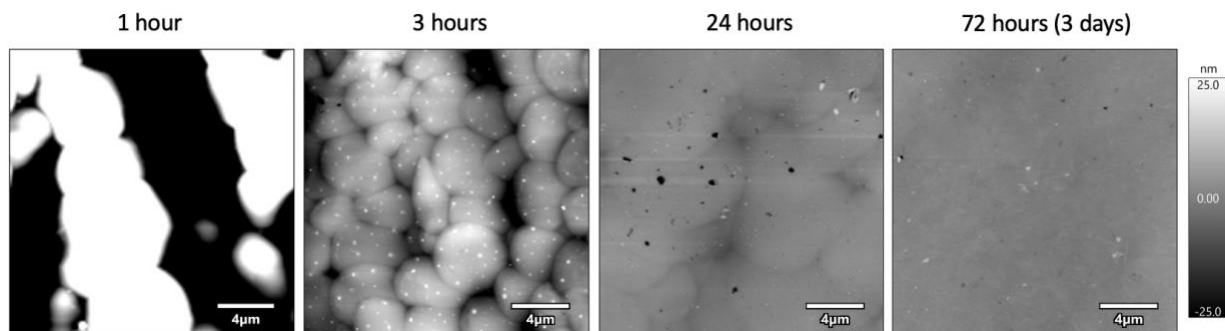


Figure S7.10: AFM topography scans at varying time points showing the evolution of the nm length scale features on the surface, evolving until 3 days.

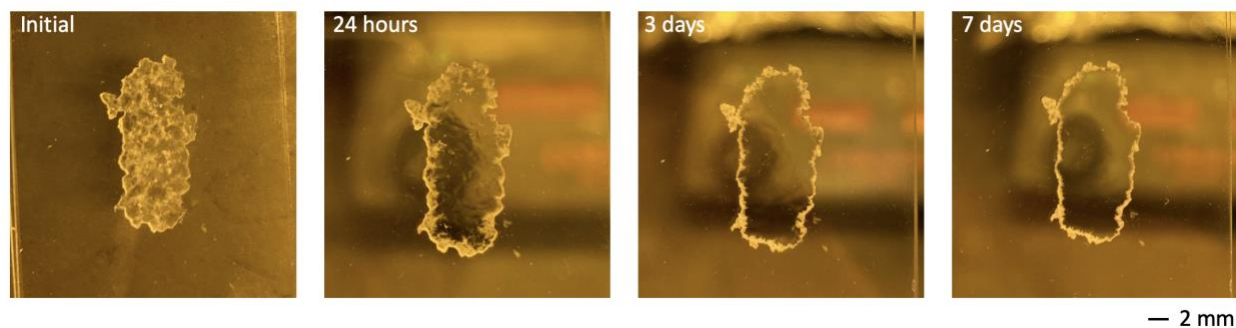


Figure S7.11: Images of particle coalescence over time and evolution of the “stained glass” appearance seen through the bulk of the film upon angling the film to light.

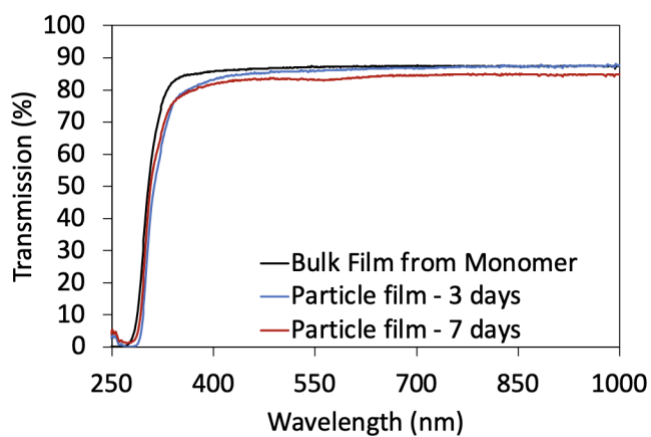


Figure S7.12: UV-vis of films made from particles after 3 and 7 days of compression in comparison to a bulk film made from monomer.

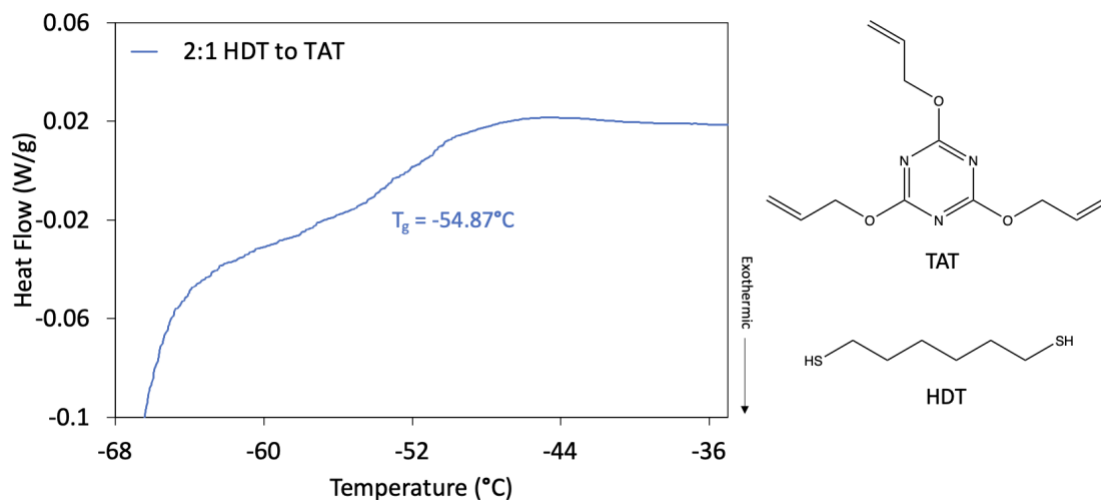


Figure S7.13: DSC trace and monomers for the secondary network.

7.7. – References

- (1) Ngo, T. D.; Kashani, A.; Imbalzano, G.; Nguyen, K. T. Q.; Hui, D. Additive Manufacturing (3D Printing): A Review of Materials, Methods, Applications and Challenges. *Composites Part B: Engineering* **2018**, *143*, 172–196. <https://doi.org/10.1016/j.compositesb.2018.02.012>.
- (2) Muralidharan, A.; Uzcategui, A. C.; McLeod, R. R.; Bryant, S. J. Stereolithographic 3D Printing for Deterministic Control over Integration in Dual-Material Composites. *Adv. Mater. Technol.* **2019**, *4* (11), 1900592. <https://doi.org/10.1002/admt.201900592>.
- (3) Yu, L.; Lei, Z.; Sun, X.; Ding, P.; Wesche, A.; Jin, Y.; Zhang, W.; Long, R. Rapid Fabrication of Fiber-Reinforced Polyimine Composites with Reprocessability, Repairability, and Recyclability. *ACS Appl. Polym. Mater.* **2021**, *3* (11), 5808–5817. <https://doi.org/10.1021/acsapm.1c01027>.
- (4) Neumann, T. V.; Dickey, M. D. Liquid Metal Direct Write and 3D Printing: A Review. *Adv. Mater. Technol.* **2020**, *5* (9), 2000070. <https://doi.org/10.1002/admt.202000070>.
- (5) Chevalier, Y.; Pichot, C.; Graillat, C.; Joanicot, M.; Wong, K.; Maquet, J.; Lindner, P.; Cabane, B. Film Formation with Latex Particles. *Colloid Polym Sci* **1992**, *270* (8), 806–821. <https://doi.org/10.1007/BF00776153>.
- (6) Zhan, Y.; Lavorgna, M.; Buonocore, G.; Xia, H. Enhancing Electrical Conductivity of Rubber Composites by Constructing Interconnected Network of Self-Assembled Graphene with Latex Mixing. *J. Mater. Chem.* **2012**, *22* (21), 10464. <https://doi.org/10.1039/c2jm31293j>.
- (7) Potts, J. R.; Shankar, O.; Du, L.; Ruoff, R. S. Processing–Morphology–Property Relationships and Composite Theory Analysis of Reduced Graphene Oxide/Natural Rubber Nanocomposites. *Macromolecules* **2012**, *45* (15), 6045–6055. <https://doi.org/10.1021/ma300706k>.

- (8) Yu, K.; Shi, Q.; Li, H.; Jabour, J.; Yang, H.; Dunn, M. L.; Wang, T.; Qi, H. J. Interfacial Welding of Dynamic Covalent Network Polymers. *Journal of the Mechanics and Physics of Solids* **2016**, *94*, 1–17. <https://doi.org/10.1016/j.jmps.2016.03.009>.
- (9) Yang, H.; Yu, K.; Mu, X.; Wei, Y.; Guo, Y.; Qi, H. J. Molecular Dynamics Studying on Welding Behavior in Thermosetting Polymers Due to Bond Exchange Reactions. *RSC Adv.* **2016**, *6* (27), 22476–22487. <https://doi.org/10.1039/C5RA26128G>.
- (10) Chen, X.; Dam, M. A.; Ono, K.; Mal, A.; Shen, H.; Nutt, S. R.; Sheran, K.; Wudl, F. A Thermally Re-Mendable Cross-Linked Polymeric Material. *Science, New Series* **2002**, *295* (5560), 1698–1702.
- (11) Liu, Y.-L.; Chuo, T.-W. Self-Healing Polymers Based on Thermally Reversible Diels–Alder Chemistry. *Polym. Chem.* **2013**, *4* (7), 2194. <https://doi.org/10.1039/c2py20957h>.
- (12) Cheng, C.; Bai, X.; Zhang, X.; Li, H.; Huang, Q.; Tu, Y. Self-Healing Polymers Based on a Photo-Active Reversible Addition-Fragmentation Chain Transfer (RAFT) Agent. *J Polym Res* **2015**, *22* (4), 46. <https://doi.org/10.1007/s10965-015-0691-9>.
- (13) Yao, L.; Rong, M. Z.; Zhang, M. Q.; Yuan, Y. C. Self-Healing of Thermoplastics via Reversible Addition–Fragmentation Chain Transfer Polymerization. *J. Mater. Chem.* **2011**, *21* (25), 9060. <https://doi.org/10.1039/c1jm10655d>.
- (14) Robinson, L. L.; Self, J. L.; Fusi, A. D.; Bates, M. W.; Read de Alaniz, J.; Hawker, C. J.; Bates, C. M.; Sample, C. S. Chemical and Mechanical Tunability of 3D-Printed Dynamic Covalent Networks Based on Boronate Esters. *ACS Macro Lett.* **2021**, *10* (7), 857–863. <https://doi.org/10.1021/acsmacrolett.1c00257>.
- (15) Fu, F.; Huang, M.; Zhang, W.; Zhao, Y.; Liu, X. Thermally Assisted Self-Healing Behavior of Anhydride Modified Polybenzoxazines Based on Transesterification. *Sci Rep* **2018**, *8* (1), 10325. <https://doi.org/10.1038/s41598-018-27942-9>.
- (16) Zheng, M.; Guo, Q.; Yin, X.; Getangama, N. N.; de Bruyn, J. R.; Xiao, J.; Bai, Y.; Liu, M.; Yang, J. Direct Ink Writing of Recyclable and *in Situ* Repairable Photothermal Polyurethane for Sustainable 3D Printing Development. *J. Mater. Chem. A* **2021**, *9* (11), 6981–6992. <https://doi.org/10.1039/D0TA11341G>.
- (17) Brown, T. E.; Carberry, B. J.; Worrell, B. T.; Dudaryeva, O. Y.; McBride, M. K.; Bowman, C. N.; Anseth, K. S. Photopolymerized Dynamic Hydrogels with Tunable Viscoelastic Properties through Thioester Exchange. *Biomaterials* **2018**, *178*, 496–503. <https://doi.org/10.1016/j.biomaterials.2018.03.060>.
- (18) Sowan, N.; Cox, L. M.; Shah, P. K.; Song, H. B.; Stansbury, J. W.; Bowman, C. N. Dynamic Covalent Chemistry at Interfaces: Development of Tougher, Healable Composites through Stress Relaxation at the Resin–Silica Nanoparticles Interface. *Adv. Mater. Interfaces* **2018**, *5* (18), 1800511. <https://doi.org/10.1002/admi.201800511>.
- (19) Shi, Q.; Yu, K.; Kuang, X.; Mu, X.; Dunn, C. K.; Dunn, M. L.; Wang, T.; Jerry Qi, H. Recyclable 3D Printing of Vitrimer Epoxy. *Mater. Horiz.* **2017**, *4* (4), 598–607. <https://doi.org/10.1039/C7MH00043J>.
- (20) Huang, Q.; Tang, Z.; Wang, D.; Wu, S.; Guo, B. Engineering Segregated Structures in a Cross-Linked Elastomeric Network Enabled by Dynamic Cross-Link Reshuffling. *ACS Macro Lett.* **2021**, *10* (2), 231–236. <https://doi.org/10.1021/acsmacrolett.0c00852>.
- (21) Lu, L.; Pan, J.; Li, G. Recyclable High-Performance Epoxy Based on Transesterification Reaction. *J. Mater. Chem. A* **2017**, *5* (40), 21505–21513. <https://doi.org/10.1039/C7TA06397K>.

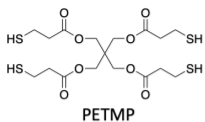
- (22) Worrell, B. T.; McBride, M. K.; Lyon, G. B.; Cox, L. M.; Wang, C.; Mavila, S.; Lim, C.-H.; Coley, H. M.; Musgrave, C. B.; Ding, Y.; Bowman, C. N. Bistable and Photoswitchable States of Matter. *Nat Commun* **2018**, *9* (1), 2804. <https://doi.org/10.1038/s41467-018-05300-7>.
- (23) De Alwis Watuthanthrige, N.; Ahammed, B.; Dolan, M. T.; Fang, Q.; Wu, J.; Sparks, J. L.; Zanjani, M. B.; Konkolewicz, D.; Ye, Z. Accelerating Dynamic Exchange and Self-Healing Using Mechanical Forces in Crosslinked Polymers. *Mater. Horiz.* **2020**, *7* (6), 1581–1587. <https://doi.org/10.1039/C9MH01938C>.
- (24) Yu, L.; Sun, X.; Jin, Y.; Zhang, W.; Long, R. Mechanics of Vitrimer Particle Compression and Fusion under Heat Press. *International Journal of Mechanical Sciences* **2021**, *201*, 106466. <https://doi.org/10.1016/j.ijmecsci.2021.106466>.
- (25) Podgórski, M.; Huang, S.; Bowman, C. N. Additive Manufacture of Dynamic Thiol–Ene Networks Incorporating Anhydride-Derived Reversible Thioester Links. *ACS Appl. Mater. Interfaces* **2021**, *13* (11), 12789–12796. <https://doi.org/10.1021/acsami.0c18979>.

Chapter 7: Appendix

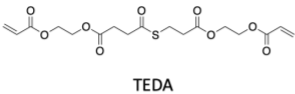
A summary of information has been generated on varying the stoichiometry for the thioester containing microparticles. The amount of excess thiol was varied, and material parameters were measured and recorded for each stoichiometry. Characterization includes optical microscopy, FTIR, and DSC.

Modulating the amount of excess thiol changes the rate with which the thiol-thioester exchange propagates. Increasing the amount excess thiol and thus the number of generated thiolate anions increases the rate of exchange. Other variables to consider when controlling the exchange rate include catalyst concentration, temperature, and applied strain. The 1.4:2 stoichiometry was chosen for the study in Ch. 7 due to its particle stability over weeks to months and its reasonably rapid exchange rate for data analysis.

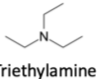
Thiol-Michael dispersion polymerization



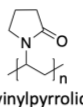
PETMP



TEDA



Triethylamine



Polyvinylpyrrolidone

Trial	Stoich.	Excess	PVP wt%	TEA wt%	Quench	Coalesce (24 hrs)	Coal. (48+hrs – 7days)	D _n (μm)	Coeff. Var. (CV)	T _g (°C)
1	1:1	100% Thiol	50	10	No	Yes	-	-	-	-
2	1:1	100% Thiol	50	10	Yes (equiv.)	Yes	-	2.0 ± 0.3	13 %	-18.7
5	1.5:2	50% Thiol	50	10	Yes (excess)	No	No – but packed/needs manual dissociation	2.6 ± 0.4	14 %	-24.5
7	1.4:2	40% Thiol	50	10	Yes (excess)	No	No	4.0 ± 0.4	10 %	-21.6
6	1.3:2	30% Thiol	50	10	Yes (excess)	No	No	3.1 ± 0.5	17 %	-22.0
8	1.2:2	20% Thiol	50	10	Yes (excess)	No	No	2.0 ± 0.3	17 %	-19.1
4	1.1:2	10% Thiol	50	10	Yes (excess)	No	No	3.0 ± 0.5	19 %	-20.2
3	0.9:2	Acrylate	50	10	Yes (excess)	No	No	2.4 ± 0.4	17 %	-20.3

Excess acetic acid to quench (30 min stir)
8 wt% monomer in MeOH
Rxn: 1 hour

ImageJ for particle analysis
100 particles randomly chosen

Figure A7.1: Table for particle stoichiometry and summary of properties. Stoichiometry read as PETMP to TEDA. Excess thiol in reference to thioester backbone.

Corresponding optical microscopy images are displayed in **Figure A7.2**. It is interesting to note that the 1:1 PETMP to TEDA stoichiometry coalesced without the addition of the base catalyst within about 48 hours (**Figure A7.3b and c**). The piece of polymer in **Figure A7.3c** was submerged in MeOH and remained a solid mass. After the dispersion polymerization is complete, the system is washed with MeOH to remove the reaction catalyst, TEA, and surfactant (see Experimental section of Ch. 7). The MeOH is poured off, but there is still a small amount left that is evaporated off by allowing the particles to sit at ambient conditions for two days. During this time, during the evaporation process capillary forces and Laplacian pressures appear to facilitate particle coalescence for the 1:1 formulation. It is possible proton transfer occurs from the free thiols to the MeOH, resulting in formation of the thiolate anion necessary to perform the thiol-thioester exchange between particle networks. Another possible avenue is the formation of a small number of disulfides, resulting in crosslinking between particles. Lowering the concentration of free thiol resulted in stable particles beyond a week if kept in the freezer. The particles could also potentially be stored in a mildly acidic environment until they are desired for use to prohibit thiolate anion formation. To mitigate disulfide formation, a radical inhibitor such as 2,6-di-tert-4-methyl phenol (BHT) could be added, which would not inhibit the thiol-Michael polymerization or the thiol-thioester exchange for the particle coalescence because those reactions do not utilize the radical reaction pathway required for disulfide formation and would simply be for stabilization of the particles in storage.

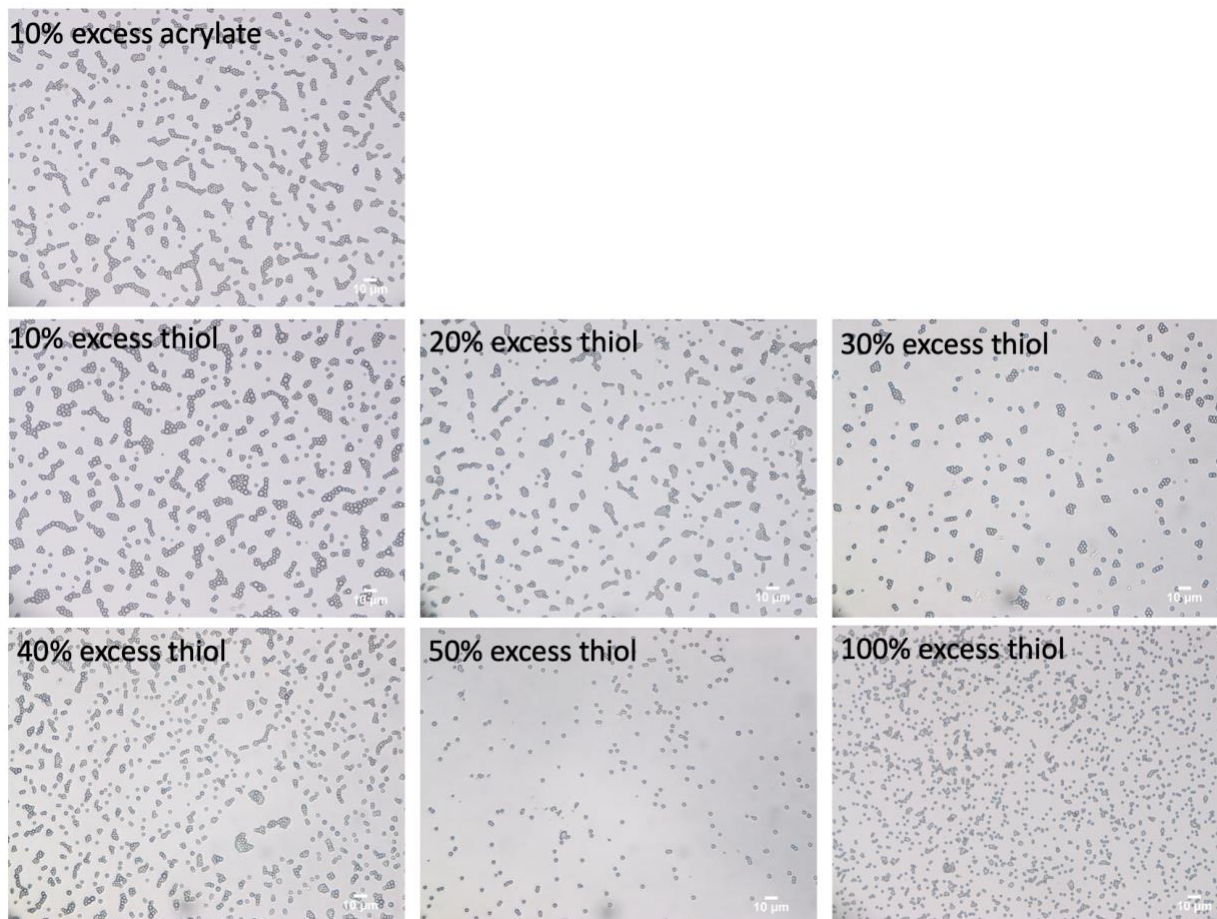


Figure A7.2: Optical microscopy for particle formulations.

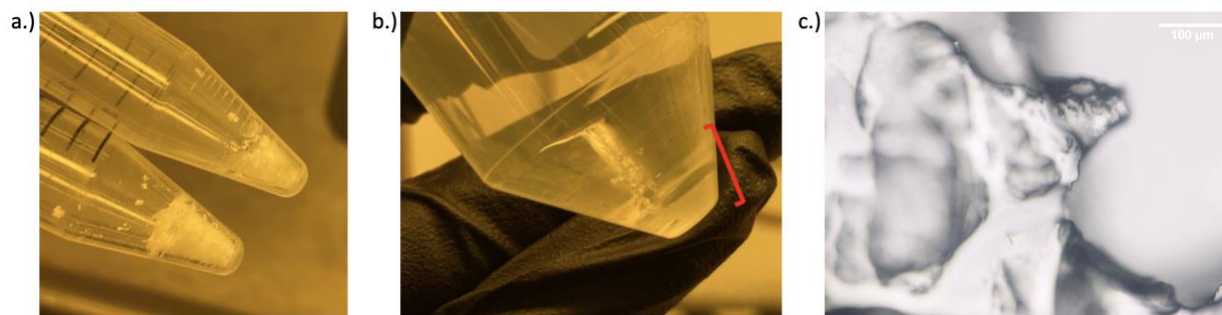


Figure A7.3: a.) Example of dry thioester particles. b.) Thioester particles with a 1:1 stoichiometry after allowing to dry over two days resulting in coalescence of particles. c.) A piece of the coalesced polymer mass from b.) under the microscope.

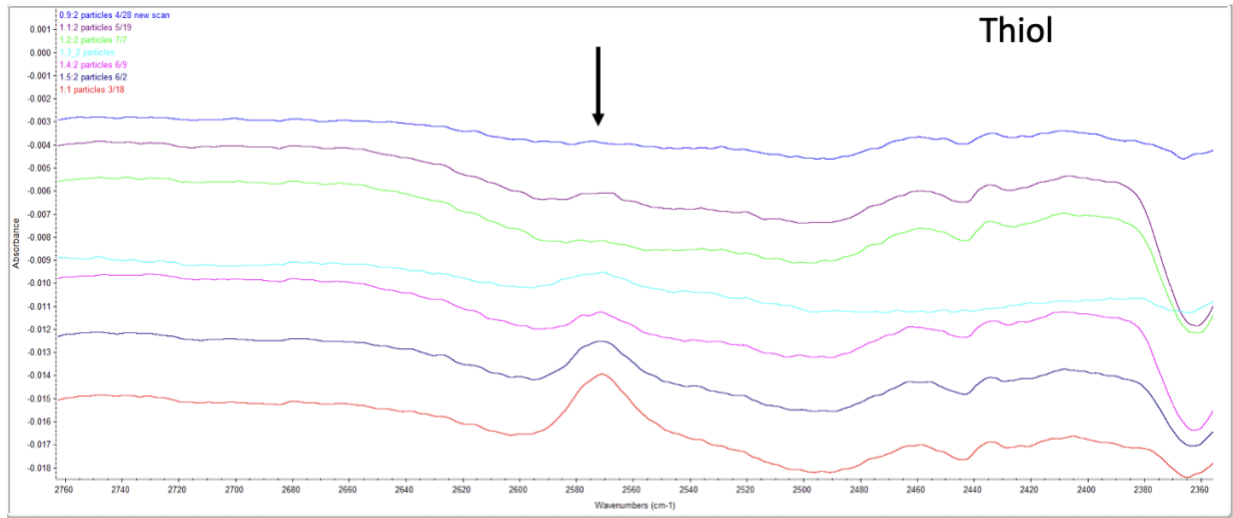


Figure A7.4: FTIR for particle formulations.

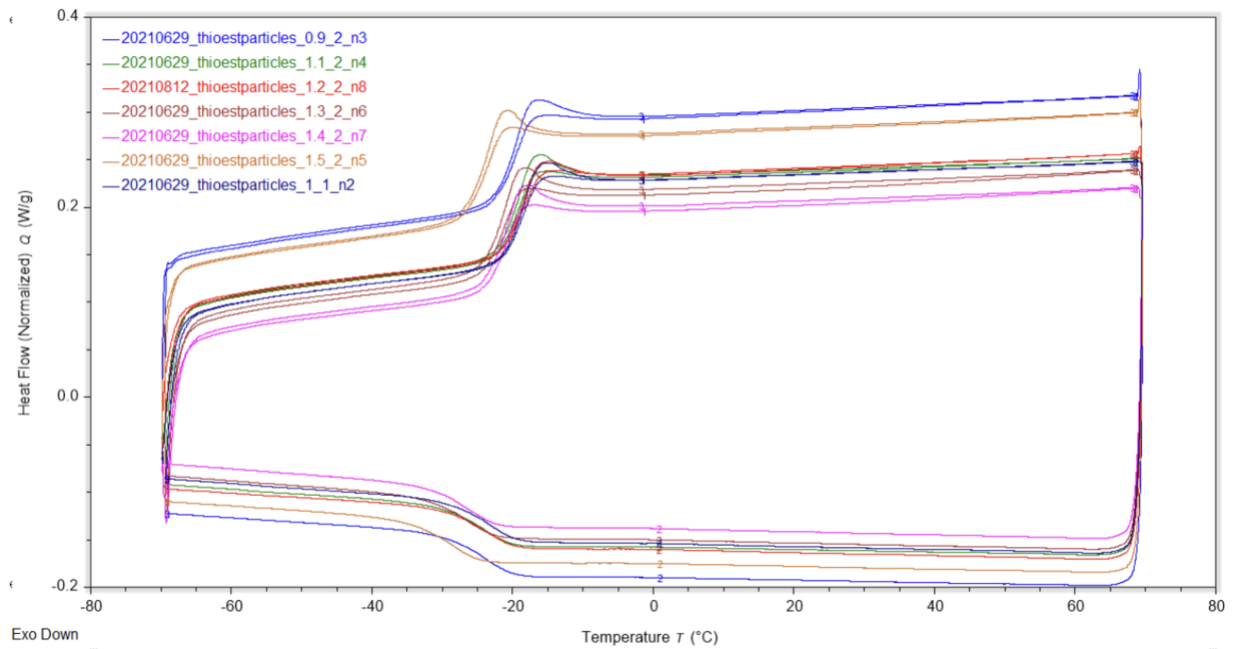


Figure A7.5: DSC for particle formulations.

Chapter 8: Conclusions and Future Recommendations

The work in this thesis has demonstrated that covalent adaptable networks (CANs) can be incorporated into a variety of polymer materials to enable modifications to the polymer network post-polymerization. By investigating the underlying molecular alignment incorporated into the polymer network, control over resulting shapes and colors of materials was realized. Utilizing the dynamic covalent chemistry (DCC) afforded by the CAN, enabled preservation and programming of the modulated molecular alignment. This thesis spans programmable structures on the macroscale ranging in a few millimeters in length, to micron-scale shape programming and actuation. Specifically, this work focused on light-initiated addition-fragmentation chain-transfer (AFT) and thiol-thioester exchange, as the chosen DCCs, which will be elaborated on in this chapter.

8.1 – Shape and Color Changing Structures

The first aim included the third chapter, which incorporated DCC into a liquid crystal elastomer (LCE) enabling complex shape programming and actuation. DCC also enabled re-writability of programmed shapes. Light initiated addition-fragmentation chain-transfer (AFT) was utilized for the third through sixth chapters in LCE materials to decouple the DCC from the thermally activated LC phase transition behavior to actuate the materials. The underlying programmed molecular alignment dictated the shapes and actuation modes that were achieved. This was important because many CAN-LCEs prior to this work utilized thermal activation of the CAN, which resulted in some limitations due to the thermal dependence of the LC phase transition, which is critical for shape actuation. The AFT chemistry proved advantageous to not only decouple the CAN activation from the LC phase transition, but temperature was investigated as an added

variable to alter and further control programming of the AFT-LCE. To generate the AFT-LCEMP, a thiol-Michael oligomerization was done first, to incorporate the allyl dithiol (ADT) monomer into the network backbone of the proceeding reaction thereafter. These AFT capable oligomers were then crosslinked via an acrylate homopolymerization to produce the AFT-LCE. The resin was pre-doped with photoinitiator to carry out the subsequent light exposed reactions. The AFT-LCE programming was dictated by modulating light exposure, temperature, and strain. After programming, the materials were then thermally cycled to repeatably actuate the programmed shape. Upon modulation of these variables, it was discovered that increased exposure times allow for prolonged rearrangement of the polymer network to relieve stress imparted from the straining event. This yielded increasingly altered final strains and thus overall shapes. Modulating the programming temperature manifested changes to both the LC shape, measured at room temperature below the T_{NI} , and the isotropic shape, measured at high temperature above the T_{NI} . Programming the AFT-LCE below the T_{NI} resulted in changes to the LC shape, but little to no effects on the isotropic shape, with the material temporarily recovering its initial starting shape during thermal cycling. Programming the AFT-LCE above the T_{NI} , resulted in significant alteration to both the LC and isotropic shapes. It was concluded that programming below the T_{NI} relieved stress in reoriented domain boundaries, without significant alteration to the entire polymer network, while programming above the T_{NI} more directly programmed the entirety of the polymer network due to the elastic behavior of the material at high temperature.

Due to the light-initiated nature of the reaction chosen, investigation was also performed on controlling the penetration depth of light through the thickness of the film to program the LC alignment. A UV absorbing chemical, Tinuvin-328 (T-328) was embedded into the polymer network. This controlled the extent of AFT activation through the thickness in the film resulting

in controllable stabilization of LC alignment. The gradient of LC alignment resulted in an out-of-plane buckling of the polymer film often utilized in shape programmed materials, where competing regions of stress within the polymer network result in 3D architectures. Ultimately, this work demonstrated that modulating variables can be utilized to control programming and shape actuation of the light facilitated AFT-LCE. Finally, the programmed structures were erased, by irradiating the programmed shapes above the T_{NI} . Irradiating the material above the T_{NI} allows for the LC mesogens to move towards an isotropic state, and comparatively stress-free network thermodynamic equilibrium.

This study led to the second aim and fourth chapter on investigating how CANs can be utilized in color modulation and programming in cholesteric LCEs (CLCEs). Color modulation is important for camouflage and other optically dependent materials, including tunable light sources, or surfaces. The color in these CLCEs is a structural phenomenon, with the underlying LC alignment giving rise to a Bragg reflection on the order of visible wavelengths. Upon doping the AFT-LC oligomer resin from the previous chapter with a cholesteric LC, a handedness of alignment induced by gentle manual shearing of the resin, resulted in a repeating structure, giving rise to a photonic crystal and interaction with light on visible length scales. The resin, doped with photoinitiator, was then crosslinked by an acrylate homopolymerization to preserve the chiral LC alignment. The material, initially red shifted, displaying a red sheen, was uniaxially deformed and resulted in blue shifting to an apparent blue reflective wavelength. This mechanical deformation altered the underlying repeating structure which resulted in the color shift. The change in color dictated at varying strains, were preserved utilizing the AFT chemistry again, to reorganize the network around the molecular alterations. Thermal cycling programmed films resulted in toggling between the blue shifted programmed shape and the red shifted initial shape. Complex patterns

were programmed utilizing photomasks. The color of the material was also erased by irradiating the AFT-CLCE above the T_{NI} . As was discovered in the previous chapter, irradiating the material above the T_{NI} enables erasure of any LC alignment maintained prior to the exposure. This chapter led to a facile means of programming and erasing color within one material.

The achievement of post-polymerization modifications found in the Chapter 3 and 4 were meaningful contributions to the scientific community on re-writable materials. Moving forward, these studies have potential, exciting applications in soft robotics, optics, and drug delivery. These LC materials are lacking in meaningful work outputs for some applications. More work needs to be done on improving efficiency and mechanical integrity for meaningful translation to application. These LC materials rely on the liquid crystal content to achieve meaningful actuation, so it is important to balance the polymer network properties with the LC phase properties and leads to challenges in optimization for application. The work reported here utilizes simple folding and straining techniques to generate complex structures due to the rubbery nature of the material, but this also results in drawbacks to robustness of shapes generated and lack of work output they can achieve. Another avenue of investigation is the 3D printing of LCEs utilizing light polymerizations and CAN reconfiguration. Light facilitated reactions have some drawbacks in penetration depth and attenuation throughout the thickness of materials. Utilizing thermal initiation has the possibility for more uniform dissipation throughout a 3D printed part. There is significant work that needs to be done in terms of creating efficient methods for 3D printing these thermally sensitive LCEs.

The color changing CLCEs have use in strain mapping, camouflage, textiles, tunable light sources, and many other optical applications. Optimization is required to increase the selectivity and improve the alignment in the initially red shifted reflection characteristics. Free-standing color

changing films have a lot of potential in strain mapping applications. A large issue in manufacturing and industrial uses are the integrity of parts made. Extreme environments or workplace accidents can damage materials unknowingly. Applying programmable strain mapping materials can track the integrity of a part throughout its lifetime. Utilizing a mechano triggered CAN stimulus would be an appropriate avenue for this application, with a strain in the part resulting in a color change and activation of the CAN to preserve the color change in the damaged region.

The materials up to this point were on millimeter length scales, and this raised the question of translation of these DCCs to micron-scale features.

8.2 – Shape Changing Microstructures

The third aim covered the remaining chapters on CANs incorporated in microstructures. Chapter 5 laid the groundwork for developing liquid crystal microparticles (LCEMPs). The LCEMPs demonstrated one and two-way shape switching. A thiol-Michael dispersion polymerization was performed to generate the LCEMPs. One-way shape switching was achieved via compression of particles to a new shape and thermal cycling to recover the original shape. Two-way shape switching was achieved via a second stage polymerization after compression, to preserve the new particle shape. These particles were then thermally cycled to demonstrate autonomous shape switching thereafter. Again, underlying molecular alignment of LCs dictated the shape switching behavior. The two-stage programming mechanism in Chapter 5 was non-reversible, which was overcome by incorporating DCC into the LCEMPs.

Chapter 6 incorporated DCC, specifically AFT, into LCEMPs, to achieve re-writable and actuatable microparticle configurations, which had not been demonstrated in the literature before.

AFT-LCEMPs enabled post-polymerization modifications to the particle shape, but also enabled reconfigurability of programmed shapes. A thiol-Michael dispersion polymerization was performed incorporating the ADT monomer to generate the AFT-LCEMPs. Particles were manually compressed at room temperature, resulting in a prolate shape. The particles pre-doped with photoinitiator were irradiated with light, which activated the AFT exchange to preserve the new particle shape and underlying LC alignment. Thermally cycling the material past its T_{NI} resulted in reversible shape switching from prolate to spherical. The prolate shape was also erased by irradiating the programmed particles above the T_{NI} , again also observed from the macroscale studies prior. Compression of the particles above the T_{NI} resulted in an oblate shape, and utilizing a diffraction grating as the superstrate, complex surface topography was programmed. The polydomain structure below the T_{NI} influenced the prolate deformed shape, while deformation above the T_{NI} in the isotropic phase allowed for more uniform deformation.

Microparticles have significant interest in control of rheological properties and drug delivery. Some drawbacks from the study included difficulty in programming and harvesting a meaningful amount of the liquid crystal elastomer microparticles (LCEMPs) for testing, which requires more optimization to move forward in studies involving measuring rheological properties in a solution of shape changing particles. There is also room to investigate more geometries by varying LC content, particle size, or programming conditions. The light stimulated AFT reaction was chosen in this study to decouple the programming stimulus with the thermally activated LC phase transitions, but there is a vast library of CANs of varying chemistries that require investigation in micro-networks. For drug delivery purposes, chemo responsive CANs networks would be an interesting avenue for study for biological applications, with the body having numerous chemo responsive signals. Thermally activated CANs would also be another viable

choice to study with a variety of biological processes and bodily functions being activated and regulated by body temperature.

8.3 – Processable Polymer Microparticles with Potential in 3D Printing

Finally, Chapter 7 investigated CAN-microparticles to generate cohesive polymer films with applications in coatings or selective direct-write 3D printing. The thiol-thioester exchange was utilized in these amorphous particles due to its controllable and rapid exchange with activation by a base catalyst. A thiol-Michael dispersion polymerization was done to generate thioester containing microparticles designed with an excess of thiols in the network. The microparticles were cast on a glass slide and upon addition of a base and compression between glass, the thiol-thioester exchange was activated, which resulted in homogenous amorphous polymer films. The material properties were characterized between films made from monomer and films made from particles to confirm structural integrity of the films made from particles. Ultra-violet visible spectroscopy (UV-vis) suggested particle coalescence is complete by day 7, and final transmission is approximately the same in comparison to films made from monomer. Uniaxial tensile tests were run to compare films made from monomer to films made from particles with the current results potentially indicating no compromise to the network integrity after particle coalescence, but more tensile tests are required to reach a definitive conclusion. A secondary network was designed with excess thiols to enable bond exchange with the thioester containing microparticles. The particles were welded to the secondary network demonstrating the welding capabilities this technology facilitates between the two chemistries. There is still ongoing investigation on the characterization of films made from particles, which will lead to a more cohesive picture on the phenomenon occurring.

These tunable films and surfaces have applications in polymer coatings to generate varying structural properties as desired by tuning the catalyst loading and time during compression. As mentioned, using the thiol-thioester containing microparticles to create cohesive films has applications in direct-write 3D printing. The next step for this work would be to implement them in a direct write type printer. A second set of thiol-thioester containing particles with different mechanical properties would also be ideal as a secondary writing ink to achieve a cohesive network with spatially controlled properties. The timescale with which relaxation happens would need to be significantly shortened, for commercialized applications in 3D printing. This technology could also be envisioned using a light facilitated CAN which would lead to an added level of spatial and temporal control. Although, challenges with the light facilitated reaction include light attenuation through the sample thickness and the relaxation time scale as compared with the rate of initiator depletion. Another avenue moving forward would be to recycle the thioester films made from microparticles. Taking the thioester containing particles and mixing them with a thiol monomer and base catalyst, will result in depolymerization of the network at appropriate quantities of thiol monomer. The network would exchange with the thiol monomer instead of a secondary network, which would result in depolymerization. Recyclable materials are at the forefront of scientific investigation in the race to address climate change and improve sustainability.

8.4 – Summary

Ultimately in this work, the underlying molecular structure dictated actuatable shape or color configurations that were made programmable by designing the materials as a CAN. Furthermore, CANs were utilized to generate new structures post-polymerization. The understanding garnered from this work contributes information to the scientific community on

how CANs can be utilized to achieve controllable shape switching structures from the macro to micron-scale, including programming of color. A systematic investigation of variables contributed to the library of information amassed in this work on controlling AFT and thioester DCC for modifying polymer materials post-polymerization. As discussed, these soft materials have drawbacks in structural robustness and ability to perform meaningful work output, so significant investigation still exists on pushing these chemistries forward for application.

Bibliography

- (1) Xie, M.; Hisano, K.; Zhu, M.; Toyoshi, T.; Pan, M.; Okada, S.; Tsutsumi, O.; Kawamura, S.; Bowen, C. Flexible Multifunctional Sensors for Wearable and Robotic Applications. *Advanced Materials Technologies* **2019**, *4* (3), 1800626. <https://doi.org/10.1002/admt.201800626>.
- (2) Belmonte, A.; Bus, T.; Broer, D. J.; Schenning, A. P. H. J. Patterned Full-Color Reflective Coatings Based on Photonic Cholesteric Liquid-Crystalline Particles. *ACS Applied Materials & Interfaces* **2019**, *11* (15), 14376–14382. <https://doi.org/10.1021/acsami.9b02680>.
- (3) Birnbaum, D. T.; Brannon-Peppas, L. Microparticle Drug Delivery Systems. In *Drug Delivery Systems in Cancer Therapy*; Brown, D. M., Ed.; Humana Press: Totowa, NJ, 2004; pp 117–135. https://doi.org/10.1007/978-1-59259-427-6_6.
- (4) Robert J. Young; Lovell, P. A. *Introduction to Polymers*, Third.; CRC Press, 2011.
- (5) Lee, T. Y.; Guymon, C. A.; Jönsson, E. S.; Hoyle, C. E. The Effect of Monomer Structure on Oxygen Inhibition of (Meth)Acrylates Photopolymerization. *Polymer* **2004**, *45* (18), 6155–6162. <https://doi.org/10.1016/j.polymer.2004.06.060>.
- (6) Paul C. Hiemenz; Lodge, T. P. *Polymer Chemistry*, 2nd ed.; Taylor and Francis Group, 2007.
- (7) Cramer, N. B.; Bowman, C. N. Kinetics of Thiol-Ene and Thiol-Acrylate Photopolymerizations with Real-Time Fourier Transform Infrared. *J. Polym. Sci. A Polym. Chem.* **2001**, *39* (19), 3311–3319. <https://doi.org/10.1002/pola.1314>.
- (8) O'Brien, A. K.; Cramer, N. B.; Bowman, C. N. Oxygen Inhibition in Thiol–Acrylate Photopolymerizations. *J. Polym. Sci. A Polym. Chem.* **2006**, *44* (6), 2007–2014. <https://doi.org/10.1002/pola.21304>.
- (9) Nair, D. P.; Podgórski, M.; Chatani, S.; Gong, T.; Xi, W.; Fenoli, C. R.; Bowman, C. N. The Thiol-Michael Addition Click Reaction: A Powerful and Widely Used Tool in Materials Chemistry. *Chemistry of Materials* **2014**, *26* (1), 724–744. <https://doi.org/10.1021/cm402180t>.
- (10) Hoyle, C. E.; Bowman, C. N. Thiol-Ene Click Chemistry. *Angewandte Chemie International Edition* **2010**, *49* (9), 1540–1573. <https://doi.org/10.1002/anie.200903924>.
- (11) McBride, M. K.; Worrell, B. T.; Brown, T.; Cox, L. M.; Sowan, N.; Wang, C.; Podgorski, M.; Martinez, A. M.; Bowman, C. N. Enabling Applications of Covalent Adaptable Networks. *Annual Review of Chemical and Biomolecular Engineering* **2019**, *10* (1), 175–198. <https://doi.org/10.1146/annurev-chembioeng-060718-030217>.
- (12) Podgórski, M.; Fairbanks, B. D.; Kirkpatrick, B. E.; McBride, M.; Martinez, A.; Dobson, A.; Bongiardina, N. J.; Bowman, C. N. Toward Stimuli-Responsive Dynamic Thermosets through Continuous Development and Improvements in Covalent Adaptable Networks (CANs). *Adv. Mater.* **2020**, *32* (20), 1906876. <https://doi.org/10.1002/adma.201906876>.
- (13) Kloxin, C. J.; Scott, T. F.; Adzima, B. J.; Bowman, C. N. Covalent Adaptable Networks (CANs): A Unique Paradigm in Cross-Linked Polymers. *Macromolecules* **2010**, *43* (6), 2643–2653. <https://doi.org/10.1021/ma902596s>.
- (14) Moad, G.; Rizzardo, E.; Thang, S. H. RAFT Polymerization and Some of Its Applications. *Chem. Asian J.* **2013**, *8* (8), 1634–1644. <https://doi.org/10.1002/asia.201300262>.
- (15) Fortman, D. J.; Brutman, J. P.; Cramer, C. J.; Hillmyer, M. A.; Dichtel, W. R. Mechanically Activated, Catalyst-Free Polyhydroxyurethane Vitrimers. *J. Am. Chem. Soc.* **2015**, *137* (44), 14019–14022. <https://doi.org/10.1021/jacs.5b08084>.
- (16) Otera, J. Transesterification. *American Chemical Society* **1993**, No. 93, 22.

- (17) Amamoto, Y.; Kamada, J.; Otsuka, H.; Takahara, A.; Matyjaszewski, K. Repeatable Photoinduced Self-Healing of Covalently Cross-Linked Polymers through Reshuffling of Trithiocarbonate Units. *Angew. Chem.* **2011**, *123* (7), 1698–1701. <https://doi.org/10.1002/ange.201003888>.
- (18) Christensen, P. R.; Scheuermann, A. M.; Loeffler, K. E.; Helms, B. A. Closed-Loop Recycling of Plastics Enabled by Dynamic Covalent Diketoenamine Bonds. *Nat. Chem.* **2019**, *11* (5), 442–448. <https://doi.org/10.1038/s41557-019-0249-2>.
- (19) Brutman, J. P.; Fortman, D. J.; De Hoe, G. X.; Dichtel, W. R.; Hillmyer, M. A. Mechanistic Study of Stress Relaxation in Urethane-Containing Polymer Networks. *J. Phys. Chem. B* **2019**, *123* (6), 1432–1441. <https://doi.org/10.1021/acs.jpcc.8b11489>.
- (20) Chen, X.; Dam, M. A.; Ono, K.; Mal, A.; Shen, H.; Nutt, S. R.; Sheran, K.; Wudl, F. A Thermally Re-Mendable Cross-Linked Polymeric Material. *Science, New Series* **2002**, *295* (5560), 1698–1702.
- (21) Denissen, W.; Winne, J. M.; Du Prez, F. E. Vitrimers: Permanent Organic Networks with Glass-like Fluidity. *Chem. Sci.* **2016**, *7* (1), 30–38. <https://doi.org/10.1039/C5SC02223A>.
- (22) Cash, J. J.; Kubo, T.; Bapat, A. P.; Sumerlin, B. S. Room-Temperature Self-Healing Polymers Based on Dynamic-Covalent Boronic Esters. *Macromolecules* **2015**, *48* (7), 2098–2106. <https://doi.org/10.1021/acs.macromol.5b00210>.
- (23) Kloxin, C. J.; Scott, T. F.; Bowman, C. N. Stress Relaxation via Addition–Fragmentation Chain Transfer in a Thiol-Ene Photopolymerization. *Macromolecules* **2009**, *42* (7), 2551–2556. <https://doi.org/10.1021/ma802771b>.
- (24) Bracher, P. J.; Snyder, P. W.; Bohall, B. R.; Whitesides, G. M. The Relative Rates of Thiol–Thioester Exchange and Hydrolysis for Alkyl and Aryl Thioalkanoates in Water. *Orig Life Evol Biosph* **2011**, *41* (5), 399–412. <https://doi.org/10.1007/s11084-011-9243-4>.
- (25) Michal, B. T.; Jaye, C. A.; Spencer, E. J.; Rowan, S. J. Inherently Photohealable and Thermal Shape-Memory Polydisulfide Networks. *ACS Macro Lett.* **2013**, *2* (8), 694–699. <https://doi.org/10.1021/mz400318m>.
- (26) Leung, D.; Bowman, C. N. Reducing Shrinkage Stress of Dimethacrylate Networks by Reversible Addition-Fragmentation Chain Transfer. *Macromol. Chem. Phys.* **2012**, *213* (2), 198–204. <https://doi.org/10.1002/macp.201100402>.
- (27) Photoinduced Plasticity in Cross-Linked Polymers | Science <https://science.sciencemag.org/content/308/5728/1615.long> (accessed 2019 -05 -03).
- (28) Ryu, J.; D’Amato, M.; Cui, X.; Long, K. N.; Jerry Qi, H.; Dunn, M. L. Photo-Origami—Bending and Folding Polymers with Light. *Appl. Phys. Lett.* **2012**, *100* (16), 161908. <https://doi.org/10.1063/1.3700719>.
- (29) Kloxin, C. J.; Scott, T. F.; Park, H. Y.; Bowman, C. N. Mechanophotopatterning on a Photoresponsive Elastomer. *Adv. Mater.* **2011**, *23* (17), 1977–1981. <https://doi.org/10.1002/adma.201100323>.
- (30) Cheng, C.; Bai, X.; Zhang, X.; Li, H.; Huang, Q.; Tu, Y. Self-Healing Polymers Based on a Photo-Active Reversible Addition-Fragmentation Chain Transfer (RAFT) Agent. *J Polym Res* **2015**, *22* (4), 46. <https://doi.org/10.1007/s10965-015-0691-9>.
- (31) Cargoët, M.; Diemer, V.; Snella, B.; Desmet, R.; Blanpain, A.; Drobecq, H.; Agouridas, V.; Melnyk, O. Catalysis of Thiol–Thioester Exchange by Water-Soluble Alkyldiselenols Applied to the Synthesis of Peptide Thioesters and SEA-Mediated Ligation. *J. Org. Chem.* **2018**, *83* (20), 12584–12594. <https://doi.org/10.1021/acs.joc.8b01903>.

- (32) Worrell, B. T.; McBride, M. K.; Lyon, G. B.; Cox, L. M.; Wang, C.; Mavila, S.; Lim, C.-H.; Coley, H. M.; Musgrave, C. B.; Ding, Y.; Bowman, C. N. Bistable and Photoswitchable States of Matter. *Nat Commun* **2018**, *9* (1), 2804. <https://doi.org/10.1038/s41467-018-05300-7>.
- (33) Wang, C.; Mavila, S.; Worrell, B. T.; Xi, W.; Goldman, T. M.; Bowman, C. N. Productive Exchange of Thiols and Thioesters to Form Dynamic Polythioester-Based Polymers. *ACS Macro Lett.* **2018**, *7* (11), 1312–1316. <https://doi.org/10.1021/acsmacrolett.8b00611>.
- (34) Podgórski, M.; Worrell, B. T.; Sinha, J.; McBride, M. K.; Bowman, C. N. Thermal Metamorphosis in (Meth)Acrylate Photopolymers: Stress Relaxation, Reshaping, and Second-Stage Reaction. *Macromolecules* **2019**, *52* (21), 8114–8123. <https://doi.org/10.1021/acs.macromol.9b01678>.
- (35) Brown, T. E.; Carberry, B. J.; Worrell, B. T.; Dudaryeva, O. Y.; McBride, M. K.; Bowman, C. N.; Anseth, K. S. Photopolymerized Dynamic Hydrogels with Tunable Viscoelastic Properties through Thioester Exchange. *Biomaterials* **2018**, *178*, 496–503. <https://doi.org/10.1016/j.biomaterials.2018.03.060>.
- (36) Worrell, B. T.; Mavila, S.; Wang, C.; Kontour, T. M.; Lim, C.-H.; McBride, M. K.; Musgrave, C. B.; Shoemaker, R.; Bowman, C. N. A User's Guide to the Thiol-Thioester Exchange in Organic Media: Scope, Limitations, and Applications in Material Science. *Polym. Chem.* **2018**, *9* (36), 4523–4534. <https://doi.org/10.1039/C8PY01031E>.
- (37) Hubbard, A. M.; Mailen, R. W.; Zikry, M. A.; Dickey, M. D.; Genzer, J. Controllable Curvature from Planar Polymer Sheets in Response to Light. *Soft Matter* **2017**, *13* (12), 2299–2308. <https://doi.org/10.1039/C7SM00088J>.
- (38) Imran Khan M., Zagho M.M., Shakoor R.A. *Smart Polymer Nanocomposites. A Brief Overview of Shape Memory Effect in Thermoplastic Polymers.*; Springer, Cham, 2017.
- (39) Liu, Y.; Shaw, B.; Dickey, M. D.; Genzer, J. Sequential Self-Folding of Polymer Sheets. *Sci. Adv.* **2017**, *3* (3), e1602417. <https://doi.org/10.1126/sciadv.1602417>.
- (40) McBride, M. K.; Podgorski, M.; Chatani, S.; Worrell, B. T.; Bowman, C. N. Thermoreversible Folding as a Route to the Unique Shape-Memory Character in Ductile Polymer Networks. *ACS Appl. Mater. Interfaces* **2018**, *7*.
- (41) Chung, T.; Romo-Uribe, A.; Mather, P. T. Two-Way Reversible Shape Memory in a Semicrystalline Network. *Macromolecules* **2008**, *41* (1), 184–192. <https://doi.org/10.1021/ma071517z>.
- (42) Li, M.; Guan, Q.; Dingemans, T. J. High-Temperature Shape Memory Behavior of Semicrystalline Polyamide Thermosets. *ACS Appl. Mater. Interfaces* **2018**, *10*.
- (43) Meng, Y.; Yang, J.-C.; Lewis, C. L.; Jiang, J.; Anthamatten, M. Photoinscription of Chain Anisotropy into Polymer Networks. *Macromolecules* **2016**, *49* (23), 9100–9107. <https://doi.org/10.1021/acs.macromol.6b01990>.
- (44) Jin, B.; Song, H.; Jiang, R.; Song, J.; Zhao, Q.; Xie, T. Programming a Crystalline Shape Memory Polymer Network with Thermo- and Photo-Reversible Bonds toward a Single-Component Soft Robot. *Sci. Adv.* **2018**, *4* (1), eaao3865. <https://doi.org/10.1126/sciadv.aao3865>.
- (45) An, N.; Li, M.; Zhou, J. Predicting Origami-Inspired Programmable Self-Folding of Hydrogel Trilayers. *Smart Mater. Struct.* **2016**, *25* (11), 11LT02. <https://doi.org/10.1088/0964-1726/25/11/11LT02>.

- (46) Zheng, N.; Fang, Z.; Zou, W.; Zhao, Q.; Xie, T. Thermoset Shape-Memory Polyurethane with Intrinsic Plasticity Enabled by Transcarbamylation. *Angew. Chem. Int. Ed.* **2016**, *55* (38), 11421–11425. <https://doi.org/10.1002/anie.201602847>.
- (47) White, T. J.; Broer, D. J. Programmable and Adaptive Mechanics with Liquid Crystal Polymer Networks and Elastomers. *Nature Materials* **2015**, *14* (11), 1087–1098. <https://doi.org/10.1038/nmat4433>.
- (48) Ube, T.; Kawasaki, K.; Ikeda, T. Photomobile Liquid-Crystalline Elastomers with Rearrangeable Networks. *Adv. Mater.* **2016**, *28* (37), 8212–8217. <https://doi.org/10.1002/adma.201602745>.
- (49) Ohm, C.; Brehmer, M.; Zentel, R. Liquid Crystalline Elastomers as Actuators and Sensors. *Adv. Mater.* **2010**, *22* (31), 3366–3387. <https://doi.org/10.1002/adma.200904059>.
- (50) K pfer, J.; Finkelmann, H. Nematic Liquid Single Crystal Elastomers. *Makromol. Chem., Rapid Commun.* **1991**, *12* (12), 717–726. <https://doi.org/10.1002/marc.1991.030121211>.
- (51) Yakacki, C. M.; Saed, M.; Nair, D. P.; Gong, T.; Reed, S. M.; Bowman, C. N. Tailorable and Programmable Liquid-Crystalline Elastomers Using a Two-Stage Thiol–Acrylate Reaction. *RSC Advances* **2015**, *5* (25), 18997–19001. <https://doi.org/10.1039/C5RA01039J>.
- (52) Ware, T. H.; McConney, M. E.; Wie, J. J.; Tondiglia, V. P.; White, T. J. Voxellated Liquid Crystal Elastomers. *Science* **2015**, *347* (6225), 982–984. <https://doi.org/10.1126/science.1261019>.
- (53) Kloxin, C. J.; Scott, T. F.; Adzima, B. J.; Bowman, C. N. Covalent Adaptable Networks (CANs): A Unique Paradigm in Cross-Linked Polymers. *Macromolecules* **2010**, *43* (6), 2643–2653. <https://doi.org/10.1021/ma902596s>.
- (54) Pei, Z.; Yang, Y.; Chen, Q.; Terentjev, E. M.; Wei, Y.; Ji, Y. Mouldable Liquid-Crystalline Elastomer Actuators with Exchangeable Covalent Bonds. *Nature Mater* **2014**, *13* (1), 36–41. <https://doi.org/10.1038/nmat3812>.
- (55) Wen, Z.; McBride, M. K.; Zhang, X.; Han, X.; Martinez, A. M.; Shao, R.; Zhu, C.; Visvanathan, R.; Clark, N. A.; Wang, Y.; Yang, K.; Bowman, C. N. Reconfigurable LC Elastomers: Using a Thermally Programmable Monodomain To Access Two-Way Free-Standing Multiple Shape Memory Polymers. *Macromolecules* **2018**, *51* (15), 5812–5819. <https://doi.org/10.1021/acs.macromol.8b01315>.
- (56) Wang, Z.; Tian, H.; He, Q.; Cai, S. Reprogrammable, Reprocessible, and Self-Healable Liquid Crystal Elastomer with Exchangeable Disulfide Bonds. *ACS Appl. Mater. Interfaces* **2017**, *9* (38), 33119–33128. <https://doi.org/10.1021/acsami.7b09246>.
- (57) Sun, D.; Zhang, J.; Li, H.; Shi, Z.; Meng, Q.; Liu, S.; Chen, J.; Liu, X. Toward Application of Liquid Crystalline Elastomer for Smart Robotics: State of the Art and Challenges. *Polymers* **2021**, *13* (11), 1889. <https://doi.org/10.3390/polym13111889>.
- (58) Bamfield, P.; Hutchings, M. *Chromic Phenomena - Technological Applications of Colour Chemistry*, 3rd ed.; Royal Society of Chemistry, 2018.
- (59) Zhang, H.; Chen, Y.; Lin, Y.; Fang, X.; Xu, Y.; Ruan, Y.; Weng, W. Spiropyran as a Mechanochromic Probe in Dual Cross-Linked Elastomers. *Macromolecules* **2014**, *47* (19), 6783–6790. <https://doi.org/10.1021/ma500760p>.
- (60) Datta, B. C.; Ortiz, C. Methods for Design and Fabrication of Bio-Inspired Nanostructures Exhibiting Structural Coloration. In *Advanced Fabrication Technologies for Micro/Nano Optics and Photonics XIII*; von Freymann, G., Blasco, E., Chanda, D., Eds.; SPIE: San Francisco, United States, 2020; p 33. <https://doi.org/10.1117/12.2544398>.

- (61) Nicole, L.; Laberty-Robert, C.; Rozes, L.; Sanchez, C. Hybrid Materials Science: A Promised Land for the Integrative Design of Multifunctional Materials. *Nanoscale* **2014**, *6* (12), 6267–6292. <https://doi.org/10.1039/C4NR01788A>.
- (62) Berthier, S. *Photonique Des Morphos*; Springer-Verlag: Paris, 2010.
- (63) Zhao, Q.; Finlayson, C. E.; Snoswell, D. R. E.; Haines, A.; Schäfer, C.; Spahn, P.; Hellmann, G. P.; Petukhov, A. V.; Herrmann, L.; Burdet, P.; Midgley, P. A.; Butler, S.; Mackley, M.; Guo, Q.; Baumberg, J. J. Large-Scale Ordering of Nanoparticles Using Viscoelastic Shear Processing. *Nat Commun* **2016**, *7* (1), 11661. <https://doi.org/10.1038/ncomms11661>.
- (64) Finkelmann, H.; Kim, S. T.; Muñoz, A.; Palffy-Muhoray, P.; Taheri, B. Tunable Mirrorless Lasing in Cholesteric Liquid Crystalline Elastomers. *Advanced Materials* **2001**, *13* (14), 1069–1072. [https://doi.org/10.1002/1521-4095\(200107\)13:14<1069::AID-ADMA1069>3.0.CO;2-6](https://doi.org/10.1002/1521-4095(200107)13:14<1069::AID-ADMA1069>3.0.CO;2-6).
- (65) Mulder, D. J.; Schenning, A. P. H. J.; Bastiaansen, C. W. M. Chiral-Nematic Liquid Crystals as One Dimensional Photonic Materials in Optical Sensors. *J. Mater. Chem. C* **2014**, *2* (33), 6695–6705. <https://doi.org/10.1039/C4TC00785A>.
- (66) Natarajan, L. V.; Wofford, J. M.; Tondiglia, V. P.; Sutherland, R. L.; Koerner, H.; Vaia, R. A.; Bunning, T. J. Electro-Thermal Tuning in a Negative Dielectric Cholesteric Liquid Crystal Material. *Journal of Applied Physics* **2008**, *103* (9), 093107. <https://doi.org/10.1063/1.2913326>.
- (67) Kizhakidathazhath, R.; Geng, Y.; Jampani, V. S. R.; Charni, C.; Sharma, A.; Lagerwall, J. P. F. Facile Anisotropic Deswelling Method for Realizing Large-Area Cholesteric Liquid Crystal Elastomers with Uniform Structural Color and Broad-Range Mechanochromic Response. *Advanced Functional Materials* **2020**, *30* (7), 1909537. <https://doi.org/10.1002/adfm.201909537>.
- (68) Varanytsia, A.; Nagai, H.; Urayama, K.; Palffy-Muhoray, P. Tunable Lasing in Cholesteric Liquid Crystal Elastomers with Accurate Measurements of Strain. *Scientific Reports* **2015**, *5* (1). <https://doi.org/10.1038/srep17739>.
- (69) Kim, D.-Y.; Lee, K. M.; White, T. J.; Jeong, K.-U. Cholesteric Liquid Crystal Paints: In Situ Photopolymerization of Helicoidally Stacked Multilayer Nanostructures for Flexible Broadband Mirrors. *NPG Asia Materials* **2018**, *10* (11), 1061–1068. <https://doi.org/10.1038/s41427-018-0096-4>.
- (70) White, T. J.; Bricker, R. L.; Natarajan, L. V.; Tondiglia, V. P.; Green, L.; Li, Q.; Bunning, T. J. Electrically Switchable, Photoaddressable Cholesteric Liquid Crystal Reflectors. *Optics Express* **2010**, *18* (1), 173. <https://doi.org/10.1364/OE.18.000173>.
- (71) Brannum, M. T.; Steele, A. M.; Venetos, M. C.; Korley, L. T. J.; Wnek, G. E.; White, T. J. Light Control with Liquid Crystalline Elastomers. *Advanced Optical Materials* **2019**, *7* (6), 1801683. <https://doi.org/10.1002/adom.201801683>.
- (72) Moirangthem, M.; Schenning, A. P. H. J. Full Color Camouflage in a Printable Photonic Blue-Colored Polymer. *ACS Applied Materials & Interfaces* **2018**, *10* (4), 4168–4172. <https://doi.org/10.1021/acsami.7b17892>.
- (73) Patravale, V. B.; Mandawgade, S. D. Novel Cosmetic Delivery Systems: An Application Update: Novel Cosmetic Delivery Systems. *International Journal of Cosmetic Science* **2008**, *30* (1), 19–33. <https://doi.org/10.1111/j.1468-2494.2008.00416.x>.
- (74) Mueller, S.; Llewellyn, E. W.; Mader, H. M. The Rheology of Suspensions of Solid Particles. *Proceedings of the Royal Society A: Mathematical, Physical and Engineering Sciences* **2010**, *466* (2116), 1201–1228. <https://doi.org/10.1098/rspa.2009.0445>.

- (75) Landfester, K. Miniemulsion Polymerization and the Structure of Polymer and Hybrid Nanoparticles. *Angewandte Chemie International Edition* **2009**, *48* (25), 4488–4507. <https://doi.org/10.1002/anie.200900723>.
- (76) Ho, C. C.; Keller, A.; Odell, J. A.; Ottewill, R. H. Preparation of Monodisperse Ellipsoidal Polystyrene Particles. *Colloid & Polymer Science* **1993**, *271* (5), 469–479. <https://doi.org/10.1007/BF00657391>.
- (77) Hessberger, T.; Braun, L.; Zentel, R. Microfluidic Synthesis of Actuating Microparticles from a Thiol-Ene Based Main-Chain Liquid Crystalline Elastomer. *Polymers* **2016**, *8* (12), 410. <https://doi.org/10.3390/polym8120410>.
- (78) Bhaskar, S.; Pollock, K. M.; Yoshida, M.; Lahann, J. Towards Designer Microparticles: Simultaneous Control of Anisotropy, Shape, and Size. *Small* **2010**, *6* (3), 404–411. <https://doi.org/10.1002/smll.200901306>.
- (79) Wischke, C.; Schossig, M.; Lendlein, A. Shape-Memory Effect of Micro-/Nanoparticles from Thermoplastic Multiblock Copolymers. *Small* **2014**, *10* (1), 83–87. <https://doi.org/10.1002/smll.201202213>.
- (80) Klinger, D.; Wang, C. X.; Connal, L. A.; Audus, D. J.; Jang, S. G.; Kraemer, S.; Killops, K. L.; Fredrickson, G. H.; Kramer, E. J.; Hawker, C. J. A Facile Synthesis of Dynamic, Shape-Changing Polymer Particles. *Angewandte Chemie International Edition* **2014**, *53* (27), 7018–7022. <https://doi.org/10.1002/anie.201400183>.
- (81) Wang, C.; Podgórski, M.; Bowman, C. N. Monodisperse Functional Microspheres from Step-Growth “Click” Polymerizations: Preparation, Functionalization and Implementation. *Mater. Horiz.* **2014**, *1* (5), 535–539. <https://doi.org/10.1039/C4MH00082J>.
- (82) Wang, C.; Zhang, X.; Podgórski, M.; Xi, W.; Shah, P.; Stansbury, J.; Bowman, C. N. Monodispersity/Narrow Polydispersity Cross-Linked Microparticles Prepared by Step-Growth Thiol–Michael Addition Dispersion Polymerizations. *Macromolecules* **2015**, *48* (23), 8461–8470. <https://doi.org/10.1021/acs.macromol.5b02146>.
- (83) Cox, L. M.; Sun, X.; Wang, C.; Sowan, N.; Killgore, J. P.; Long, R.; Wu, H.-A.; Bowman, C. N.; Ding, Y. Light-Stimulated Permanent Shape Reconfiguration in Cross-Linked Polymer Microparticles. *ACS Applied Materials & Interfaces* **2017**, *9* (16), 14422–14428. <https://doi.org/10.1021/acsami.7b02759>.
- (84) Kawaguchi, S.; Ito, K. Dispersion Polymerization. In *Polymer Particles*; Okubo, M., Ed.; Advances in Polymer Science; Springer Berlin Heidelberg: Berlin, Heidelberg, 2005; Vol. 175, pp 299–328. <https://doi.org/10.1007/b100118>.
- (85) Liu, X.; Xu, Y.; Heuts, J. P. A.; Debije, M. G.; Schenning, A. P. H. J. Monodisperse Liquid Crystal Network Particles Synthesized via Precipitation Polymerization. *Macromolecules* **2019**, *52* (21), 8339–8345. <https://doi.org/10.1021/acs.macromol.9b01852>.
- (86) Liu, X.; Pan, X. Programmable Liquid Crystal Elastomer Microactuators Prepared via Thiol-Ene Dispersion Polymerization. *Soft Matter* **2020**, *13* (45), 8368–8378. <https://doi.org/10.1039/C7SM01619K>.
- (87) Neumann, T. V.; Dickey, M. D. Liquid Metal Direct Write and 3D Printing: A Review. *Adv. Mater. Technol.* **2020**, *5* (9), 2000070. <https://doi.org/10.1002/admt.202000070>.
- (88) Chevalier, Y.; Pichot, C.; Graillat, C.; Joanicot, M.; Wong, K.; Maquet, J.; Lindner, P.; Cabane, B. Film Formation with Latex Particles. *Colloid Polym Sci* **1992**, *270* (8), 806–821. <https://doi.org/10.1007/BF00776153>.
- (89) Wang, C. Step-Growth Nano/Micro Polymer Networks. **2018**, 212.

- (90) Sowan, N.; Cox, L. M.; Shah, P. K.; Song, H. B.; Stansbury, J. W.; Bowman, C. N. Dynamic Covalent Chemistry at Interfaces: Development of Tougher, Healable Composites through Stress Relaxation at the Resin–Silica Nanoparticles Interface. *Adv. Mater. Interfaces* **2018**, *5* (18), 1800511. <https://doi.org/10.1002/admi.201800511>.
- (91) Belmonte, A.; Bus, T.; Broer, D. J.; Schenning, A. P. H. J. Patterned Full-Color Reflective Coatings Based on Photonic Cholesteric Liquid-Crystalline Particles. *ACS Applied Materials & Interfaces* **2019**, *11* (15), 14376–14382. <https://doi.org/10.1021/acsami.9b02680>.
- (92) Wang, J.-N.; Liu, Y.-Q.; Zhang, Y.-L.; Feng, J.; Wang, H.; Yu, Y.-H.; Sun, H.-B. Wearable Superhydrophobic Elastomer Skin with Switchable Wettability. *Adv. Funct. Mater.* **2018**, *28* (23), 1800625. <https://doi.org/10.1002/adfm.201800625>.
- (93) Xie, M.; Hisano, K.; Zhu, M.; Toyoshi, T.; Pan, M.; Okada, S.; Tsutsumi, O.; Kawamura, S.; Bowen, C. Flexible Multifunctional Sensors for Wearable and Robotic Applications. *Advanced Materials Technologies* **2019**, *4* (3), 1800626. <https://doi.org/10.1002/admt.201800626>.
- (94) Birnbaum, D. T.; Brannon-Peppas, L. Microparticle Drug Delivery Systems. In *Drug Delivery Systems in Cancer Therapy*; Brown, D. M., Ed.; Humana Press: Totowa, NJ, 2004; pp 117–135. https://doi.org/10.1007/978-1-59259-427-6_6.
- (95) Liu, Y.; Genzer, J.; Dickey, M. D. “2D or Not 2D”: Shape-Programming Polymer Sheets. *Progress in Polymer Science* **2016**, *52*, 79–106. <https://doi.org/10.1016/j.progpolymsci.2015.09.001>.
- (96) Meng, Y.; Jiang, J.; Anthamatten, M. Shape Actuation via Internal Stress-Induced Crystallization of Dual-Cure Networks. *ACS Macro Lett.* **2015**, *4* (1), 115–118. <https://doi.org/10.1021/mz500773v>.
- (97) Han, Z.; Wang, P.; Mao, G.; Yin, T.; Zhong, D.; Yiming, B.; Hu, X.; Jia, Z.; Nian, G.; Qu, S.; Yang, W. Dual PH-Responsive Hydrogel Actuator for Lipophilic Drug Delivery. *ACS Appl. Mater. Interfaces* **2020**, *12* (10), 12010–12017. <https://doi.org/10.1021/acsami.9b21713>.
- (98) Lou, J.; Liu, Z.; Yang, L.; Guo, Y.; Lei, D.; You, Z. A New Strategy of Discretionarily Reconfigurable Actuators Based on Self-Healing Elastomers for Diverse Soft Robots. *Adv. Funct. Mater.* **2021**, *31* (11), 2008328. <https://doi.org/10.1002/adfm.202008328>.
- (99) Küpfer, J.; Finkelmann, H. Nematic Liquid Single Crystal Elastomers. *Makromol. Chem., Rapid Commun.* **1991**, *12* (12), 717–726. <https://doi.org/10.1002/marc.1991.030121211>.
- (100) Portugall, M.; Ringsdorf, H.; Zentel, R. Synthesis and Phase Behaviour of Liquid Crystalline Polyacrylates. *Macromolecular Chemistry and Physics* **1982**, *183* (10), 2311–2321. <https://doi.org/10.1002/macp.1982.021831003>.
- (101) Ware, T. H.; McConney, M. E.; Wie, J. J.; Tondiglia, V. P.; White, T. J. Voxellated Liquid Crystal Elastomers. *Science* **2015**, *347* (6225), 982–984. <https://doi.org/10.1126/science.1261019>.
- (102) Kowalski, B. A.; Guin, T. C.; Auguste, A. D.; Godman, N. P.; White, T. J. Pixelated Polymers: Directed Self Assembly of Liquid Crystalline Polymer Networks. *ACS Macro Lett.* **2017**, *6* (4), 436–441. <https://doi.org/10.1021/acsmacrolett.7b00116>.
- (103) Fortman, D. J.; Brutman, J. P.; Cramer, C. J.; Hillmyer, M. A.; Dichtel, W. R. Mechanically Activated, Catalyst-Free Polyhydroxyurethane Vitrimers. *J. Am. Chem. Soc.* **2015**, *137* (44), 14019–14022. <https://doi.org/10.1021/jacs.5b08084>.
- (104) Otera, J. Transesterification. *American Chemical Society* **1993**, No. 93, 22.

- (105) Amamoto, Y.; Kamada, J.; Otsuka, H.; Takahara, A.; Matyjaszewski, K. Repeatable Photoinduced Self-Healing of Covalently Cross-Linked Polymers through Reshuffling of Trithiocarbonate Units. *Angew. Chem.* **2011**, *123* (7), 1698–1701. <https://doi.org/10.1002/ange.201003888>.
- (106) Christensen, P. R.; Scheuermann, A. M.; Loeffler, K. E.; Helms, B. A. Closed-Loop Recycling of Plastics Enabled by Dynamic Covalent Diketoenamine Bonds. *Nat. Chem.* **2019**, *11* (5), 442–448. <https://doi.org/10.1038/s41557-019-0249-2>.
- (107) Pei, Z.; Yang, Y.; Chen, Q.; Terentjev, E. M.; Wei, Y.; Ji, Y. Mouldable Liquid-Crystalline Elastomer Actuators with Exchangeable Covalent Bonds. *Nature Mater* **2014**, *13* (1), 36–41. <https://doi.org/10.1038/nmat3812>.
- (108) Curk, T.; Dobnikar, J.; Frenkel, D. Liquid Crystalline Epoxy Networks with Exchangeable Disulfide Bonds. *Soft Matter* **2016**, *12* (1), 35–44. <https://doi.org/10.1039/C5SM02144H>.
- (109) Wen, Z.; McBride, M. K.; Zhang, X.; Han, X.; Martinez, A. M.; Shao, R.; Zhu, C.; Visvanathan, R.; Clark, N. A.; Wang, Y.; Yang, K.; Bowman, C. N. Reconfigurable LC Elastomers: Using a Thermally Programmable Monodomain To Access Two-Way Free-Standing Multiple Shape Memory Polymers. *Macromolecules* **2018**, *51* (15), 5812–5819. <https://doi.org/10.1021/acs.macromol.8b01315>.
- (110) McBride, M. K.; Martinez, A. M.; Cox, L.; Alim, M.; Childress, K.; Beiswinger, M.; Podgorski, M.; Worrell, B. T.; Killgore, J.; Bowman, C. N. A Readily Programmable, Fully Reversible Shape-Switching Material. *Science Advances* **2018**, *4* (8), eaat4634. <https://doi.org/10.1126/sciadv.aat4634>.
- (111) Fridrikh, S. V.; Terentjev, E. M. Polydomain-Monodomain Transition in Nematic Elastomers. *Phys. Rev. E* **1999**, *60* (2), 1847–1857. <https://doi.org/10.1103/PhysRevE.60.1847>.
- (112) Ware, T. H.; Biggins, J. S.; Shick, A. F.; Warner, M.; White, T. J. Localized Soft Elasticity in Liquid Crystal Elastomers. *Nature Communications* **2016**, *7* (1). <https://doi.org/10.1038/ncomms10781>.
- (113) Kuentler, A. S. Light-Induced Shape Morphing of Thin Films. *Interface Science* **2019**, *17*.
- (114) Qin, L.; Gu, W.; Yu, Y. Photodeformable Liquid Crystalline Polymers LCPs. In *Polymers and Polymeric Composites: A Reference Series*; Palsule, S., Ed.; Springer Berlin Heidelberg: Berlin, Heidelberg, 2018; pp 1–29. https://doi.org/10.1007/978-3-642-37179-0_52-1.
- (115) Ma, S. J.; Mannino, S. J.; Wagner, N. J.; Kloxin, C. J. Photodirected Formation and Control of Wrinkles on a Thiol–Ene Elastomer. *ACS Macro Letters* **2013**, *2* (6), 474–477. <https://doi.org/10.1021/mz400166e>.
- (116) Bienz, E. F. (Thermal Camouflage). *U.S. Patent*. 4,156,033. **1979**.
- (117) Han, T.; Bai, X.; Thong, J. T. L.; Li, B.; Qiu, C.-W. *Adv. Mater.* **2014**, *26*, 1731.
- (118) Yu, H.; Shao, S.; Yan, L.; Meng, H.; He, Y.; Yao, C.; Xu, P.; Zhang, X.; Hu, W.; Huang, W. *J Mater. Chem.* **2016**, *4*, 2269.
- (119) Ramsley, A. O. (Camouflage Patterns - Effects of Size and Color). *U.S. Army NATICK R&D. Natick/TR-79/030*. **1979**.
- (120) Teyssier, J.; Saenko, S. V.; van der Marel, D.; Milinkovitch, M. C. *Nat. Commun.* **2015**, *6*, 1.
- (121) Zhang, W.; Kragt, S.; Schenning, A. P. H. J.; de Haan, L. T.; Zhou, G. *ACS Omega* **2017**, *2*, 3475.
- (122) Kim, Y.; Tamaoki, N. *J. Mater. Chem.* **2014**, *2*, 9258.

- (123) White, T. J.; Bricker, R. L.; Natarajan, L. V.; Tondiglia, V. P.; Green, L.; Li, Q.; Bunning, T. J. *Optics Express* **2010**, *18*, 174.
- (124) Ge, J.; Yin, Y. *Angew.* **2011**, *50*, 1492.
- (125) Moirangthem, M.; Schenning, A. P. H. J. *ACS Applied Materials & Interfaces* **2018**, *10*, 4168.
- (126) Burton, E. R. (Color Changing Contact Lenses). *U.S. Patent*. US 8,542,325 B2. **2013**.
- (127) Kim, D.-Y.; Lee, K. M.; White, T. J.; Jeong, K.-U. *NPG Asia Materials* **2018**, *10*, 1061.
- (128) Finkelmann, H.; Kim, S. T.; Muñoz, A.; Palffy-Muhoray, P.; Taheri, B. *Adv. Mater.* **2001**, *13*, 1069.
- (129) Xie, M.; Hisano, K.; Zhu, M.; Toyoshi, T.; Pan, M.; Okada, S.; Tsutsumi, O.; Kawamura, S.; Bowen, C. *Adv. Mater. Tech.* **2019**, *4*, 1800626.
- (130) Kragt, A. J. J.; Broer, D. J.; Schenning, A. P. H. J. *Adv. Funct. Mater.* **2018**, *28*, 1704756.
- (131) White, T. J.; McConney, M. E.; Bunning, T. J. *J. Mater. Chem.* **2010**, *20*, 9832.
- (132) Mulder, D. J.; Schenning, A. P. H. J.; Bastiaansen, C. W. M. *J. Mater. Chem.* **2014**, *2*, 6695.
- (133) Brannum, M. T.; Steele, A. M.; Venetos, M. C.; Korley, L. T. J.; Wnek, G. E.; White, T. J. *Adv. Opt. Mater.* **2019**, *7*, 1801683.
- (134) Kizhakidathazhath, R.; Geng, Y.; Jampani, V. S. R.; Charni, C.; Sharma, A.; Lagerwall, J. P. F. *Adv. Funct. Mater.* **2020**, *30*, 1909537.
- (135) McBride, M. K.; Martinez, A. M.; Cox, L.; Alim, M.; Childress, K.; Beiswinger, M.; Podgorski, M.; Worrell, B. T.; Killgore, J.; Bowman, C. N. *Sci. Adv.* **2018**, *4*, 1.
- (136) Yakacki, C. M.; Saed, M.; Nair, D. P.; Gong, T.; Reed, S. M.; Bowman, C. N. *RSC Adv.* **2015**, *5*, 18997.
- (137) White, T. J.; Broer, D. J. *Nat. Mater.* **2015**, *14*, 1087.
- (138) Kloxin, C. J.; Scott, T. F.; Adzima, B. J.; Bowman, C. N. *Macromolecules* **2010**, *43*, 2643.
- (139) Zhang, G.; Peng, W.; Wu, J.; Zhao, Q.; Xie, T. *Nat. Commun.* **2018**, *9*, 1.
- (140) Cicuta, P.; Tajbakhsh, A. R.; Terentjev, E. M. *Phys. Rev.* **2004**, *70*, 011704.
- (141) Min Lee, K.; Tondiglia, V. P.; Godman, N. P.; Middleton, C. M.; White, T. J. *Soft Matter* **2017**, *13*, 5842.
- (142) Cicuta, P.; Tajbakhsh, A. R.; Terentjev, E. M. *Phys. Rev.* **2002**, *65*, 051704.
- (143) Stille, W. *Eur. Phys. J. Plus* **2009**, *28*, 57.
- (144) Warner, M.; Terentjev, E. M.; Meyer, R. B.; Mao, Y. *Phys. Rev. Lett.* **2000**, *85*, 2320.
- (145) Varanytsia, A.; Nagai, H.; Urayama, K.; Palffy-Muhoray, P. *Sci. Rep.* **2015**, *5*, 1.
- (146) Patravale, V. B.; Mandawgade, S. D. Novel Cosmetic Delivery Systems: An Application Update: Novel Cosmetic Delivery Systems. *International Journal of Cosmetic Science* **2008**, *30* (1), 19–33. <https://doi.org/10.1111/j.1468-2494.2008.00416.x>.
- (147) Birnbaum, D. T.; Brannon-Peppas, L. Microparticle Drug Delivery Systems. In *Drug Delivery Systems in Cancer Therapy*; Brown, D. M., Ed.; Humana Press: Totowa, NJ, 2004; pp 117–135. https://doi.org/10.1007/978-1-59259-427-6_6.
- (148) Belmonte, A.; Bus, T.; Broer, D. J.; Schenning, A. P. H. J. Patterned Full-Color Reflective Coatings Based on Photonic Cholesteric Liquid-Crystalline Particles. *ACS Applied Materials & Interfaces* **2019**, *11* (15), 14376–14382. <https://doi.org/10.1021/acsami.9b02680>.
- (149) Marshall, J. E.; Gallagher, S.; Terentjev, E. M.; Smoukov, S. K. Anisotropic Colloidal Micromuscles from Liquid Crystal Elastomers. *Journal of the American Chemical Society* **2014**, *136* (1), 474–479. <https://doi.org/10.1021/ja410930g>.

- (150) Kishi, R.; Osada, Y. Reversible Volume Change of Microparticles in an Electric Field. *Journal of the Chemical Society, Faraday Transactions 1: Physical Chemistry in Condensed Phases* **1989**, 85 (3), 655. <https://doi.org/10.1039/f19898500655>.
- (151) Uto, K.; Ebara, M. Magnetic-Responsive Microparticles That Switch Shape at 37 °C. *Applied Sciences* **2017**, 7 (11), 1203. <https://doi.org/10.3390/app7111203>.
- (152) Cox, L. M.; Sun, X.; Wang, C.; Sowan, N.; Killgore, J. P.; Long, R.; Wu, H.-A.; Bowman, C. N.; Ding, Y. Light-Stimulated Permanent Shape Reconfiguration in Cross-Linked Polymer Microparticles. *ACS Applied Materials & Interfaces* **2017**, 9 (16), 14422–14428. <https://doi.org/10.1021/acsami.7b02759>.
- (153) Hessberger, T.; Braun, L.; Zentel, R. Microfluidic Synthesis of Actuating Microparticles from a Thiol-Ene Based Main-Chain Liquid Crystalline Elastomer. *Polymers* **2016**, 8 (12), 410. <https://doi.org/10.3390/polym8120410>.
- (154) Ohm, C.; Serra, C.; Zentel, R. A Continuous Flow Synthesis of Micrometer-Sized Actuators from Liquid Crystalline Elastomers. *Advanced Materials* **2009**, 21 (47), 4859–4862. <https://doi.org/10.1002/adma.200901522>.
- (155) Haseloh, S.; Ohm, C.; Smallwood, F.; Zentel, R. Nanosized Shape-Changing Colloids from Liquid Crystalline Elastomers. *Macromolecular Rapid Communications* **2011**, 32 (1), 88–93. <https://doi.org/10.1002/marc.201000324>.
- (156) Yang, Z.; Huck, W. T. S.; Clarke, S. M.; Tajbakhsh, A. R.; Terentjev, E. M. Shape-Memory Nanoparticles from Inherently Non-Spherical Polymer Colloids. *Nature Materials* **2005**, 4 (6), 486–490. <https://doi.org/10.1038/nmat1389>.
- (157) Vennes, M.; Martin, S.; Gisler, T.; Zentel, R. Anisotropic Particles from LC Polymers for Optical Manipulation. *Macromolecules* **2006**, 39 (24), 8326–8333. <https://doi.org/10.1021/ma0613279>.
- (158) Cairns, D. R.; Sibulkin, M.; Crawford, G. P. Switching Dynamics of Suspended Mesogenic Polymer Microspheres. *Applied Physics Letters* **2001**, 78 (18), 2643–2645. <https://doi.org/10.1063/1.1367292>.
- (159) Vennes, M.; Zentel, R. Liquid-Crystalline Colloidal Particles. *Macromolecular Chemistry and Physics* **2004**, 205 (17), 2303–2311. <https://doi.org/10.1002/macp.200400296>.
- (160) Liu, X.; Xu, Y.; Heuts, J. P. A.; Debije, M. G.; Schenning, A. P. H. J. Monodisperse Liquid Crystal Network Particles Synthesized via Precipitation Polymerization. *Macromolecules* **2019**, 52 (21), 8339–8345. <https://doi.org/10.1021/acs.macromol.9b01852>.
- (161) Liu, X.; Pan, X. Programmable Liquid Crystal Elastomer Microactuators Prepared via Thiol-Ene Dispersion Polymerization. *Soft Matter* **2020**, 13 (45), 8368–8378. <https://doi.org/10.1039/C7SM01619K>.
- (162) Wang, C.; Zhang, X.; Podgórski, M.; Xi, W.; Shah, P.; Stansbury, J.; Bowman, C. N. Monodispersity/Narrow Polydispersity Cross-Linked Microparticles Prepared by Step-Growth Thiol–Michael Addition Dispersion Polymerizations. *Macromolecules* **2015**, 48 (23), 8461–8470. <https://doi.org/10.1021/acs.macromol.5b02146>.
- (163) Wang, X.; Xu, M.; Ren, H.; Wang, Q. A Polarization Converter Array Using a Twisted-Azimuthal Liquid Crystal in Cylindrical Polymer Cavities. *Opt. Express* **2013**, 21 (13), 16222. <https://doi.org/10.1364/OE.21.016222>.
- (164) Ware, T. H.; Biggins, J. S.; Shick, A. F.; Warner, M.; White, T. J. Localized Soft Elasticity in Liquid Crystal Elastomers. *Nature Communications* **2016**, 7 (1). <https://doi.org/10.1038/ncomms10781>.

- (165) Patravale, V. B.; Mandawgade, S. D. Novel Cosmetic Delivery Systems: An Application Update: Novel Cosmetic Delivery Systems. *International Journal of Cosmetic Science* **2008**, *30* (1), 19–33. <https://doi.org/10.1111/j.1468-2494.2008.00416.x>.
- (166) Birnbaum, D. T.; Brannon-Peppas, L. Microparticle Drug Delivery Systems. In *Drug Delivery Systems in Cancer Therapy*; Brown, D. M., Ed.; Humana Press: Totowa, NJ, 2004; pp 117–135. https://doi.org/10.1007/978-1-59259-427-6_6.
- (167) Xia, Y.; Gates, B.; Yin, Y.; Lu, Y. Monodispersed Colloidal Spheres: Old Materials with New Applications. *Advanced Materials* **2000**, *12* (10), 693–713. [https://doi.org/10.1002/\(SICI\)1521-4095\(200005\)12:10<693::AID-ADMA693>3.0.CO;2-J](https://doi.org/10.1002/(SICI)1521-4095(200005)12:10<693::AID-ADMA693>3.0.CO;2-J).
- (168) van Kuringen, H. P. C.; Mulder, D. J.; Beltran, E.; Broer, D. J.; Schenning, A. P. H. J. Nanoporous Polymer Particles Made by Suspension Polymerization: Spontaneous Symmetry Breaking in Hydrogen Bonded Smectic Liquid Crystalline Droplets and High Adsorption Characteristics. *Polymer Chemistry* **2016**, *7* (29), 4712–4716. <https://doi.org/10.1039/C6PY00865H>.
- (169) Bhaskar, S.; Pollock, K. M.; Yoshida, M.; Lahann, J. Towards Designer Microparticles: Simultaneous Control of Anisotropy, Shape, and Size. *Small* **2010**, *6* (3), 404–411. <https://doi.org/10.1002/smll.200901306>.
- (170) Cox, L. M.; Killgore, J. P.; Li, Z.; Long, R.; Sanders, A. W.; Xiao, J.; Ding, Y. Influences of Substrate Adhesion and Particle Size on the Shape Memory Effect of Polystyrene Particles. *Langmuir* **2016**, *32* (15), 3691–3698. <https://doi.org/10.1021/acs.langmuir.6b00588>.
- (171) Mueller, S.; Llewellyn, E. W.; Mader, H. M. The Rheology of Suspensions of Solid Particles. *Proceedings of the Royal Society A: Mathematical, Physical and Engineering Sciences* **2010**, *466* (2116), 1201–1228. <https://doi.org/10.1098/rspa.2009.0445>.
- (172) Uto, K.; Ebara, M. Magnetic-Responsive Microparticles That Switch Shape at 37 °C. *Applied Sciences* **2017**, *7* (11), 1203. <https://doi.org/10.3390/app7111203>.
- (173) Marshall, J. E.; Gallagher, S.; Terentjev, E. M.; Smoukov, S. K. Anisotropic Colloidal Micromuscles from Liquid Crystal Elastomers. *Journal of the American Chemical Society* **2014**, *136* (1), 474–479. <https://doi.org/10.1021/ja410930g>.
- (174) Liu, X.; Pan, X.; Debije, M.; Huets, J.; Mulder, D.; Schenning, A. Programmable Liquid Crystal Elastomer Microactuators Prepared via Thiol-Ene Dispersion Polymerization. *Soft Matter* **2020**, *13* (45), 8368–8378. <https://doi.org/10.1039/C7SM01619K>.
- (175) Klinger, D.; Wang, C. X.; Connal, L. A.; Audus, D. J.; Jang, S. G.; Kraemer, S.; Killops, K. L.; Fredrickson, G. H.; Kramer, E. J.; Hawker, C. J. A Facile Synthesis of Dynamic, Shape-Changing Polymer Particles. *Angewandte Chemie International Edition* **2014**, *53* (27), 7018–7022. <https://doi.org/10.1002/anie.201400183>.
- (176) Wischke, C.; Schossig, M.; Lendlein, A. Shape-Memory Effect of Micro-/Nanoparticles from Thermoplastic Multiblock Copolymers. *Small* **2014**, *10* (1), 83–87. <https://doi.org/10.1002/smll.201202213>.
- (177) Ho, C. C.; Keller, A.; Odell, J. A.; Ottewill, R. H. Preparation of Monodisperse Ellipsoidal Polystyrene Particles. *Colloid & Polymer Science* **1993**, *271* (5), 469–479. <https://doi.org/10.1007/BF00657391>.
- (178) Rešetič, A.; Milavec, J.; Zupančič, B.; Domenici, V.; Zalar, B. Polymer-Dispersed Liquid Crystal Elastomers. *Nature Communications* **2016**, *7* (1). <https://doi.org/10.1038/ncomms13140>.

- (179) Belmonte, A.; Bus, T.; Broer, D. J.; Schenning, A. P. H. J. Patterned Full-Color Reflective Coatings Based on Photonic Cholesteric Liquid-Crystalline Particles. *ACS Applied Materials & Interfaces* **2019**, *11* (15), 14376–14382. <https://doi.org/10.1021/acsami.9b02680>.
- (180) Ohm, C.; Serra, C.; Zentel, R. A Continuous Flow Synthesis of Micrometer-Sized Actuators from Liquid Crystalline Elastomers. *Advanced Materials* **2009**, *21* (47), 4859–4862. <https://doi.org/10.1002/adma.200901522>.
- (181) Yu, H.; Liu, H.; Kobayashi, T. Fabrication and Photoresponse of Supramolecular Liquid-Crystalline Microparticles. *ACS Applied Materials & Interfaces* **2011**, *3* (4), 1333–1340. <https://doi.org/10.1021/am2001289>.
- (182) Ryabchun, A.; Bobrovsky, A. Photocontrollable Deformations of Polymer Particles in Elastic Matrix. *Advanced Optical Materials* **2019**, *7* (24), 1901486. <https://doi.org/10.1002/adom.201901486>.
- (183) Vennes, M.; Zentel, R. Liquid-Crystalline Colloidal Particles. *Macromolecular Chemistry and Physics* **2004**, *205* (17), 2303–2311. <https://doi.org/10.1002/macp.200400296>.
- (184) Yang, Z.; Huck, W. T. S.; Clarke, S. M.; Tajbakhsh, A. R.; Terentjev, E. M. Shape-Memory Nanoparticles from Inherently Non-Spherical Polymer Colloids. *Nature Materials* **2005**, *4* (6), 486–490. <https://doi.org/10.1038/nmat1389>.
- (185) Haseloh, S.; Ohm, C.; Smallwood, F.; Zentel, R. Nanosized Shape-Changing Colloids from Liquid Crystalline Elastomers. *Macromolecular Rapid Communications* **2011**, *32* (1), 88–93. <https://doi.org/10.1002/marc.201000324>.
- (186) Haseloh, S.; Zentel, R. Synthesis of Liquid-Crystalline Colloids in Nonpolar Media and Their Manipulation in Electric Fields. *Macromolecular Chemistry and Physics* **2009**, *210* (17), 1394–1401. <https://doi.org/10.1002/macp.200900122>.
- (187) Hessberger, T.; Braun, L.; Zentel, R. Microfluidic Synthesis of Actuating Microparticles from a Thiol-Ene Based Main-Chain Liquid Crystalline Elastomer. *Polymers* **2016**, *8* (12), 410. <https://doi.org/10.3390/polym8120410>.
- (188) Fleischmann, E.-K.; Forst, F. R.; Köder, K.; Kapernaum, N.; Zentel, R. Microactuators from a Main-Chain Liquid Crystalline Elastomer via Thiol-Ene “Click” Chemistry. *Journal of Materials Chemistry C* **2013**, *1* (37), 5885. <https://doi.org/10.1039/c3tc30272e>.
- (189) White, T. J.; Broer, D. J. Programmable and Adaptive Mechanics with Liquid Crystal Polymer Networks and Elastomers. *Nature Materials* **2015**, *14* (11), 1087–1098. <https://doi.org/10.1038/nmat4433>.
- (190) Yakacki, C. M.; Saed, M.; Nair, D. P.; Gong, T.; Reed, S. M.; Bowman, C. N. Tailorable and Programmable Liquid-Crystalline Elastomers Using a Two-Stage Thiol-Acrylate Reaction. *RSC Advances* **2015**, *5* (25), 18997–19001. <https://doi.org/10.1039/C5RA01039J>.
- (191) Liu, X.; Xu, Y.; Heuts, J. P. A.; Debije, M. G.; Schenning, A. P. H. J. Monodisperse Liquid Crystal Network Particles Synthesized via Precipitation Polymerization. *Macromolecules* **2019**, *52* (21), 8339–8345. <https://doi.org/10.1021/acs.macromol.9b01852>.
- (192) Wang, C.; Zhang, X.; Podgórski, M.; Xi, W.; Shah, P.; Stansbury, J.; Bowman, C. N. Monodispersity/Narrow Polydispersity Cross-Linked Microparticles Prepared by Step-Growth Thiol-Michael Addition Dispersion Polymerizations. *Macromolecules* **2015**, *48* (23), 8461–8470. <https://doi.org/10.1021/acs.macromol.5b02146>.
- (193) Durham, O. Z.; Shipp, D. A. Polymer Colloids from Step-Growth Thiol-X Polymerizations. *Polymer Reviews* **2020**, 1–26. <https://doi.org/10.1080/15583724.2020.1743307>.

- (194) McBride, M. K.; Worrell, B. T.; Brown, T.; Cox, L. M.; Sowan, N.; Wang, C.; Podgorski, M.; Martinez, A. M.; Bowman, C. N. Enabling Applications of Covalent Adaptable Networks. *Annual Review of Chemical and Biomolecular Engineering* **2019**, *10* (1), 175–198. <https://doi.org/10.1146/annurev-chembioeng-060718-030217>.
- (195) Kloxin, C. J.; Scott, T. F.; Adzima, B. J.; Bowman, C. N. Covalent Adaptable Networks (CANs): A Unique Paradigm in Cross-Linked Polymers. *Macromolecules* **2010**, *43* (6), 2643–2653. <https://doi.org/10.1021/ma902596s>.
- (196) Hanzon, D. W.; Traugott, N. A.; McBride, M. K.; Bowman, C. N.; Yakacki, C. M.; Yu, K. Adaptable Liquid Crystal Elastomers with Transesterification-Based Bond Exchange Reactions. *Soft Matter* **2018**, *14* (6), 951–960. <https://doi.org/10.1039/C7SM02110K>.
- (197) Saed, M. O.; Gablier, A.; Terentejv, E. M. Liquid Crystalline Vitrimers with Full or Partial Boronic-Ester Bond Exchange. *Advanced Functional Materials* **2020**, *30* (3), 1906458. <https://doi.org/10.1002/adfm.201906458>.
- (198) McBride, M. K.; Martinez, A. M.; Cox, L.; Alim, M.; Childress, K.; Beiswinger, M.; Podgorski, M.; Worrell, B. T.; Killgore, J.; Bowman, C. N. A Readily Programmable, Fully Reversible Shape-Switching Material. *Science Advances* **2018**, *4* (8), eaat4634. <https://doi.org/10.1126/sciadv.aat4634>.
- (199) Cox, L. M.; Sun, X.; Wang, C.; Sowan, N.; Killgore, J. P.; Long, R.; Wu, H.-A.; Bowman, C. N.; Ding, Y. Light-Stimulated Permanent Shape Reconfiguration in Cross-Linked Polymer Microparticles. *ACS Applied Materials & Interfaces* **2017**, *9* (16), 14422–14428. <https://doi.org/10.1021/acsami.7b02759>.
- (200) Ware, T. H.; Biggins, J. S.; Shick, A. F.; Warner, M.; White, T. J. Localized Soft Elasticity in Liquid Crystal Elastomers. *Nature Communications* **2016**, *7* (1). <https://doi.org/10.1038/ncomms10781>.
- (201) Yu, H.; Dong, C.; Zhou, W.; Kobayashi, T.; Yang, H. Wrinkled Liquid-Crystalline Microparticle-Enhanced Photoresponse of PDLC-Like Films by Coupling with Mechanical Stretching. *Small* **2011**, *7* (21), 3039–3045. <https://doi.org/10.1002/sml.201101098>.
- (202) Liu, J.; Liu, Y.; Xue, Y.; Ren, Y.; Fan, X.; Wang, R.; Zhang, H.; Zhang, B.; Zhang, Q. Fabrication and Characterization of Controllable Wrinkled-Surface Polymer Microparticles. *Journal of Materials Science* **2019**, *54* (7), 5852–5864. <https://doi.org/10.1007/s10853-018-2421-2>.
- (203) Ngo, T. D.; Kashani, A.; Imbalzano, G.; Nguyen, K. T. Q.; Hui, D. Additive Manufacturing (3D Printing): A Review of Materials, Methods, Applications and Challenges. *Composites Part B: Engineering* **2018**, *143*, 172–196. <https://doi.org/10.1016/j.compositesb.2018.02.012>.
- (204) Muralidharan, A.; Uzcategui, A. C.; McLeod, R. R.; Bryant, S. J. Stereolithographic 3D Printing for Deterministic Control over Integration in Dual-Material Composites. *Adv. Mater. Technol.* **2019**, *4* (11), 1900592. <https://doi.org/10.1002/admt.201900592>.
- (205) Yu, L.; Lei, Z.; Sun, X.; Ding, P.; Wesche, A.; Jin, Y.; Zhang, W.; Long, R. Rapid Fabrication of Fiber-Reinforced Polyimine Composites with Reprocessability, Repairability, and Recyclability. *ACS Appl. Polym. Mater.* **2021**, *3* (11), 5808–5817. <https://doi.org/10.1021/acsapm.1c01027>.
- (206) Neumann, T. V.; Dickey, M. D. Liquid Metal Direct Write and 3D Printing: A Review. *Adv. Mater. Technol.* **2020**, *5* (9), 2000070. <https://doi.org/10.1002/admt.202000070>.

- (207) Chevalier, Y.; Pichot, C.; Graillat, C.; Joanicot, M.; Wong, K.; Maquet, J.; Lindner, P.; Cabane, B. Film Formation with Latex Particles. *Colloid Polym Sci* **1992**, *270* (8), 806–821. <https://doi.org/10.1007/BF00776153>.
- (208) Zhan, Y.; Lavorgna, M.; Buonocore, G.; Xia, H. Enhancing Electrical Conductivity of Rubber Composites by Constructing Interconnected Network of Self-Assembled Graphene with Latex Mixing. *J. Mater. Chem.* **2012**, *22* (21), 10464. <https://doi.org/10.1039/c2jm31293j>.
- (209) Potts, J. R.; Shankar, O.; Du, L.; Ruoff, R. S. Processing–Morphology–Property Relationships and Composite Theory Analysis of Reduced Graphene Oxide/Natural Rubber Nanocomposites. *Macromolecules* **2012**, *45* (15), 6045–6055. <https://doi.org/10.1021/ma300706k>.
- (210) Yu, K.; Shi, Q.; Li, H.; Jabour, J.; Yang, H.; Dunn, M. L.; Wang, T.; Qi, H. J. Interfacial Welding of Dynamic Covalent Network Polymers. *Journal of the Mechanics and Physics of Solids* **2016**, *94*, 1–17. <https://doi.org/10.1016/j.jmps.2016.03.009>.
- (211) Yang, H.; Yu, K.; Mu, X.; Wei, Y.; Guo, Y.; Qi, H. J. Molecular Dynamics Studying on Welding Behavior in Thermosetting Polymers Due to Bond Exchange Reactions. *RSC Adv.* **2016**, *6* (27), 22476–22487. <https://doi.org/10.1039/C5RA26128G>.
- (212) Chen, X.; Dam, M. A.; Ono, K.; Mal, A.; Shen, H.; Nutt, S. R.; Sheran, K.; Wudl, F. A Thermally Re-Mendable Cross-Linked Polymeric Material. *Science, New Series* **2002**, *295* (5560), 1698–1702.
- (213) Liu, Y.-L.; Chuo, T.-W. Self-Healing Polymers Based on Thermally Reversible Diels–Alder Chemistry. *Polym. Chem.* **2013**, *4* (7), 2194. <https://doi.org/10.1039/c2py20957h>.
- (214) Cheng, C.; Bai, X.; Zhang, X.; Li, H.; Huang, Q.; Tu, Y. Self-Healing Polymers Based on a Photo-Active Reversible Addition-Fragmentation Chain Transfer (RAFT) Agent. *J Polym Res* **2015**, *22* (4), 46. <https://doi.org/10.1007/s10965-015-0691-9>.
- (215) Yao, L.; Rong, M. Z.; Zhang, M. Q.; Yuan, Y. C. Self-Healing of Thermoplastics via Reversible Addition–Fragmentation Chain Transfer Polymerization. *J. Mater. Chem.* **2011**, *21* (25), 9060. <https://doi.org/10.1039/c1jm10655d>.
- (216) Robinson, L. L.; Self, J. L.; Fusi, A. D.; Bates, M. W.; Read de Alaniz, J.; Hawker, C. J.; Bates, C. M.; Sample, C. S. Chemical and Mechanical Tunability of 3D-Printed Dynamic Covalent Networks Based on Boronate Esters. *ACS Macro Lett.* **2021**, *10* (7), 857–863. <https://doi.org/10.1021/acsmacrolett.1c00257>.
- (217) Fu, F.; Huang, M.; Zhang, W.; Zhao, Y.; Liu, X. Thermally Assisted Self-Healing Behavior of Anhydride Modified Polybenzoxazines Based on Transesterification. *Sci Rep* **2018**, *8* (1), 10325. <https://doi.org/10.1038/s41598-018-27942-9>.
- (218) Zheng, M.; Guo, Q.; Yin, X.; Getangama, N. N.; de Bruyn, J. R.; Xiao, J.; Bai, Y.; Liu, M.; Yang, J. Direct Ink Writing of Recyclable and *in Situ* Repairable Photothermal Polyurethane for Sustainable 3D Printing Development. *J. Mater. Chem. A* **2021**, *9* (11), 6981–6992. <https://doi.org/10.1039/D0TA11341G>.
- (219) Brown, T. E.; Carberry, B. J.; Worrell, B. T.; Dudaryeva, O. Y.; McBride, M. K.; Bowman, C. N.; Anseth, K. S. Photopolymerized Dynamic Hydrogels with Tunable Viscoelastic Properties through Thioester Exchange. *Biomaterials* **2018**, *178*, 496–503. <https://doi.org/10.1016/j.biomaterials.2018.03.060>.
- (220) Sowan, N.; Cox, L. M.; Shah, P. K.; Song, H. B.; Stansbury, J. W.; Bowman, C. N. Dynamic Covalent Chemistry at Interfaces: Development of Tougher, Healable Composites

- through Stress Relaxation at the Resin–Silica Nanoparticles Interface. *Adv. Mater. Interfaces* **2018**, *5* (18), 1800511. <https://doi.org/10.1002/admi.201800511>.
- (221) Shi, Q.; Yu, K.; Kuang, X.; Mu, X.; Dunn, C. K.; Dunn, M. L.; Wang, T.; Jerry Qi, H. Recyclable 3D Printing of Vitrimer Epoxy. *Mater. Horiz.* **2017**, *4* (4), 598–607. <https://doi.org/10.1039/C7MH00043J>.
- (222) Huang, Q.; Tang, Z.; Wang, D.; Wu, S.; Guo, B. Engineering Segregated Structures in a Cross-Linked Elastomeric Network Enabled by Dynamic Cross-Link Reshuffling. *ACS Macro Lett.* **2021**, *10* (2), 231–236. <https://doi.org/10.1021/acsmacrolett.0c00852>.
- (223) Lu, L.; Pan, J.; Li, G. Recyclable High-Performance Epoxy Based on Transesterification Reaction. *J. Mater. Chem. A* **2017**, *5* (40), 21505–21513. <https://doi.org/10.1039/C7TA06397K>.
- (224) Worrell, B. T.; McBride, M. K.; Lyon, G. B.; Cox, L. M.; Wang, C.; Mavila, S.; Lim, C.-H.; Coley, H. M.; Musgrave, C. B.; Ding, Y.; Bowman, C. N. Bistable and Photoswitchable States of Matter. *Nat Commun* **2018**, *9* (1), 2804. <https://doi.org/10.1038/s41467-018-05300-7>.
- (225) De Alwis Watuthanthrige, N.; Ahammed, B.; Dolan, M. T.; Fang, Q.; Wu, J.; Sparks, J. L.; Zanjani, M. B.; Konkolewicz, D.; Ye, Z. Accelerating Dynamic Exchange and Self-Healing Using Mechanical Forces in Crosslinked Polymers. *Mater. Horiz.* **2020**, *7* (6), 1581–1587. <https://doi.org/10.1039/C9MH01938C>.
- (226) Yu, L.; Sun, X.; Jin, Y.; Zhang, W.; Long, R. Mechanics of Vitrimer Particle Compression and Fusion under Heat Press. *International Journal of Mechanical Sciences* **2021**, *201*, 106466. <https://doi.org/10.1016/j.ijmecsci.2021.106466>.
- (227) Podgórski, M.; Huang, S.; Bowman, C. N. Additive Manufacture of Dynamic Thiol–Ene Networks Incorporating Anhydride-Derived Reversible Thioester Links. *ACS Appl. Mater. Interfaces* **2021**, *13* (11), 12789–12796. <https://doi.org/10.1021/acsmi.0c18979>.